

Spring 5-2010

A Study of the Effective Interfacial Tension Between Miscible Fluids by Spinning Drop Tensiometer and Microfluidics

Gloria Dollie Viner
University of Southern Mississippi

Follow this and additional works at: <https://aquila.usm.edu/dissertations>

 Part of the [Chemistry Commons](#)

Recommended Citation

Viner, Gloria Dollie, "A Study of the Effective Interfacial Tension Between Miscible Fluids by Spinning Drop Tensiometer and Microfluidics" (2010). *Dissertations*. 946.
<https://aquila.usm.edu/dissertations/946>

This Dissertation is brought to you for free and open access by The Aquila Digital Community. It has been accepted for inclusion in Dissertations by an authorized administrator of The Aquila Digital Community. For more information, please contact Joshua.Cromwell@usm.edu.

ABSTRACT

A STUDY OF THE EFFECTIVE INTERFACIAL TENSION BETWEEN MISCIBLE FLUIDS BY SPINNING DROP TENSIO METER AND MICROFLUIDICS

by Gloria Dollie Viner

May 2010

A miscible system is a system in which two fluids can completely dissolve in one another. A sharp concentration gradient can be observed in miscible systems. We studied the concentration gradient or miscible interface between IBA (isobutyric acid) and water, a miscible system near a consolute point (close to the system's upper critical solution temperature [UCST]). The original hypothesis was that the sharp concentration gradient of IBA/water was due to barodiffusion, a diffusion effect driven by pressure. We tested this hypothesis by studying IBA/water at five different rotation rates and three different temperatures. At 20 °C, increasing rotation acceleration from 6000 to 15000 rpm resulted in increasing dissolution rate, thus demonstrating that barodiffusion did not cause the sharp concentration gradient. However, the rotation acceleration did not affect the dissolution rate at higher temperatures. Increasing the temperature from 20 °C to 27 °C caused EIT (effective interfacial tension) to decrease. Since surfactants generally lower the interfacial tension between immiscible fluids, we tested an anionic and cationic surfactant and evaluated how its concentration within cmc (critical micelle concentration) affected the EIT of a miscible system. With increasing surfactant concentration, the EITs generally

decreased. At 20 °C, the ITs of IBA/water systems using surfactants were slightly higher than IBA/water systems without surfactant, which is unusual. At 30 °C, increasing and decreasing the rotation rate resulted in the averaged EIT and radii getting higher. We had some unusual behavior in the microfluidic device that we did not observe in the SDT (spinning drop tensiometer) because of mixing and the microsystem was done on a smaller scale so that larger effects from surface tension occurred, but some behaviors were the same, thus indicating that the behavior of the IBA/water system was not solely due to the instrument used.

ACKNOWLEDGEMENTS

The writer would like to thank her major advisor and members of her committee for their support and feedback. Thanks to former and current members of the Pojman lab who conducted research related to what I did. I would also like to thank my family for their support and encouragement through the six years to achieve my master's and then my doctoral degree in chemistry.

TABLE OF CONTENTS

ABSTRACT.....	ii
ACKNOWLEDGEMENTS.....	iv
LIST OF TABLES.....	vii
LIST OF ILLUSTRATIONS.....	viii
CHAPTER	
I. INTRODUCTION AND GOALS.....	1
Project Goals	
Importance of the Research	
II. BACKGROUND AND LITERATURE REVIEW.....	4
Interfacial Tension and Effective Interfacial Tension	
Isobutyric Acid and Water	
Spinning Drop Tensiometry	
SDT Research in Pojman Lab	
Diffusion and Fick's Law	
Barodiffusion	
Surfactants	
Microfluidics	
III. EXPERIMENTAL PROCEDURES AND PRELIMINARY ANALYSIS METHOD.....	27
SDT	
Microfluidics	
Preliminary Analysis Method of Volume of IBA Drop as Function of Time	
IV. IBA VOLUME EXPERIMENTS	36
Results and Observed Behavior	
Development of Method for Analysis	
Analysis	
Conclusions	

V.	SURFACTANTS	86
	Distinguishing Drops	
	Comparison of Behavior	
	EIT and Surfactant Concentration	
	Conclusions	
VI.	MICROFLUIDICS.....	150
	PMMA and PC Microfluidic Devices	
	Polydimethylsiloxane (PDMS) Microfluidic Device	
	Conclusions	
VII.	CONCLUSIONS AND FUTURE WORK.....	187
	REFERENCES.....	197

LIST OF TABLES

Table

3.1.	List of Reagents Used.....	27
4.1.	Summary of Rates of Dissolving IBA Drops at Different Temperatures and Rotation Rates.....	65
4.2.	Averaged EIT and IT of IBA/water at Different Rotation Rates and Temperatures.....	76
5.1.	Summary of EIT for Different Surfactants at 30 °C.....	134
5.2.	Summary of EIT and Slopes for Different Surfactants at 30 °C.....	138
5.3.	Summary of IT for Different Surfactants at 20 °C.....	139
5.4.	Summary of IT and Slopes for Different Surfactants at 20 °C.....	141
6.1.	Contact Angles of Various Systems on Different Surfaces.....	173

LIST OF ILLUSTRATIONS

Figure

2.1.	Concentration profile of an interface	5
2.2.	Structure of Isobutyric Acid (IBA).....	9
2.3.	Phase diagram of IBA/water.....	9
2.4.	Schematic of a Spinning Drop Tensiometer (SDT).....	10
2.5.	Drop expansion in monomer/polymer system over 7 minutes	13
2.6.	An example of a polymer's wide transition zone.....	13
2.7.	An example of a drop evolution for IBA/water.	14
2.8.	Drop evolution of n-butanol in water at 20 °C and $\omega = 8000$ rpm.....	15
2.9.	Diffusion of bromophenol blue over a period of 24 hours with images taken about every five hours.....	15
2.10.	Diffusion plot	17
2.11.	An image of a T conjunction in a microfluidic device, a T sensor.....	22
2.12.	An image of an H conjunction in a microfluidic device, an H filter.....	22
2.13.	An image of a microfluidic device that uses large Péclet numbers.....	23
2.14.	An image of a microfluidic device and a close-up of its Y-junction	25
3.1.	Image of Evolving Drop.....	34
3.2.	A graph of the volume/SA vs. time of the second Knud-Thomsen approximation of IBA/water at 25 °C for 8500 rpm and 8000 rpm.....	35
4.1.	A long drop of IBA that started to pinch off at 8000 rpm above UCST	40
4.2.	Small drops of IBA that would not merge and only lasted 10 seconds or less at 10000 rpm above UCST.....	40

4.3.	A really long drop of IBA that would form into smaller drops after a rotational rate decrease and then start to dissolve at 8000 rpm at 27°C.	41
4.4.	A really long drop of IBA that had a decreased rotation rate that broke up into smaller drops at 10000 rpm above UCST.....	41
4.5.	A continuation of Figure 4.4 where the smaller drops would start to merge despite the higher or lower rotation being used at 10000 rpm above UCST.....	42
4.6.	A long drop that extended outside the field of view and became diffuse at 8000 rpm at 30 °C.....	42
4.7.	Graphs of Princen et al. table of correction factors.....	47
4.8.	Image of IBA/water drop at 6000 rpm 20 °C, 25 °C, and 27 °C.....	51
4.9.	Image of IBA/water drop at 8000 rpm 20 °C, 25 °C, and 27 °C.....	51
4.10.	Image of IBA/water drop at 10000 rpm 20 °C, 25 °C, and 27 °C.....	51
4.11.	Image of IBA/water drop at 12000 rpm 20 °C, 25 °C, and 27 °C.....	51
4.12.	Image of IBA/water drop at 14000 rpm 20 °C, 25 °C, and 27 °C.....	52
4.13.	Graph of Volume/SA vs. Time of IBA/water at 20 °C for 6000 rpm.....	52
4.14.	Graph of Volume/SA vs. Time of IBA/water at 20 °C for 8000 rpm.....	53
4.15.	Graph of Volume/SA vs. Time of IBA/water at 20 °C for 10000 rpm.....	53
4.16.	Graph of Volume/SA vs. Time of IBA/water at 20 °C for 12000 rpm.....	54
4.17.	Graph of Volume/SA vs. Time of IBA/water at 20 °C for 14000 rpm.....	54
4.18.	Graph of Volume/SA vs. Time of IBA/water at 25 °C for 6000 rpm.....	55
4.19.	Graph of Volume/SA vs. Time of IBA/water at 25 °C for 8000 rpm.....	55
4.20.	Graph of Volume/SA vs. Time of IBA/water at 25 °C for 10000 rpm.....	56
4.21.	Graph of Volume/SA vs. Time of IBA/water at 25 °C for 12000 rpm.....	56
4.22.	Graph of Volume/SA vs. Time of IBA/water at 25 °C for 14000 rpm.....	57
4.23.	Graph 2 of Volume/SA vs. Time of IBA/water at 25 °C for 14000 rpm.....	57

4.24.	Graph of Volume/SA vs. Time of IBA/water at 27 °C for 6000 rpm.....	58
4.25.	Graph of Volume/SA vs. Time of IBA/water at 27 °C for 8000 rpm.....	58
4.26.	Graph of Volume/SA vs. Time of IBA/water at 27 °C for 10000 rpm.....	59
4.27.	Graph of Volume/SA vs. Time of IBA/water at 27 °C for 12000 rpm.....	59
4.28.	Graph of Volume/SA vs. Time of IBA/water at 27 °C for 14000 rpm.....	60
4.29.	A series of images depicting how an IBA drop changes shape with 0.1 seconds elapsing between the second through tenth images and two seconds between the first and second image.....	62
4.30.	IBA/water drop at 6000 and 27 °C with diffuse edges.....	63
4.31.	IBA/water drops at 6000 at 27 °C and 8000 at 20 °C with unidentifiable component the same size as IBA-rich drops	63
4.32.	IBA-rich drops merging at 8000 rpm and 20 °C with two seconds passing between the left and center images and 0.25 seconds between the center and right images.....	63
4.33.	An IBA-rich drop becoming obliterated by an air bubble at 14000 rpm and 20 °C and 25 °C.....	64
4.34.	Image of small air bubble (dark drop) in IBA/water at 8000 rpm and 27 °C and at 10000 rpm and 20 °C	79
4.35.	Image of medium air bubble (dark drop) in IBA/water at 6000 rpm and 27 °C at 10000 rpm and 25 °C and at 14000 rpm and 20 °C	79
4.36.	IBA/water drop emerging from large air bubble at 12000 rpm 27 °C.....	79
4.37.	IBA/water drop at 6000 rpm and 27°C with ten and sixteen seconds elapsing between the left and center and center and right images	79
4.38.	IBA/water drop at 10000 rpm and 20°C with five seconds elapsing between the left and center and center and right images.....	80
4.39.	IBA/water drop at 14000 rpm and 20°C with two and three seconds elapsing between the left and center and center and right images.....	80
4.40.	Rate of diffusion versus rotation rate squared.....	84

5.1.	IBA-rich phase coming from left side of capillary at 7000 rpm at 24 °C....	89
5.2.	IBA-rich drop coming from left side of capillary at 4000 rpm at 20 °C.....	90
5.3.	IBA/SDS/Water at 9000 rpm at 29 °C	92
5.4.	IBA/SDS/Water at 9000 rpm and 7000 rpm at 29 °C	92
5.5.	IBA/SDS/Water with black air bubble at 10000 rpm at 29 °C.....	92
5.6.	IBA/SDS/Water at 8000 rpm at 29 °C	94
5.7.	IBA/water and IBA/surfactant/water systems at 20 °C	95
5.8.	IBA/water and IBA/surfactant/water systems above the UCST between 27-30 °C. Images A and C: IBA/SDS/water at 8000 rpm at 29 °C. Image B: IBA/water at 8000 rpm at 27 °C. Image D: IBA/water at 8000 rpm at 29 °C.	95
5.9.	IBA/SDS/water at 29 °C at 8000 rpm.....	97
5.10.	IBA/SDS/water at 29 °C between 7000 rpm to 15000 rpm	98
5.11.	IBA/SDS/water and IBA/water at 29 °C at 8000 rpm.	99
5.12.	IBA/SDS/water at 29°C and 0 rpm	101
5.13.	IBA being injected into water-rich phase at 24 °C.....	102
5.14.	Fluid motions in IBA/water system between 27 °C and 28 °C.....	102
5.15.	IBA/surfactant/water system at 0 rpm and above UCST.....	103
5.16.	IBA/surfactant/water system at 8000 rpm and above the UCST.....	103
5.17.	IBA/water/surfactant system at 0 rpm and above the UCST with a needle taking a small IBA drop from a larger IBA drop.....	105
5.18.	An example of IBA/water/SDS with a drop of IBA inside of long SDS-rich water drop which is in the bulk water-rich phase at 25 °C at 7000 rpm.....	106

5.19.	An example of IBA/water/SDS with an IBA-rich drop inside of long SDS-rich water drop which is in the bulk water-rich phase at 29°C at 7000 rpm.....	107
5.20.	IBA/Water and IBA/SDS/Water above the UCST.....	108
5.21.	IBA/Water at 7000 rpm and above the UCST showing the IBA's sharp boundary fading.....	109
5.22.	IBA/SDS/Water system at 8000 rpm above the UCST; the IBA's sharp boundary fading.....	110
5.23.	IBA/SDS/Water system that was 3 minutes later after Figure 5.22.....	110
5.24.	IBA/SDS/Water system that was 8 minutes later after Figure 5.22.....	110
5.25.	Marangoni effect in IBA/water at 20 °C.....	111
5.26.	Marangoni effect for IBA/SDS/water at 20 °C.....	111
5.27.	IBA/water endpinching at 27 °C and 8000 rpm.....	112
5.28.	IBA/dodecyltrimethylammonium chloride/water endpinched at 20 °C and 15000 rpm.....	112
5.29.	IBA/SDS/water almost end pinching at 27 °C and 29 °C at 8000 rpm....	113
5.30.	IBA/SDS/water at 20 °C and 4000 rpm with drops merging.....	114
5.31.	IBA/SDS/water above the UCST and 8000 rpm with drops merging.....	114
5.32.	IBA/SDS/water at 20 °C and 3000 rpm.....	114
5.33.	IBA/SDS/water at 27 °C and 7000 rpm with the IBA drops merging.....	116
5.34.	IBA/SDS/water above the UCST and 8000 rpm with one short and two long IBA drops merging.....	116
5.35.	IBA/SDS/water drops merging at 24 °C at 7000 rpm going from image A to image D (between A to B and B to C, 0.25 seconds passed; between C to D, 1-2 seconds passed).....	116
5.36.	Graph of r^{-3} vs. ω^2 for IBA/SDS/water of 0.0006 M SDS at 20 and 30 °C.....	118

5.37. Graph of r^{-3} vs. ω^2 for IBA/SDS/water of 0.312 mM SDS at 20 and 30 °C.....	118
5.38. Another graph of r^{-3} vs. ω^2 for IBA/SDS/water of 0.312 mM SDS at 20 and 30 °C.....	118
5.39. A graph of r^{-3} vs. ω^2 for IBA/SDS/water of 0.312 mM SDS with second and third rotational increases and decreases at 30 °C.....	119
5.40. Graph of r^{-3} vs. ω^2 for IBA/SDS/water of 0.06 mM SDS at 30 °C.....	119
5.41. A graph of r^{-3} vs. ω^2 for IBA/SDS/water of 0.06 mM SDS with third and fourth rotational increases and decreases at 30 °C.....	119
5.42. Graph of r^{-3} vs. ω^2 for IBA/SDS/water of 0.06 mM SDS at 20 and 30 °C.....	120
5.43. An extension of the graph of r^{-3} vs. ω^2 for IBA/SDS/water of 0.06 mM SDS with third and fourth rotational increases and decreases at 30 °C.	120
5.44. Graph of r^{-3} vs. ω^2 for IBA/SDS/water of 11.8 mM SDS at 30 °C.....	121
5.45. A graph of r^{-3} vs. ω^2 for IBA/SDS/water of 11.8 mM SDS with third and fourth rotational increases and decreases at 30 °C.....	121
5.46. Graph of r^{-3} vs. ω^2 for IBA/SDS/water of 11.8 mM SDS at 30 °C.....	122
5.47. A graph of r^{-3} vs. ω^2 for IBA/SDS/water of 11.8 mM SDS with fourth, fifth, and sixth rotational increases and decreases at 30 °C.....	122
5.48. Graph of r^{-3} vs. ω^2 for IBA/DTAC/water of 5.74 mM DTAC at 20 and 30 °C.....	123
5.49. Graph of r^{-3} vs. ω^2 for IBA/DTAC/water of 5.74 mM DTAC at 30 °C.....	123
5.50. Graph of r^{-3} vs. ω^2 for IBA/DTAC/water of 0.610 mM DTAC at 30 °C....	123
5.51. Graph of r^{-3} vs. ω^2 for IBA/SDS /water of 11.8 mM SDS at 20 °C.....	124
5.52. Graph of r^{-3} vs. ω^2 for IBA/SDS/water of 0.312 mM SDS at 20 °C.....	124
5.53. Graph of r^{-3} vs. ω^2 for IBA/SDS/water of 0.06 mM SDS at 20 °C.....	125
5.54. Graph of r^{-3} vs. ω^2 for IBA/SDS/water of 0.603 mM SDS at 20 °C.....	125

5.55.	A graph of r^3 vs. ω^2 for IBA/SDS/water of 0.603 mM SDS with the fourth and fifth rotational rate increase and third rotational rate decrease at 20 °C.....	126
5.56.	Graph of r^3 vs. ω^2 for IBA/DTAC/water of 5.74 mM DTAC.....	126
5.57.	Graph of r^3 vs. ω^2 for IBA/DTAC/water of 0.610 mM DTAC at 20 °C....	127
5.58.	Graphs of EIT of IBA/surfactant/Water vs. Concentration at 30 °C.....	142
5.59.	Graphs of EIT of IBA/surfactant/Water vs. Concentration at 30 °C.....	143
5.60.	Graphs of EIT of IBA/SDS/Water vs. Concentration at 20 and 30 °C.....	143
5.61.	Graphs of EIT of IBA/DTAC/Water versus Concentration at 20 and 30 °C.....	144
5.62.	Graphs of EIT of IBA/surfactant/Water vs. Change in Rotation Rate at 30 °C.....	144
5.63.	Graphs of EIT of IBA/surfactant/Water vs. Change in Rotation Rate at 20 °C.....	145
6.1.	A drawing of the microfluidic device that we used.....	154
6.2.	Images of the microfluidic device.....	154
6.3.	An image of the microfluidic device in which the IBA-rich phase was in the center and the water-rich phase was in the side channels, and more of the IBA-rich phase was flowing in than the water-rich phase.....	155
6.4.	An image of the microfluidic device in which the IBA-rich phase was in the center and the water-rich phase was in the side channels, and more of the water-rich phase was flowing in than the IBA-rich phase.....	156
6.5.	An image of the microfluidic device in which the water-rich phase was in the center and the IBA-rich phase was in the side channels, and the more of the IBA-rich phase was flowing in than the water-rich phase....	156
6.6.	An image of the microfluidic device in which the water-rich phase was in the center and the IBA-rich phase was in the side channels, and more of the water-rich phase was flowing in than the IBA-rich phase.....	157
6.7.	An image of the partially dissolved PMMA after one day in IBA/water...	158

6.8.	An image of the PC after four days in IBA/water.....	159
6.9.	Microfluidic device with IBA/water at 20 °C.....	159
6.10.	Microfluidic device with different injection flows of IBA/H ₂ O at 23 °C and had 2-mm wide channels.....	160
6.11.	Ethanol being injected into 5-mm PC microfluidic device.....	161
6.12.	The ethanol became fainter or more diffuse as it was continually injected.....	161
6.13.	The syringes being pulled out and both ethanol and water flowed backwards through the central channel.....	162
6.14.	Faint lines of ethanol in a 5-mm PC microfluidic device.....	163
6.15.	Faint lines of ethanol widening in a 5-mm PC microfluidic device.....	163
6.16.	The faint lines of ethanol narrowing in a 5-mm PC microfluidic device...	164
6.17.	Ethanol dissolving in the upper part of the 5-mm PC microfluidic device.....	164
6.18.	PC Microfluidic device with IBA/water in 5-mm wide channel.....	165
6.19.	Another image of a PC microfluidic device with IBA/water in 5-mm wide channel.....	166
6.20.	PC Microfluidic device with IBA/water in 3-mm wide channel.....	166
6.21.	Another image of a PC microfluidic device with IBA/water in 3-mm wide channel.....	167
6.22.	PC Microfluidic device with IBA/water in 2-mm wide channel.....	168
6.23.	PC Microfluidic device with n-butanol/water in 5-mm wide channel.....	169
6.24.	PC Microfluidic device with n-butanol/water in 3-mm wide channel.....	170
6.25.	PC Microfluidic device with n-butanol/water in 2-mm wide channel.....	171
6.26.	Another image of a PC microfluidic device with n-butanol/water in 3-mm wide channel.....	172
6.27.	Underside view of the PDMS microfluidic device.....	176

6.28.	Y-junction of PDMS microfluidic chip and initial break up.....	178
6.29.	Streams start to drift towards one side of channel.....	178
6.30.	Three streams become two streams.....	179
6.31.	Long cylindrical drop breaks up into smaller drops.....	179
6.32.	Initial start of drop break up.....	180
6.33.	Part of IBA stream starts to hit upper, outer channel of water so that the IBA drop breaks off.....	180
6.34.	The IBA drops are completely broken off and become more clearly defined as separate drops.....	181
6.35.	Cylindrical IBA drop of breaks up into smaller drops in PDMS chip.....	181
6.36.	Continuation of cylindrical IBA drop breaking into smaller drops in PDMS chip.....	182

CHAPTER I

INTRODUCTION AND GOALS

Project Goals

The goal of this project was to study 'miscible interfaces,' i.e., concentration gradients between miscible fluids, specifically IBA (isobutyric acid) and water. Pojman *et al.* demonstrated with spinning drop tensiometry that an effective interfacial tension exists and can be measured for isobutyric acid and water, n-butanol and water, and dodecyl acrylate/poly(dodecyl acrylate).¹⁻³

We used spinning drop tensiometry to measure the effective interfacial tension (EIT) for systems near their consolute points. For isobutyric acid and water, we determined if the rotational acceleration affected diffusion by studying the temporal evolution of the drop volume/surface area as a function of rotation rate.

We used spinning drop tensiometry to determine how an anionic and a cationic surfactant each affected the IBA-water system in the immiscible and miscible regimes.

We used microfluidics as a method to study IBA/water and to determine what type of microfluidic device worked best for studying different types of systems such as IBA/water and n-butanol/water. We compared the microfluidic behavior of a system such as IBA/water to the microfluidic behavior of a system we were unable to study because of the mixing of the SDT such as ethanol/water system.

Importance of The Research

Pojman *et al.* proposed that there were three types of miscible systems:¹

1) Miscible in all proportions, like honey-water, dodecyl acrylate-poly(dodecyl acrylate), or ethanol-water. In such systems the width of the transition zone grows with time.

2) Partially miscible but not near a consolute point (LCST or UCST), like n-butanol and water. The transition zone does not become wider nor does the EIT relax with time. The gradient is fixed by the solubility limit. For example, n-butanol can only penetrate into water up to the concentration equal to the solubility.

3) Systems near a consolute point. The concentration gradient remains sharp as the system relaxes to equilibrium. An example of this system is isobutyric acid and water near its UCST (Upper Critical Solution Temperature).

Prior research in the Pojman lab¹⁻³ has considered all three types of systems, but in this dissertation, we focused on the second and third types of miscible systems because we wanted to determine if the behavior shown by IBA/water near its consolute point is unique or if other systems near their consolute point behave similarly to IBA/water. Systems close to a consolute point like IBA/water above its UCST act like a system that is miscible in all proportions. Systems with finite solubility like n-butanol/water can also act like IBA/water near its consolute point because the concentration gradient is limited by the solubility and large persistent concentration gradients can occur.

Because the diffusion coefficient near the consolute point is very small, the rotational acceleration of the SDT may affect the diffusional flux. So, we studied the dissolution of drops of IBA in water at different temperatures above and below the UCST as a function of the rotational acceleration.

Since surfactants generally lower the interfacial tension between immiscible fluids, we wanted to test how surfactants affect the EIT of miscible systems. We used SDT to determine how the IT (interfacial tension) and EIT of the IBA-water system is a function of concentration and type of surfactant (anionic or cationic). We tested different concentrations of surfactant because we can observe how increasing the surfactant concentration, up to the cmc, would affect the interfacial tension.

Microfluidics can allow us to study other systems that we could not use with the SDT such as ethanol/water because the ethanol would dissolve into water when the SDT started spinning. Both methods, SDT and microfluidics, allows us to observe sharp concentration gradients in miscible and partially miscible systems such as IBA/water and n-butanol/water. We wanted to see if we could observe the capillary instability with miscible fluids in a microfluidic device.

CHAPTER II

BACKGROUND AND LITERATURE REVIEW

Interfacial Tension and Effective Interfacial Tension

Van der Waals was one of the first people to explain how intermolecular forces relate to pressure, volume, and temperature. Van der Waals forces play a large part in keeping liquid molecules close together. When an interface forms between two different fluids, molecules near this interface have fewer favorable interactions since they have fewer neighbors with their same energetically favorable interactions, thus generating interfacial tension. To reduce this tension and minimize the number of molecules in these unfavorable interactions, the liquid will minimize its surface area. Energy per area (J/m^2) or force per length (N/m) is used to express interfacial tension:

$$\sigma = \frac{\partial F}{\partial A} \quad (\text{Eq. 1})$$

where

$$F = E - TS \quad (\text{Eq. 2})$$

F is free energy; S is entropy; T is temperature; and E is internal energy or enthalpy.

A model of an interface as an infinitely thin layer where there is a discontinuous transition from one homogeneous phase to another is not strictly correct⁴ because “the one liquid will always be soluble in the other to some degree, however small.”⁵ Yet, since the length of the zone separating most phases is approximately 100 nm or less, an infinitely thin interface is a valid

approximation.⁶ These phase changes occurring over short distances have smooth transitions from one phase to another as shown in Figure 2.1.

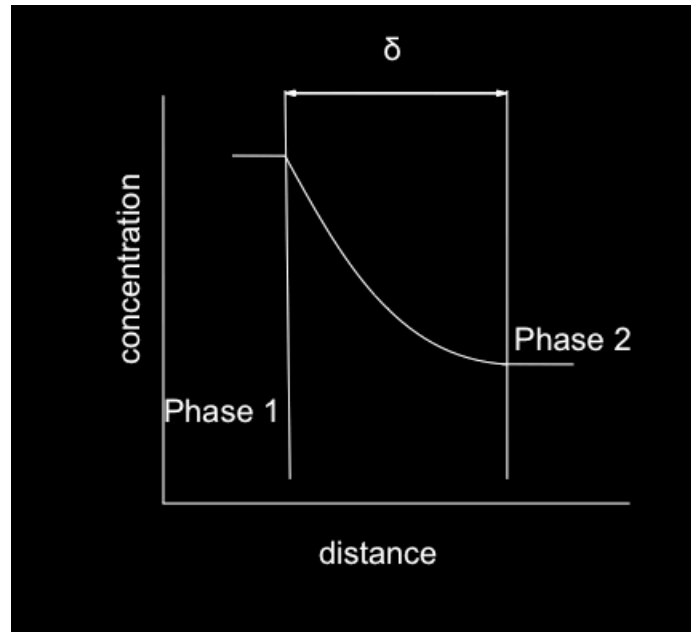


Figure 2.1. Concentration profile of an interface.

Delta in Figure 2.1 represents the width of the interface.

In 1893, Van der Waals proposed that equations of state can predict the width of the interface.⁷ This theory showed that the interface's width increases exponentially as a mixture reaches its critical point, making the interface larger than the distances over which molecular interactions occur.⁸ Cahn and Hilliard used Van der Waals' theory to develop their model.

Joseph and Renardy gave a thorough examination of this topic, interfacial tension and the behavior of a system with miscible fluids, in a review of the fluid dynamics that take place in systems with two miscible fluids.⁹ In 1871, Bosscha

noted the appearance of tension-like behavior in miscible systems. Korteweg, in a 1901 paper, noted Bosscha's results and wrote about the stresses caused by sharp concentration gradients that occur when miscible fluids are in contact with each other.¹⁰ Quinke was the first to attempt to quantify this apparent interfacial tension.¹¹

Smith *et al.* furthered the study of effective interfacial tension (EIT) by using Van der Waals's as well as Cahn's and Hilliard's equilibrium equations to express the free energy caused by the concentration gradient between miscible fluids.¹² Smith, Van den Ven, and Mason's equation was for effective interfacial tension:

$$\sigma = k \int_{-x_0}^{x_0} \left(\frac{\partial c}{\partial x} \right)^2 dx \quad (\text{Eq. 3})$$

where c is a mole fraction; σ is the effective interfacial tension; and $(-x_0, x_0)$ is the interfacial region. A proportionality constant changes Equation 3 to:

$$\sigma = k \int_{-x_0}^{x_0} \left(\frac{\partial c}{\partial x} \right)^2 dx \quad (\text{Eq. 4})$$

where k is a constant defined as the square gradient parameter with units of Newtons. Assuming the concentration gradient is linear, Equation 4 can be reduced to:¹³

$$\sigma = k \frac{\Delta c^2}{\delta} \quad (\text{Eq. 5})$$

where δ is the width of the transition zone.

Zeldovich explained interfacial tension in a different manner using the concept of impossibility of negative surface tension to show surface tension as a

real, positive result and through changing surface areas. Zeldovich assumed that the diffusion process takes place at time t_1 at a constant surface S_1 with the thickness x_1 equal to $(D*t_1)^{0.5}$ where D is the diffusion coefficient so that decreasing of the free energy of the system (F) is proportional to the amount of the mixture (M , which equals $\rho * S_1 * (D*t_1)^{0.5}$ where ρ is density of the liquid).¹⁴ The derived equation is

$$F = F - \alpha * M \quad (\text{Eq. 6})^{14}$$

where α is the positive coefficient. Increasing the surface rapidly will not cause any change in the amount mixture at the moment the surface changes. Instead the layer will stretch so that x_1 will decrease inversely proportional to the surface.

Zeldovich states the increase in M and subsequent decrease in F occurs in the irreversible process of diffusion after the increase in surface and not at the moment of surface increase.¹⁴ For this reason, the decrease in free energy, which is a result as an increase in surface, cannot be transformed into mechanical energy of the walls so that a negative value cannot be considered as negative surface tension or the force applied to the walls in the direction of the increasing surface cannot occur. Thus, Zeldovich states that assuming negative surface tension would result in self-bending and drop breakup of a surface boundary and, in the case of completely miscible fluids, resulting in acceleration of the mixture formation.

Using equation 7,

$$\left. \frac{\partial F}{\partial S} \right|_{x=\text{constant}} = -A_1 * x_0 + \frac{A_2}{x_0} \quad (\text{Eq. 7})^{14}$$

where σ_m is the surface tension of miscible liquids, Zeldovich states that these values for the surface tension present real, positive surface tension at the boundary of two miscible liquids. According to this equation, as surface area (A) decreases, the layer thickens and the gradient and F decrease. This decrease is independent of diffusion and can be transformed into mechanical energy. Thus, σ_m can be measured as a force that acts on part of a device and that can move while surface area is changing and so is not different from common surface tension of the boundary between two immiscible fluids, which is inversely proportional to the layer thickness of the mixture formed at the boundary during the diffusion process. This surface tension decreases with time.

An example of an effective interfacial tension (EIT) is in the system of isobutyric acid (IBA)/water. When IBA/water are below their Upper Critical Temperature (UCST) of 26.3 °C, a water-rich phase and an acid phase exist in equilibrium. As the temperature is raised, diffusion starts to occur because the system is no longer in equilibrium. Once the temperature exceeds the UCST, the two phases start to become one phase. When the interface is gone, an interfacial tension no longer exists.

Isobutyric Acid and Water

Understanding of the phase behavior of IBA and water is important for SDT and microfluidic studies. IBA has a polar carboxylic acid group and a non-polar alkyl group:

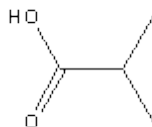


Figure 2.2. Structure of Isobutyric Acid (IBA).

The polar group makes IBA soluble in water while the non-polar iso-butyric group tends to reduce IBA's solubility.

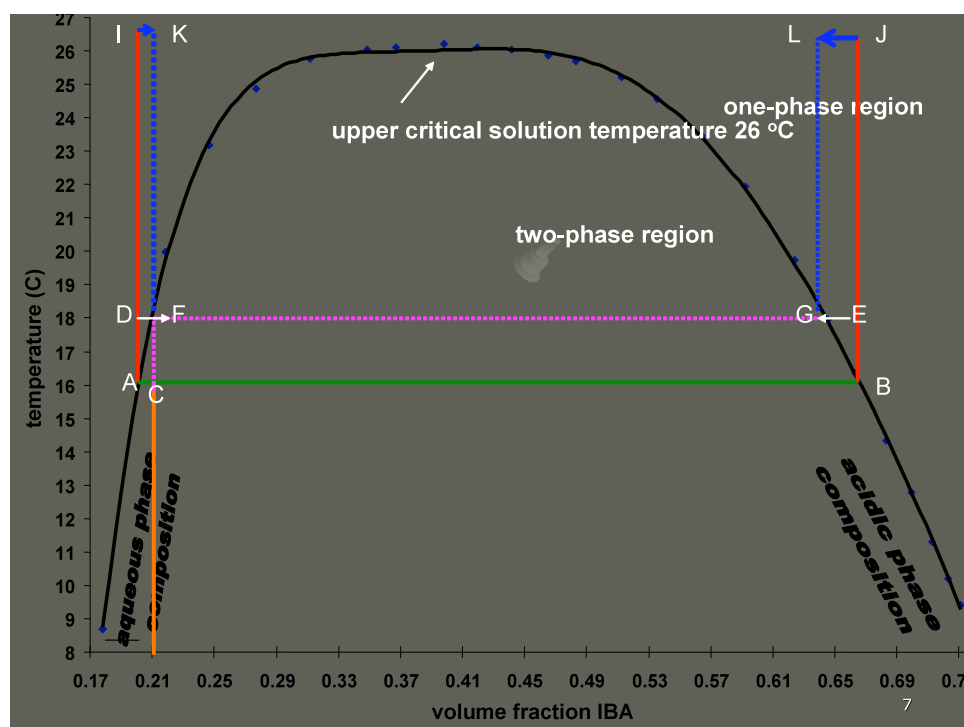


Figure 2.3. Phase diagram of IBA/water.¹² (Image courtesy of C. Whitmore)

This phase diagram can be used to understand how an increase in temperature produces a nonequilibrium situation. If the temperature is suddenly raised from 16 °C to 18 °C, the water-rich and acidic phases will move up the dashed lines from points A and B to points D and E, respectively. Points D and E are in the

one-phase region and, hence, have more free energy than the corresponding points F and G. Since the water-rich and acidic phases are in contact, mass transfer will ensue and bring these phases' compositions to points F and G. The upper critical solution temperature (UCST) for IBA/water system is 26 °C, which means that above 26 °C, one phase exist but below 26 °C two phases exist.

Spinning Drop Tensiometry

Spinning drop tensiometry (SDT) was developed by Bernard Vonnegut in the 1940s.¹⁵ This technique was originally a method to measure interfacial tension between air and water. A modern spinning drop tensiometer is depicted in Figure 2.4.

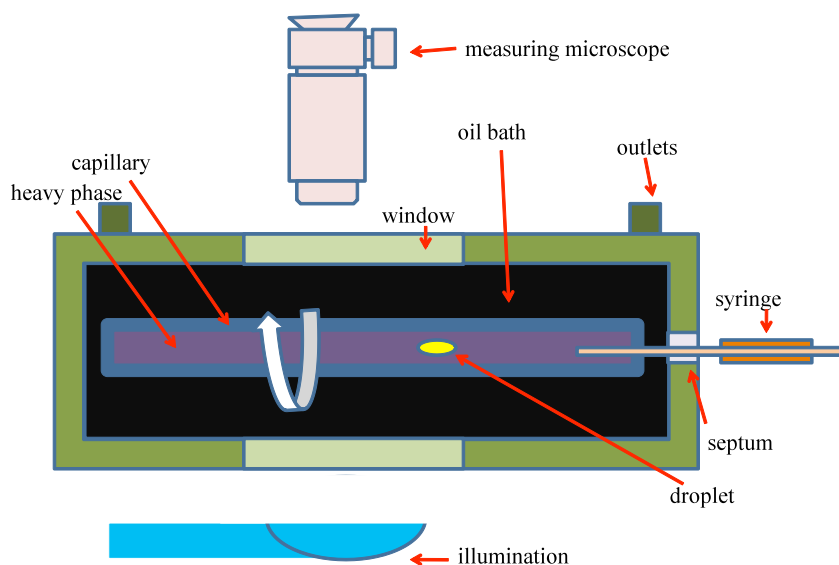


Figure 2.4. Schematic of a Spinning Drop Tensiometer (SDT).

In this technique, a drop of less dense fluid is placed in a cylinder that contains a more dense fluid; this cylinder is then rotated at high velocities, resulting in the less dense drop moving to the central axis of the cylinder. This forced migration causes the drop to elongate and become thinner. The rotational force is countered by interfacial tension, which is trying to minimize the surface area and, so, shortening and fattening the drop. Hence, the more interfacial tension the fatter the drop. By minimizing the total energy with respect to the radius of the drop, interfacial tension can be calculated:

$$\sigma = \frac{\Delta\rho\omega^2 r^3}{4} \quad (\text{Eq. 8})$$

where ω^2 is rate of rotation in radians/s; $\Delta\rho$ is the difference between the densities; and r is the drop radius. This equation assumes that the drop is shaped like a cylinder with hemispherical ends. It can only be applied accurately when the drop's length is at least four times its diameter. If this assumption is not the case, then Princen *et al.*¹⁶ derived another equation based on the same principles but with the drop's length being less than four times its width:

$$\sigma = \frac{\Delta\rho\omega^2}{4C} \quad (\text{Eq. 9})$$

where C is a correction factor based on the drop's half length and half width. Princen *et al.* made a table of these correction factors for these ellipsoidal drops for different values of C . This equation is called the "modified" Vonnegut equation.

Chan *et al.* give a summary of factors that can affect the accuracy of SDT measurements.¹⁷ One of these errors is from reading the drop's radius. Taking

high resolution images of the drop and getting the number of pixels in these drops ensure accurate measurements, but high rotation rates decrease this accuracy by blurring the edges of these drops. This blurriness can be corrected by strobe illumination. Another major source of error comes from buoyancy or gravity effects.^{18, 19} These effects were ignored in Vonnegut's analysis but at low rotation rates, buoyancy can be a problem. To prove that the calculated interfacial tension is not affected by buoyancy, a plot of r^{-3} vs. ω^2 is made, and if the line is straight, then the interfacial tension is independent of the rotation rate. Other problems include secondary flows²⁰ within the capillary, inhomogeneities in temperature control, and the liquid lagging behind the capillary's rotation rate. Secondary flows and inhomogeneities are problems that can be noticed and be considered when describing what occurs in the capillary, but the liquid's lagging is not a problem if the capillary's diameter is small enough.

SDT Research in Pojman Lab

In Figure 2.5, research by Pojman *et al.* done with a miscible monomer-polymer system in a spinning drop tensiometer showed that a drop of a monomer that was miscible with its polymer in the polymer matrix expanded with time.^{21, 22}

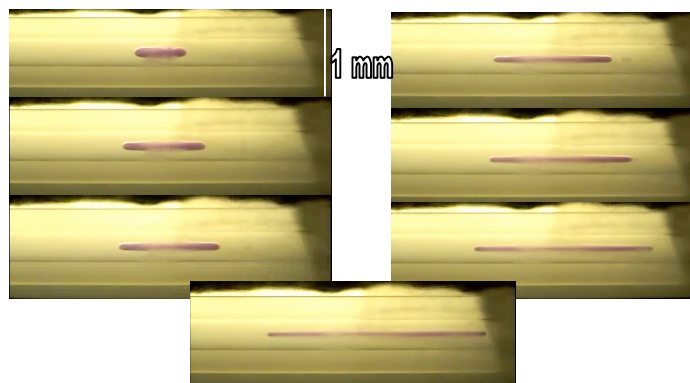


Figure 2.5. Drop expansion in monomer/polymer system over 7 minutes. (Images courtesy of Brian Zoltowski)

In dodecyl acrylate/ poly(dodecyl acrylate) systems, the transition zone was observed to be diffuse as shown in Figure 2.6.

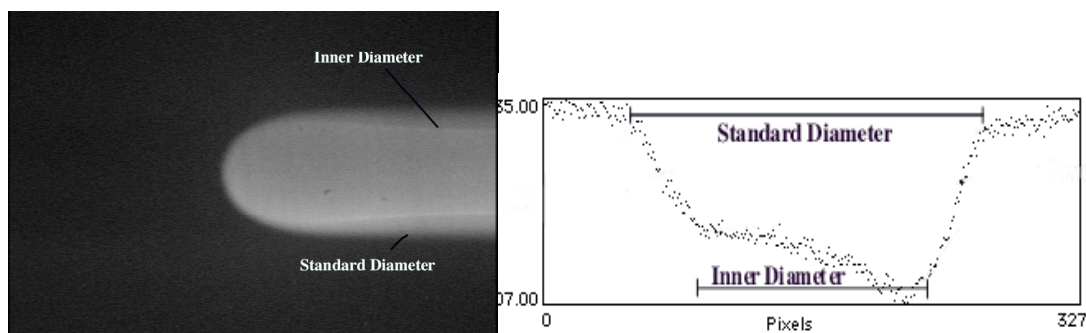


Figure 2.6. An example of a polymer's wide transition zone. (Image courtesy of Brian Zoltowski)

However, another system, IBA/water, had a sharp transition zone and the water-rich phase was “eating” the acidic phase, meaning that the IBA was diffusing faster into the water-rich phase than water was diffusing into the acidic phase. An example of this drop evolution is shown in Figure 2.7.

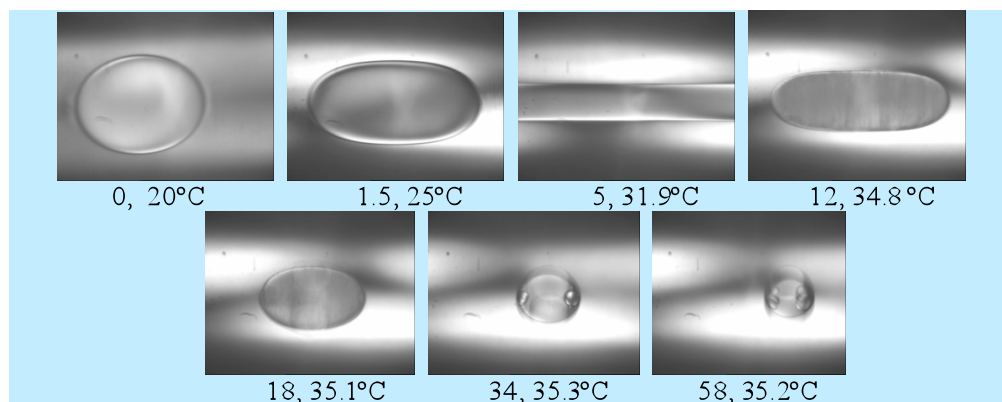


Figure 2.7. An example of a drop evolution for IBA/water. (Image courtesy of C. Whitmore)

Figure 2.7 shows that as the temperature was increased the drop stretched, but once the upper critical solution temperature was passed, the drop volume of IBA began to decrease with time.

Another system that showed similar behavior to the IBA/water system with sharp transition zones was n-butanol and water. The drop evolution of n-butanol and water is shown in Figure 2.8 with the sharpness of the boundary due to the sharp concentration gradient or an artifact.

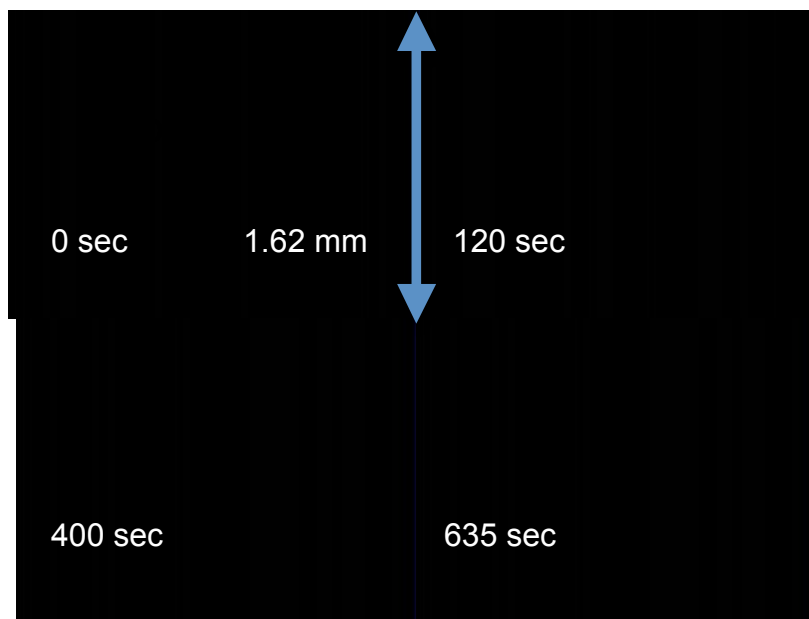


Figure 2.8. Drop evolution of n-butanol in water at 20 °C and $\omega = 8000$ rpm.
(From unpublished lab results.)

Diffusion and Fick's Law

Diffusion is the transport of matter caused by gradients of chemical potential. Diffusion of bromophenol blue, a pH indicator, in water containing agar gel (to prevent convection) is shown in Figure 2.9:

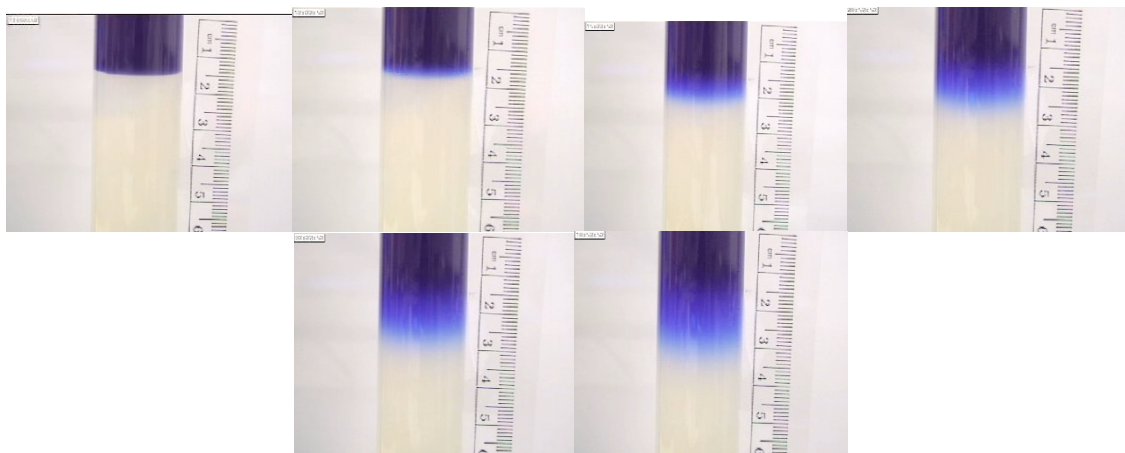


Figure 2.9. Diffusion of bromophenol blue over a period of 24 hours with images taken about every five hours. (Image courtesy of J. Pojman)

In this series of images, the bromophenol blue, which is present as a dilute water-rich solution, is diffusing into agar gel over 24 hours. One can see that the bromophenol blue's color is becoming lighter than its initial dark blue. This lighter blue, or transition zone, shows the diffusion's progress over about 1.5 centimeters.

Diffusion can be represented by Fick's laws. Alfred Fick's first hypothesis defined a one-dimensional flux J_1 as

$$J_1 = A j_1 = -AD \left(\frac{\partial c_1}{\partial x} \right) \quad (\text{Eq. 10})$$

where A is the area across which diffusion occurs; j_1 is the flux per unit area; c_1 is concentration; D is the diffusion coefficient, often with units of cm^2/s ; and x is distance. This equation became Fick's first law. Fick also determined a more general conservation equation:

$$\left(\frac{\partial c_1}{\partial t} \right) = D \left[\left(\frac{\partial^2 c_1}{\partial x^2} \right) + \left(\frac{1}{A} \right) \left(\frac{\partial A}{\partial x} \right) \left(\frac{\partial c_1}{\partial x} \right) \right] \quad (\text{Eq. 11})$$

which became the basis for the one-dimensional unsteady-state diffusion or Fick's second law. When no convection occurs, Equation 12 simplifies to:

$$\frac{\partial c}{\partial t} = D \frac{\partial^2 c}{\partial x^2} \quad (\text{Eq. 12}).$$

Assuming D is a constant, the solution to Equation 13 can be used to illustrate the diffusion for two liquids initially separated at time $t = 0$ and $x = 0$ with concentrations c_1 and c_2 :

$$c(x,t) = \frac{c_1 + c_2}{2} + \frac{c_2 - c_1}{2} \operatorname{erf}\left(\frac{x}{2\sqrt{Dt}}\right) \quad (\text{Eq. 13})$$

where the error function erf is defined as

$$\operatorname{erf}(z) = \frac{2}{\sqrt{\pi}} \int_0^z e^{-t^2} dt. \quad (\text{Eq. 14}).$$

The temporal evolution of a concentration gradient, based on Equations 13 and 14, is illustrated in Figure 2.10.

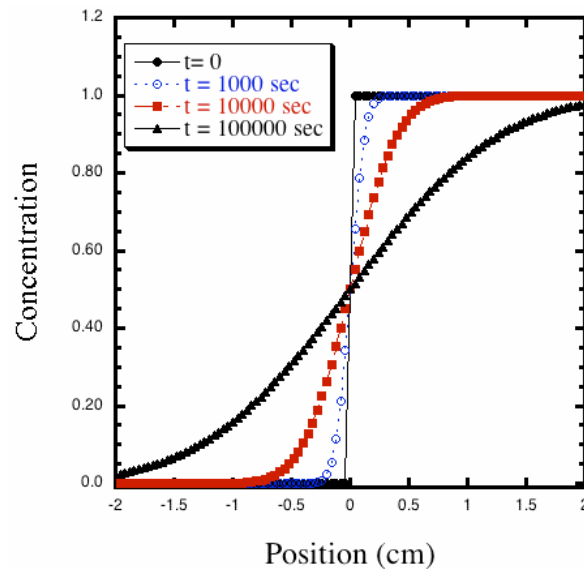


Figure 2.10. Diffusion plot. (Image courtesy of J. Pojman)

Figure 2.10 shows how a concentration gradient relaxes with time. Note that the position of the inflection point of the gradient does not change, indicating that the maximum gradient does not move and so the transition zone does not move but the upper and lower edges of the transition zone move outward symmetrically.

This symmetrical movement indicates a single concentration-independent

diffusion coefficient can accurately be used to calculate the spatial concentration and distribution as a function of time.

Barodiffusion

Barodiffusion is the diffusion effect due to pressure gradients.²³ Landau and Lifshitz define barodiffusion in terms of

$$j = \rho D \left[\nabla C + \frac{k_T}{T} \nabla T + \frac{k_p}{p} \nabla p \right] \quad (\text{Eq. 8})^{23}$$

where k_p is the barodiffusion coefficient. The equation is defined in terms of diffusion flux that corresponds the effect of a pressure gradient and the barodiffusion gradient. In the SDT, liquids are exposed to accelerations much greater than 1 g (acceleration from gravity) so that a drop with a radius of 2 mm with a rotation rate of 14000 rpm will experience an acceleration of 41 g's. Gravity can affect diffusion in binary systems near a critical solution temperature.²⁴⁻²⁹ Using supersaturated binary solutions, Ismailov and Myerson studied concentration gradients that were induced by gravity.^{30, 31} In 2004, Jamshidi-Ghaleh *et al.* stated that barodiffusion could affect the diffusion of sugar in water.³²

Giglio and Vendramini calculated for the first time the magnitude of the steady-state concentration gradient due to gravity using a laser-beam deflection technique.³³ They measured this gradient in a binary mixture near a consolute critical temperature and compared their calculations to values derived by osmotic compressibility data. Due to gravitational forces, large concentration and density gradients are expected to form when a binary liquid mixture approaches a

consulate critical point. Giglio and Vendramini found that even though the temperature change occurred in a matter of minutes, the gravitationally-induced concentration gradient changed over a longer time period.

Hicks *et al.* found that for a system to be in equilibrated, a barodiffusion gradient must exist and studied this concentration gradient with an aniline-cyclohexane system.³⁴ They found that small changes in temperature could cause significant concentration gradient changes in the aniline-cyclohexane system. These changes in the steady-state values occurred even though the authors expected equilibrium behavior when no temperature gradient was applied.

Vailati and Giglio studied barodiffusion and free diffusion in binary liquid mixtures.³⁵ For free diffusion, a comparison of predicted data and experimental results were in good agreement, thus demonstrating that the fluctuations with the equilibrium values increase during the transition from the transient state to the steady state, but in the case of barodiffusion, the fluctuations are smaller than the equilibrium one because the gravitational gradient lowers the equilibrium fluctuations below their thermodynamic values during the early phases of the transient stage. This happens because “the buoyancy actually ‘hides away’ spontaneous fluctuations by drifting them along the gradient until they rest in a density-matching layer.”³⁵

Surfactants

A surfactant is a substance, which is usually in low concentrations, that has the property of adsorbing onto surfaces or interfaces of the system and of altering the interfacial free energies.³⁶ Interfacial free energy is the minimum amount of work required to create that interface.³⁷ Surfactants can be important for emulsions, foams, and dispersions of solids and heterogeneous catalysis, corrosion, detergency, or flotation; surfactants can be used in the making of different products such as soap, lubricating oil additives, or foaming agents for concrete.³⁷

Surfactants have the ability to reduce the interfacial tension of systems by replacing the components of the binary system at the original interface so that the stronger bond between the hydrophobic group of the surfactant and the acid phase and the between the hydrophilic group of the surfactant and water-rich phase occurs.²⁰ These new, stronger interactions should result in reduced tension across the interface in the cmc (critical micelle concentration).³⁷

Research has shown that the interfacial tension of a surfactant-containing solution decreases steadily as the bulk concentration of the surfactant is increased until the concentration reaches a value known as the critical micelle concentration (cmc), above which the tension remains virtually unchanged.³⁷ This point is also very close to the minimum tension that the system can achieve.³⁷

Microfluidics

Microfluidics is the study of miniaturized systems and fluidic manipulation and offers a variety of possibilities from solving biological and chemical system integration problems to studying microfluidic physics.³⁸ Over the past decade, new research has been developed to miniaturize chemical and biochemical analysis and reaction devices, trying to integrate a lab-on-a-chip systems.^{39, 40}

A circular tubing has an outward centrifugal force while a fluid flowing through a contraction or expansion has the force pointing towards the wide end of the channel.¹⁶ In circular tubing with the radius of the curvature being larger than the channel radius of a microfluidic device, centrifugal forces on the fluids drive a secondary flow.¹⁶ Typically, the Reynolds number, which relates the inertial forces to viscous forces, is low in microfluidic devices, resulting in laminar flows, but this number can be forced higher, making turbulent flows.¹⁶ Because of the low Reynolds number and laminar flows in most microfluidic devices, mixing between fluids occurs via diffusion.¹⁶

The rate of mixing can be a problem for some uses of the microfluidic devices because the faster the mixing, the harder the separation.¹⁶ So, controlling the dispersion can be the most important in building a microfluidic device. In a T junction, shown in Figure 2.11, “two fluid streams are brought to flow alongside each other down a channel” with “solute molecules in each stream” diffusing into each other, forming an interdiffusion zone.¹⁶

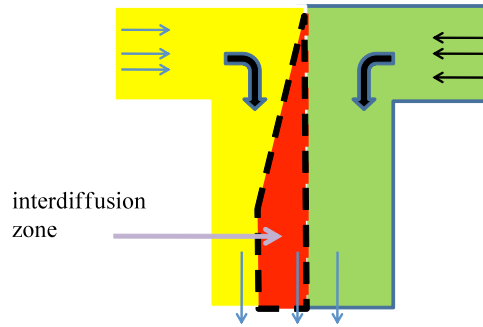


Figure 2.11. An image of a T conjunction in a microfluidic device, a T sensor.

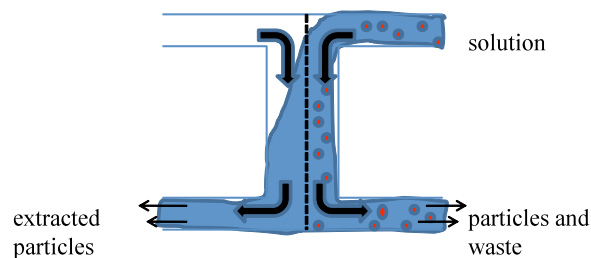


Figure 2.12. An image of an H conjunction in a microfluidic device, an H filter.

In Figures 2.11 and 2.12, the Péclet number, which relates convection to diffusion, is in the intermediate range, in which the “T sensor requires the interface to spread diffusively on appropriate time and length scales,” and the H filter is optimal when the smaller Péclet number is for the extracted component and the larger Péclet number is for the “waste.”¹⁶ In microfluidic devices that utilize large Péclet numbers, the “multiple fluid streams can flow alongside each other over long distances with minimal mixing.”¹⁶ One example of this, shown in Figure 2.13, is a three-electrode system fabricated within existing microchannels.

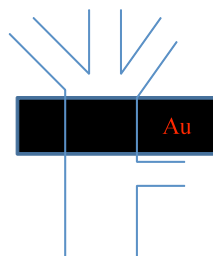


Figure 2.13. An image of a microfluidic device that uses large Péclet numbers.

In the microfluidic device that we built, we wanted to study behavior of miscible systems that were not mixing. So that, a type of microfluidic device similar to Figure 2.13 would work better than either an H conjunction or a J conjunction because this type of device would allow multiple laminar flows.

If two immiscible fluids are placed into the microfluidic device, an interfacial tension between the two fluids affects the dynamics of the free surface.¹⁶ For example, Thorsen *et al.* injected a stream of water into a stream of oil, and the jet of water was destabilized by the Rayleigh-Plateau instability, which is an instability that breaks up a cylinder-shaped fluid into smaller droplets, and small, monodisperse droplets formed.¹⁶ From this research, Thorsen *et al.* showed that microfluidic devices can be used to create controllable droplet emulsions in immiscible fluids.¹⁶ If no interfacial tension existed between the oil and water, then the streams would flow alongside each other but the interfacial tension works to reduce the interfacial area as viscous stress work to extend and drag the interface downstream.¹⁶ The interface is destabilized by these competing stresses, causing droplets to form.¹⁶ Smaller droplets can be formed

through flow focusing of either increasing shear gradients or by drawing the stream into a thin jet that breaks up by the Rayleigh-Plateau instability.¹⁶

One problem with the large surface-to-volume ratios of microfluidic devices are the surface effects, particularly when free fluid surfaces are present.¹⁶ The interfacial tensions can cause bulk liquid movement, meaning that, because of capillary forces, fluids tend to wet microchannels.¹⁶ Previous research showed that fluids that are not continuously flowing through the channels moved to the more highly wetting side and to even travel uphill on a surface with interfacial tension gradient.¹⁶ So, in building our microfluidic device, we must make sure that the neither fluid was overly attracted to or reacted with or destroyed the microchannels.

The interfacial tension of the two fluids depends upon temperature, electrostatic potential, and surfactant concentration; the surface tension gradients can be created by externally inducing a gradient in any of these three properties.¹⁶ The two fluids' behavior may also be affected by gravity because, with two different densities, buoyant forces can drive the more dense fluid downward into the less dense fluid and vice versa.

Sugii *et al.* studied a system of ethanol and water. They used a Y-shaped junction, shown in Figure 2.14, in which ethanol was pumped from one channel and water was pumped into the other channel.

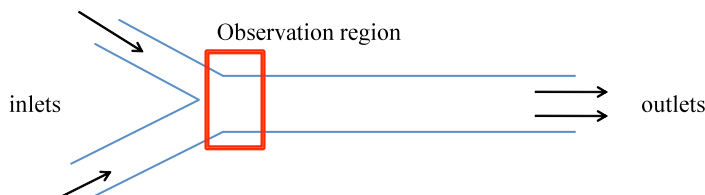


Figure 2.14. An image of a microfluidic device and a close-up of its Y-junction.

Sugii *et al.* observed an imbalance of the shear stress at the interface and believed that imbalance was from a Korteweg stress that existed between the interface of ethanol and water.¹⁸ The Korteweg stress was balanced at the interface of the miscible two-layer flow but was similar to a Marangoni effect, which drives the fluid towards the region of largest interfacial tension.¹⁸ These results are consistent with those predicted in numerical simulations by Bessonov *et al.*⁴¹ This stable interface was created by applying different inlet flow rates of water and ethanol.¹⁸

The Rayleigh-Plateau instability occurs when the cylindrical length of one fluid in another fluid is much greater than $2\pi r$ and is driven by capillary instability, which can be from interfacial tension.⁴² The unconstrained cylinder has a final drop size of $2\pi r$. When the drop breaks up into smaller droplets, the drop loses surface area but retains the same volume. The rate of drop break up is a function of viscosity and interfacial tension. The smaller droplets will also have the same diameter as the original drop.⁴³

The rate of the droplet breakup and fluid shape is influenced by the confinement shape, fluid affinity to one of the walls, and the contact angle of the

two fluids meeting.¹⁹ If either the fluid closest to the wall or the central fluid has a higher affinity for one of the capillary walls, droplet breakup time increases compared to neutral affinity, but if the central fluid has a high affinity for the wall, the rate of droplet breakup decreases.¹⁹ Smaller confinements showed a slower breakup than a larger confinement, but in order to obtain a similar slowing down of drop breakup, the “extent of confinement” needs to be larger for a two parallel plates than for a tube.²⁰ Flexible boundaries that arise from surrounding fluids can also influence drop breakup; in some cases, the flexible boundaries increased stabilities while, in other cases, these boundaries decreased stabilities.¹⁹

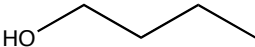
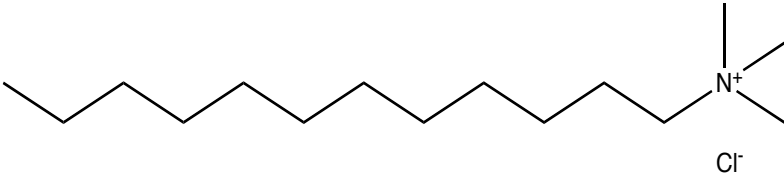
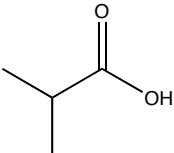
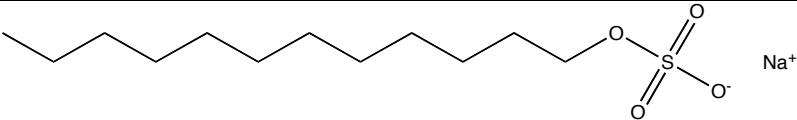
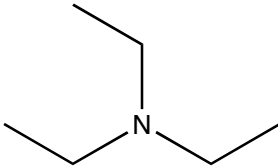
CHAPTER III

EXPERIMENTAL PROCEDURES AND PRELIMINARY ANALYSIS METHOD

All of the reagents used were 99% pure or higher. SDS was recrystallized from alcohol rather than used as-is for some of the surfactant experiments. The rest of the reagents were used as received.

Table 3.1

List of Reagents Used

Structure	Name
 n-Butanol	n-butanol
 Dodecyltrimethylammonium Chloride	Dodecyltrimethylammonium Chloride
 Isobutyric Acid	Isobutyric Acid (IBA)
 Sodium Dodecyl Sulfate	Sodium Dodecyl Sulfate (SDS)
 Triethylamine	Triethylamine (TEA)

SDT

The spinning drop tensiometer was a Krüss SITE100 with drop shape analysis software. Temperature control was provided by a VWR 1166 circulator that flowed oil around the capillary. The oil also functioned as a lubricant for the bearings. Illumination came from two rows of independently operated LEDs, one row on the back, opposite the camera (labeled horizontal) and one row below (labeled vertical). Rotation from 0 to 15000 rpm was controlled by drop shape analysis (DSA-II) software, which also recorded the temperature inside the barrel. A PAL-standard CCD camera, a Toshiba TELI CCD color camera, was used to record the interfacial phenomena occurring in the capillary. The CCD camera was hooked directly to the computer. Movies were recorded with the program Falcon Avi-SoftComp. VirtualDubMod, another computer program, was used to grab selected frames from the recorded movie. ImageJ was used to measure the diameter of the drops.

To perform a calibration, a pre-measured needle was used to insert a drop of either n-butanol or IBA. From the same movie of the behavior of the drop, several images of the pre-measured needle were captured. In this study, the pre-measured needle had a diameter of 457 microns. Using VirtualDubMod, frames of the pre-measured needle were selected. ImageJ was used to measure the width of the pre-measured needle in pixels. If the needle were 65 pixels and the needle 457 microns, then the calibration factor would be 457 microns/65 pixels or $7.03 * 10^{-6}$ m/pixel.

To make a typical Vonnegut interfacial tension measurement, the matrix, via a 20-mL glass syringe, was inserted into the capillary through one of the endcaps, and the syringe injected the matrix until both endcaps and the capillary are filled. The drop was then injected by a 10-uL syringe. Next, the initial rotation speed of the capillary was started and the drop was located by adjusting the position and focus of the camera. The Falcon AVI-SoftComp was then set to record. As the drop's actions were recorded, the rotation was increased in increments, normally by 500 rpm. Each increase/decrease of rotation was recorded along with the time that the rotation was increased/decreased. After the rotation had finished being increased and decreased, the movie was saved and frames from each rotation rate and/or temperature were selected in VirtualDubMod. The drop's diameter from each selected frame was measured in pixels with the program ImageJ. This distance was converted to meters. The measured rotation rate was converted from rpm to radians/sec by multiplying by $2\pi/60$.

The rotational acceleration is calculated from ω^2 times radius of the capillary. The diameter of the capillary is about 3 mm and the rotation range was between 0 to 15000 rpm so that the SDT had an acceleration range of 0 to 94 m/s^2 with the rotation rates of 0 to 15000 rpm:

$$15000 \text{ rpm} \times 15000 \text{ rpm} \times 1.5 \text{ mm} / (60 \text{ seconds} \times 60 \text{ seconds} \times 1000) = 94 \text{ m/s}^2$$

In our range of the small volume of IBA/water, we looked from 15 to 82 m/s^2 for the rotational rates of 6000 rpm to 14000 rpm. The distance and rotation rate

along with other parameters in the Vonnegut equation were used to determine the interfacial tension.

To calculate the interfacial tension from one of the SDT trials: first the diameter of the drop was converted from pixels to meters by multiplying the diameter by a meter/pixel conversion. The meter/pixel conversion was found from measuring the width of the injecting needle (457 μm) in the program ImageJ and then converting the number of pixels that the needle is to meters. Then the rotation rate in rpm was converted to radians/sec by multiplying the rotation rate rpm by $2\pi/60$, and the drop's radius was cubed and the rotation rate was squared. Then, the cubed radius was plotted versus the squared rotation rate. From Vonnegut's formula, the density difference was multiplied by 1000 (in order to make mN/m rather than N/m) and divided by the slope of this graph and four, giving the interfacial tension. The density differences used were: 15.4 kg/m^3 for IBA-water.²

For the systems used in the temperature jumps, 50 mL of water was added to a 100-mL glass jar. Then, for IBA/water or n-butanol/water, 50 mL of either IBA or n-butanol was added to the 100-mL container. The 100-mL jar was shaken 24 hours before each temperature jump and allowed to equilibrate. For the temperature jumps with surfactant, the surfactant was added to the water; the container shaken and mixed until all of the visible surfactant was dissolved. Then the IBA was added and the container shaken again.

For the volume experiments, separate containers of IBA, n-butanol, and water were kept at room temperature and then either heated, cooled, or left at

room temperature (depending on the temperature) for 10 minutes before each volume experiment.

Microfluidics

The microfluidic chips were pre-made by two different groups: the PC (polycarbonate) and PMMA (poly(methyl methacrylate)) chips were made by the Soper lab at Louisiana State University, and the PDMS (polydimethylsiloxane) chips were made by the Kumacheva lab at University of Toronto. Glass capillaries with an outer diameter of 360 micrometers and an inner diameter of 180 micrometers were glued to the microfluidic chips using Gorilla Glue. Glass capillaries were connected to a glass connector that was inserted in a plastic connector, which was attached to a 1-mL plastic syringe.

At the beginning of each experiment, the plastic syringes were filled with the appropriate lighter and heavier phases and then hooked up to the glass and plastic connectors. Then, the connectors were attached to the glass capillaries. The microfluidic devices were placed on the top or to the side of the site 100 spinning drop tensiometer and the spinning drop tensiometer camera (a Toshiba TELI CCD color camera) was used to record the movies of the microfluidic devices. The movie was recorded with the program Falcon Avi-SoftComp. VirtualDubMod was used to grab selected frames from the recorded movie.

Most of the experiments were done at room temperature, but for experiments with increased temperature, the SDT's circulator was heated between 40 °C to 60 °C to increase the surface temperature of the microfluidic

device to 26 °C to 30 °C. An Omega 450 AKT thermocouple reader with a type K wire was used to measure the temperature of the microfluidic chip.

Preliminary Analysis Method of Volume of IBA Drop as Function of Time

A variety of equations were tested on trying to determine which equation best fit the volume and surface area of the observed dissolving drop. The dissolving drop changed from an ellipsoid to a regular spherical shape, which is why the modified Knud-Thomsen equation (shown below in Equation 17) was used. Originally, we were going to use either a prolate or regular Knud-Thomsen equation to measure surface area. We calculated volume and surface area included using initially the prolate surface area but then decided to use the regular Knud-Thomsen ellipsoid formula because of the ellipsoid shape of the drop. Because we were unsure how to plot the initial data from the dissolving drop, we initially plotted rotation rate squared vs. volume squared, volume vs. time, rotation rate vs. time, initial volume of drop vs. time, and initial volume vs. rotation rate. None of these plots were used because they were not linear or did not take into account how volume changed with surface area. So, we then used the modified Knud-Thomsen equation that assumed a change in shape from ellipsoid to spherical.

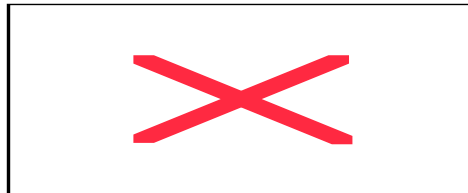
We measured volume several different ways by measuring r squared and l different ways and inputted the data into the prolate formula, original Knud-Thomsen equation for ellipsoid shape, and modified Knud-Thomsen equation. We measured the area of the drop and then multiplying by an assumed one unit

of length to equal volume. A second method used a computer program designed by Chip Fillingane that automatically measured the radius. For a third way, we measured the length and diameter of the drop and then putting these measurements into the prolate formula, a Knud-Thomsen ellipsoid formula, or the modified Knud-Thomsen formula.

Some of the initial work tested used IBA/water at 8000 and 8500 rpm at 25 °C. The volume was calculated using the volume formula for an ellipsoid of

$$V = r^2 \times (l/2) \times (4/3) \times 3.14 \text{ (Eq. 16)}^{44}$$

where V is volume, r is the radius of the drop, and l is the length of the drop. The surface area was calculated using the Knud-Thomsen approximation for spherical surface area:⁴⁴



(Eq. 17)⁴⁴

where a is the length of the drop divided by two, b and c are the radii of the drop (only used one radii, which was the same for b and c), SA is surface area, $p = \ln(2)/\ln(\pi/2)$ and k is ~ 0.0942 .⁴⁴ This formula gave a relative error between -0.204% to +0.187%. This equation was used because, over time, the drops evolved from a prolate ellipsoid to a more spherical shape. The Knud-Thomsen approximation fit the drop evolution best (the shape of the drop changing from ellipsoid to sphere) because the original Knud-Thomsen fit the spherical shape best. An image of a drop with evolving shape is shown in Figure 3.1.

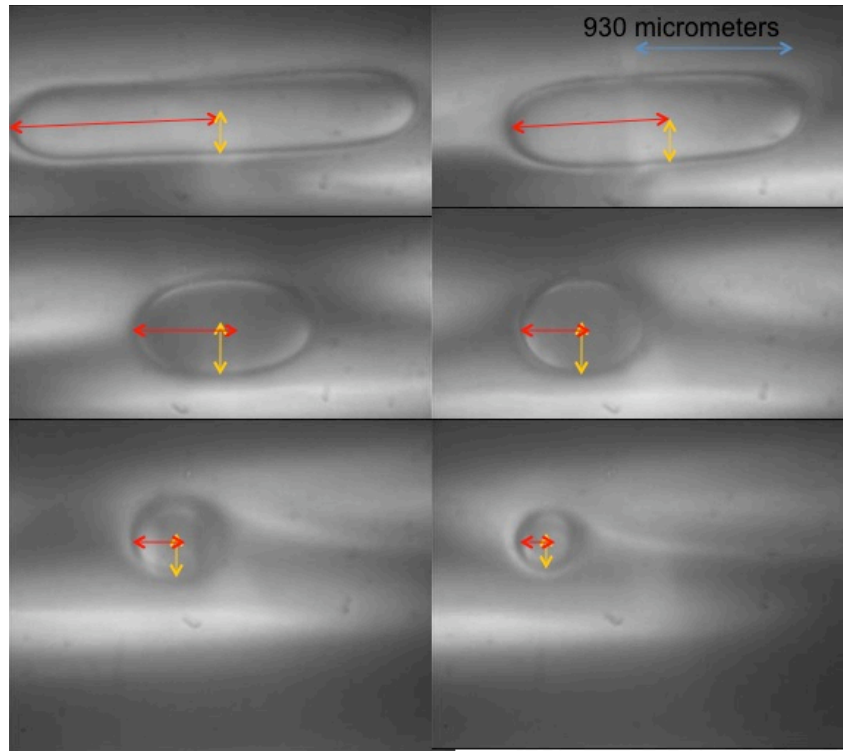


Figure 3.1. Image of Evolving Drop.

Some of the drops are tilted because the camera was tilted. In Figure 3.1, red arrows correspond to a for Equation 17. Yellow/orange arrows correspond to radius b and c , which are the same radii in this dissertation, for Equation 17. The blue arrow corresponds to the scale bar for the image and typically is the length of the drop. The volume/surface area vs. time was plotted to see how the volume evolved over time; volume/surface area vs. time was used rather than volume vs. time because dividing by surface area corrects for changes to surface area at different rotation rates, which would affect the diffusive flux.

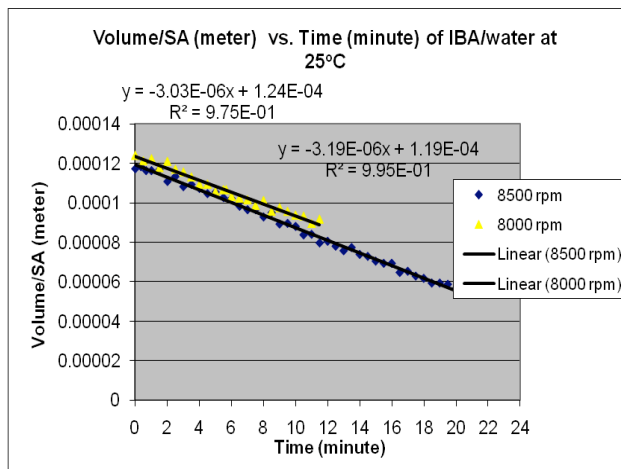


Figure 3.2. A graph of the volume/SA vs. time of the second Knud-Thomsen approximation of IBA/water at 25 °C for 8500 rpm and 8000 rpm.

Figure 3.2 showed a linear decrease for volume/SA vs. time. Because the rate of change for volume/SA vs. time was the same for 8000 rpm and 8500 rpm, barodiffusion had no effect on the rate that IBA dissolves into water over this small range of rotation rates. So, a larger range of rotation rate and temperature range was used.

CHAPTER IV

IBA VOLUME EXPERIMENTS

In the Pojman lab, the original experiment of IBA and water had a long drop of IBA come from the saturated water-rich phase at a low temperature, raised the temperature, and then decreased the rotation rate from a large rotation rate to a much smaller rotation rate.¹ This experiment resulted in the dissolving of the IBA-rich phase into the water-rich phase even though the systems had sharp boundaries. Also, this experiment gave us the idea that this experiment could be easily repeated with the same results at higher rotation rates of 6000-15000 rpm since the rotational acceleration of the SDT could affect the diffusional flux due to the very small diffusion coefficient near the consolute point. This experiment could give us further explanation of how barodiffusion or rotation rate affected the dissolving of an IBA-rich drop into the water-rich phase and still have the boundaries of the system remain sharp. We theorized that barodiffusion was causing this experimental result and predicted that miscible fluids such as IBA and water would exhibit an effective interfacial tension when brought in contact with each other.

To test if barodiffusion caused the sharp boundaries, experiments were performed at 3 different temperatures (20 °C, 25 °C, and 27 °C) at five different rotation rates (6000 rpm, 8000 rpm, 10000 rpm, 12000 rpm, and 14000 rpm). Barodiffusion occurs because of a pressure gradient, and gravity causes a pressure gradient in a liquid. (hydrostatic pressure = $\rho \cdot g \cdot h$) Rotational acceleration can cause a pressure gradient so that barodiffusion could affect the

EIT. The SDT acts like a little centrifuge. These experiments measured the rate of a small volume drop dissolving and required taking the surface area into consideration so that plots of volume/surfaces area vs. time were done. The surface area has to be accounted for because as the rotation rate was increased, the drop increased in surface, which would necessarily increase the rate at which the volume decreased with time. We chose 20 °C, 25 °C, and 27 °C for the temperatures because IBA-water systems have an UCST at 26.3 °C and the temperatures were close to the consolute point. Five different rotation rates were selected because the rotational acceleration of the SDT could affect the diffusional flux due to the very small diffusion coefficient near the consolute point.

Results and Observed Behavior

One of the first set of experiments was with ~10 mL of equilibrated water-rich phase injected at 25 °C. We then decreased the temperature to 20 °C and let the water-rich phase settle for ~20 minutes. At 20 °C, we started the rotation rate at 8000 rpm and increased the temperature to 30 °C. With this set of experiments, we got two different results: (1) a long drop of IBA that end-pinched and then these smaller drops dissolved between 24 °C and 28 °C (the drops dissolved within 30 seconds, generally about 10 seconds once the temperature was 26 °C and above); (2) little or no drops of IBA. When these results occurred, we tried using 28 °C (we tried 28 °C because we thought that the final temperature was too much above the UCST, and the drops were dissolving too quickly before the temperature reached 30 °C) but got the same results as the

previous temperatures. With different rotation rates, we thought that the drops would have a slightly different shape and possibly be more stable. However, when we tried 6000 rpm and 10000 rpm rather than 8000 rpm, we still got little to no drops or a long drop of IBA that end-pinched and then had smaller drops dissolve between 24 and 28 °C.

We also tried building up to the selected rotation rate by starting the initial rotation rate of 0 rpm, 1000 rpm, 2000 rpm, etc. until the selected rotation of 6000 rpm or 8000 rpm because we thought that the gradual increase of rotation rate would slowly pull out more of the IBA and let the smaller IBA drops merge. This method did allow for the smaller IBA drops to merge but the end results were still the same as described above. We also tried letting the drops settle for 30 minutes, 45 minutes, 1 hour, and 2 hours at 20 °C before starting the initial rotation rate, testing whether the system had reached equilibrium. In this set of experiments, we also started the rotation rate at either 6000 rpm or 8000 rpm and then letting the drop rotate at 6000 rpm or 8000 rpm for 20 minutes, 30 minutes, 1 hour, and 2 hours at 20 °C and then increasing the temperature to 28 °C or 30 °C. With this slight change, we thought that the IBA might not have separated long enough and this method would settle the IBA-rich drops more. However, we still got the same results as above.

The next set of experiments we tried injecting ~10 mL of equilibrated water-rich phase and 10-40 µL of equilibrated IBA at 25 °C. We then decreased the temperature to 20 °C and let the water-rich phase equilibrate for ~20 minutes. At 20 °C, we started the rotation rate at 8000 rpm and increased the temperature

to 28 °C. We thought that this procedure would give larger IBA-rich droplets and a lower final temperature would allow us to observe the drop for a longer time. We also thought that we would be able to better control the amount of IBA that formed in a drop since the other method always had a variety of IBA-rich drops despite if all other conditions such as final temperature and time to settle were the same. With these set of experiments, the results were: (1) a long drop of IBA that end-pinched and then these smaller drops dissolved between 24 °C and 28 °C (the drops dissolved within 30 seconds between these two temperatures but generally about 10 seconds once the temperature was 26 °C and above) as seen in Figure 4.1; (2) little or no drops of IBA (generally at 10-20 μL L of IBA) as seen in Figure 4.2; (3) a really long drop of IBA-rich phase that extended beyond the field of view and had smaller IBA-rich droplets form after decreasing the rotation rate and then the smaller drops would dissolve within 30 seconds as seen in Figure 4.3; (4) a really long drop of IBA that was outside the field of view and had smaller IBA-rich droplets form after decreasing the rotation rate and then the smaller drops would re-merge into a larger drop that was extended beyond the field of view, and the middle of the drop became diffuse and dissolved before the two ends of the drop came into the field of view, as seen in Figure 4.4 and 4.5; (5) a really long drop of IBA that was extended outside the field of view, and the middle of the drop became diffuse and dissolved before the two ends of the drop came into the field of view, as seen in Figure 4.6; and (6) a long drop of IBA that had a diameter that was decreasing without end pinching or shrinking as the drop length stretched out.

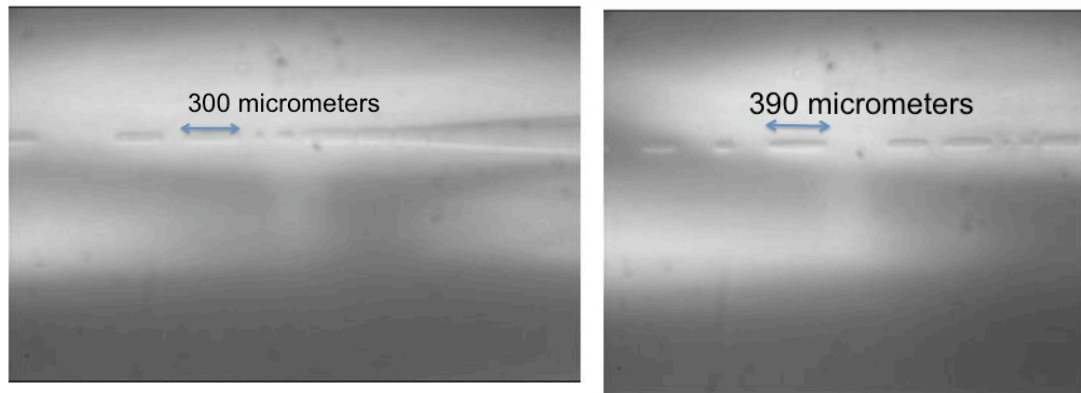


Figure 4.1. A long drop of IBA that started to pinch off at 8000 rpm above UCST.

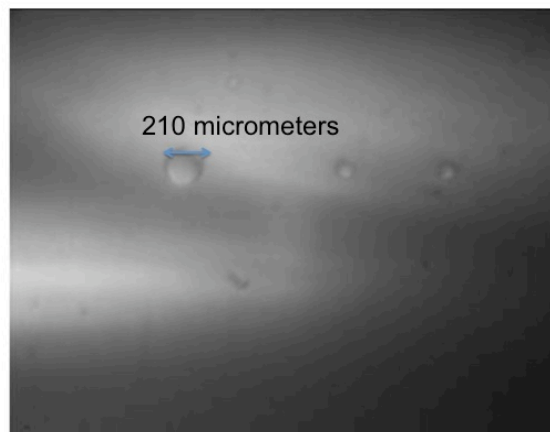


Figure 4.2. Small drops of IBA that would not merge and only lasted 10 seconds or less at 10000 rpm above UCST.

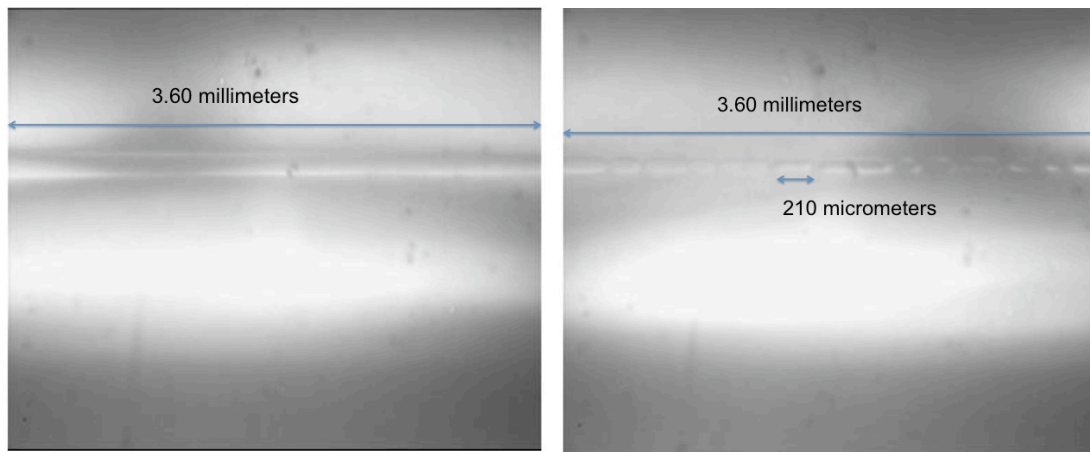


Figure 4.3. A really long drop of IBA that would form into smaller drops after a rotational rate decrease and then start to dissolve at 8000 rpm at 27 °C.

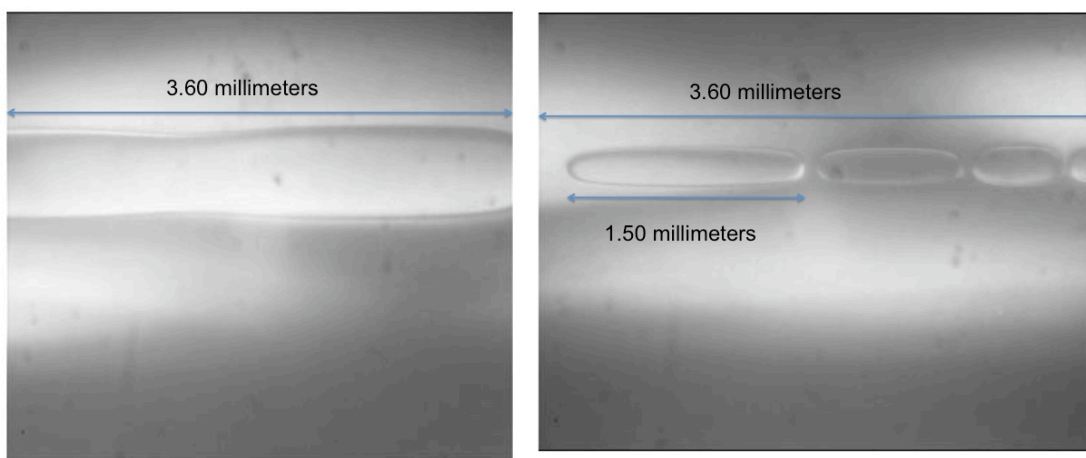


Figure 4.4. A long drop of IBA that had a decreased rotation rate that broke up into smaller drops at 10000 rpm above UCST.

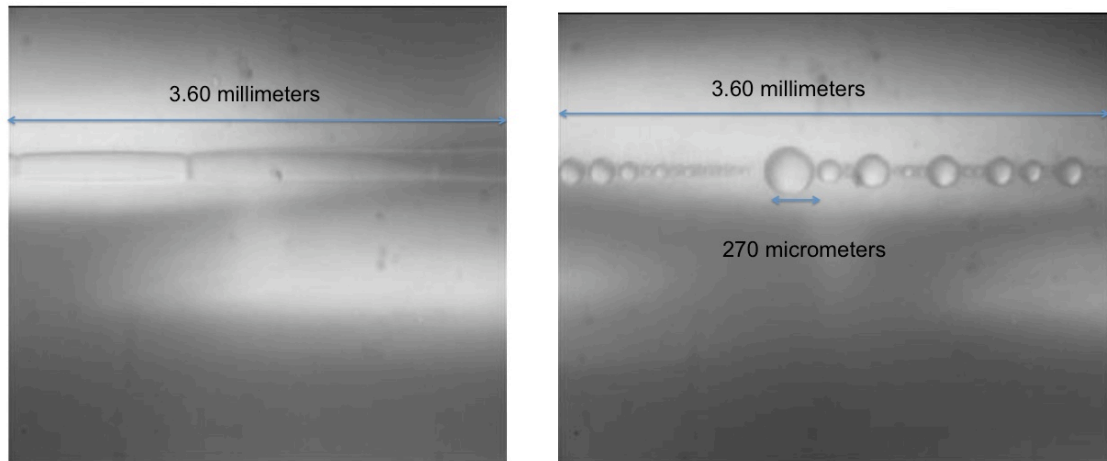


Figure 4.5. A continuation of Figure 4.4 where the smaller drops would start to merge despite the higher or lower rotation being used at 10000 rpm above UCST.

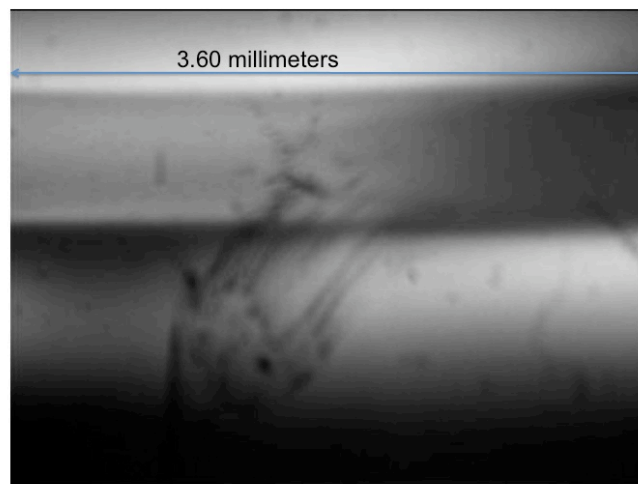


Figure 4.6. A long drop that extended outside the field of view and became diffuse at 8000 rpm at 30 °C.

Though we had some better control of the amount of IBA-rich phase that formed, we still had some variation of the amount of IBA that separated from the water-rich phase even if we used the same settlement time. We used this same set of procedures with 20 minutes, 30 minutes, 1 hour, and 2 hours of settlement

time at 20 °C and starting the initial rotation rate and then letting the drop rotate at 6000 or 8000 rpm for 30 minutes, 1 hour, and 2 hours. We still obtained the same five results listed above. The longer the separation time or the larger amount of equilibrated IBA the longer the IBA drop. We tried a variety of combinations of equilibrated IBA and settlement times but still got a different IBA-rich drop lengths. We also tried a gradual buildup in rotation rate as described in the previous paragraph; the results again had the smaller drops merge but the end results were still the same except for results number two. In comparing this method to the one above, we were able to get more consistent results and some of the drops did last about 5-20 seconds longer but the drops still dissolved within 30 seconds between 26 °C and 28 °C when the temperature was still increasing. In two results, the final temperature was stable at 28 °C, and the drops dissolved for about 10-20 seconds but the dissolving IBA-rich drops would blur in and out so that no clear image of the drops could be seen. In this procedure, we also tried pure IBA and pure water at 8000 rpm and settling for 20 minutes, 1 hour, and 2 hours at 20 °C, rotating at 8000 rpm, and then increasing the temperature to 28 °C. The IBA-rich drops were small enough to be seen but the drops seem to dissolve much quicker than the equilibrated results.

Another set of experiments involved an initial temperature of 25 °C and then raising the temperature to 28 °C or 30 °C. We would inject 20-40 μ L of equilibrated IBA and ~10 mL of equilibrated water at 25 °C, start the rotation at 6000 or 8000 rpm, and then increase the temperature to either 28 °C or 30 °C. With this method, we did have much better control of how much IBA-rich droplets

formed but the results were the same as when the initial temperature was 20 °C: (1) a long drop of IBA that end-pinched and then these smaller drops dissolved between 24 °C and 28 °C (the drops dissolved within 30 seconds, generally about 10 seconds once the temperature was 26 °C and above); (2) little or no drops of IBA (generally at 20 µL of IBA); (3) a really long drop of IBA that extended beyond the field of view and had smaller IBA droplets form after decreasing the rotation rate and then the smaller drops would dissolve within 30 seconds; and (4) a really long drop of IBA that extended beyond the field of view and had smaller IBA droplets form after decreasing the rotation rate and then the smaller drops would re-merge into a larger drop that extended beyond the field of view of the camera, and the middle of the drop became diffuse and dissolved before the two ends of the drop came into camera-view. We also tried this method with pure IBA and pure water and got the same results except the IBA seemed to dissolve more quickly.

In all of the above methods, the jar or jars that contained either the pure IBA, pure water, or mixed solution of IBA-water was shaken and then allowed to equilibrate between 30 minutes to 24 hours, which varied the amount of IBA that formed in droplets) at 25 °C. We tried equilibrating the jars for 24 hours at 20 °C. We then injected about ~10 mL of saturated water-rich phase at 20 °C and let the sample settle for 30 minutes at 20 °C. We then started the rotation at 8000 rpm and let the drops rotate for 30 minutes at 8000 rpm at 20 °C. We did all of these steps in order to make sure that the IBA drops were as separated as possible. We then increased the temperature to 28 °C. We obtained three results from this

set of experiments: (1) a long drop of IBA that end-pinched and then these smaller drops dissolved between 24 °C and 28 °C (the drops dissolved within 30 seconds, generally about 10 seconds once the temperature was 26 °C and above); (2) a very long drop of IBA that extended beyond the field of view and had smaller IBA-rich droplets form after decreasing the rotation rate and then the smaller drops would dissolve within 30 seconds; and (3) a really long drop of IBA that extended beyond the field of view and had smaller IBA-rich droplets form after decreasing the rotation rate and then the smaller drops would re-merge into a larger drop that extended beyond the field of view of the camera, and the middle of the drop became diffuse and dissolved before the two ends of the drop came into camera-view. These IBA-rich drops were the largest of all of the procedures that we tried, but the time it took for them to dissolve was still the same.

The last method that we used was the most successful but not quite in the way that we had hoped. We let the jars of pure IBA, pure water, and mixed solution equilibrate at 20 °C, 25 °C, 27 °C, 28 °C, or 30 °C. We would then add either ~10 mL of the saturated water-rich phase and 30-40 µL of saturated IBA or 10 mL of pure water and 1-120 µL of pure IBA (the amount of pure IBA depended on the temperature and rotation rate: the smaller the rotation rate or smaller temperature had the smaller amount of pure IBA) at one of the above temperatures and start the selected rotation rate between 6000 rpm – 14000 rpm. The equilibrated solution had the drops dissolve slower than the unequilibrated solution. Lower temperatures and lower rotation rates had fatter

(bigger radii across) drops that dissolved slower. Above 27 °C, the drops dissolved too quickly to be seen; the drops would dissolve as they were initially mixed or injected. Another problem was air bubbles in this procedure and the other procedures described in the above paragraphs. A third problem was that, when the drops became 10-30 pixels wide by 10-30 pixels high, the IBA-rich drops would oscillate or change quickly from oval to elliptical to oval, blurring the image.

Development of Method for Analysis

The EIT was calculated using Princen *et al.*⁴⁵ Vonnegut stated that for a long volume drop, the drop is assumed to be a cylinder shape with its length four times (or more) the diameter.³⁷ His formula was a static-based method that stated:

$$\sigma = \frac{\Delta\rho\omega^2 r^3}{4} \quad (\text{Eq. 18})$$

where σ is interfacial tension, $\Delta\rho$ is density difference, ω is rotation rate, and r is radius. For Princen *et al.*,⁴⁵ he modified Vonnegut's formula so that the interfacial tension could be calculated for drops whose length was less than four times the diameter. Princen *et al.*⁴⁵ included a correction factor, C , so that the formula was now:

$$\sigma = \frac{\Delta\rho\omega^2}{4C} \quad (\text{Eq. 19})$$

The correction factor is determined from the ratio of the length to the diameter volume. The correction factor is only good for drops with a ratio of 1:1 to 4:1.

Princen *et al.*⁴⁵ included a table. We graphed this table (Figure 4.7)

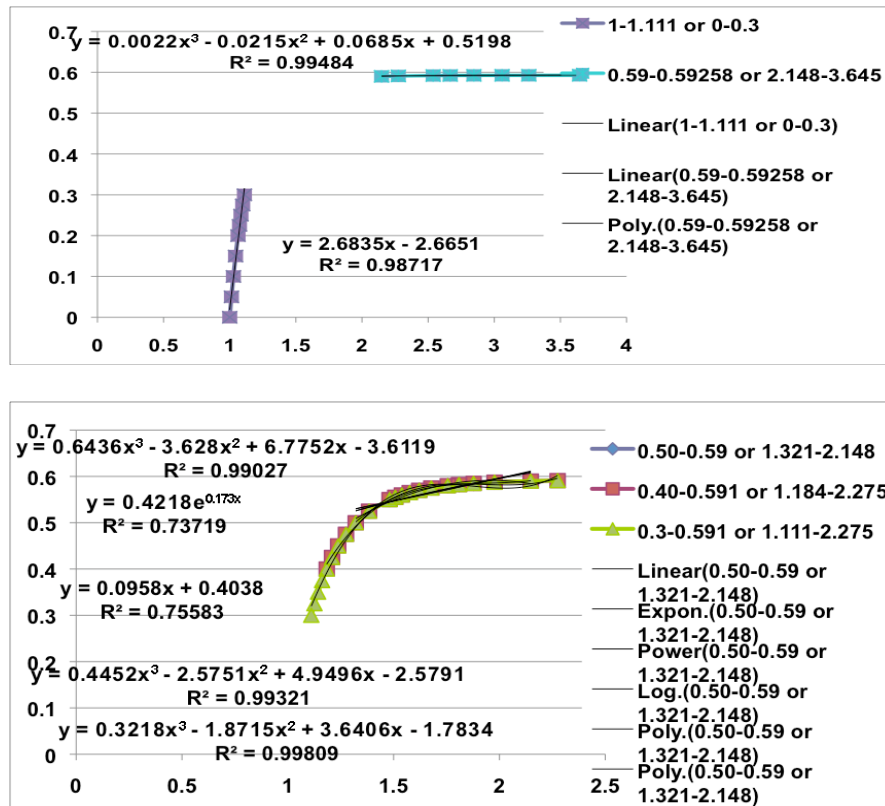


Figure 4.7. Graphs of Princen *et al.*⁴⁵ table of correction factors.

but the table was not a simple linear, polynomial, or exponential graph so that we divided the table into three linear regression lines of

$$0.0022*(BL19^3)-(0.0215*(BL19^2))+(0.0685*BL19)+0.5198 \quad (\text{Eq. 20})$$

$$(0.6436*(BL19^3))-(3.628*(BL19^2))+(6.7752*BL19)-3.6119 \quad (\text{Eq. 21})$$

$$2.6835*(BL19)-2.6651 \quad (\text{Eq. 22})$$

where BL19 is the ratio of length to the diameter.

Equations 20, 21, and 22 were for ratios of, respectively, 2.148-3.645, 1.111-2.275, and 1.000-1.111. Each of the equations had a R^2 of 0.95 or better. For example, from 8000 rpm and 25 °C, the ratio of length to diameter was 1.173 so that, for Princen *et al.*'s table, the correction factor would have been between 0.375 and 0.4 for the length to diameter ratios, respectively of 1.162 and 1.184. From equation 26, the corrected value would have been 0.383. For drops whose ratio was between 3.65 and 4, the correction factor of 16/27 was used. For all of the drops with ratios between 1:1 and 4:1, the Princen *et al.* formula was used, but for the few drops whose length was four times the diameter (only for the first few seconds), the original Vonnegut formula was used.

For the short volume, we graphed the table into three parts. Anything above the 3.640 ratio, required the Vonnegut formula. Ratios of 2.148-3.645 used the equation:

$$0.0022*(BL19^3)-(0.0215*(BL19^2))+(0.0685*BL19)+0.5198 \quad (\text{Eq. 23})$$

where BL19 is the ratio of x/y from the Corrections Table⁴⁵ in the Princen *et al.* paper. The equation yielded the “corrected multiple” used that was multiplied in Princen's formula. For example, BL19 from 8000 rpm IBA water 25 C was 2.65 and this equation gave a corrected multiple of 0.591 so that the EIT was calculated to be:

$(837.76^2) * 1000 * 52.8 * 0.25 * (K19^3)$ (the radius)*BR19 (corrected multiple) =
0.0606 mN/m

Ratios of 1.111-2.275 used the equation:

$$(0.6436 * (BL19^3)) - (3.628 * (BL19^2)) + (6.7752 * BL19) - 3.6119 \quad (\text{Eq. 24})$$

Ratios of 1-1.111 used the equation:

$$2.6835 * (BL19) - 2.6651 \quad (\text{Eq. 25})$$

Ratios of less than one could not be used according to the Corrections Table from the paper by Princen *et al.*⁴⁵

We color-coordinated each of ratios and then went back and applied the appropriate formula to calculate either the “corrected multiple” or EIT.

For ratios larger than 3.645, the regular formula of

$$(\text{rotation rate})^2 * 1000 * (\text{density difference}) * (\text{radius})^3 * 0.25 \quad (\text{Eq. 26})$$

was used to calculate EIT (multiples in shades of blue).

For ratios between 1-3.645, the formula from the paper by Princen *et al.*

$$(\text{rotation rate})^2 * 1000 * (\text{density difference}) * (\text{radius})^3 * 0.25 * (\text{“corrected multiple”})$$

$$(\text{Eq. 27})$$

was used to calculate EIT (shades of green represent ratios of 2.148-3.645, shades of white represent the majority of the calculated small volumes and ratios of 1.111-2.275, shades of yellow represent the ratios between 1.000-1.111). For

ratios below 1, shades of red or brown represented nonusable EIT. Shades of black were used to represent unused calculated EITs of small volumes.

Each of the three formulas used to calculate the “corrected multiples” had R^2 of 0.9948 for green, 0.9903 for white, and 0.9872 for yellow. There was a better correlation for white if the formula of

$$y = 0.3218x^3 - 1.8715x^2 + 3.6406x - 1.7834 \quad (\text{Eq. 28})$$

with a $R^2 = 0.9981$ was used, but this graph had a smaller number of points and we were trying to get as many points as possible while having a R^2 value of 0.99 or better. For the ratios that fell between 2.148-2.275, we would use the green or white formula, depending on whether there were more green or more white shaded cells/points surrounding that particular point.

Analysis

Experiments were done with pure IBA/water at 5 different rotation rates (6000, 8000, 10000, 12000, and 14000 rpm) at 3 different temperatures (20 °C, 25 °C, 27 °C). Figures 4.8-4.12 show drops of IBA/water at 6000, 8000, 10000, 12000, and 14000 rpm at 20 °C, 25 °C, and 27 °C. In these figures, except in cases noted above (two drops merged, etc.), the drops became smaller in length and thinner in radii as the temperature and rotation rate increased. One thing that happened to all of the drops was a more diffuse boundary as the temperature was increased.

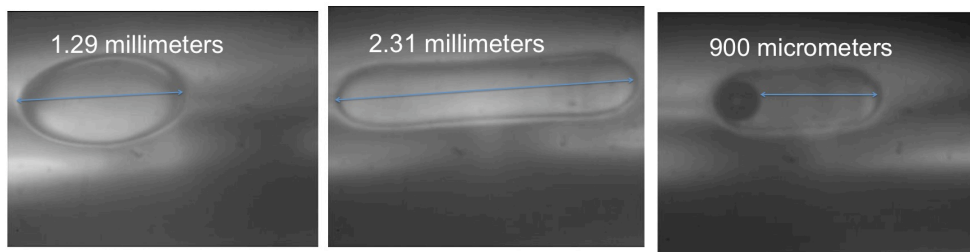


Figure 4.8. Image of IBA/water drop at 6000 rpm 20 °C (left), 25 °C (center), and 27 °C (right).

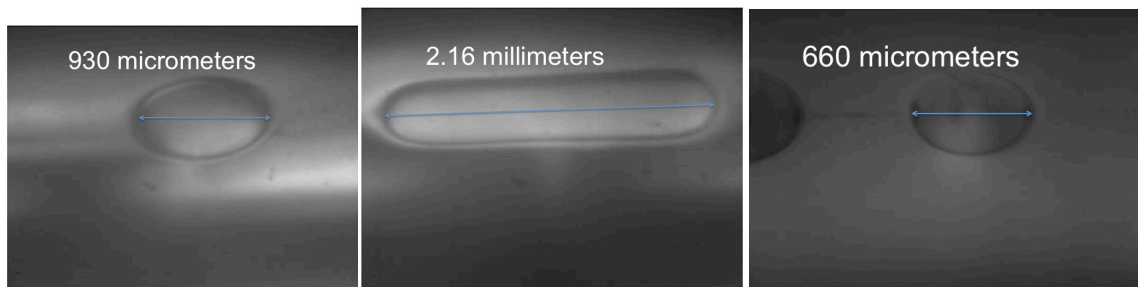


Figure 4.9. Image of IBA/water drop at 8000 rpm 20 °C (left), 25 °C (center), and 27 °C (right); images are tilted because the camera was out of position.

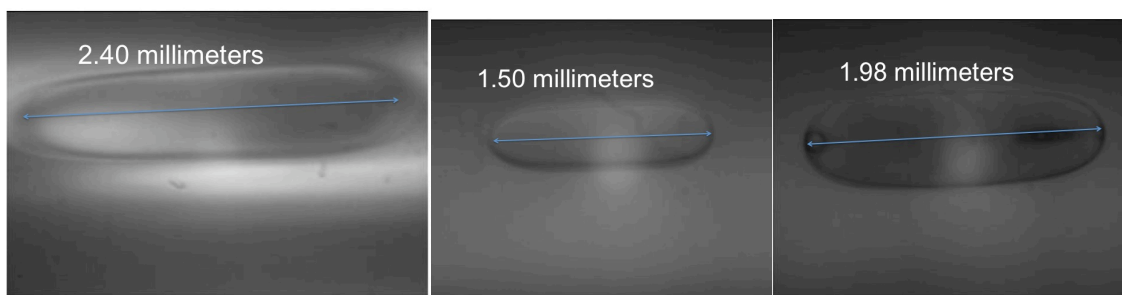


Figure 4.10. Image of IBA/water drop at 10000 rpm 20 °C (left), 25 °C (center), and 27 °C (right); images are tilted because the camera was out of position.

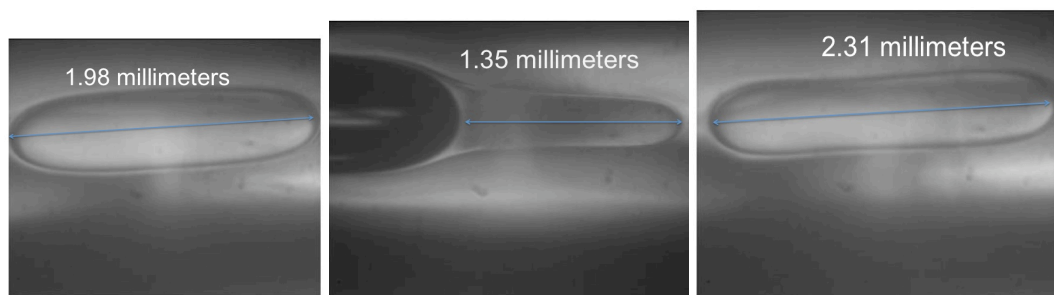


Figure 4.11. Images of IBA/water drop at 12000 rpm 20 °C (left), 25 °C (center), and 27 °C (right); images are tilted because the camera was out of position.

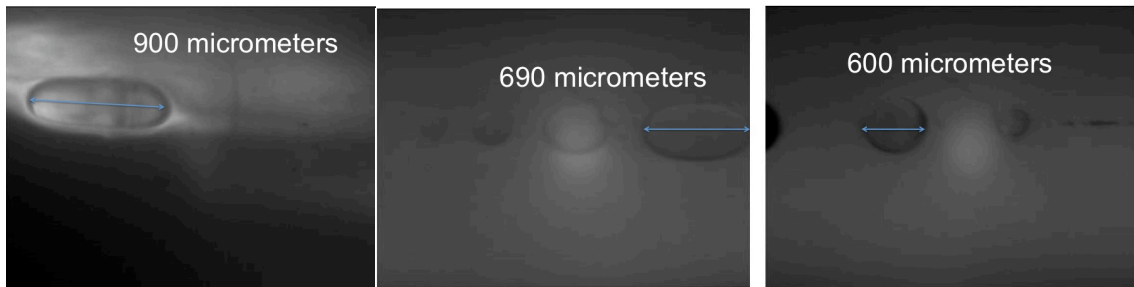


Figure 4.12. Images of IBA/water drop at 14000 rpm 20 °C (left), 25 °C (center), and 27 °C (right).

Figures 4.13-4.17 show the graphs of IBA/water at 20 °C and rotation rates between 6000-14000 rpm. Figures 4.18-4.23 show the graphs of IBA/water at 25 °C and rotation rates between 6000-14000 rpm. Figures 4.24-4.28 show the graphs of IBA/water at 27 °C and rotation rates between 6000-14000 rpm. All of the graphs show a linear regression line for each drop for the volume/surface area versus time.

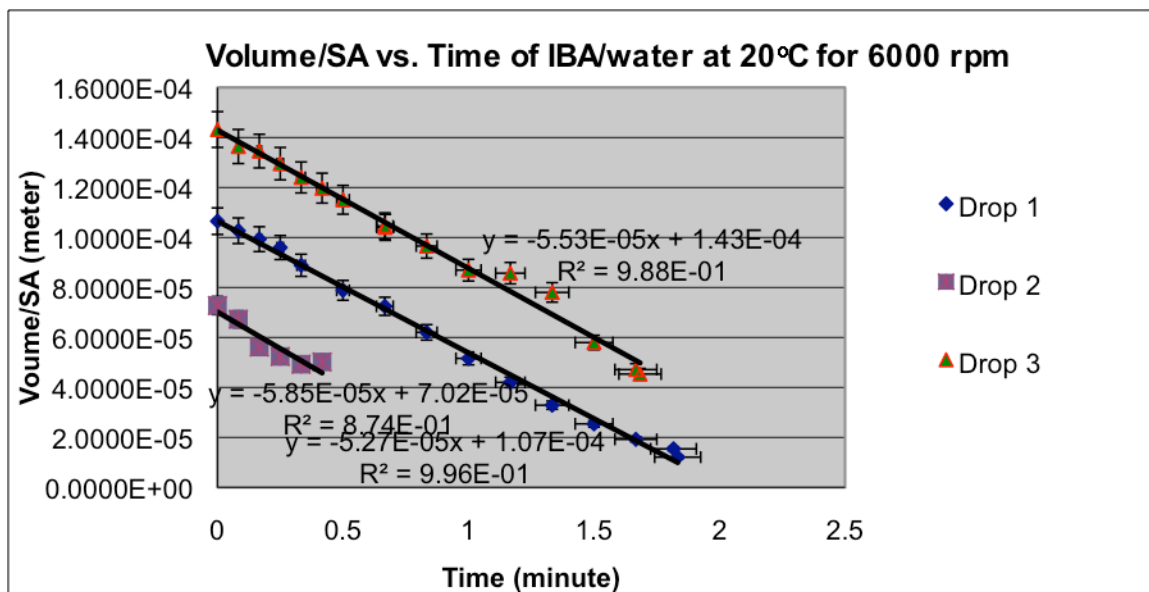


Figure 4.13. Graph of Volume/SA vs. Time of IBA/water at 20 °C for 6000 rpm.

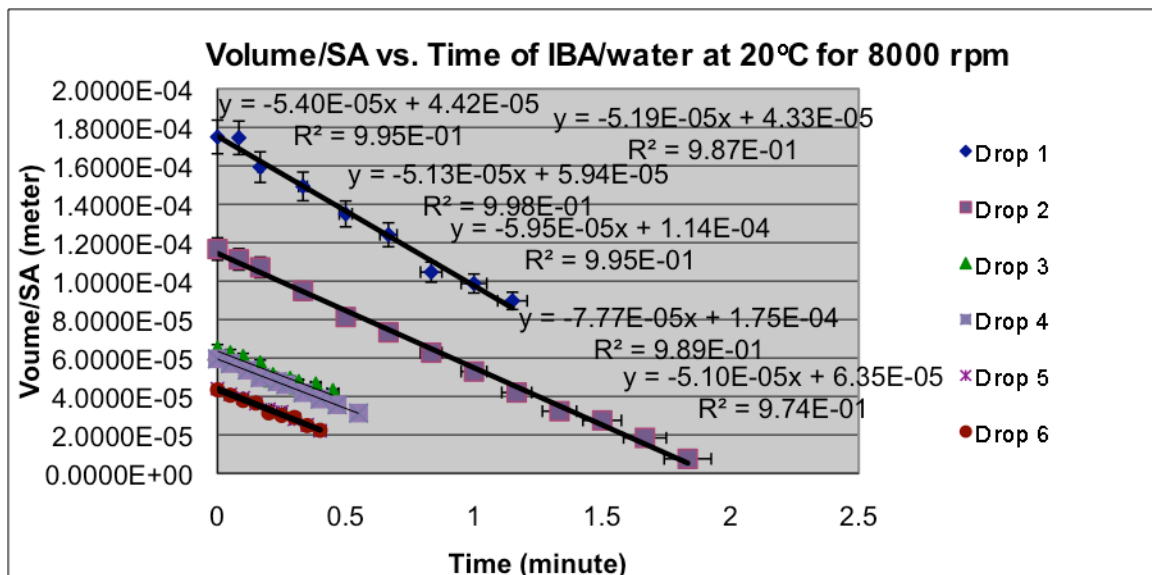


Figure 4.14. Graph of Volume/SA vs. Time of IBA/water at 20 °C for 8000 rpm.

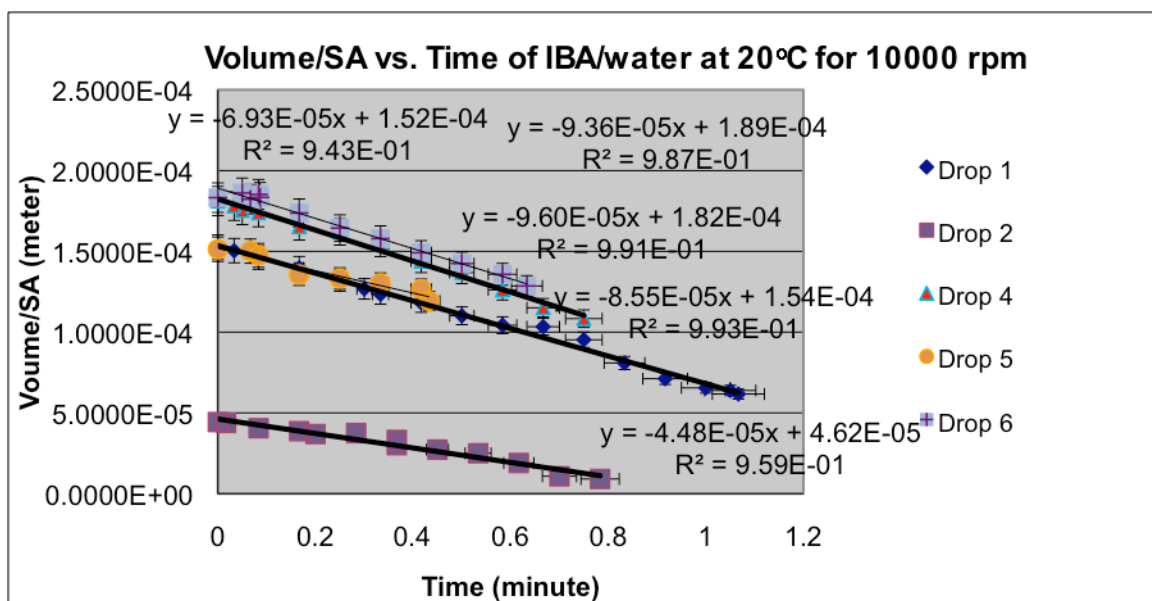


Figure 4.15. Graphs of Volume/SA vs. Time of IBA/water at 20 °C for 10000 rpm.

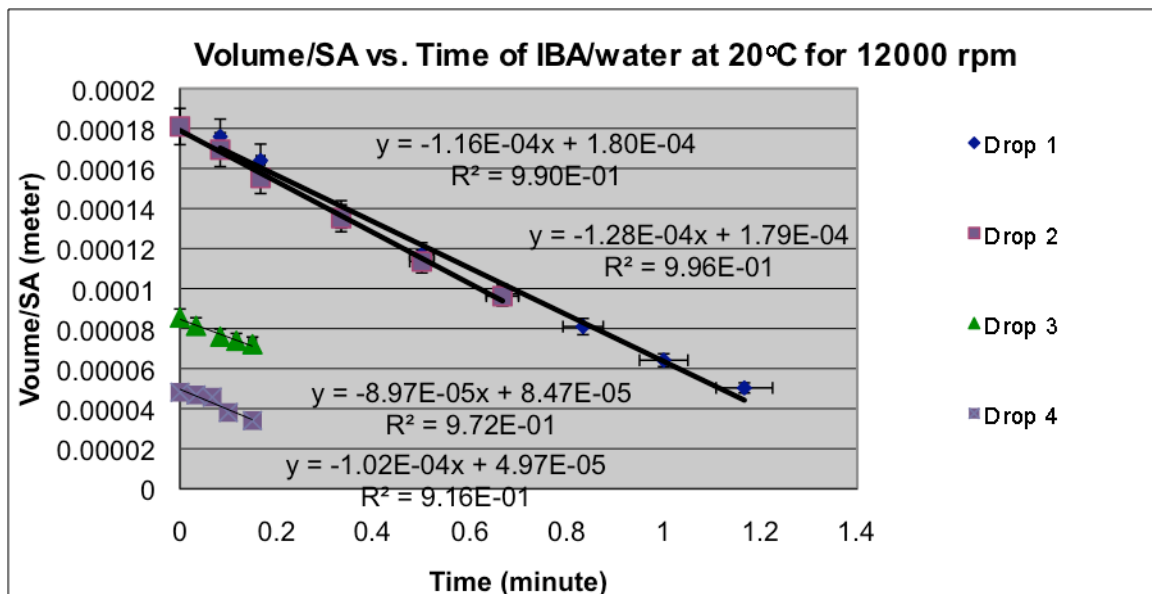


Figure 4.16. Graphs of Volume/SA vs. Time of IBA/water at 20 °C for 12000 rpm.

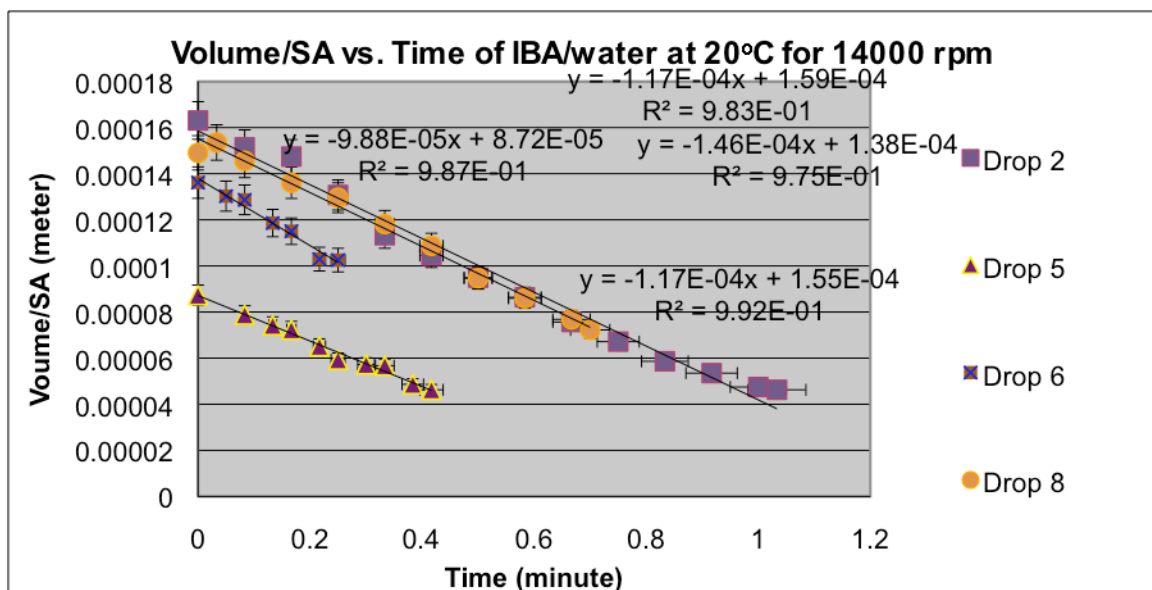


Figure 4.17. Graphs of Volume/SA vs. Time of IBA/water at 20 °C for 14000 rpm.

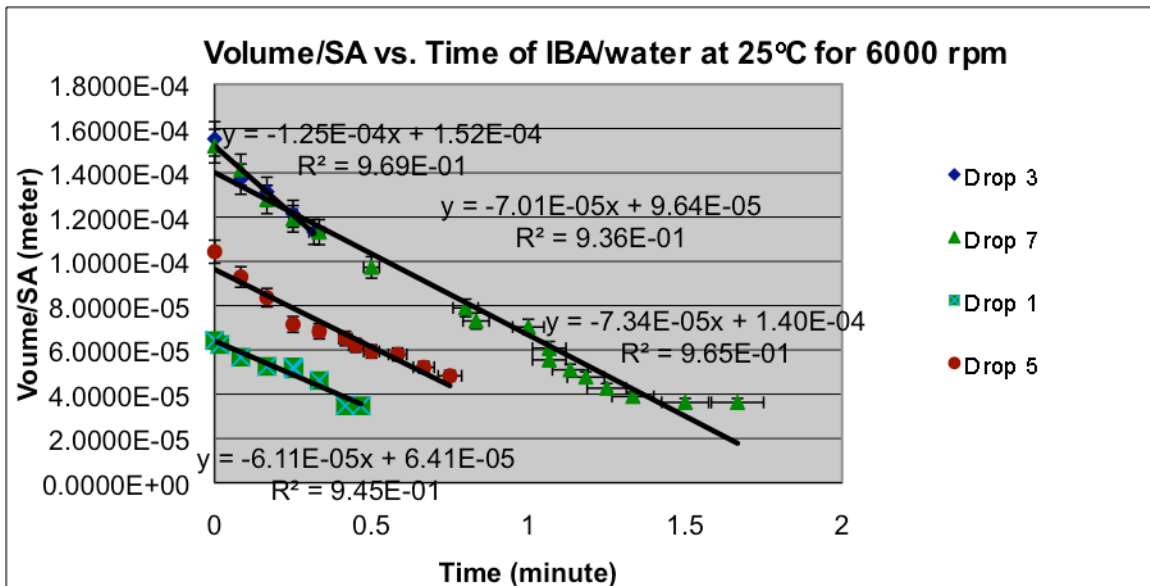


Figure 4.18. Graphs of Volume/SA vs. Time of IBA/water at 25 °C for 6000 rpm.

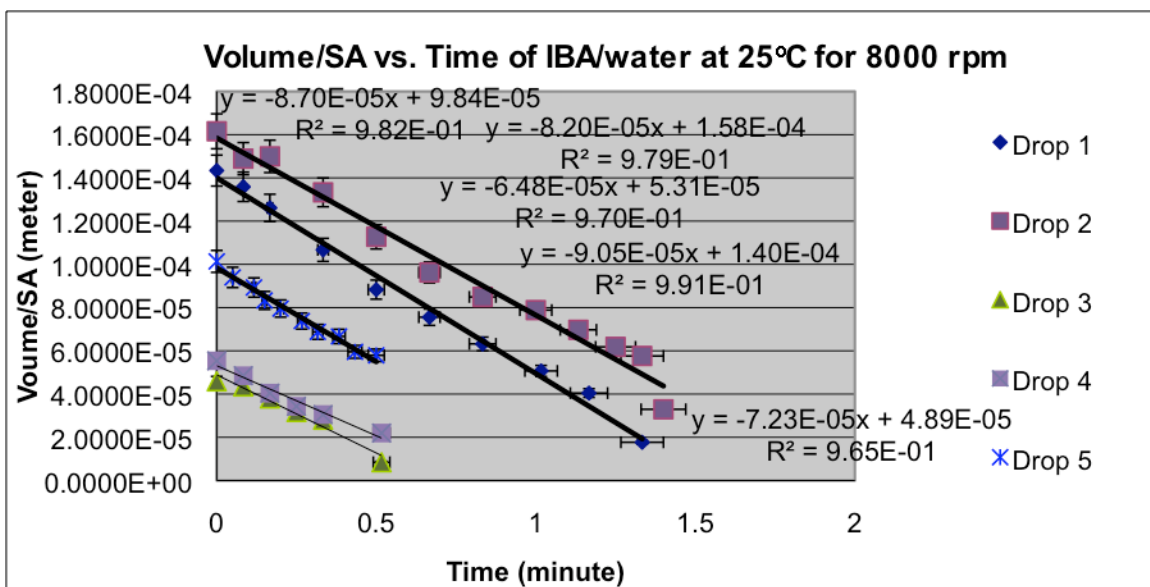


Figure 4.19. Graphs of Volume/SA vs. Time of IBA/water at 25 °C for 8000 rpm.

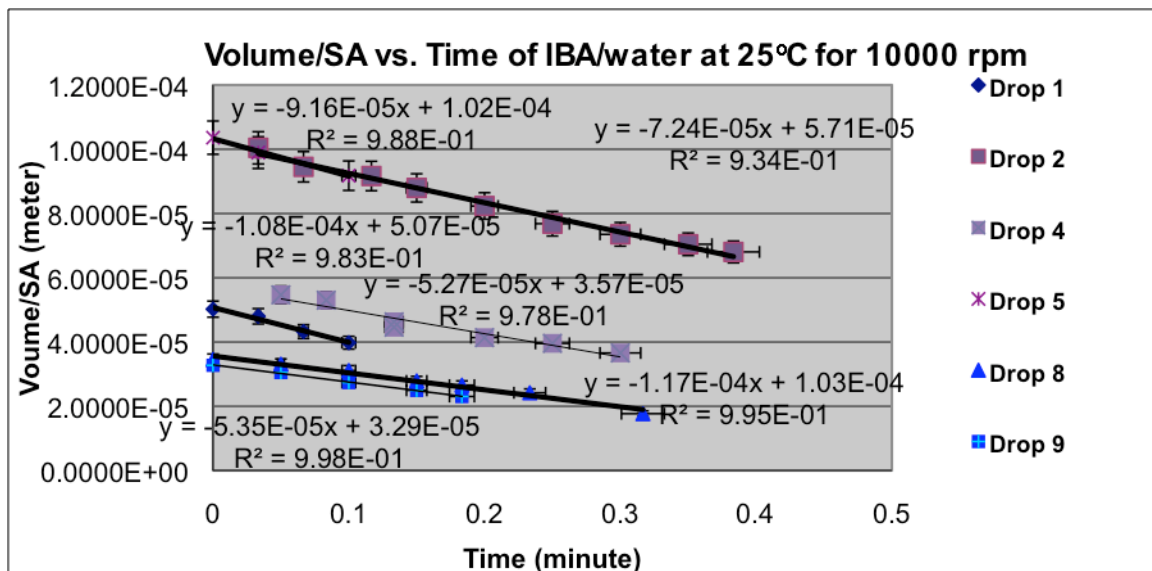


Figure 4.20. Graphs of Volume/SA vs. Time of IBA/water at 25 °C for 10000 rpm.

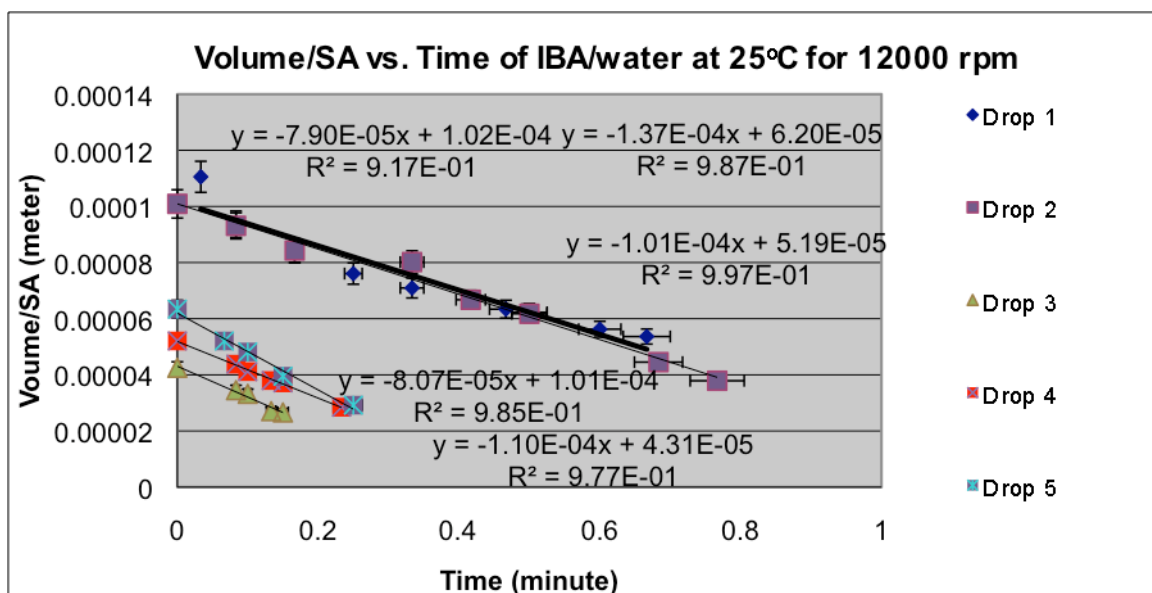


Figure 4.21. Graphs of Volume/SA vs. Time of IBA/water at 25 °C for 12000 rpm.

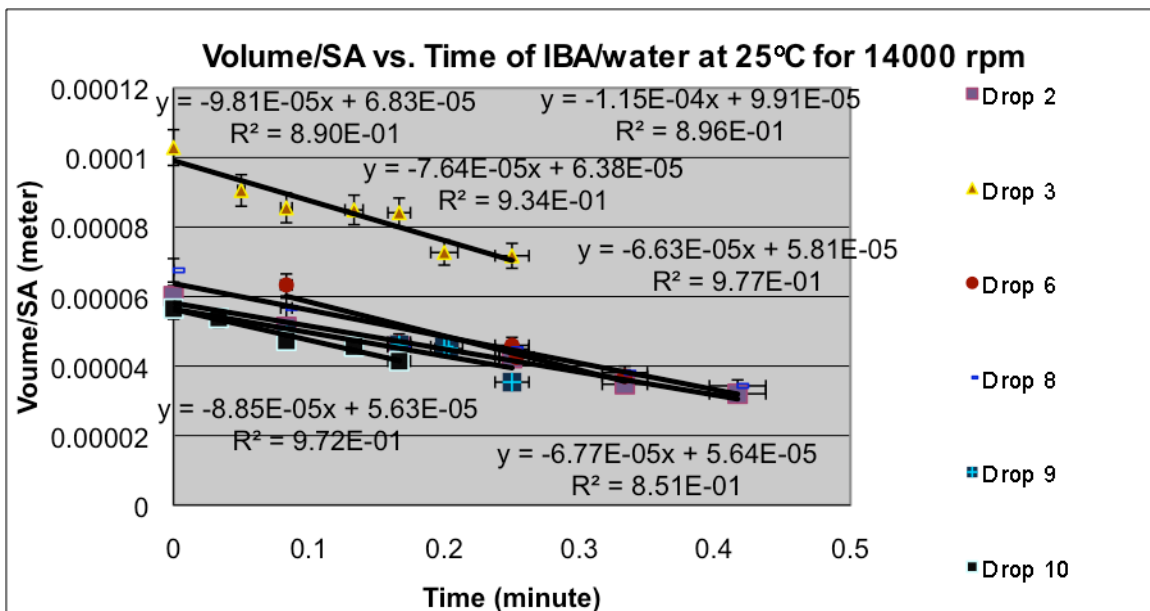


Figure 4.22. Graphs of Volume/SA vs. Time of IBA/water at 25 °C for 14000 rpm.

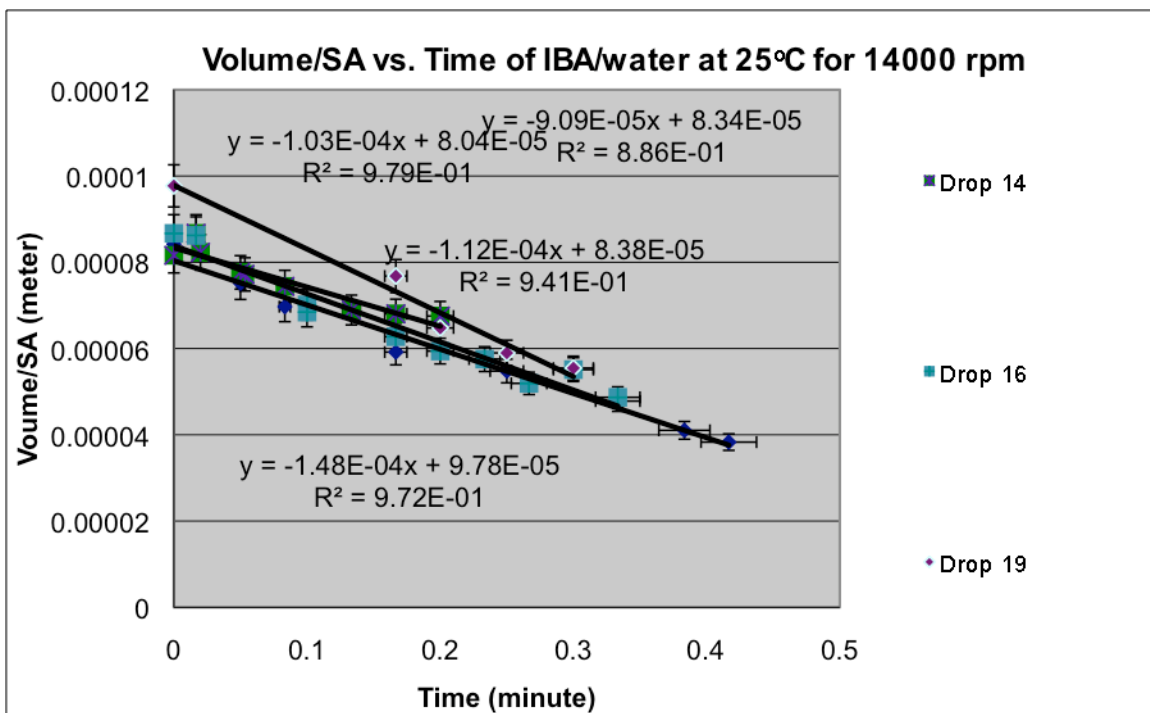


Figure 4.23. Graph 2 of Volume/SA vs. Time of IBA/water at 25 °C for 14000 rpm.

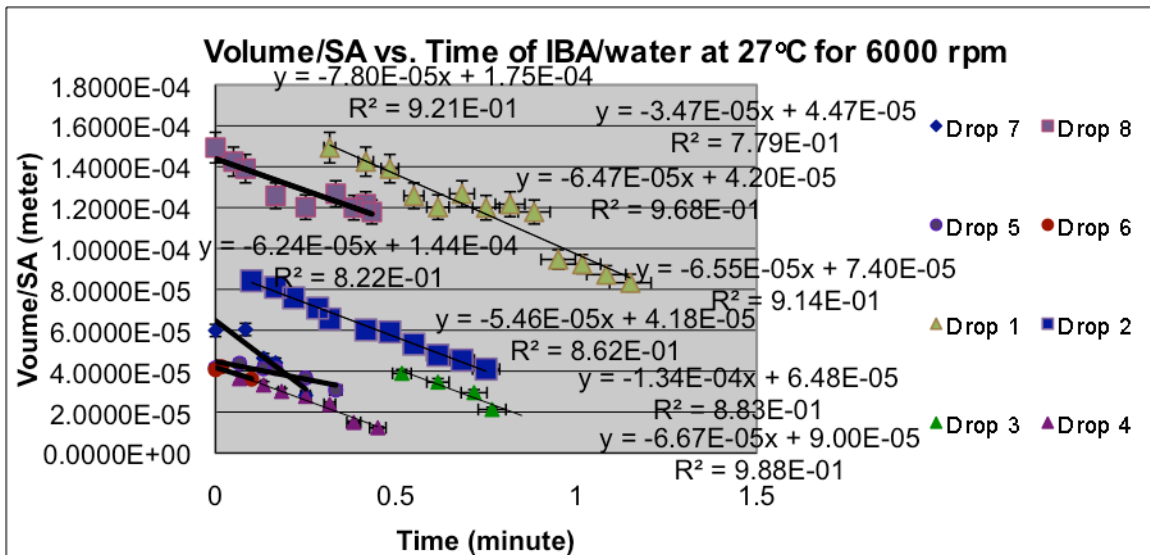


Figure 4.24. Graph of Volume/SA vs. Time of IBA/water at 27 °C for 6000 rpm.

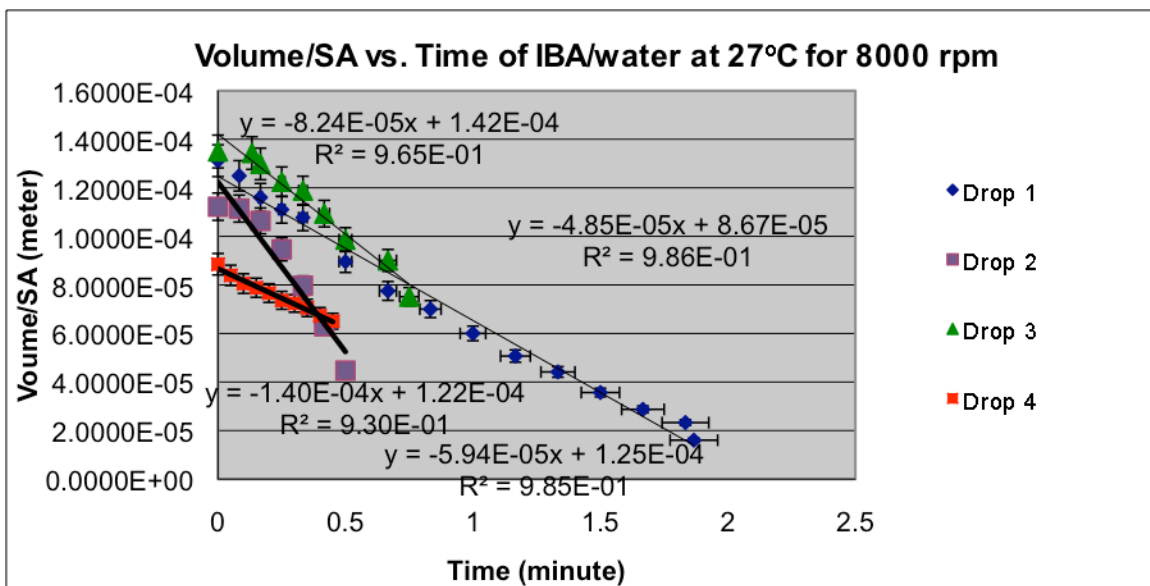


Figure 4.25. Graphs of Volume/SA vs. Time of IBA/water at 27 °C for 8000 rpm.

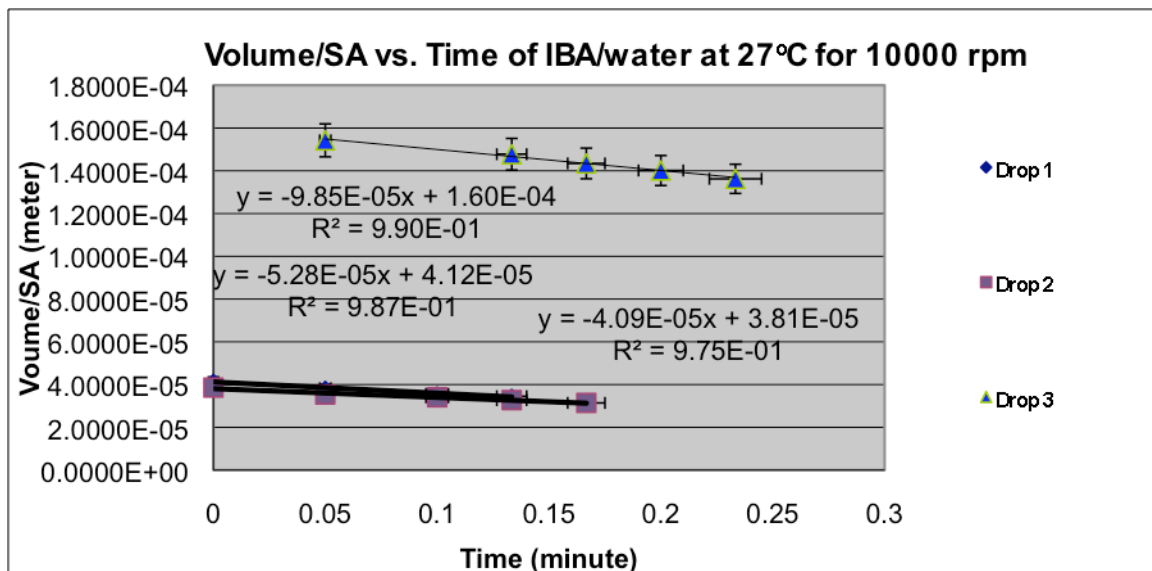


Figure 4.26. Graphs of Volume/SA vs. Time of IBA/water at 27 °C for 10000 rpm.

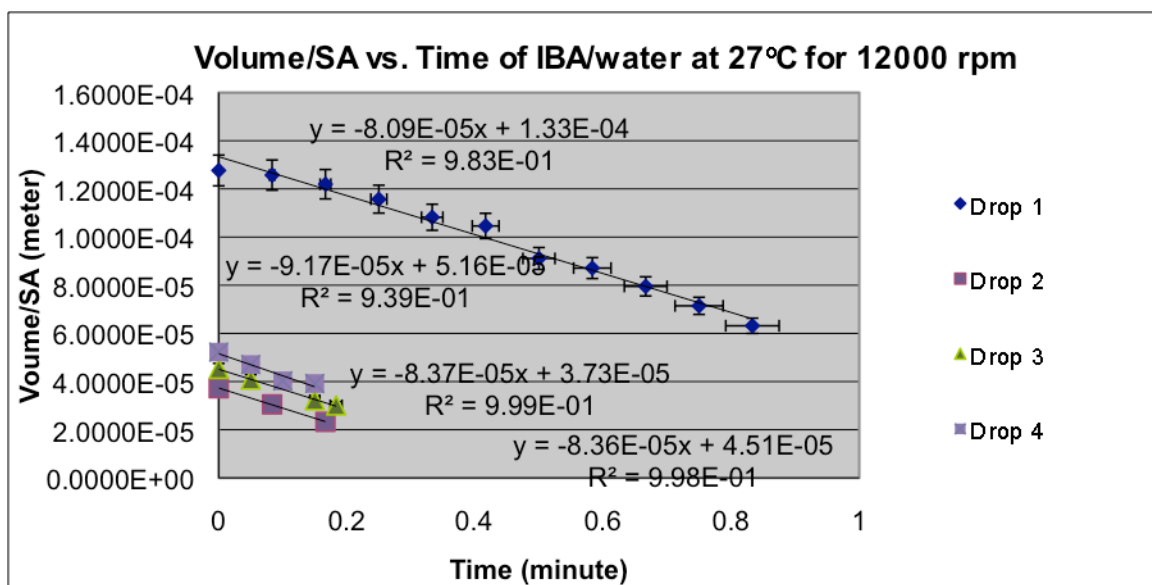


Figure 4.27. Graphs of Volume/SA vs. Time of IBA/water at 27 °C for 12000 rpm.

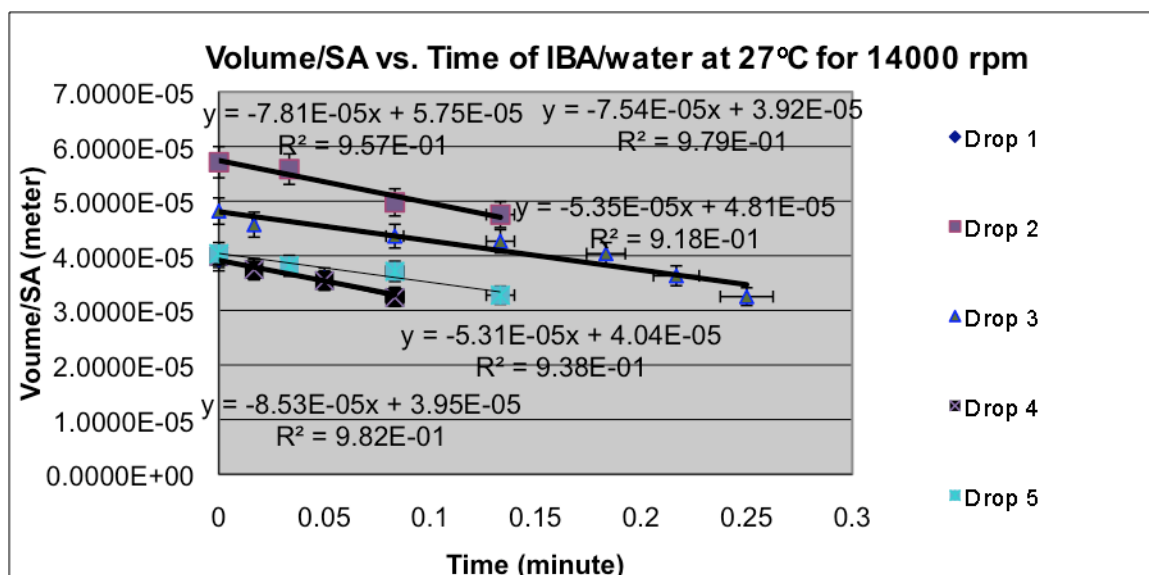


Figure 4.28. Graphs of Volume/SA vs. Time of IBA/water at 27 °C for 14000 rpm.

Each of the graphs has at least three drops; some of the drops have more than three drops because: (1) the time frame was small (10 seconds or less); (2) an air bubble was present; (3) pixels length and/or diameter would be between 10-25 pixels (generally, IBA drops would stretch and lengthen or oscillate between an ellipsoid and sphere when either the drop's diameter or drop's length was between 10-25 pixels); (4) drop's boundary became diffuse (generally only at 27 °C); (5) IBA-rich drop would have a differently shaded, unknown compound drop inside that became the same size as IBA-rich drop dissolved; (6) drops would merge; and/or (7) drops became obliterated by an air bubble. Figures 4.31-4.35 show examples of cases 3-7. Figure 4.29 shows how the IBA-rich drop changes shapes when the pixel length and/or diameter was between 10-25 pixels. This behavior occurred for most of the IBA-rich drops. Figure 4.30 shows how a drop's boundary becomes diffuse. Figure 4.2 shows how an unknown component inside a drop can hinder an IBA-rich drop's measurement of length

and radius since the impurity is almost as large as the IBA-rich drop itself. Figure 4.32 shows how two IBA drops merging; with two drops merging, a new drop measurement is then started, shortchanging the original drop's length and requiring finding an IBA drop with a longer time duration. Figure 4.33 shows how air bubbles shortened a drop's existence and time duration by hitting the IBA-rich drop so that no IBA-rich drop can be seen after the air bubble collides with it. This behavior was also another very common occurrence.

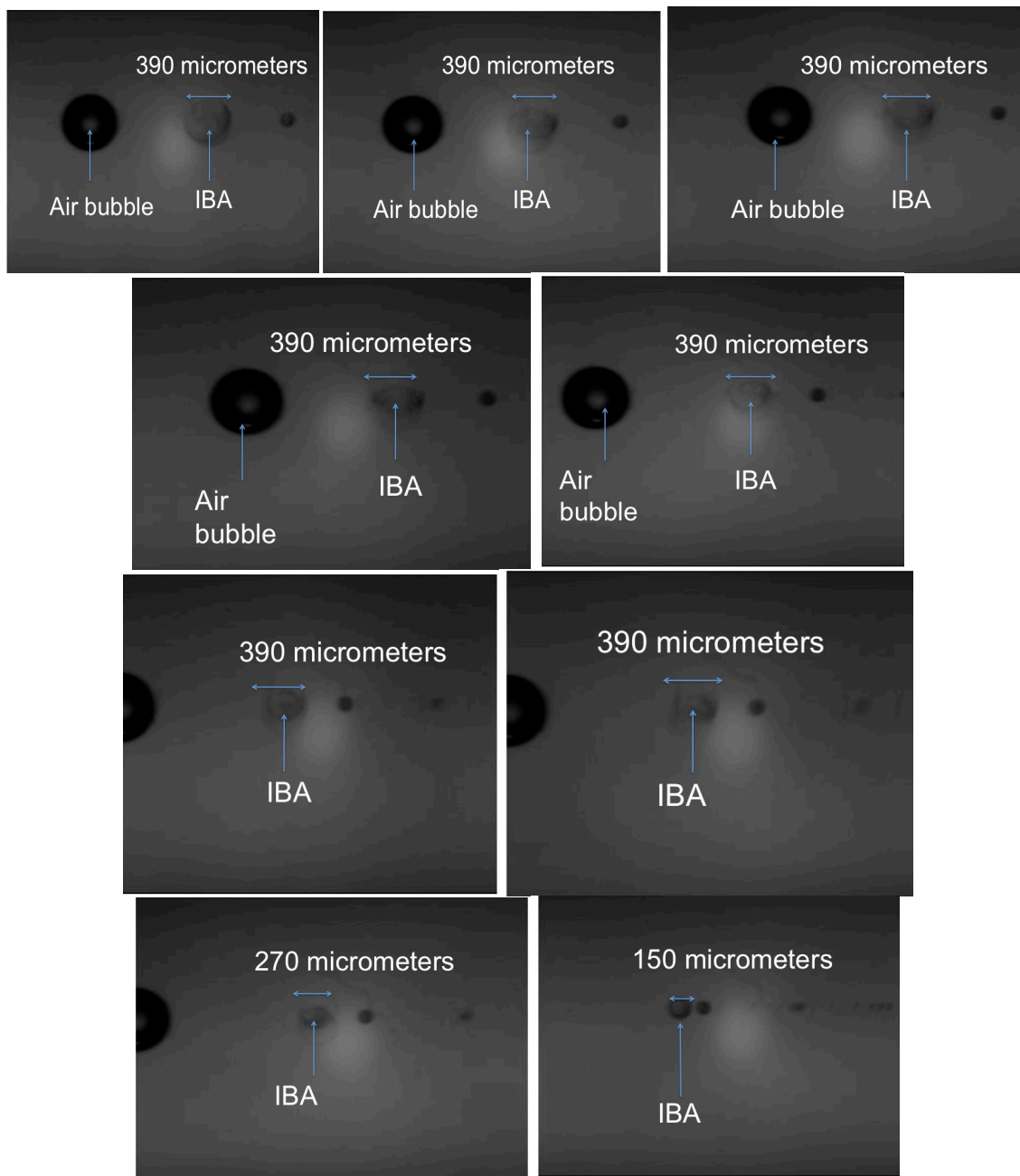


Figure 4.29. A series of images depicting how an IBA drop changes shape with 0.1 seconds elapsing between the second through tenth images and two seconds between the first and second image.

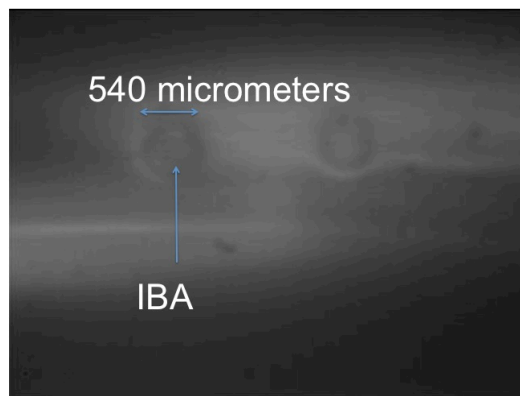


Figure 4.30. IBA/water drop at 6000 and 27 °C with diffuse edges.

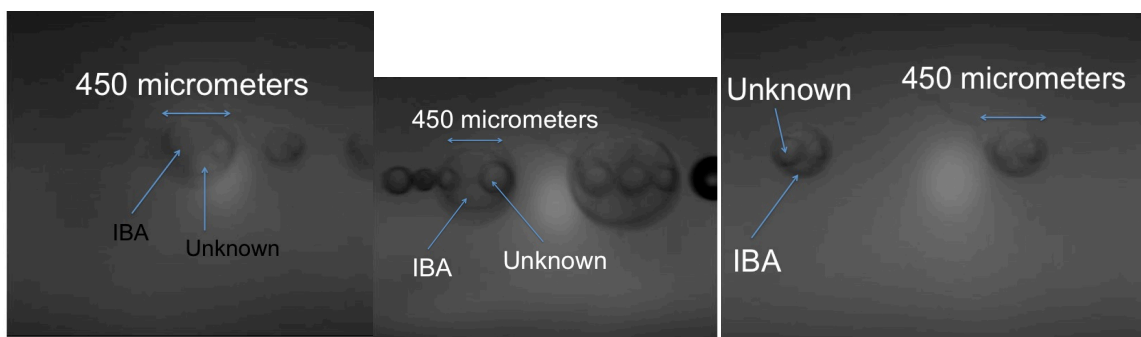


Figure 4.31. IBA/water drops at 6000 at 27 °C (left and center) and 8000 at 20 °C (right) with unidentifiable component the same size as IBA-rich drops.

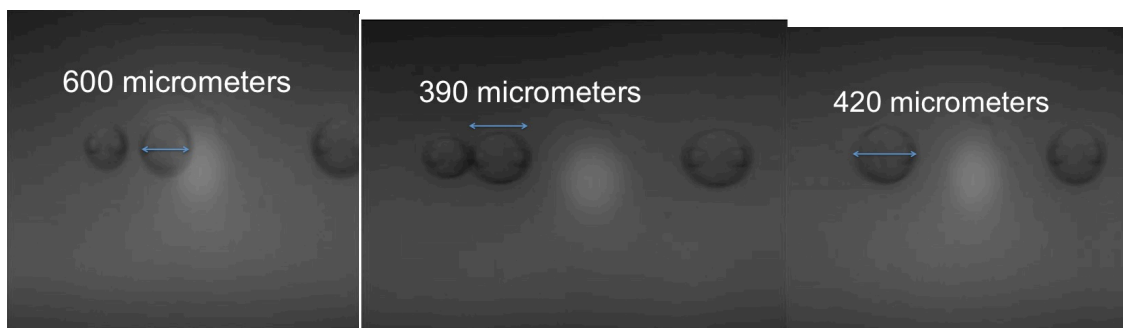


Figure 4.32. IBA-rich drops merging at 8000 rpm and 20 °C with two seconds passing between the left and center images and 0.25 seconds between the center and right images.

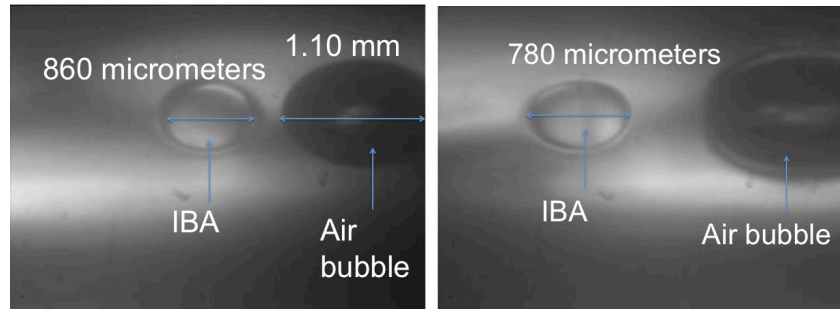


Figure 4.33. An IBA-rich drop becoming obliterated by an air bubble at 14000 rpm and 20 °C (left) and 25 °C (right).

Table 4.1 shows the rates of the dissolving IBA-rich drops along with rotation rate, temperature, and time range. At 20 °C, the rates increased between 6000 and 14000 rpm. The dissolution rate for 10000 rpm and 20 °C would have been -10.15×10^{-5} if a drop with an air bubble had been included. The 20×10^{-5} , which was the dissolution rate for the 10000 rpm and 20 °C, was due to an air bubble that was large, subtracting out the air bubble did not make a difference in changing the rate. The highest rate of dissolving of -11.96×10^{-5} for 14000 rpm and 20 °C was due to its largest rotation rate; with the air bubbles, the averaged dissolution rate would have been -22.6×10^{-5} . Overall, for the rates at 20 °C, the rates slightly rose as the rotation rate increased.

Table 4.1

Summary of Rates of Dissolving IBA Drops at Different Temperatures and Rotation Rates

Slope Range of SA/Volume vs. Time	Average Slope	Temperature (°C)	Rotation Rate (rpm)	Time Range for Dissolving Drop (sec)	Time Average (sec)	Standard Deviation
-5.27 - - 5.85 *10 ⁻⁵	-5.55*10 ⁻⁵	20	6.00*10 ³	25-110	79	2.37*10 ⁻⁶
-5.10 - - 7.77 *10 ⁻⁵	-5.76*10 ⁻⁵	20	8.00*10 ³	24-110	48	9.93*10 ⁻⁶
-4.48 - - 9.60 *10 ⁻⁵	-7.78*10 ⁻⁵	20	1.00*10 ⁴	20-64	41	1.90*10 ⁻⁵
-8.97 - - 12.8 *10 ⁻⁵	-10.9*10 ⁻⁵	20	1.20*10 ⁴	9-70	32	1.44*10 ⁻⁵
-9.88 - - 14.6 *10 ⁻⁵	-12.0*10 ⁻⁵	20	1.40*10 ⁴	15-62	29	1.69*10 ⁻⁵
-6.11 - - 12.5 *10 ⁻⁵	-8.24*10 ⁻⁵	25	6.00*10 ³	19-100	48	2.50*10 ⁻⁵
-6.48 - - 9.05 *10 ⁻⁵	-7.93*10 ⁻⁵	25	8.00*10 ³	33-84	66	9.50*10 ⁻⁶
-5.27 - - 11.7 *10 ⁻⁵	-8.25*10 ⁻⁵	25	1.00*10 ⁴	6-19	11	2.50*10 ⁻⁵
-7.90 - - 13.7 *10 ⁻⁵	-10.2*10 ⁻⁵	25	1.20*10 ⁴	9-50	27	2.13*10 ⁻⁵
-6.63 - - 14.8 *10 ⁻⁵	-9.66*10 ⁻⁵	25	1.40*10 ⁴	10-31	20	2.35*10 ⁻⁵
-3.47 - - 13.4*10 ⁻⁵	-7.01*10 ⁻⁵	27	6.00*10 ³	6-69	38	2.68*10 ⁻⁵
-4.85 - - 14.0 *10 ⁻⁵	-8.26*10 ⁻⁵	27	8.00*10 ³	27-112	54	3.53*10 ⁻⁵
-4.09 - - 9.85 *10 ⁻⁵	-6.41*10 ⁻⁵	27	1.00*10 ⁴	10-14	11	2.48*10 ⁻⁵
-8.09 - - 9.17 *10 ⁻⁵	-8.50*10 ⁻⁵	27	1.20*10 ⁴	10-55	22	4.03*10 ⁻⁶
-5.31 - - 8.53 *10 ⁻⁵	-6.91*10 ⁻⁵	27	1.40*10 ⁴	5-15	8	1.33*10 ⁻⁵

For the rates between 6000, 8000, 10000, 12000, and 14000 rpm at 25 °C and 27 °C, the range was between -6.41 – -10.15*10⁻⁵. The rates at 27 °C were

all the closest between all of the temperatures with only 2.11×10^{-5} difference while the rates at 25°C differed by 2.32×10^{-5} . The range and rate of dissolving would probably have been higher if the drops had lasted longer at the higher rotation rates. In general, the shorter times had the smaller dissolution rates because the drops were smaller in radius and length and the shorter time had the smallest volume/surface area ratio because the drops were smaller in radius and length. For example, the three drops of 12000 rpm at 25°C had an average rate of about -8×10^{-5} when the drops lasted less than 0.2 minutes but had a rate of about -10×10^{-5} when the drops lasted about 0.8 minutes.

If all of the drops had lasted the same amount of time, the rate of dissolving would have increased slightly with each increasing rotation rate. For 20°C , the rates would also increase with increasing time; for example, a drop that lasted 110, 70, and 30 seconds for 8000 rpm at 20°C would have rates of, respectively, -7.77 , -5.95 , and -5.10×10^{-5} . The rate increased about -1×10^{-5} for each 0.67 minute in the first minute at 20°C but increased about -2×10^{-5} for 0.6 minute in the first minute at 25°C . These examples were true in cases where the longer the drop, the larger the dissolution rate. In these two cases, the smallest drops had the shortest time, but for the 20°C , the medium time had the largest initial volume/surface area ratio. Looking at another example of this behavior with 10000 rpm at 20°C : when the drops have the similar ratios of volume/surface area, the longer time will have the larger ratio rate. The longer time of 0.41 minutes had a greater $\sim -2 \times 10^{-5}$ dissolution rate in the first minute; however, when the drop had a larger ratio of volume/surface area, the longest

time had the same rate as the drop with the largest volume/surface area ratio.

When comparing similar ratios and similar times between 8000, 10000, and 12000 rpm, the dissolution rate increased by $\sim -1 \times 10^{-5}$ between each increasing rotation rate and between the temperatures of 20 °C and 25 °C.

There were some cases that did not follow the larger the volume/surface area the larger the dissolution rate or the longer the time length the larger the dissolution rate. Examples include cases like 6000 rpm at 20 °C. In this instance, all of the dissolution rates were the same despite the shortest time length having the smallest volume/surface area ratio. Another difference case was 6000 at 25 °C in which the shorter time in comparison with a similar volume/surface area ratio had the larger dissolution rate. This is attributed to the fact that both of the ratios had the same dissolution rate of about -10×10^{-5} in the first 0.5 minutes but as the time lengthened to almost two minutes for the dissolution rate dropped to $\sim -8 \times 10^{-5}$. However, when comparing similar time lengths and ratios for 6000 rpm at temperatures 20 °C and 25 °C, the dissolution rate increased between $-2 - 3 \times 10^{-5}$.

In looking at 14000 rpm and 25 °C, there was a case in which the volume/surface area ratio and time lengths were similar but one had a dissolution rate of -9.81×10^{-5} and the other had a rate of -6.63×10^{-5} . This difference was because the -6.63×10^{-5} had a 25% smaller radius and length, thus resulting in some discrepancies in general trends. Also, like in 6000 and 25 °C, there was another occurrence of a shorter time length having a larger dissolution rate than one with a similar volume/surface area ratio and, like the 6000 rpm, the drops

had similar starting rates, but as the time went on, the dissolution rate decreased. Also, like 6000 at 20 °C, the drops of 14000 rpm at 20 °C had drops with different volume/surface area and time lengths having the same dissolution rate.

Comparing drops with similar volume/surface ratio and time lengths was not really possible for 14000 rpm at 20 °C and 25 °C because, with increasing temperatures, the drops had smaller lengths, radii, volume/surface ratios, and time lengths. So, that drops with higher temperatures and smaller time lengths, volume/surface ratio, lengths, and radii had the small dissolution rate as the lower 20 °C temperature drops. Between 6000 and 14000 rpm at 20 °C, the rate increased by about $4 \cdot 10^{-5}$ for drops (without air bubbles) with similar and different volume/surface ratios and time lengths. Between 6000 and 14000 rpm at 25 °C with drops of similar volume/surface ratios and time lengths, the rate increased between $3-4 \cdot 10^{-5}$, but with drops of different volume/surface ratios and smaller time lengths for 14000 rpm, the rate was the same.

At 27 °C, the range of dissolution rate differed between 1 and $2 \cdot 10^{-5}$. Like the other 10000 and 12000 rpm at 20 °C and 25 °C, the drops with larger dissolution rates either had a larger volume/surface area ratio and/or longer time length. For 8000 at 27 °C, similar to other cases at 6000 and 14000 rpm at 20 °C, two drops had the same volume/surface area ratio but the longer time length had the shorter dissolution rate; like the other cases, the dissolution rates became the same when the time was shortened to same time. Another unusual instance for 8000 rpm at 27 °C was that the one drop done at Louisiana State University (LSU) had the highest dissolution rate despite having a shorter time

length and smaller volume/surface area ratio. One possible reason is that the LSU instrument had the drops moving more quickly from one end of the capillary to the other end of the capillary. A second possible reason is that the drops in the LSU instrument could go up and down as they moved across whereas the drops in the University of Southern Mississippi (USM) instrument always moved linearly across. Other than these two cases, the shortest time and smallest volume/surface area ratio of the three USM drops of 8000 and 27 °C had the smallest dissolution rate.

Like the other 14000 rpm, this 14000 rpm at 27 °C had several different cases from the normal rule of larger dissolution rate had either a larger volume/surface area and/or time. One similar case to the 14000 rpm was that two drops with the same volume/surface area and time length had different dissolution rates because of a 25% larger radius. One striking difference was that despite how close the drops were in time duration and volume/surface area was that two of three higher volume/surface area ratios and time duration had two of the smallest dissolution rates; this difference was because they had changed the smallest in length compared to the other three.

The 6000 rpm at 27 °C had more similarities to 10000 and 12000 rpm at any temperature than it did to 6000 rpm at 20 °C or 25 °C: the 6000 rpm at 27 °C, in general, had the largest dissolution rate associated with either a larger time duration or larger volume/surface area ratio. However, like the other 6000 rpm, there were some differences. One notable difference was that a larger dissolution rate was not with an air bubble even if the air bubble was not

subtracted. In this 6000rpm case, the air bubbles did not seem to affect how the dissolution rate was, possibly because air bubbles were in five out of eight drops that were measured. Another interesting case was that the smallest dissolution rates were the drops with the smallest radii and lengths; they were about 50% smaller than the other drops.

In comparing the 14000 rpm drops at different temperatures, the drops generally decreased in volume/surface area and halved in time as the temperature went from 20 °C to 25 °C to 27 °C so that the dissolution rates were about the same, but if times were shortened and the volume/surface ratios were similar, the higher temperature would have had a slightly higher dissolution rate. For 12000 rpm, the rates did increase between 20 °C and 25 °C, but at 27 °C, the dissolution rates for drops with similar time durations but smaller volume/surface area ratios were similar between 25 °C and 27 °C. So, if the drops had similar time durations and volume/surface area ratios, the 27 °C would probably have had a slightly higher dissolution rate. For 10000 rpm, when the time durations were shortened to be the same or left at its original time, the two higher temperatures for drops with similar volume/surface area ratios had the same dissolution rates, making 20 °C the smallest dissolving out of the three temperatures. For 8000 rpm, the highest dissolution rate was at 25 °C with drops of similar volume/surface area ratios (both with shortened and original times) and the lowest dissolution rate was with 20 °C. For 6000 rpm, the highest and lowest dissolution rate were at, respectively, 27 °C and 20 °C.

For the overall trend, in general, in comparing the rotation rates for each of the temperatures, from 6000 to 14000 rpm, the dissolution rates increased. At 20 and 25 °C, from 6000 to 14000 rpm, the rate increased between 6.41×10^{-5} and 1.42×10^{-5} . At 20 °C, the highest and lowest dissolution rates were at, respectively, 14000 and 6000 rpm while 12000 rpm had the highest dissolution rate for 25 °C and 27 °C and the lowest dissolution rate was at, respectively, 8000 and 10000 rpm. Though, at 27 °C, 10000 rpm had the lowest dissolution rate while 12000 rpm had the highest dissolution rate, the dissolution rate did increase from 6000 rpm to 8000 rpm to 12000 rpm and the rate increased from 10000 rpm to 14000 rpm. One reason that 10000 rpm and 14000 rpm's dissolution rates were so low for 27 °C was because the drops were smaller since they were done at LSU while the majority of the other drops done at the other rotation rates and temperatures were done at USM. A second reason that the 25 °C and 27 °C did not have the lowest and highest rotation rates being at, respectively, 6000 and 14000 rpm is that air bubbles appeared more frequently at 10000 and 14000 rpm, disrupting the dissolving times by making the dissolving time shorter and making it harder to get larger radii and length, which would have increased the dissolution rates. A third reason is that the 10000 and 14000 rpm have a lower range in the volume/surface area ratio than the 12000 rpm's volume/surface area ratio. So, when comparing similar ratios with similar time lengths, the higher temperature had the higher dissolution rate and higher rotation rate had the higher dissolution rate. Thus, larger ratios of volume/surface area, bigger changes in radii or length, longer time durations,

higher rotation rates, higher temperatures, or air bubbles will give larger dissolution rates. Smaller dissolution rates occur with smaller volume/surface area, smaller changes in radii or length, shorter time durations, smaller rotation rates, and lower temperatures.

The standard deviation increased with more variety in volume/surface area ratio. For example, because drops 10000 and 14000 rpm at 20 °C varied more in volume/surface area ratios than 12000 rpm at 20 °C even though 10000 and 14000 rpm had a smaller value range of volume to surface area ratios. Standard deviation also increased with increasing temperature from the immiscible region to the miscible region between 20-25 °C and 20-27 °C. Between 25 °C to 27 °C, the standard deviation either decreased or increased, depending on the rotation rate: for the lower rotation rates of 6000 and 8000 rpm, the rates increased while, for the higher rotation rates of 10000, 12000, and 14000 rpm, the rates decreased. One reason that the standard deviation increased from the immiscible region to the miscible region but not between the two temperatures near the UCST is that the drops varied more in the volume/surface area ratio with increasing temperature between the immiscible and miscible region, but, near the UCST, equal amounts of IBA and water diffuse into each so that, between 25 °C to 27 °C (the temperatures surrounding the UCST), the drops varied similarly in their volume/surface ratios and had less consistency in the volume amounts.

For 20 °C, standard deviation also, in general, increased with increasing rotation rate, mainly because with increasing rotation rate less consistency

occurred. This trend, however, did not occur for 25 °C or 27 °C. At 25 °C, the standard deviation was about the same while, at 27 °C, the standard deviation tended to decrease between the lower and higher rotation rates. This probably happened because the amount of the IBA injected into the water-rich phase and how quickly the IBA dissolved before the SDT started mixing. At 20 °C, only five microliters or less of IBA was injected into the water-rich phase, but, for the higher temperatures of 25 °C and 27 °C, twenty to fifty microliters (with the higher volume used at 27 °C than at 25 °C) of IBA was injected into the water-rich phase. Since IBA was dissolving more quickly before the rotation rate was started at the higher temperatures, larger amounts of IBA had to be used.

At 14000 rpm and 27 °C, the drops would have been much smaller in radii and length than the drops at 6000 rpm and 27 °C so that 6000 rpm would have been able to have more variety in its length and radii and so a larger standard deviation would occur. At 6000 rpm and 20 °C, the drops would have been the largest in radii and length so that a lot of the drops would have more conformity than the drops at 14000 rpm and 20 °C. At 14000 rpm, there would be more mixing and greater IT/EIT so that drops would have been smaller in radii and length. At 20 °C, this would mean more variety in radii and length since the drops could break up into a variety of lengths while the 6000 rpm would mainly have longer lengths, but, for 25 °C or 27 °C, the increased temperature would have decreased the length and radii compared to the drops at 20 °C so that drops at 14000 rpm would be more uniform in their smaller lengths while, 6000 rpm, which had been previously repressed in its variety in length due to its

tendency to form longer lengths no matter the temperature, can now have more variety in its length since the higher temperature allow smaller lengths and so more variety. So, drops length and radii will affect the standard deviation and drops length and radii are dependent on temperature and rotation rate.

The curve in determining the length and radii is like a Gaussian curve, with one end being 6000 rpm and 20 °C at one end and the other end being 14000 and 27 °C and the middle being all other rotation rates and temperatures. Hence, decreasing temperatures had more consistency in volume/surface area ratio but without any correlation between the dissolution time or the volume/surface area value and so had smaller standard deviations, but the values of the radii and length were dependent on the rotation rate and temperature and did affect the standard deviations.

Table 4.2 shows the averaged EIT (for 25 °C and 27 °C) and IT (for 20 °C) along with rotation rate, temperature, and time range. In general, the drops with the larger radii had the larger EIT or IT and longer time durations. For IBA/water, going from 6000 to 14000 rpm for large volume had an overall increase in EIT and IT. So, the small drop volumes should follow the same trend. In the immiscible region at 20 °C, the ITs did have an overall increase between 6000 and 14000 rpm. However, the 12000 rpm had a smaller IT than the 10000 rpm, possibly due to its 10% smaller radii. For IBA/water going from 6000 to 14000 at 25 °C, the EITs at 25 °C also had an overall increase. However, like the 20 °C group, there were some increases and decreases between the 8000 and 12000 rpm. For 25 °C, 8000 rpm and 10000 rpm had, respectively, the largest and

smallest averaged EIT, possibly because of 8000 had an averaged radii that was twice as large as 10000 rpm and 33% larger for 12000 rpm and 14000 rpm. The 10000 rpm had the smallest averaged radii by 50% compared to 12000 and 14000 rpm, perhaps explaining why its averaged EIT was so low. For 27 °C, the EITs also had an overall increase between 6000 and 14000 rpm, and, just like the other two temperatures, there were some increases and decreases in between 6000 and 14000 rpm. For 27 °C, the highest to lowest EITs were, in decreasing value, 10000, 8000, 12000, 14000, and 6000. The values for 10000 rpm and 8000 rpm were probably higher than the 12000 rpm and 14000 rpm because their averaged radii were 25-33% larger than 12000 rpm's and 14000 rpm's averaged radii. The 12000 rpm's and 14000 rpm's averaged radii were the same but 12000 rpm still have a slightly higher averaged EIT, possibly due to 12000 rpm having about three times the time duration. However, overall, the ITs and EITs did have an overall increase in their averaged values going from 6000 rpm to 14000 rpm.

Table 4.2

Averaged EIT and IT of IBA/water at Different Rotation Rates and Temperatures

IT/EIT Range (mN/m)	Average d IT/ EIT (mN/m)	Temperature (°C)	Rotation Rate (rpm)	Time Range (sec)	Time Average (sec)	Radius Range (*10 ⁻⁵ m)	Averaged Radii (*10 ⁻⁵ m)
0.00782-0.0468	0.0262	20	6.00*10 ³	25-110	79	17-25	20
0.0531-0.233	0.139	20	8.00*10 ³	24-110	48	10-27	16
0.108-0.298	0.186	20	1.00*10 ⁴	20-64	41	8-29	23
0.0205-0.245	0.134	20	1.20*10 ⁴	9-70	32	12-27	20
0.0699-0.356	0.204	20	1.40*10 ⁴	15-62	29	17-27	22
0.00690-0.0386	0.0206	25	6.00*10 ³	19-100	48	16-22	19
0.0388-0.0659	0.0498	25	8.00*10 ³	33-84	66	18-23	21
0.00271-0.0723	0.0186	25	1.00*10 ⁴	6-19	11	7-20	10
0.00438-0.0637	0.0323	25	1.20*10 ⁴	9-50	27	9-19	14
0.0217-0.0930	0.0445	25	1.40*10 ⁴	10-31	20	12-18	14
0.00103-0.0220	0.0119	27	6.00*10 ³	6-69	38	7-20	15
0.0209-0.0835	0.0419	27	8.00*10 ³	27-112	54	13-22	18
0.00505-0.122	0.0446	27	1.00*10 ⁴	10-14	11	10-24	15
0.00546-0.0612	0.0227	27	1.20*10 ⁴	10-55	22	9-15	12
0.0103-0.380	0.0183	27	1.40*10 ⁴	5-15	8	11-14	12

In comparing the individual rotation rates between temperatures, there was an overall decrease in going from 20 °C to 27 °C for most of the rotation rates. This was not too surprising since the radii significantly decreased

(generally 50%) between 20 °C to 27 °C. For 6000, 8000, 12000, and 14000 rpm, there was a steady decrease from 20 °C to 27 °C. For 6000 rpm, the decrease from 20 °C to 27 °C was 0.0262 mN/m to 0.0206 mN/m to 0.0119 mN/m. For 8000 rpm, the decrease from 20 °C to 27 °C was 0.139 mN/ m to 0.0498 mN/m to 0.0419 mN/m. For 12000 rpm, the decrease from 20 °C to 27 °C was 0.140 mN/ m to 0.0323 mN/m to 0.0227 mN/m. For 14000 rpm, the decrease from 20 °C to 27 °C was 0.204 mN/ m to 0.0445 mN/m to 0.0183 mN/m. For 6000 rpm, the decrease was regular decline whereas for 8000, 12000, and 14000 rpm the values decreased considerably between 20 °C and 25 °C. This large decrease occurred between 20 °C and 25 °C because the drops were becoming much smaller, dissolving in shorter amounts of times, and being closer to the UCST of 26 °C.

In comparing the individual rotation rates between temperatures, 10000 rpm was the only one without a steady decrease between 20 °C and 27 °C. Instead, for 10000 rpm, there was a steady decrease from 20 °C to 25 °C of 0.1858 mN/ m to 0.0186 mN/m but an increase from to 0.0446 mN/m at 27 °C. Like 8000, 12000, and 14000 rpm, there was a considerable decrease between 20 °C and 25 °C. This decrease occurred for the same reason. However, unlike the other rotation rates, an increase occurred between 25 °C and 27 °C. This increase probably happened for two reasons. One reason is that, for all of the other rotation rates, either a steady decrease in time duration or averaged drop radii occurred while 10000 rpm actually had the averaged drops' radii increase by 50%. A second, most likely, reason is that, for some unknown reason, 10000

rpm had the largest number of air bubbles, even though air bubbles will appear more quickly at 14000 rpm than at 10000 rpm. Air bubbles can affect the way that drops dissolve and the drops' ITs/EITs.

Different sizes of air bubbles sometimes affected the rate that IBA dissolved and the measured IT/EIT. Figures 4.34, 4.35, and 4.36 show examples, respectively, of small, medium, and large air bubbles. Small, medium, and large air bubbles are air bubbles that, respectively, are 25% or less, 25-100%, or twice the size of the IBA-rich drop. If the air bubble was 25% or less the size of the IBA-rich drop, then the rate of dissolving IBA and the averaged EIT were not really affected by the air bubble. If the air bubble was at least twice the size of the IBA-rich drop and was present when the IBA drop first formed, then the rate of dissolving IBA and EIT was not affected as long as the air bubble was not included in the measurements of diameter and length of the IBA-rich drop. If the air bubble is between 25-100% size of the IBA drop and is either present when the drop was first seen or becomes that way when a smaller air bubble becomes larger from the time the IBA drop was first seen, then the EIT and rate of dissolving are affected even if the air bubble is included in or subtracted out of the measurements. Figures 4.37-4.39 show examples of IBA-rich drops that dissolved around the air bubble. In these figures, the air bubbles were between 10-25% the size of the initial IBA-rich drop and, over a matter of seconds, became 50% or more the size of the IBA drop.

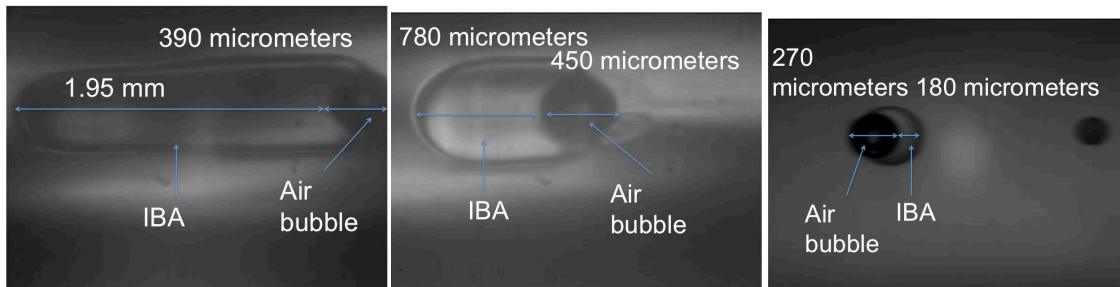


Figure 4.34. Image of small air bubble (dark drop) in IBA/water at 8000 rpm and 27 °C (left) and at 10000 rpm and 20 °C (center and right).

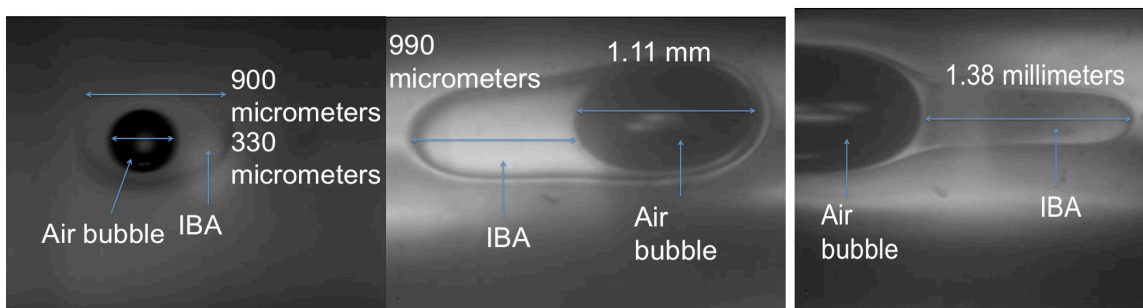


Figure 4.35. Image of medium air bubble (dark drop) in IBA/water at 6000 rpm and 27 °C (left), at 10000 rpm and 25 °C (center) and at 14000 rpm and 20 °C (right).

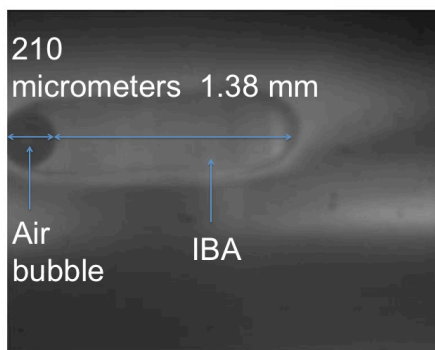


Figure 4.36. IBA/water drop emerging from large air bubble at 12000 rpm 27 °C.

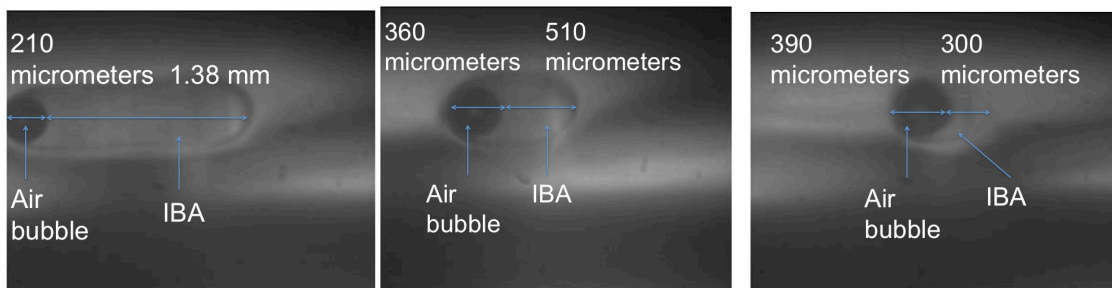


Figure 4.37. IBA/water drop at 6000 rpm and 27 °C with ten and sixteen seconds elapsing between the left and center and center and right images.

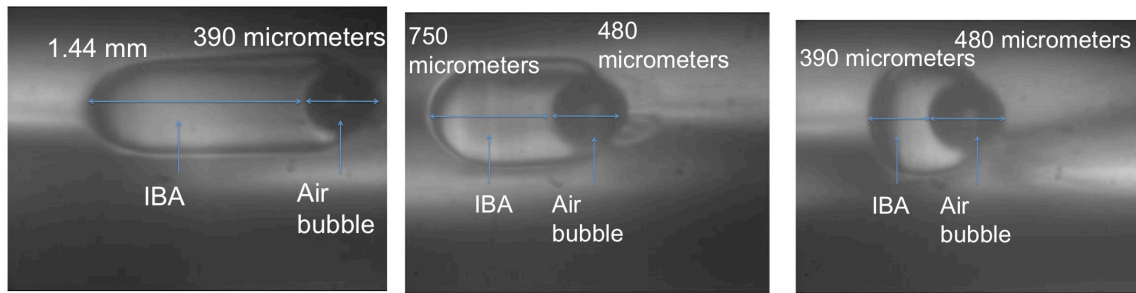


Figure 4.38. IBA/water drop at 10000 rpm and 20 °C with five seconds elapsing between the left and center and center and right images.

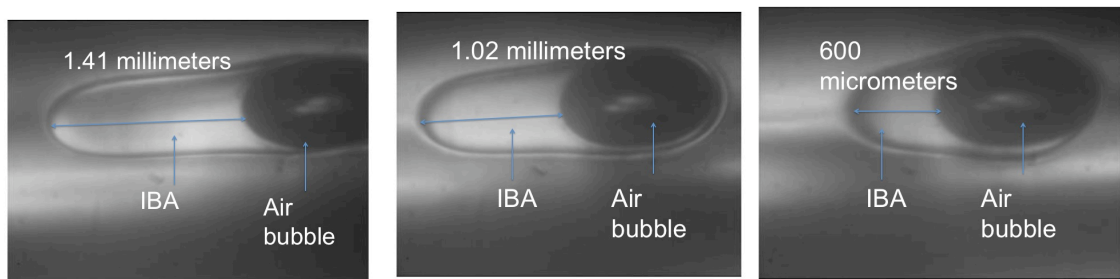


Figure 4.39. IBA/water drop at 14000 rpm and 20 °C with two and three seconds elapsing between the left and center and center and right images.

Conclusions

Before analyzing our results, we initially ran experiments because we wanted to see if we could replicate the results of the original experiment involving IBA-water. Two of the issues with these experiments were that the drops above 26 °C dissolved after 10 seconds and little or no drops occurred. Different temperatures and rotation rates were evaluated to determine which were the best ones for obtaining enough drops to analyze. With unequilibrated systems, drops of varying sizes occurred.

For equilibrated systems, we tested several different methods, evaluated how long the systems should be allowed to sit or equilibrate, and tested different initial rotation rate and initial temperatures. We used equilibrated systems

because we thought that we would be able to better control the amount of IBA that formed in a drop. From these different methods, we found that lower temperatures and lower rotation rates had fatter (bigger radii across) drops that tended to dissolve slower, thus making them easier to analyze and producing more consistent results. From different procedures, we also found that long drops of IBA/water can have blurry boundaries after half an hour of spinning at high rotation rates and at the UCST. This behavior was not seen before in other experiments. The blurry boundaries most likely mean that the barodiffusion is not the reason for the sharp concentration gradients but that the sharp boundary might be an artifact.

According to Cussler, the two fluids near a critical or consolute point are on the verge of a phase separation and the two fluids form small clusters of molecules of one species rather than being randomly distributed.⁴⁶ Near a consolution point, the diffusion coefficient approaches zero.⁴⁶ Cussler gives a couple of explanations for why this happens to the diffusion coefficient.⁴⁶ One reason is that diffusion coefficient is expected to decrease as the temperature is decreased to the consolute point. A second explanation assumes that “long-range fluctuations dominate behavior near the consolute point” and that diffusion occurs when the fluctuations of concentration and fluid velocity combine. Away from the consolution point, the motion of single molecules dominate the concentration fluctuations, but near the critical point, the fluctuations continue even as the average fluid velocity is zero, resulting in a turbulent “eddy diffusion coefficient” without flow.

Another interesting result from the different procedures was that end pinching occurred. End pinching would indicate Korteweg stress and EIT were present. For the USM instrument versus the LSU instrument, the USM had more end pinching occurring at 27 °C and 25 °C and rarely at 20 °C while end pinching occurred more frequently at 20 °C at LSU than at USM. End pinching and EIT can occur in immiscible systems and other miscible systems like dodecylacrylate/polydodecylacrylate.¹

A third unusual result from the IBA small volume experiments was how the drop shape changed when it reached a certain point of between 0.05 and 0.20 mm. The drop would rapidly change between an spherical and ellipsoid shape and, after this rapid back and forth, the drop would seem to burst into a drop that was two or more times smaller than before the rapid shape-shifting. This behavior was unique to IBA/water and occurred at all temperatures and rotation rates.

From the various equations, we found that the Knud-Thomsen approximation fit the drop evolution best since the original Knud-Thomsen formula fit the spherical shape best. By plotting volume/surface area vs. time and dividing volume by surface area, we were able to correct for changes to surface area at different rotation rates, which could affect the diffusive flux. For calculating EIT, we used the formula of Princen *et al.*⁴⁵ but had to use a set of formulas with different correction factors rather than simply one because the different ratios required different correction factors.

At 20 °C with increasing rotation rate, the dissolution rate increased and the averaged IT/EIT decreased. We still haven't figured out why an IBA drop dissolves faster at higher rotation rates at 20 °C, but the data indicate exactly that. We also found that when we increased the temperature from 20 °C to 25 °C or 27 °C, the averaged EIT/IT decreased. The decreasing of the averaged IT/EIT with increased temperature is different from what Pojman *et al.*¹ They found that EIT stay almost constant over time and temperature. The difference could have been in the averaged drop radii and the duration the drop was present. Another difference was that my results were done using pure IBA/pure water while Pojman *et al.*¹ used an equilibrated IBA/water. In the some of our initial experiments for small volume IBA/water in this dissertation, we also used equilibrated IBA/water and the EITs and their dissolution rates were smaller. The dissolution rates were smaller by a magnitude of 10 while the volume/surface area was slightly larger than the pure IBA/pure water.

The results in this dissertation also show that dissolution rate was more affected at 20 °C with a steady increase of dissolution rate with increasing rotation rate while a not-so-steady increase at 25 and 27 °C: with increasing temperature, the dissolution rate seems to be relaxing like the relaxation of the concentration gradient over time. Figure 4.40 shows this result.

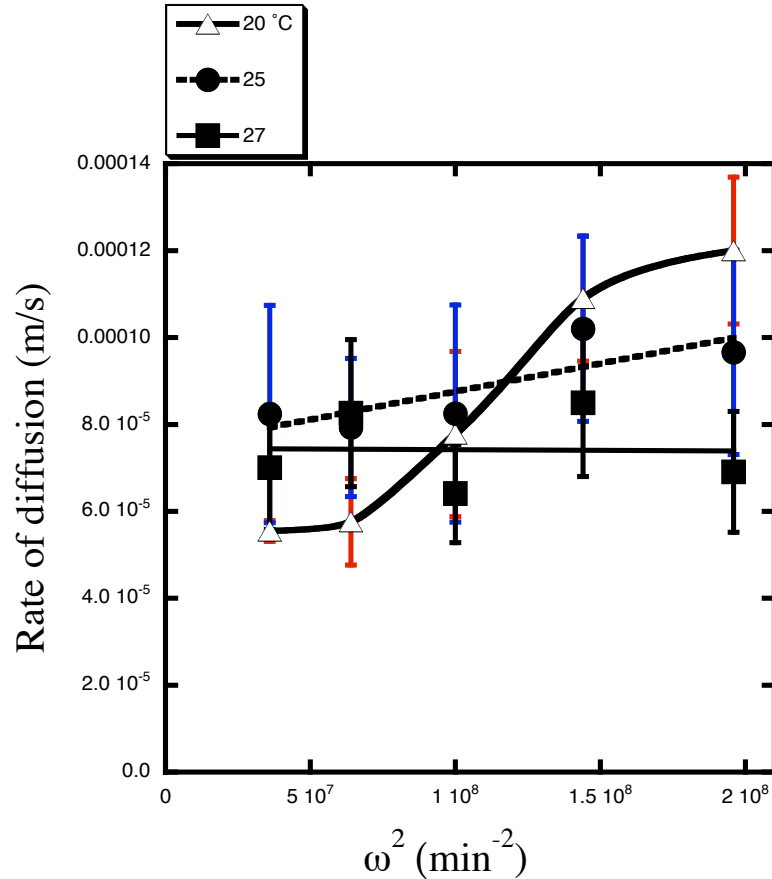


Figure 4.40. Rate of diffusion versus rotation rate squared.

Other research has shown that diffusion near a critical solution temperature are affected by gravitational forces.^{24, 26, 33, 35, 47, 48} With increasing rotation rate, the rotational acceleration increases. Only at 20 °C is there is an increase of the rate of diffusion with increasing rotational acceleration. We believe is this is due to the larger density difference between IBA and water at 20 °C compared to the other temperatures.

Formation of air bubbles sometimes adversely affected the dissolution rate and the averaged IT/EIT. These results demonstrated that barodiffusion did affect the dissolution rate but not the sharp concentration gradient. Korteweg stresses caused by large concentration gradients can lead to EIT and so could

have caused an increase in the EIT/IT values.

Larger standard deviations increased as values for volume/surface area ratio varied more or were no longer closer in value to each other. For 20 °C, standard deviation also, in general, increased with increasing rotation rate, mainly because with increasing rotation rate less consistency occurred. This trend did not occur with other temperatures because of the amount of IBA injected into the water-rich phase and how quickly the IBA dissolved before the SDT started rotating.

CHAPTER V

SURFACTANTS

Surfactants, which are substances that have the ability to adsorb onto surfaces or interfaces of the system and of altering the interfacial free energies of those interfaces, can lower the interfacial tension between immiscible fluids.³⁶ We used spinning drop tensiometry to determine how two different surfactants, SDS (sodium dodecylsulfate) and dodecyltrimethyl ammonium chloride (DTAC) affected the interfacial tension of IBA and water. Mainly, we examined EIT/IT as a function of concentration and type of surfactant and predicted that the surfactants generally would lower the interfacial tension between IBA and water.

The first step in the surfactant experiments was to identify the different components in the IBA/surfactant/water system. In order to distinguish between surfactant and IBA, the IBA/surfactant/water systems was compared with the IBA/water systems. Identification of the different components is easiest when there are sharp color contrasts among the different components of the system. Because the appearance of an IBA-rich drop varies at different temperatures, temperature was a factor for being able to identify the different components of the system. Also, in the SDT, color contrast can be indicative of whether IBA was equilibrated because equilibrated IBA is darker in color (shades of gray) or grayer than IBA that is not equilibrated.

In instances where similar color contrasts occurred, SDS-rich phase can be identified by its lack of a real boundary. Also, the IBA-rich phase has a

sharper, darker boundary that can be identified by decreasing and then increasing the rotation rate.

Besides identification of components, color contrast and differences in the boundaries were also used for comparing the behaviors of IBA/water and IBA/surfactant/water. Differences in radii of the drops, length of time the drops appeared, fluid motion, and the actual appearance of the drops were also used to compare the behaviors of the two systems. Also, the Marangoni instability was studied in IBA/water systems with and without surfactant. Comparing and contrasting the behaviors of IBA/water and IBA/surfactant/water systems can demonstrate what effect the surfactant had on the behavior of the IBA/water system.

The EIT or IT (interfacial tension) of systems with different concentrations of SDS and DTAC were studied at different temperatures. We selected concentrations that were below and above the critical micelle concentration because the EIT above the cmc should not change as the concentration is increased since the EIT should not be dependent upon the concentration above the cmc. We expect this result because this finding is true for equilibrium systems, but it is unknown whether this result is true for nonequilibrium systems. However, below the cmc, the EIT should decrease as the concentration of the surfactant increased. A plot of radius of the drop cubed vs. rotation rate squared was used to determine EIT and IT (interfacial tension). These plots demonstrate how the concentration of the surfactant and the type of surfactant affected the EIT of the system.

Besides, the effect of surfactant concentration on EIT, the impact of temperature on interfacial tension and EIT was studied at 20 °C and 30 °C, respectively. At 20 °C, the IBA/SDS/water systems are in the immiscible phase, but at 30 °C, they are in the miscible phase. The effect of rotational rate or decreasing and then increasing the rotational rate was used to study the EIT and IT what happens to EIT and IT over time and compared to IBA/water systems without surfactant.

Distinguishing Drops

The first surfactant procedure, which involved SDS, was done similarly to the IBA volume experiments' procedures: 10 mL of the water-rich phase was injected at 25 °C into the capillary, followed by 10-25 uL of the lighter IBA phase at 25 °C and the temperature lowered to 20 °C, where the system left between 5-30 minutes in order for the system to equilibrate with the temperature and have more IBA-rich phase come from the water-rich-rich phase. A larger container of 50 mL of water and 50 mL of IBA was shaken the night before the experiments were run and left to equilibrate overnight. Occasionally, some surfactants as crystals or soap-bubble-like were seen between the IBA-rich and water-rich phases in the 125-mL glass jars. The IBA-rich phase was injected in order to make sure that enough IBA was present because the first volume experiments had little IBA present in the water-rich phase when the water-rich phase was injected at 25 °C and then had the temperature lowered to 20 °C. The IBA-rich phase was injected to the end of the capillary rather than in the center because,

sometimes, too much IBA was present in the water-rich phase when the temperature was lowered from 25 °C to 20 °C. The above procedure allowed some unusual results to happen, but enough IBA was present so that the EIT of a surfactant system in IBA/water could be measured.

With this procedure, the IBA-rich phase would generally be present when the rotation rate was increased to 6000 rpm and the temperature was raised from the initial 20 °C to between 24 °C to 25 °C, allowing IBA-rich drops within either other IBA-rich drops or the surfactant-rich phase. Figures 5.1 and 5.2 show a drop of IBA emerging from the left side of the capillary and being inside another drop of IBA. At times, this behavior could occur when some IBA-rich drops were off-screen and close to the endcaps with another drop IBA-rich drop was stretching out towards the endcaps. Then, these drops could merge as seen below in Figure 5.1. Figure 5.1 shows the drop appearing at 24 °C at 7000 rpm while Figure 5.2 shows the drop appearing at 20 °C at 4000 rpm.

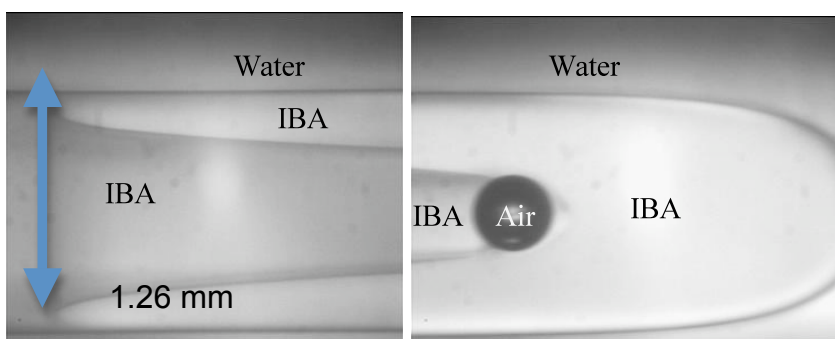


Figure 5.1. IBA-rich phase coming from left side of capillary at 7000 rpm at 24 °C.

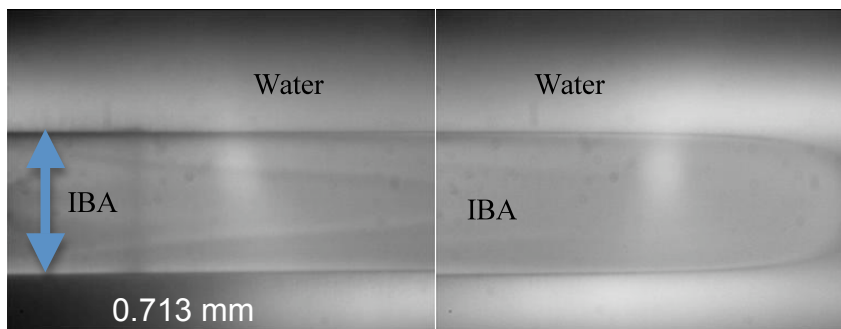


Figure 5.2. IBA-rich drop coming from left side of capillary at 4000 rpm at 20 °C.

The IBA-rich drops at 7000 rpm and 24 °C have a different color contrast while the IBA drops at 4000 rpm and 20 °C have similar color contrast. Part of this color difference is because possibly temperature difference and one IBA-rich drop is equilibrating from the cooler temperature to the higher temperature and because one IBA-rich drop has shared a boundary with surfactant. So, the IBA-rich phase that is coming from 7000 rpm and 24 °C is equilibrating with the other IBA drop while the IBA-rich drop at 20 °C and 4000 rpm is already equilibrated. The IBA drop coming from the left side at 7000 rpm and 24 °C is closer to 20 °C as seen in appearance in comparing Figures 5.1 and 5.2. The colder IBA-rich phase tends to be darker in color while the lighter color IBA-rich phase is more indicative of 24 °C. After 27 °C, the IBA-rich drops become darker and grayer. IBA drops tend to be brightest in appearance between 24 °C and 27 °C.

However, trying to distinguish among the IBA-rich phase, SDS-rich phase, and impurities from IBA (the IBA used was 99.5% pure and the surfactant was 99% or more pure) or other unknown components can be difficult when there are only slight differences in color contrast. Initial experiments were done without recrystallization because these impurities in the surfactants helped to give some

of the unusual behavior. Later experiments used recrystallized surfactant, and the data for the recrystallized surfactants were analyzed and used. Figures 5.3, 5.4, and 5.5 exemplify some instances that can be hard to tell what is what. In Figure 5.3, the outer boundary seems to be IBA/water, but inside the drop, there are smaller drops that could be impurities or IBA. The approximate ratio of the size of the smaller drops to the much larger drop indicates that the smaller drops are impurities, but a definitive answer of what the smaller drops are would be hard to achieve. However, the trail of fluid behind and around the smaller drops is IBA because, in all of the IBA/water movies, the impurities were visible drop within drop while small concentrations of IBA could form trails. Figure 5.4 shows a drop within a drop from two different movies of IBA/SDS/water. An example of uncertainty or not knowing exactly what the observed drop is: the 9000 rpm drop within a drop has a trail of smaller drops; these smaller drops tend to be IBA for an IBA/water system but the slightly larger drop has shading that could be either an impurity or IBA. The outer drop of 9000 rpm has the sharp boundary characteristic of IBA/water. The outer drop of 7000 rpm has a faded boundary; sometimes, IBA/water can have a less-than-sharp boundary but, generally, only after 20 minutes or more at 29 °C or higher or with a small concentration of IBA. The movie at 7000 rpm had a large amount (more than 40 μL) of IBA and should have had a sharp IBA/water boundary. This faded boundary might indicate it being a SDS/water boundary. The shading of the inner drop of the 7000 rpm could be either IBA or impurity. The shading is difficult to distinguish what the drop is.

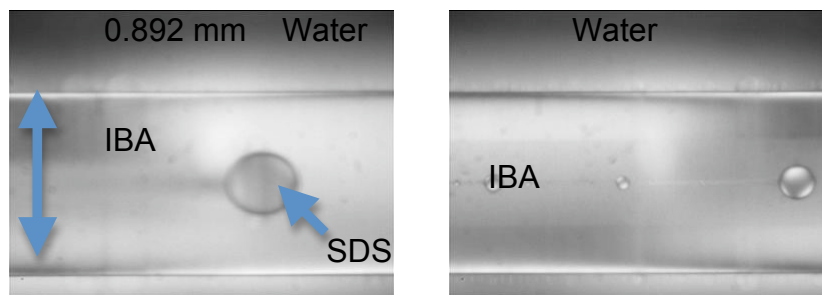


Figure 5.3. IBA/SDS/Water at 9000 rpm at 29 °C.

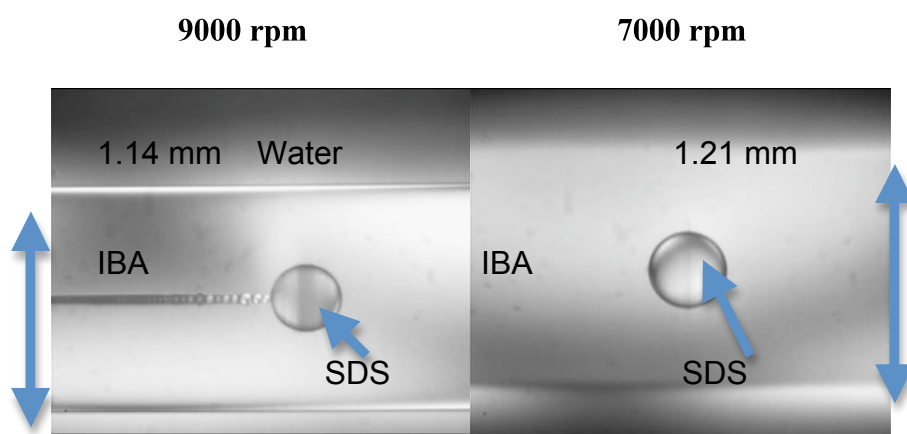


Figure 5.4. IBA/SDS/Water at 9000 rpm and 7000 rpm at 29 °C.

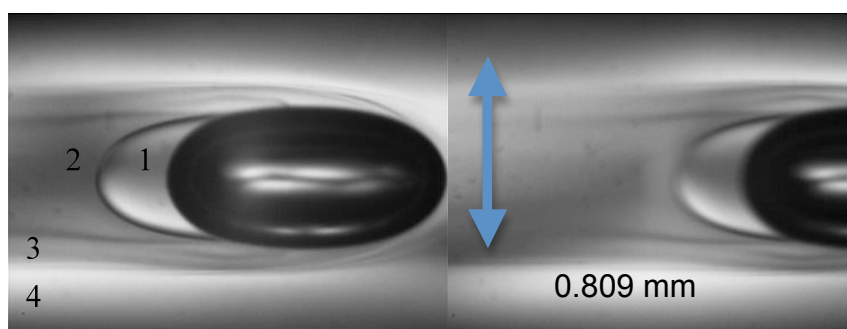


Figure 5.5. IBA/SDS/Water with black air bubble at 10000 rpm at 29 °C.

Figure 5.5 shows an air bubble (black drop) surrounded by three different boundaries. The two boundaries closest to the air bubble are probably IBA while the outermost boundary is probably SDS/water. The shading of area two is most likely IBA because that is the most typical shading of IBA at 29 °C. Area 3 is most likely SDS or the flow motions of the air bubble and IBA drops in the SDS/water-rich phase. Area 1 is most likely IBA because of its light shading. This really light shading is generally seen for IBA between 24 °C and 27 °C. Area 4 is just the water-rich phase. Figure 5.5 is an example of the ambiguous of telling the difference between IBA and SDS.

Figures 5.6-5.11 show how other images give a much clearer idea of what is the IBA-rich phase, SDS-rich phase, or an impurity or unknown component. In the left side of Figure 5.6, the two smaller drops with question marks inside are hard to tell whether the drops are impurities or the IBA-rich phase. Seconds later, on the right side of Figure 5.6, the image of the merged smaller drops are shown merging into the larger IBA-rich drop. This merging was one way to tell what a drop was. The two large drops already labeled IBA are known to be IBA because the lighter shade of the IBA was normally seen in IBA/water systems at 29 °C while the slightly darker boundary IBA was seen in IBA/SDS/water systems.

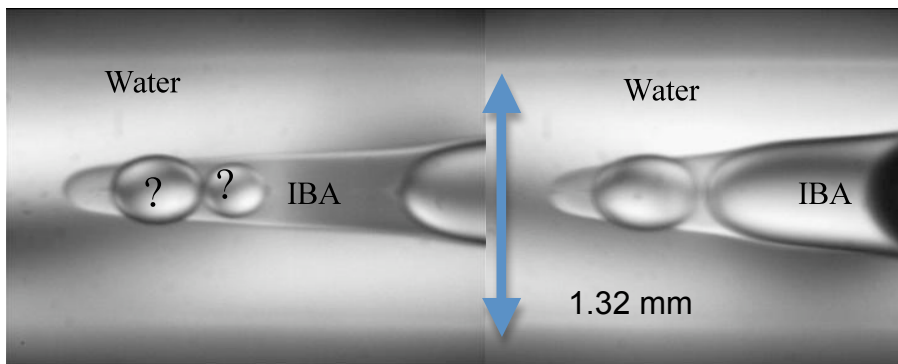


Figure 5.6. IBA/ SDS/Water at 8000 rpm at 29 °C.

The IBA-rich drops with slightly darker boundaries were identified as IBA drops because of several observations. One observation was a drop within a drop at 20 °C. Figure 5.7 shows an example of this observation. Image A of Figure 5.7 shows IBA/ dodecyltrimethylammonium chloride /water while image C of Figure 5.7 shows IBAS/DS/water; images B and D of Figure 5.7 show IBA/water. Images A and D are instances when the boundaries were not as sharp as instances B and C. In comparing A to D and C to B, the IBA/surfactant/water systems had a sharper, darker boundary than for IBA/water systems. This trend continued as the temperature increased.

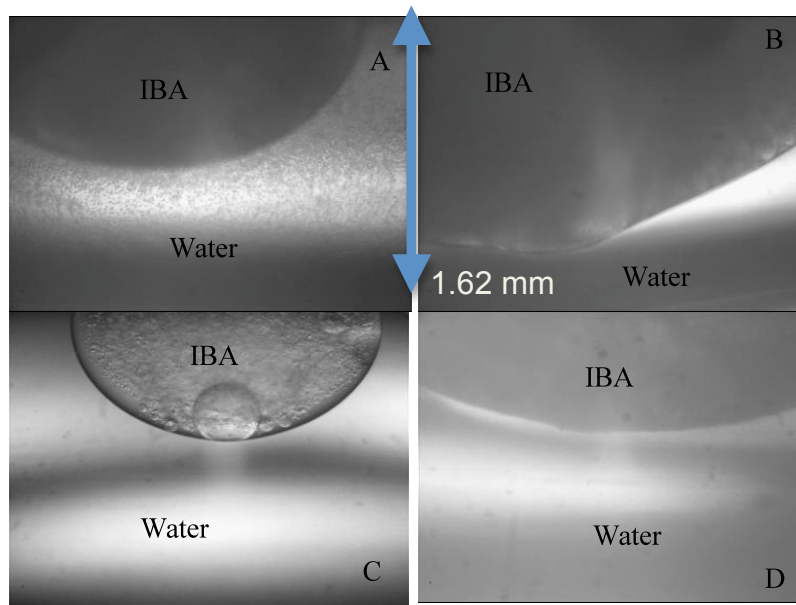


Figure 5.7. IBA/water and IBA/surfactant/water systems at 20 °C.

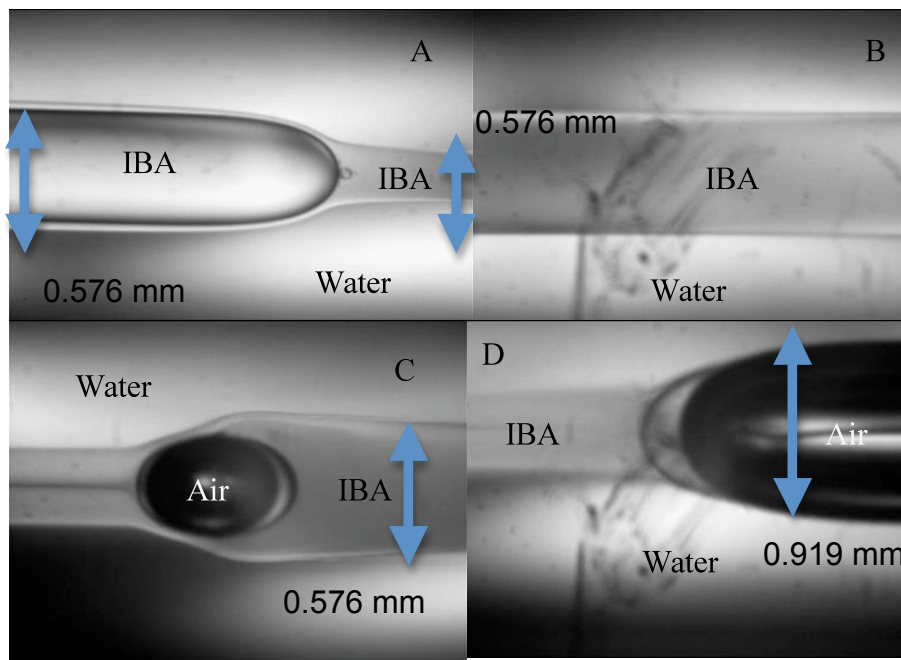


Figure 5.8. IBA/water and IBA/surfactant/water systems above the UCST between 27-30 °C. Images A and C: IBA/SDS/water at 8000 rpm at 29 °C. Image B: IBA/water at 8000 rpm at 27 °C. Image D: IBA/water at 8000 rpm at 29 °C.

Figure 5.8 shows instances of the darker, sharper boundary in IBA/surfactant/systems. Refractive index gradients can be used to measure concentration gradients because a concentration gradient causes a refractive index gradient. A larger refractive index gradient indicates a larger concentration gradient or sharper boundary if between the same species. The surfactant was causing a larger concentration gradient and hence sharper boundary. Images A and C are IBA/SDS/water at 8000 rpm at 29 °C while images B and D are IBA/water at 8000 rpm at, respectively, 27 °C and 29 °C. In comparing C and D, the air bubble is surrounded by another IBA-rich drop; this IBA drop has a sharper boundary in contrast to IBA-rich drop that is not surrounding the air bubble. However, the IBA/surfactant/water system has a darker boundary than the IBA/water system. In comparing A and B, B has a shade similar to the smaller radius diameter of the IBA-rich drop in image A but image A also has a darker, sharper boundary IBA-rich phase. The sharper, darker boundary IBA-rich drop is surrounded by the lighter boundary IBA-rich drop. Hence, in comparing the IBA/water systems to the IBA/surfactant/water systems, a drop of IBA could be identified versus an impurity or surfactant.

Figure 5.9 shows another instance that helped to identify what drops were IBA-rich phase, unknown component, or surfactant-rich phase. The images are in sequence from A to B to C to D. In image A of Figure 5.9, the SDS-rich phase is surrounding the air bubble with the IBA-rich drop off to the left. Over seconds from images A to D, the third interface, possibly SDS-rich drop, spins out from the air bubble to surround the IBA drop so that final boundaries going from

outward to the center are water/SDS, SDS/IBA, and IBA/air. The shading and boundary sharpness of the SDS-rich phase is different from the IBA-rich phase and impurities. The SDS-rich phase does not seem to have any real boundary as opposed to the IBA/water boundary or impurity/water boundary rather SDS-rich phase seems to have an interface that dissolves and is only apparent under special circumstances. In one circumstance, the air bubble allowed the SDS-rich phase to form around it and form what appears to be an interface as seen in Figure 5.8, the air bubble helps to darken and sharpen boundaries. The interface of the third drop, possibly SDS-rich phase, has more of flow/fluid motions appearing than those that are observed in a system that has not thickened or become more gel-like in appearance, the water-rich phase; i.e., fluid/flow motions that could not be observed in IBA/water can be seen in IBA/surfactant/water systems.

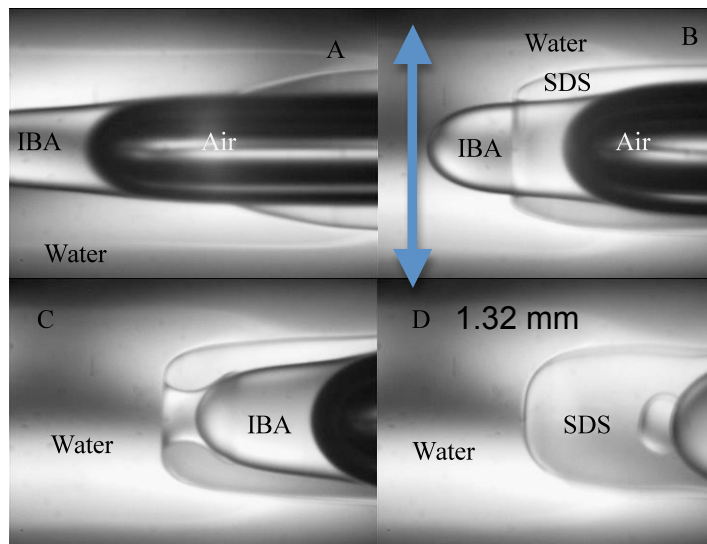


Figure 5.9. IBA/SDS/water at 29 °C at 8000 rpm.

A third instance that helped to identify the dark, sharper boundaries as IBA-rich was when we dropped the rotation rate from above 6000 rpm to zero and then increased the rotation rate back to the original value. Figure 5.10 shows this instance, which occurred multiple times. In each of the instances the rotation rate was above 6000 rpm and then dropped to zero rpm and then increased to the original rotation rate. All of the A images represent the IBA before the decreased rotation rate; all of the B images shows what happens after the rotation rate has been decreased and then increased. In all three occurrences, the B images show that the IBA drop has at least a slightly darker shade of boundary.

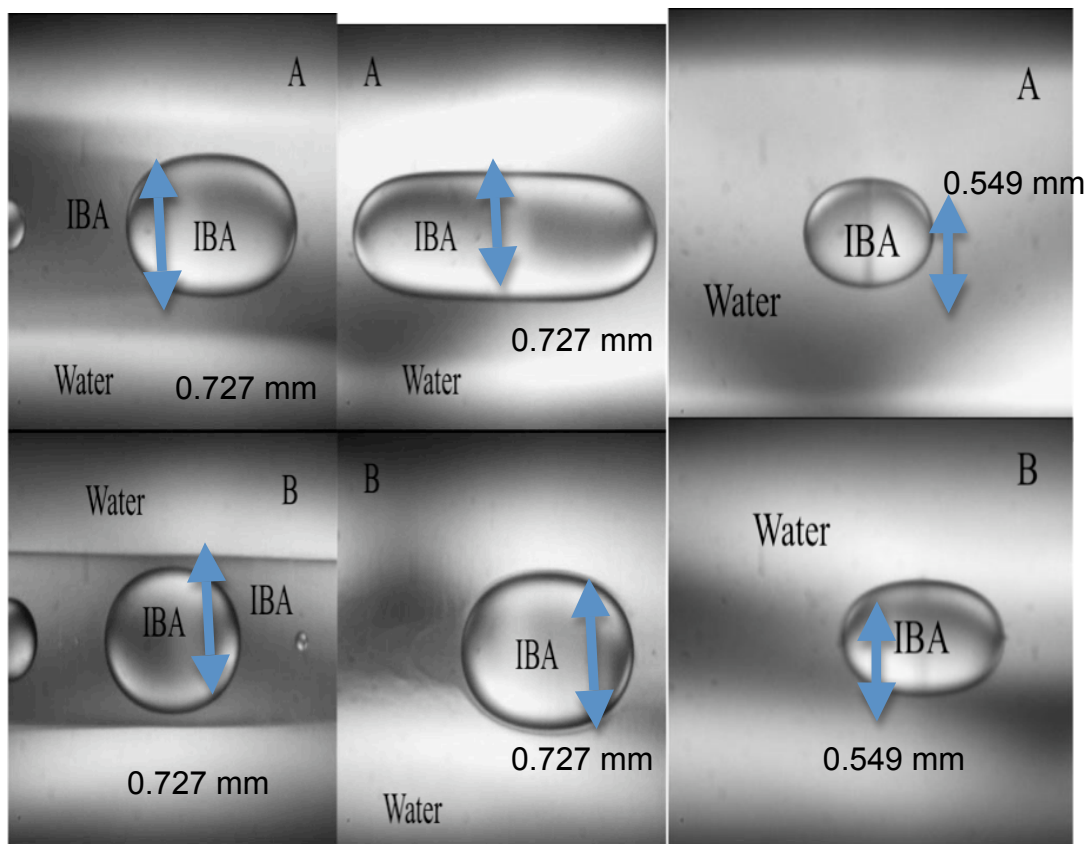


Figure 5.10. IBA/SDS/water at 29 °C between 7000 rpm to 15000 rpm.

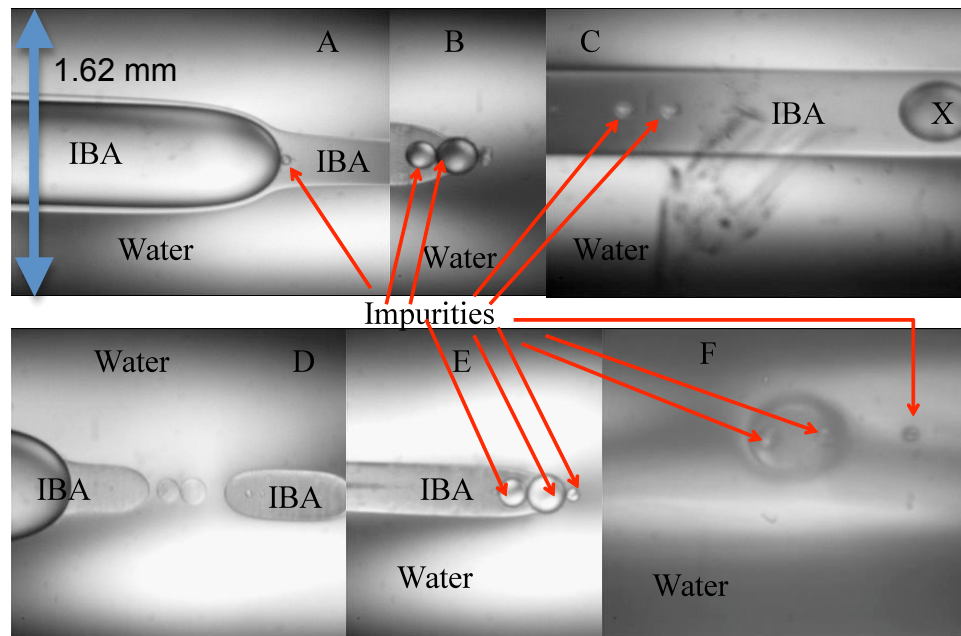


Figure 5.11. IBA/SDS/water and IBA/water at 29 °C at 8000 rpm.

Figure 5.11 shows impurities in IBA/surfactant/water and IBA/water systems at 29 °C at 8000 rpm. Images A,B, D, and E are IBA/SDS/water systems while images C and F are IBA/water systems. Impurities from the surfactant and IBA which were not 100% pure are shown by an X and red arrows. Image D shows only IBA-rich drops; image A shows only a very small impurity or unknown component. Larger impurities are shown in IBA-rich drops in IBA/SDS/water systems in B and E. C and F show large and small impurities in IBA drops in IBA/water systems. In all of the instances, the impurities drops are much smaller in radii and shape than IBA-rich drops. The impurities are also either much brighter or darker in appearance. Thus, impurities or unknown drops that cannot be attributed to the IBA-rich, water-rich, or SDS-rich phase can be identified by their smaller radii and shape and difference shading. So, Figures 5.6-5.11 show

how IBA, surfactants, and impurities can be identified based on knowledge and comparison.

Comparison of Behavior

IBA/surfactant/water systems showed some differences in behavior compared to IBA/water systems. One difference in behavior was briefly mentioned above in regards to Figure 5.10. From Figure 5.10, in the group to the far right, the A image of IBA-rich phase was at 15000 rpm and the B image was at 13000 rpm. Generally, above the UCST, the higher rotation rates of IBA/water have a darker boundary but, in this instance, the surfactant in the IBA/surfactant/water system helped to darken the IBA-rich boundary. In the group to the far left, the IBA-rich phase surrounding the smaller IBA-rich drop became markedly darker; this is another difference from IBA/water systems: in IBA/water systems, when the rotation rate is increased, decreased, and then increased, the IBA drop will decrease in radius and have a lighter, less sharp boundary. In the middle group, the A image had only had the small IBA-rich drop but the B image had two IBA-rich drops; image B shows a faint IBA drop that is to the left of the lone IBA-rich drop seen in image A. This behavior would not have occurred in IBA/water systems. These differences in behavior helped to identify the IBA-rich phase from impurities and surfactant-rich drops. Figure 5.12 shows what happened when the rotation rate had been decreased to zero rpm: a darker drop was surrounded by a lighter, more transparent drop.

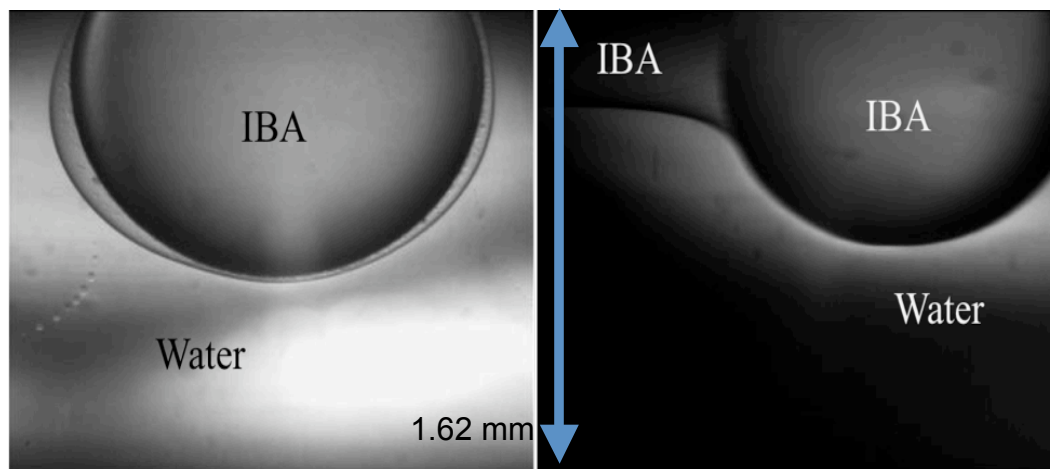


Figure 5.12. IBA/SDS/water at 29 °C and 0 rpm.

In both images of Figure 5.12, the water-rich phase surrounds the darker IBA-rich drop that is surrounded by another lighter IBA-rich drop. This behavior is exclusive to the IBA/surfactant/water systems. Other IBA/water systems might have impurities inside of the IBA drop but no IBA-rich drop within IBA-rich drop was observed in any of the experiments that we conducted.

Another difference in behavior that was briefly mentioned above was that the IBA/surfactant systems show fluid/flow motions. In IBA/water systems, any fluid/flow motions are seen when a needle is injecting IBA or an air bubble behaves in an unusual manner in a long drop of IBA, which has either a small, medium, or large concentration. Figures 5.13 and 5.14 shows these behaviors.

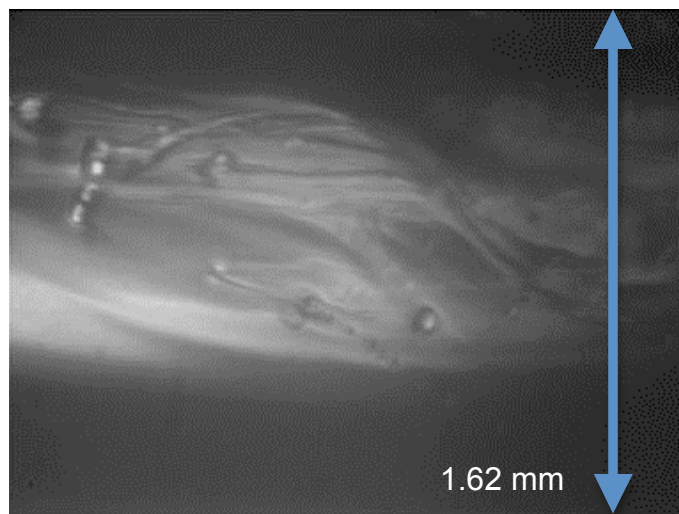


Figure 5.13. IBA being injected into water-rich phase at 24 °C.

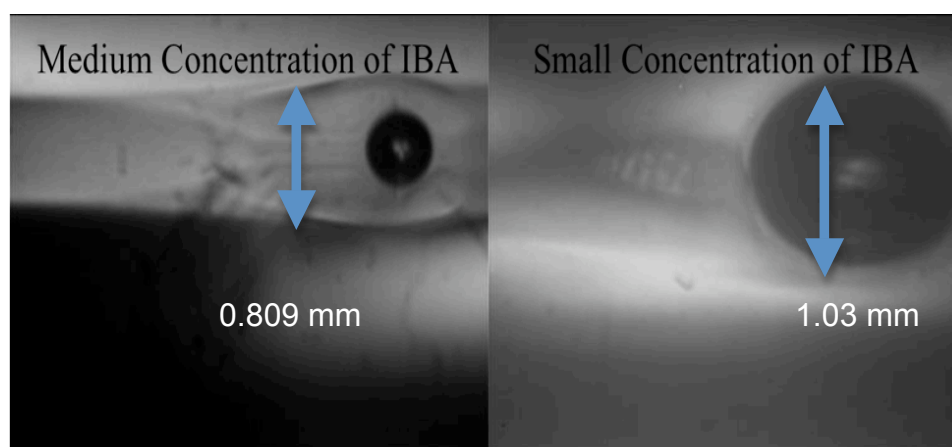


Figure 5.14. Fluid motions in IBA/water system between 27 °C and 28 °C.

IBA/surfactant/water systems will have additional fluid/flow observed even when the rotation rates have been decreased to zero. The IBA/surfactant/water systems also have fluid/flow motions shown more distinctly. Figures 5.15 and 5.16 exemplify these behaviors.

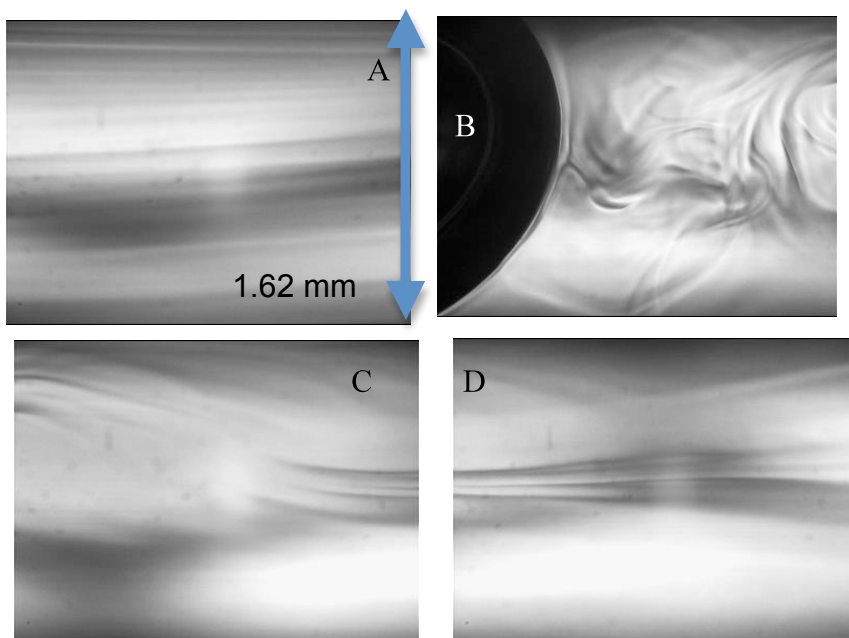


Figure 5.15. IBA/surfactant/water system at 0 rpm and above UCST.

Image A from Figure 5.15 shows what happens after the air bubble has gone past. Images B, C, and D shows fluid/flow motions after the rotation rate has dropped to zero.

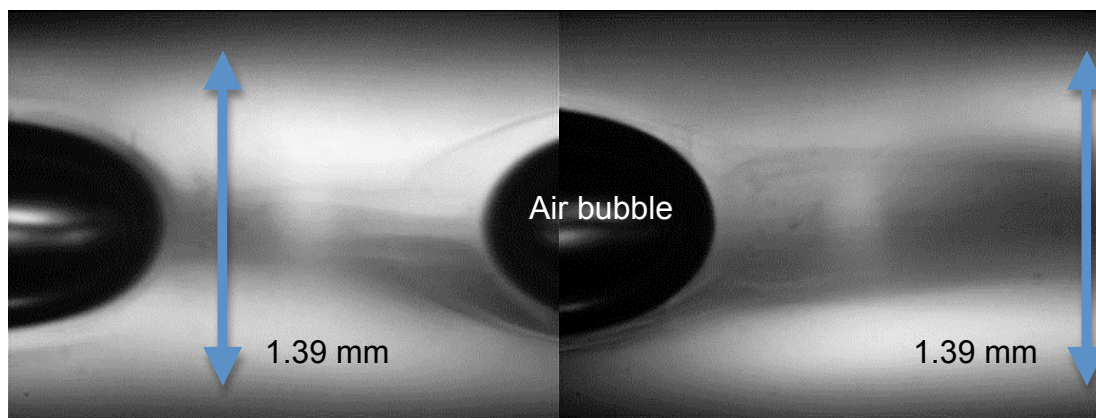


Figure 5.16. IBA/surfactant/water system at 8000 rpm and above the UCST.

Figure 5.16 shows how fluid flow can be seen between the two air bubbles and trailing after an air bubble. IBA/water system would only have shown fluid flow if an IBA-rich drop were between the air bubbles or trailing after an air bubble.

A third difference is the appearance of the IBA-rich drops in IBA/water systems versus IBA/surfactant/water systems. At times, the IBA drops are similar in shading or levels of grayness; when the IBA-rich drop is above the UCST and not interacting with surfactant, the IBA-rich phase is the same shading and similar radii as an IBA-rich drop in IBA/water systems. When the IBA-rich phase is interacting with the surfactant, the IBA-rich drop has a darker, sharper boundary and, generally, has a larger radius as seen when comparing the lighter IBA-rich phase that both surrounds and trails behind the darker IBA-rich phase.

A fourth difference is how the IBA drop seems to adhere to the needle above the UCST in an IBA/surfactant/water system. Generally, the IBA-rich drop does not adhere to the needle. Figure 5.17 shows how a small IBA-rich drop is taken away from a larger IBA-rich drop. The plunger was never pushed; the smaller drop simply attached itself to the needle after the needle touched the larger IBA-rich drop.

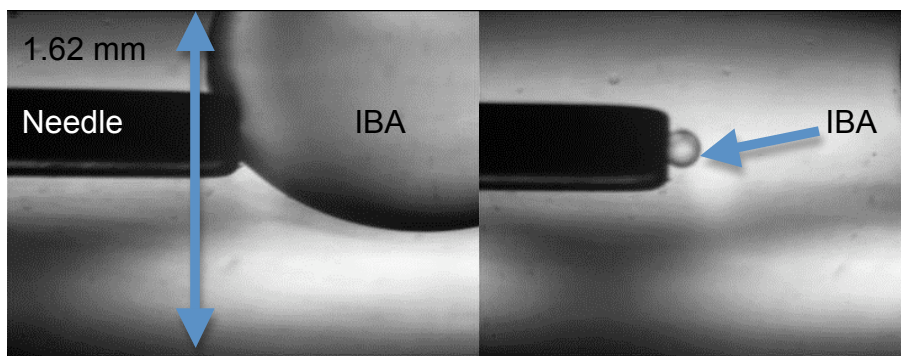


Figure 5.17. IBA/surfactant/water system at 0 rpm and above the UCST with a needle taking a small IBA drop from a larger IBA drop.

A fifth difference is how the darker and lighter IBA-rich drops in IBA/surfactant/water systems do not dissolve as quickly as the IBA-rich drops in IBA/water systems. The IBA drops in IBA/surfactant/water systems lasted much longer than the IBA drops in IBA/water systems above the UCST. While IBA-rich drops dissolved in less than five minutes above the UCST, the IBA-rich drops in IBA/surfactant/water systems could last longer than 20 minutes.

A sixth difference is that IBA/surfactant/water systems can, at times, have three phases below UCST. Then, as the temperature rises above the UCST, a third phase will start to dissolve so that only two phases are present, leaving only IBA and water. The IBA-rich phase will also eventually dissolve, but the third phase is believed to be a surfactant-rich phase because when the temperature reached 25-26 °C, the third phase would immediately dissolve whereas the IBA-rich phase would take minutes to dissolve. Also, generally, this third phase would appear when the jar containing the system was shaken. Then, a filmy bubble from the surfactant-rich phase would form between the IBA-rich and

water-rich phases. Thus, the third phase was assumed to be surfactant-rich rather than an impurity or unknown compound.

When the system of IBA/water/SDS was cooled to 20 °C and then had its temperature increased to 30 °C, a concentration gradient between SDS-rich solution and water-rich solution would appear as the rotation rate was started at 7000 rpm for 20 °C. Around 25 °C, an IBA-rich drop would travel from a spot off-camera to the center of the SDT where the SDS's concentration gradient with water-rich phase would surround it. Figure 5.18 shows an example of IBA-rich drop surrounded by SDS-rich phase which is in the bulk water-rich phase.

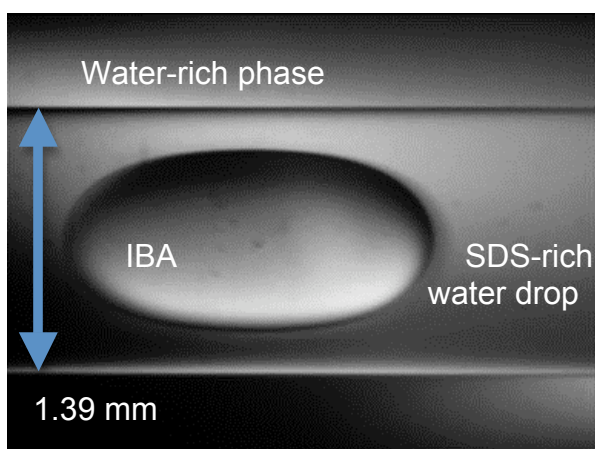


Figure 5.18. An example of IBA/water/SDS with a drop of IBA inside of long SDS-rich water drop which is in the bulk water-rich phase at 25 °C at 7000 rpm.

Generally, between 27 °C and 28 °C, the SDS-rich phase would redissolve into the water-rich phase as shown in Figure 5.19.

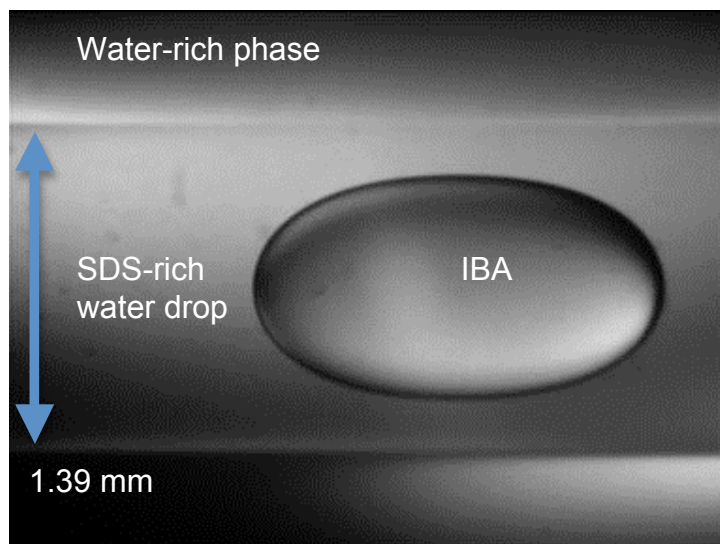


Figure 5.19. An example of IBA/water/SDS with an IBA-rich drop inside of long SDS-rich water drop which is in the bulk water-rich phase at 29 °C at 7000 rpm.

One similarity in behavior that is mentioned above is that air bubbles help to darken IBA boundaries no matter if the IBA-rich drop is in IBA/water or IBA/surfactant/water systems. Figure 5.20 shows this behavior. As long as the air bubble is large enough, the air bubble draws the IBA away from the water-rich phase and closer to the air bubble, which gives the IBA-rich drop a true interface rather than a no-so true interface with water. By drawing the IBA away from the water-rich phase, the IBA-rich drops hence have a sharper boundary. This behavior also occurs if the IBA-rich drop attaches to either the left or right side of the tensiometer's capillary.

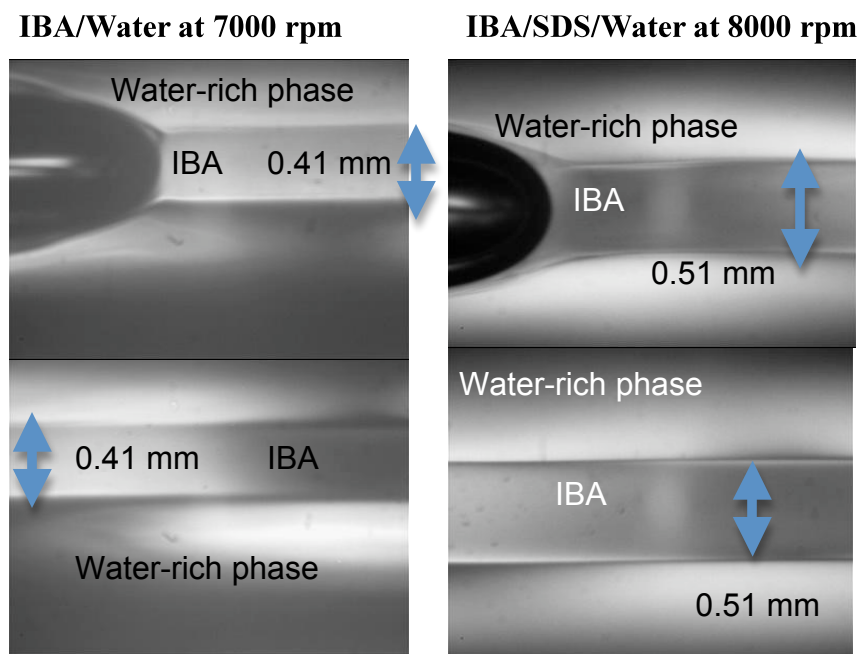


Figure 5.20. IBA/Water and IBA/SDS/Water above the UCST.

In Figure 5.20, the long drop continues in the image with the air bubble to the image below it. In the initial frame, the long IBA-rich drop of IBA/water and IBA/SDS/water look similarly sharp but the second image shows a slightly sharper IBA-rich drop in the IBA/SDS/water system than in the IBA/water system. This behavior was generally observed.

A second similarity is that as the IBA-rich phase goes further out from the air bubble, the IBA-rich phase has a lighter boundary and smaller radius. This behavior is seen in both IBA/water and IBA/surfactant/water systems. Figures 5.21-5.24 exemplify this behavior. Figure 5.21 shows the IBA/water system while Figures 5.22-5.24 show IBA/SDS/water.

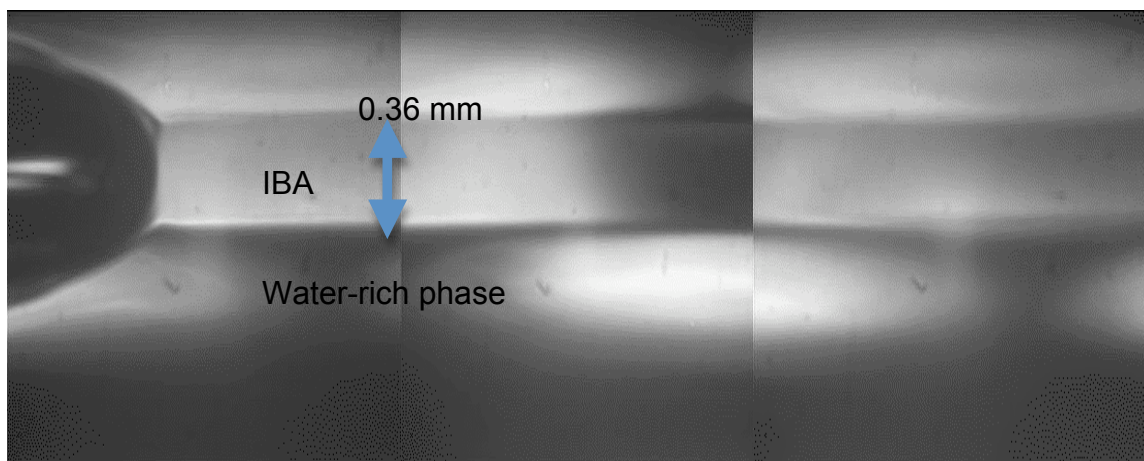


Figure 5.21. IBA/Water at 7000 rpm and above the UCST showing the IBA's sharp boundary fading.

In Figure 5.21, going from left to right, the images show a sharp boundary starting to fade as the IBA-rich drop's boundary gets further from the air bubble. The IBA-rich drop's boundary loses its sharpness as it gets further from the air bubble because the IBA is starting to lose a true interface between the air bubble and itself so that less IBA starts to dissolve into the water-rich phase and becomes more diffuse. Figure 5.22 show this same observation except that the IBA/SDS/water had a longer IBA-rich drop that stayed sharper over a longer distance. Figures 5.23 and 5.24 show how this sharpness that that air bubble initially gave fades over time. Figures 5.23 and 5.24 were taken, respectively, 3 and 8 minutes after Figure 5.22.

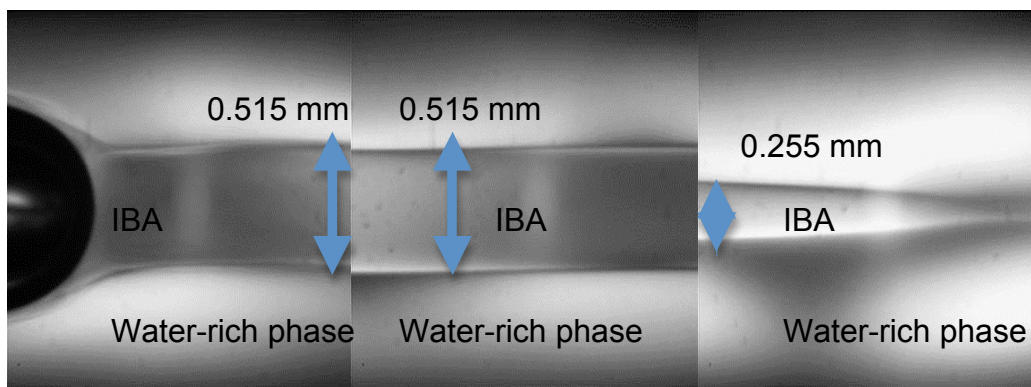


Figure 5.22. IBA/SDS/Water system at 8000 rpm above the UCST; the IBA's sharp boundary fading.

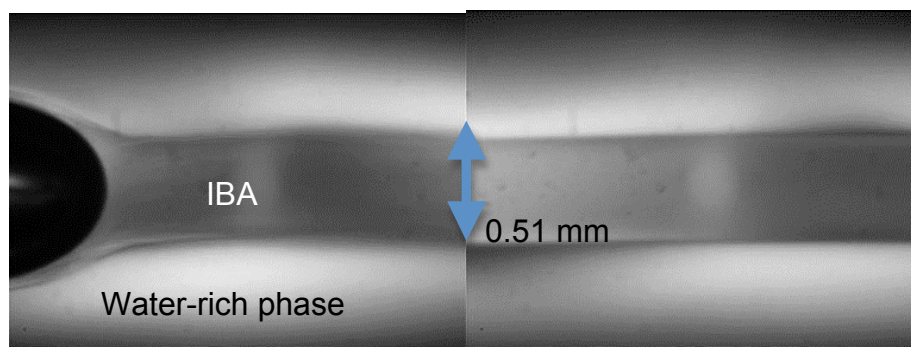


Figure 5.23. IBA/SDS/Water system that was 3 minutes later after Figure 5.22.

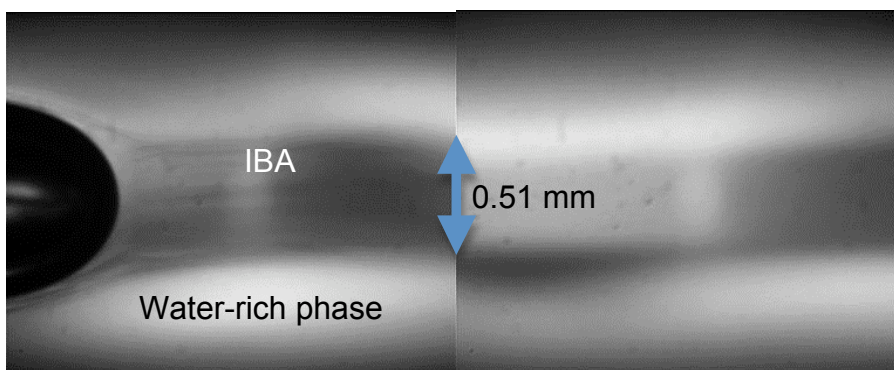


Figure 5.24. IBA/SDS/Water system that was 8 minutes later after Figure 5.22.

A third similarity is that IBA drops appear darker at 20 °C than at 29 °C or higher. The above Figures of 5.1, 5.2, and 5.7 help to show this similarity. In general, for the miscible and partially miscible systems (with a critical solution temperature) that we tested, the further the lighter phase was from the critical solution temperature and further into the immiscible region, the darker the lighter phase's drop became.

A fourth similarity is the Marangoni instability.⁴⁹ The Marangoni instability⁴⁹ was seen multiple times in IBA/surfactant/water and IBA/water systems. Figures 5.25 and 5.26 show this behavior. Both figures show the IBA-rich drop's boundary moving outward through a kicking motion.

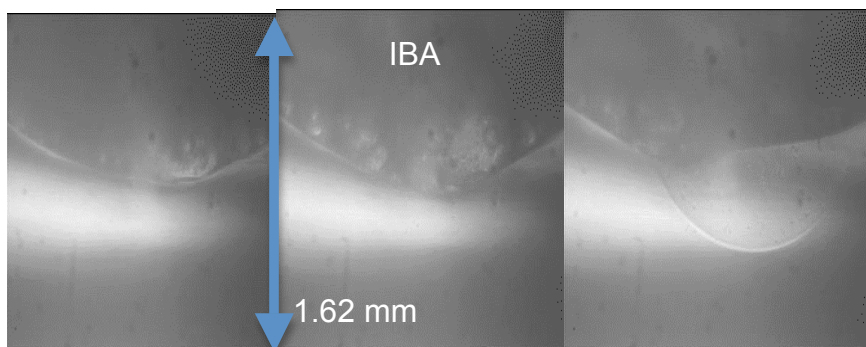


Figure 5.25. Marangoni instability in IBA/water at 20 °C.

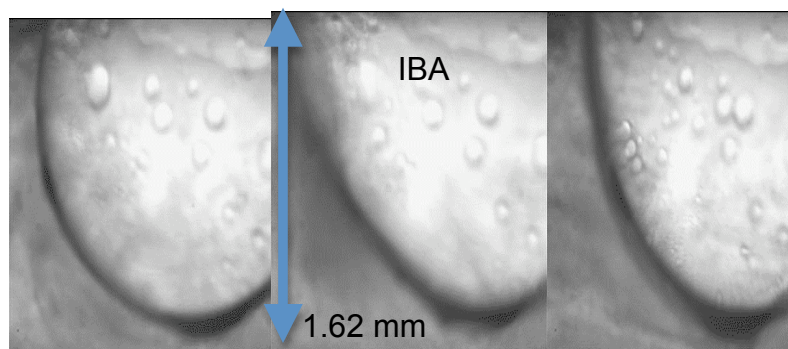


Figure 5.26. Marangoni instability for IBA/SDS/water at 20 °C.

One similarity and difference in behavior is that IBA-rich drops can still endpinch in IBA/surfactant/water systems. Figures 5.27 and 5.28 show this behavior in IBA/water and IBA/SDS/water systems.

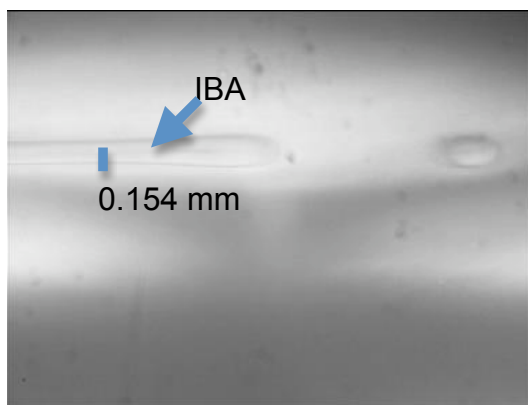


Figure 5.27. IBA/water endpinching at 27 °C and 8000 rpm.

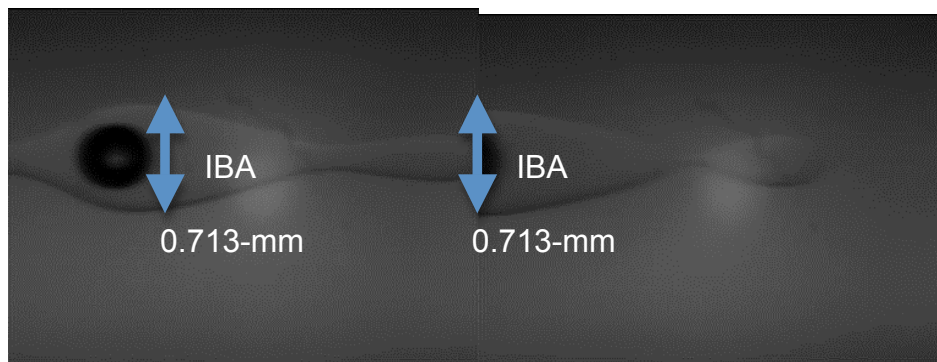


Figure 5.28. IBA/dodecyltrimethylammonium chloride/ water endpinched at 20 °C and 15000 rpm.

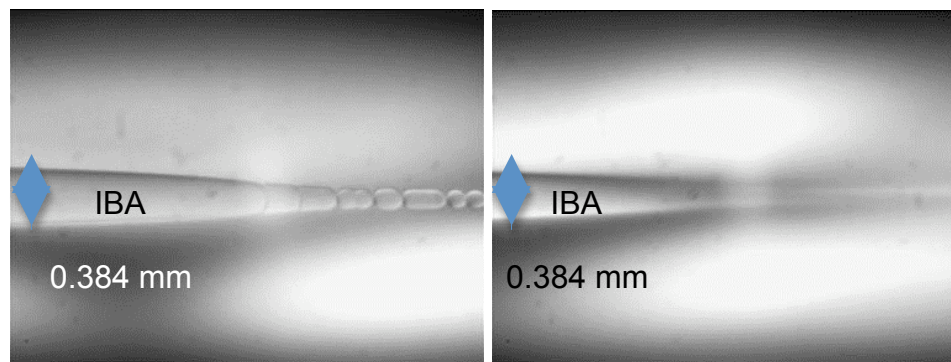


Figure 5.29. IBA/SDS/water almost end pinching at 27 °C and 29 °C at 8000 rpm.

However, the IBA/dodecyltrimethylammonium chloride/ water end-pinch at 20 °C and 15000 rpm while the IBA/water end-pinch at 27 °C and 8000 rpm, though IBA/SDS/water almost end pinched above the UCST as seen in Figure 5.29. The image to the left in Figure 5.27 is at 27 °C while the image to the right is at 29 °C. Also, the IBA/water system had more occurrences of end-pinching than the IBA/surfactant/water systems. One possible explanation for this difference is the IBA/surfactant/water systems had more volume and that less IBA had been present than end pinching would have happened more frequently.

Another behavior that was both similar and different was how drops merged. In some instances the IBA-rich drops of an IBA/surfactant/water system would merge like IBA/water would. In several other instances, the IBA drops would merge differently. Figure 5.30 shows typical IBA drops merging at 20 °C: two drops meet and their ends dissolve into each other. In general, the IBA/surfactant/water and IBA/water systems have their drops merge in this manner at any temperature or rotation, exactly like Figure 5.30 except above the UCST and higher rotation rate: one drop would merge into another without

anything unusual seen. Figure 5.31 shows typical IBA-rich drops merging.

Figure 5.32 shows an atypical IBA-rich drop merging at 20 °C and 3000 rpm.

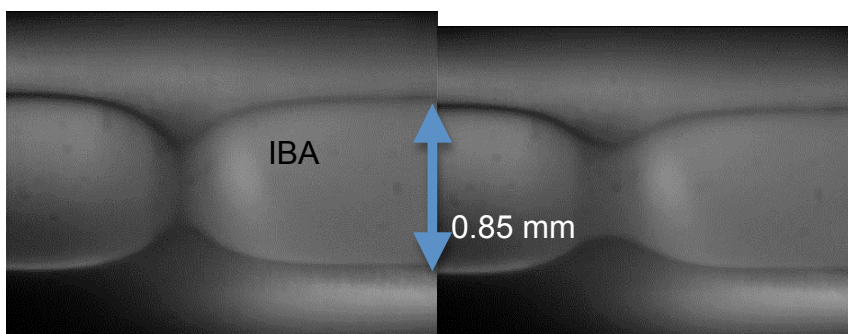


Figure 5.30. IBA/SDS/water at 20 °C and 4000 rpm with drops merging.

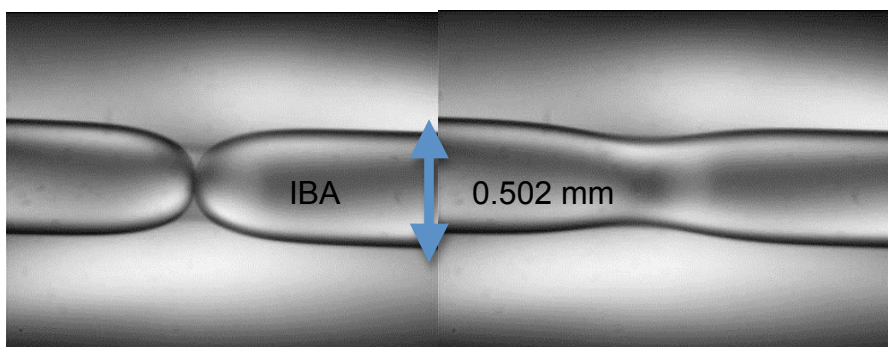


Figure 5.31. IBA/SDS/water above the UCST and 8000 rpm with drops merging.

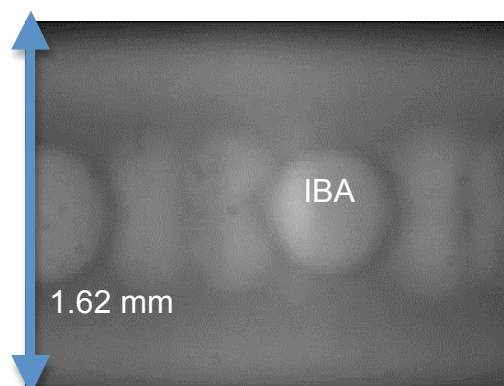


Figure 5.32. IBA/SDS/water at 20 °C and 3000 rpm.

In Figure 5.32, rather than the usual two drops merging, four smaller drops seem to merge into two drops and then those two drops merge into one drop. Figure 5.33 shows another atypical drop merge of IBA/SDS/water but this time the merging drop was at 7000 rpm and 27 °C. The IBA-rich drops were starting to end-pinch but, instead, merged. Another atypical behavior is that the merged drops show the previous length(s) of the drop(s) merged together. Usually, the two drops will merge with no distinct indication of how long the previously unmerged drops were. Figure 5.34 shows another atypical merge for IBA/SDS/water above the UCST at 8000 rpm. In this figure, the two long drops and one short drop of IBA are merging but the length of the short IBA-rich drop can still be seen after all the drops have merged. Figure 5.35 shows the last atypical IBA-rich drops merging. In this figure, the darker IBA-rich phase merges into the lighter IBA-rich phase and the darker IBA-rich phase completely overtakes the lighter IBA-rich phase, making a final dark IBA-rich drop. The IBA-rich drops merging go from image A to image B to image C to image D. So, IBA/water and IBA/surfactant/water systems can have similar merging above and below the UCST but IBA/surfactant/water can have different ways of IBA-rich drops merging.

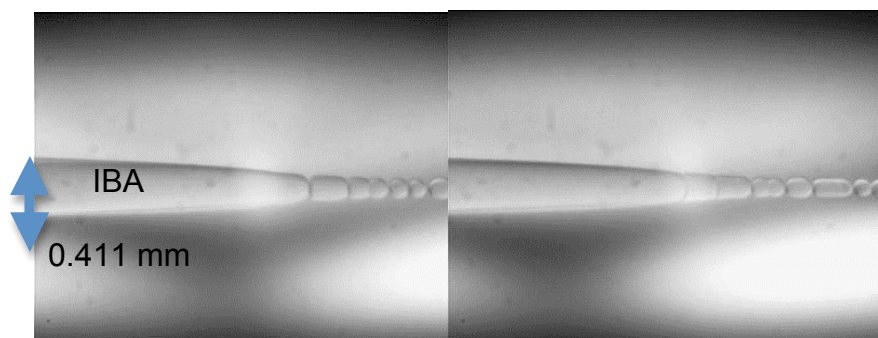


Figure 5.33. IBA/SDS/water at 27 °C and 7000 rpm with the IBA drops merging.

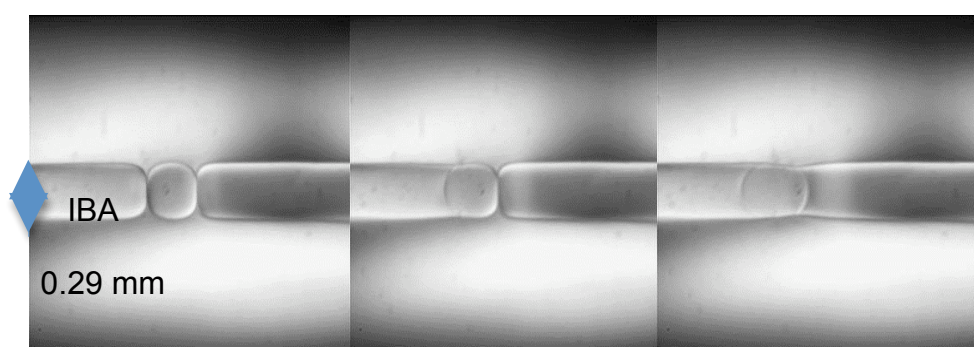


Figure 5.34. IBA/SDS/water above the UCST and 8000 rpm with one short and two long IBA drops merging.

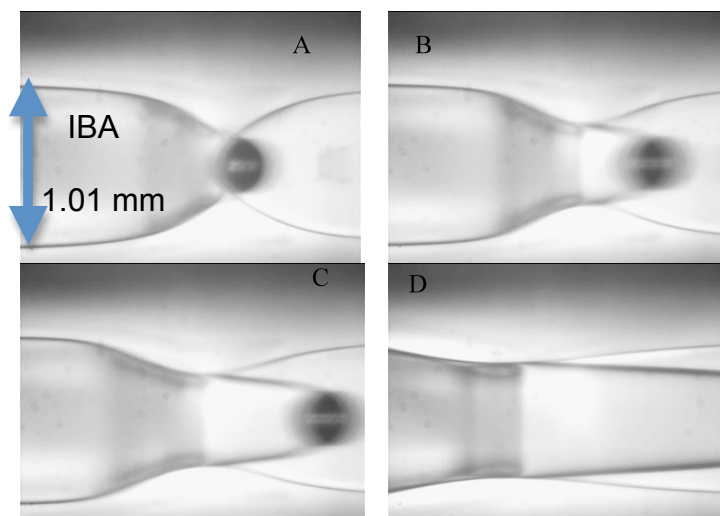


Figure 5.35. IBA/SDS/water drops merging at 24 °C at 7000 rpm going from image A to image D (between A to B and B to C, 0.25 seconds passed; between C to D, 1-2 seconds passed).

EIT and Surfactant Concentration

Besides unique and unusual behaviors in surfactant experiments, we also measured the EIT of IBA/water systems with four different concentrations (0.06 mM, 0.312 mM, 0.603 mM, and 11.8 mM) of SDS and two different concentrations (0.610 and 5.74 mM) of DTAC. These concentrations were chosen because the original concentration of 0.6 mM was determined to be below the critical micelle concentration (cmc). According to Nakamura *et al.*, the cmc of SDS in water is 3.53 mM.⁵⁰ The cmc of DTAC in water is given between 23-46 mM, depending on temperature and place of measurement (where the drop was measured).⁵¹ So, the EITs for IBA/water systems with DTAC should change since the EITs were measured below the cmc, but the cmcs may not be the same in water as they are in IBA/water. While the EITs should decrease, for the three smaller concentrations of SDS below the cmc as the concentrations increase: below the cmc, EIT should decrease as the bulk concentration increases. Figures 5.36-5.50 show the graphs of r^{-3} vs. ω^2 for these IBA/surfactant/water systems between 20 °C and 30 °C. Figures 5.51-5.57 shows the graphs of r^{-3} vs. ω^2 for these IBA/surfactant/water systems at 20 °C.

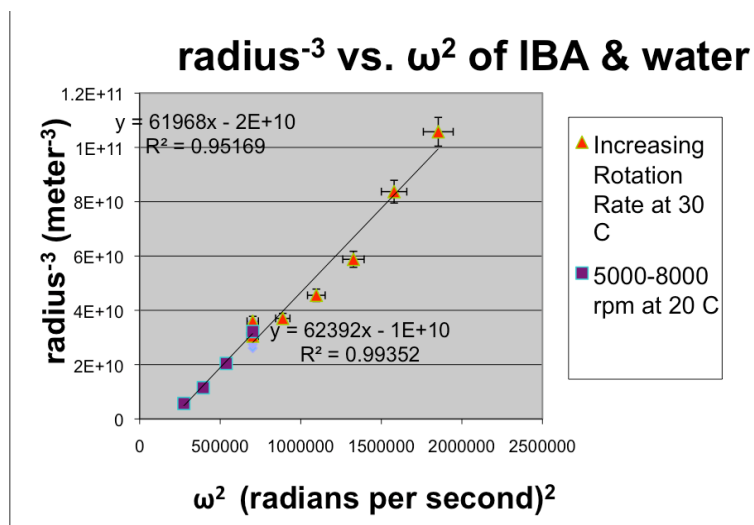


Figure 5.36. Graph of r^3 vs. ω^2 for IBA/SDS/water of 0.0006 M SDS at 20 and 30 °C.

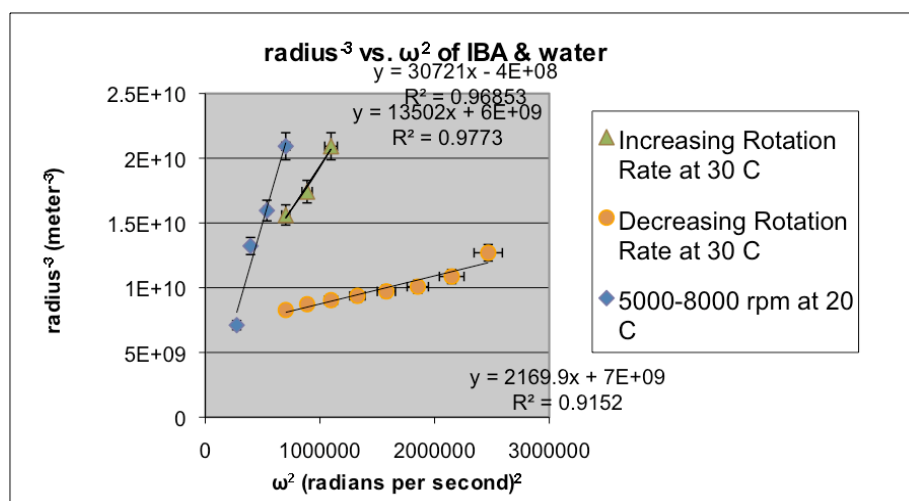


Figure 5.37. Graph of r^3 vs. ω^2 for IBA/SDS/water of 0.312 mM SDS at 20 and 30 °C.

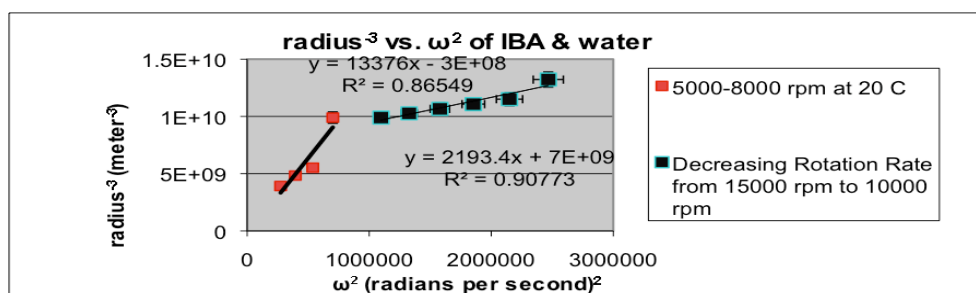


Figure 5.38. Another graph of r^3 vs. ω^2 for IBA/SDS/water of 0.312 mM SDS at 20 and 30 °C.

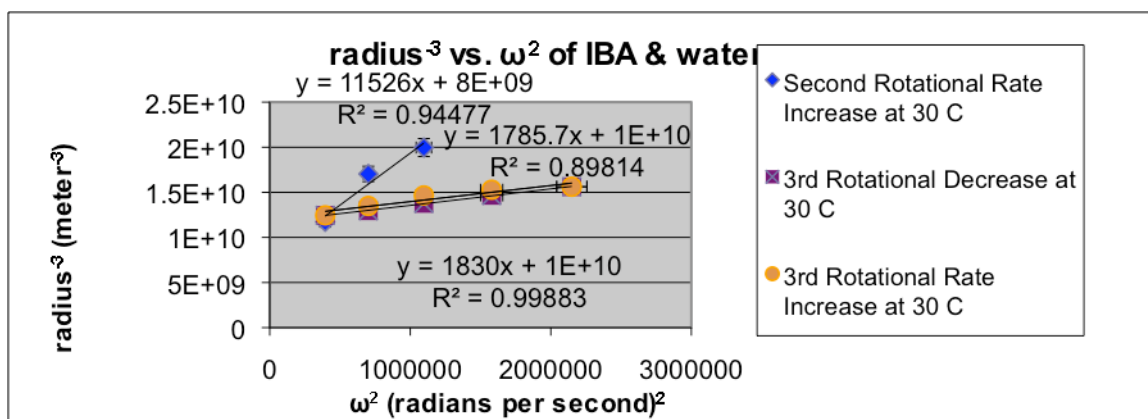


Figure 5.39. A graph of r^{-3} vs. ω^2 for IBA/SDS/water of 0.312 mM SDS with second and third rotational increases and decreases at 30 °C.

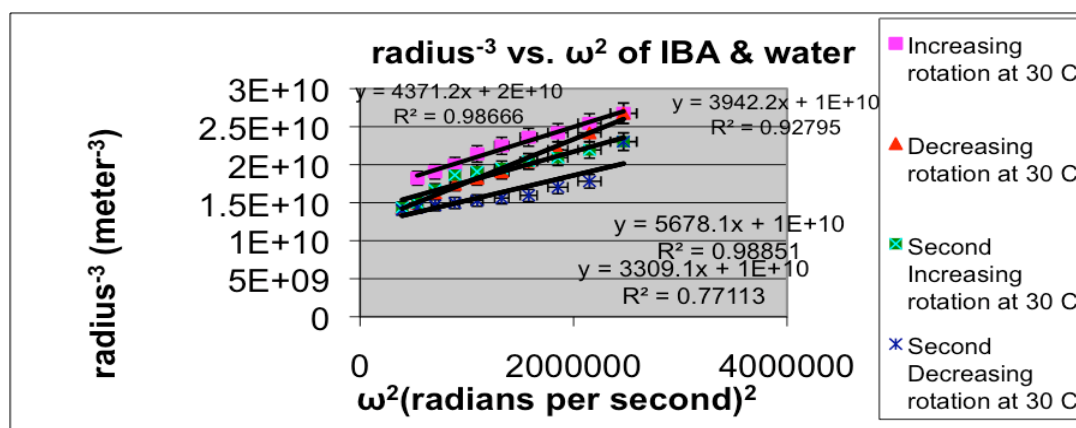


Figure 5.40. Graph of r^{-3} vs. ω^2 for IBA/SDS/water of 0.06 mM SDS at 30 °C.

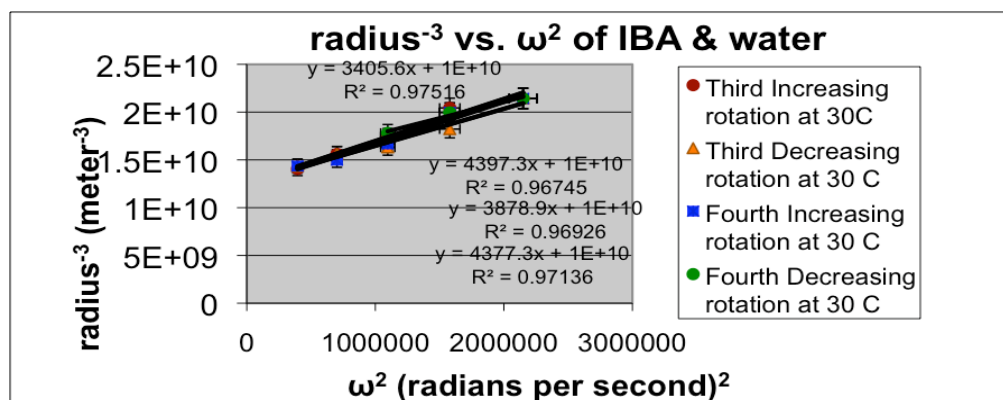


Figure 5.41. A graph of r^{-3} vs. ω^2 for IBA/SDS/water of 0.06 mM SDS with third and fourth rotational increases and decreases at 30 °C.

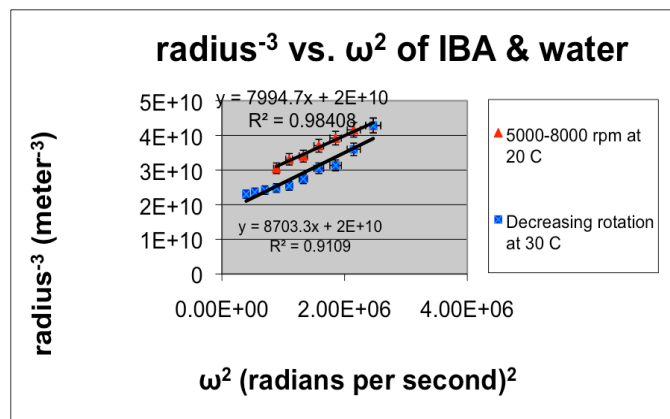


Figure 5.42. Graph of r^{-3} vs. ω^2 for IBA/SDS/water of 0.06 mM SDS at 20 and 30 °C.

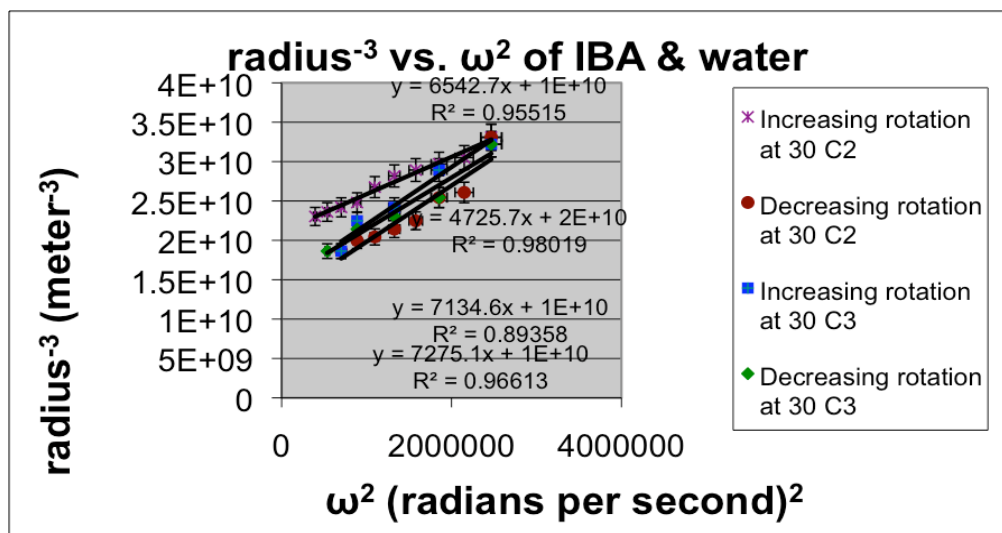


Figure 5.43. An extension of the graph of r^{-3} vs. ω^2 for IBA/SDS/water of 0.06 mM SDS with third and fourth rotational increases and decreases at 30 °C.

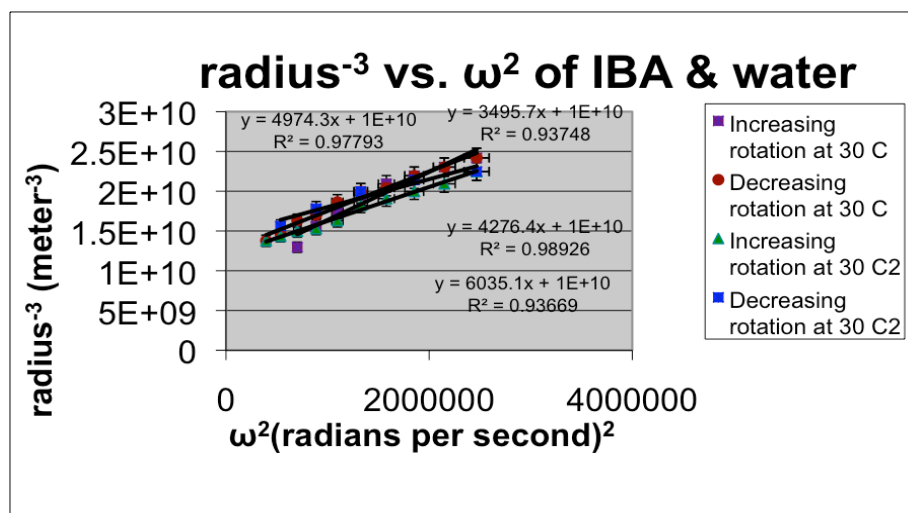


Figure 5.44. Graph of r^{-3} vs. ω^2 for IBA/SDS/water of 11.8 mM SDS at 30 °C.

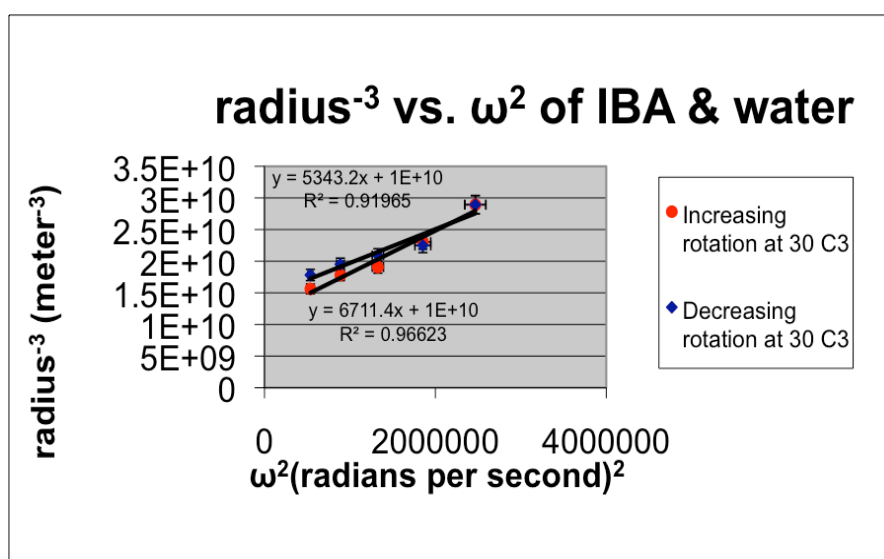


Figure 5.45. A graph of r^{-3} vs. ω^2 for IBA/SDS/water of 11.8 mM SDS with third and fourth rotational increases and decreases at 30 °C.

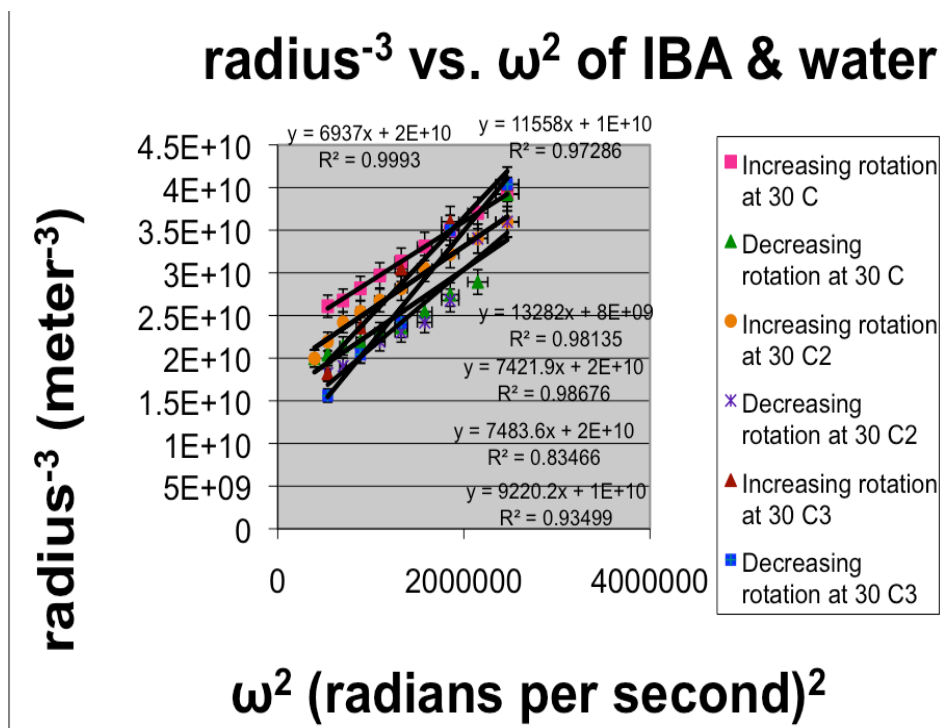


Figure 5.46. Graph of r^{-3} vs. ω^2 for IBA/SDS/water of 11.8 mM SDS at 30 °C.

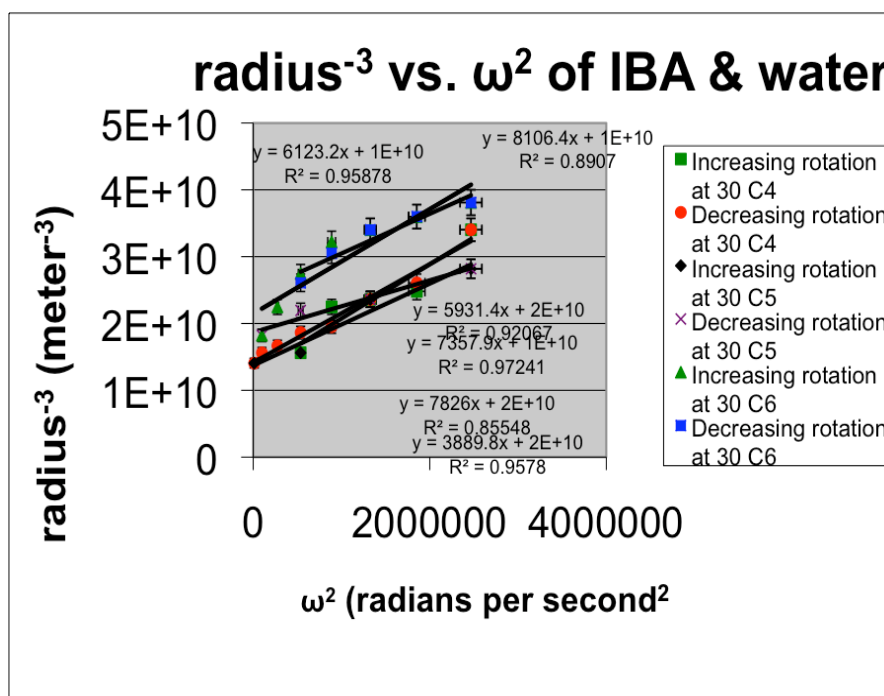


Figure 5.47. A graph of r^{-3} vs. ω^2 for IBA/SDS/water of 11.8 mM SDS with fourth, fifth, and sixth rotational increases and decreases at 30 °C.

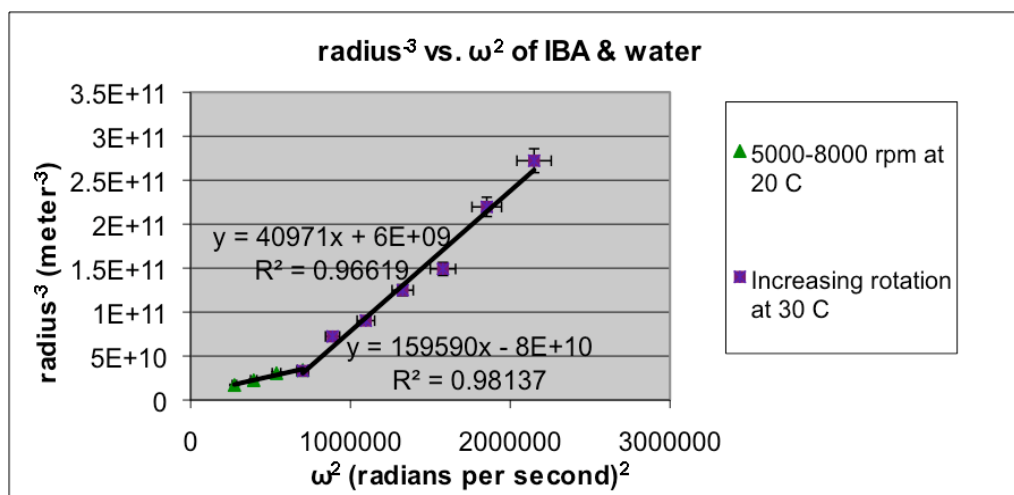


Figure 5.48. Graph of r^3 vs. ω^2 for IBA/DTAC/water of 5.74 mM DTAC at 20 and 30 °C.

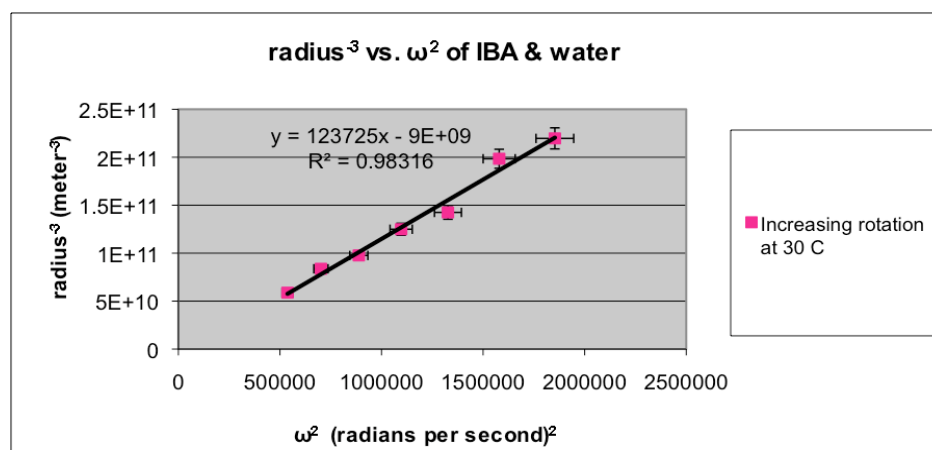


Figure 5.49. Graph of r^3 vs. ω^2 for IBA/DTAC/water of 5.74 mM DTAC at 30 °C.

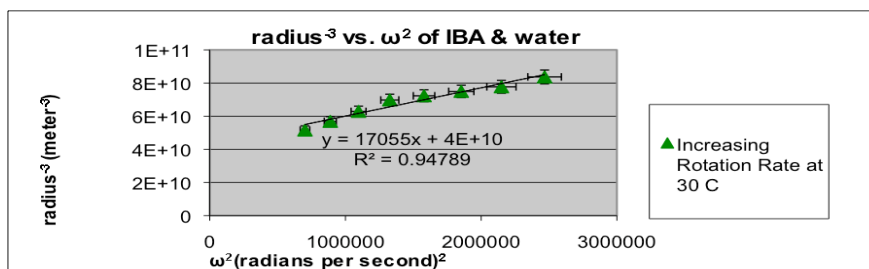


Figure 5.50. Graph of r^3 vs. ω^2 for IBA/DTAC/water of 0.610 mM DTAC at 30 °C.

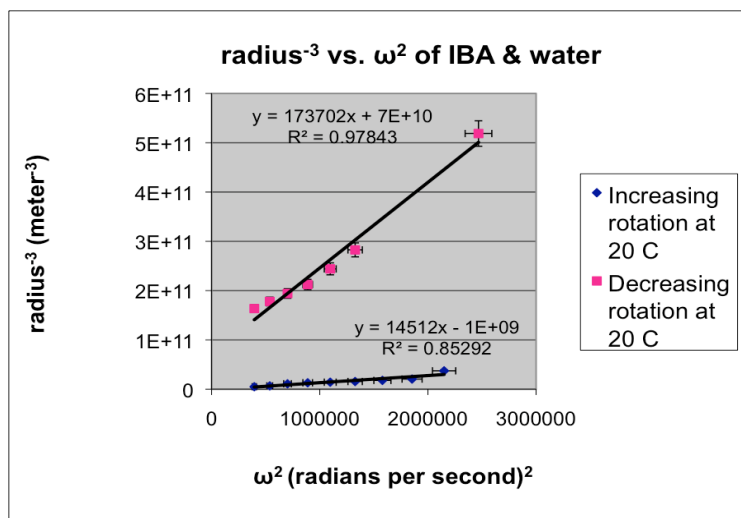


Figure 5.51. Graph of r^{-3} vs. ω^2 for IBA/SDS /water of 11.8 mM SDS at 20 °C.

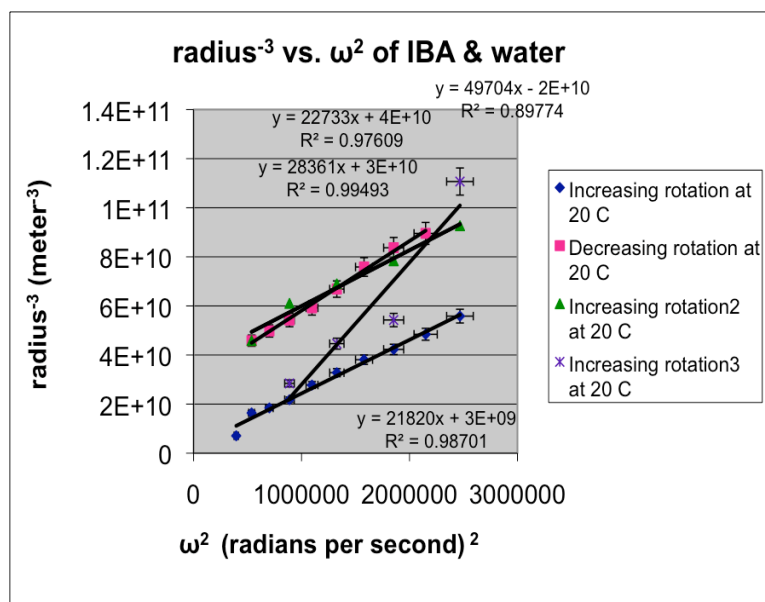


Figure 5.52. Graph of r^{-3} vs. ω^2 for IBA/SDS/water of 0.312 mM SDS at 20 °C.

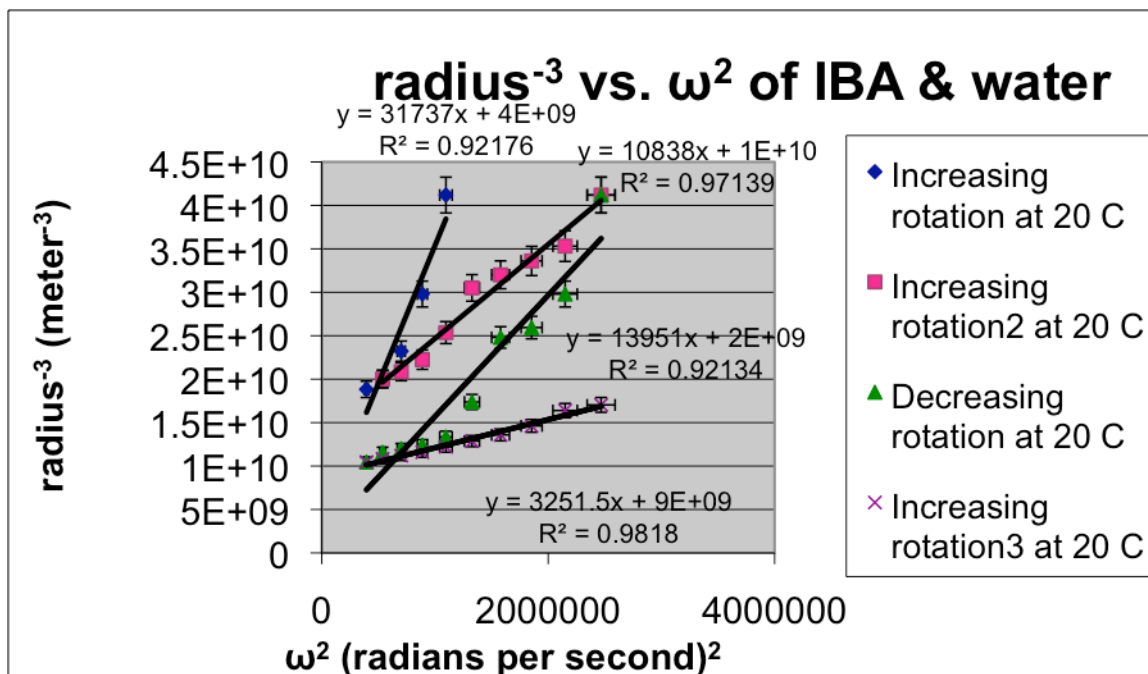


Figure 5.53. Graph of r^{-3} vs. ω^2 for IBA/SDS/water of 0.06 mM SDS at 20 °C.

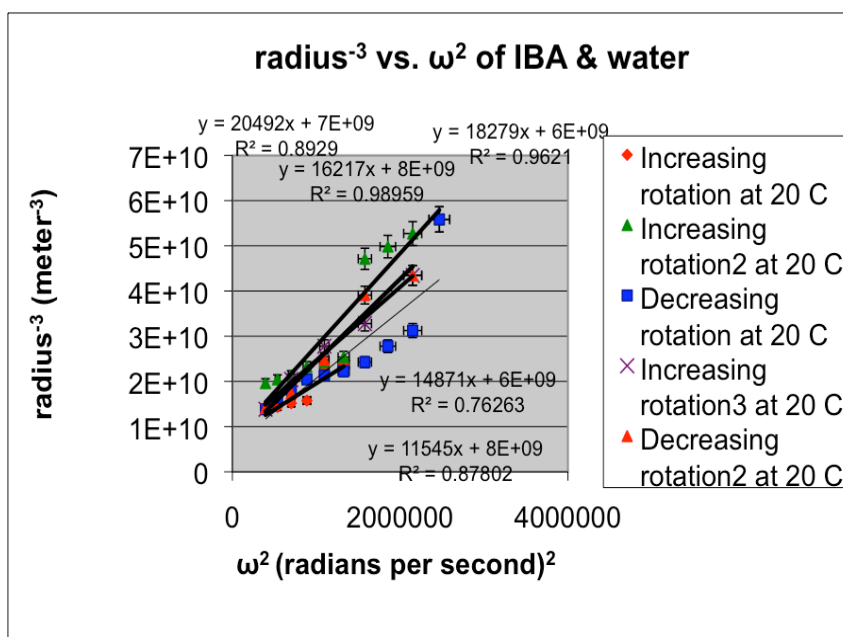


Figure 5.54. Graph of r^{-3} vs. ω^2 for IBA/SDS/water of 0.603 mM SDS at 20 °C.

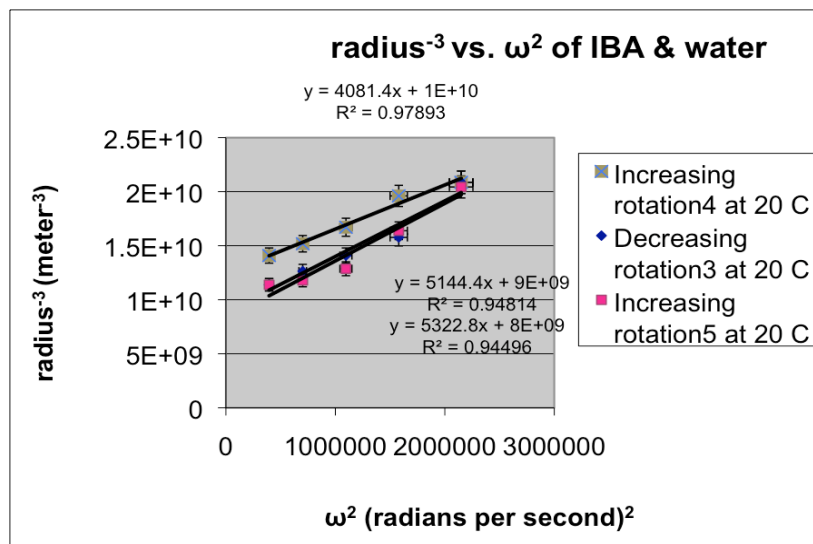


Figure 5.55. A graph of r^{-3} vs. ω^2 for IBA/SDS/water of 0.603 mM SDS with the fourth and fifth rotational rate increase and third rotational rate decrease at 20 °C.

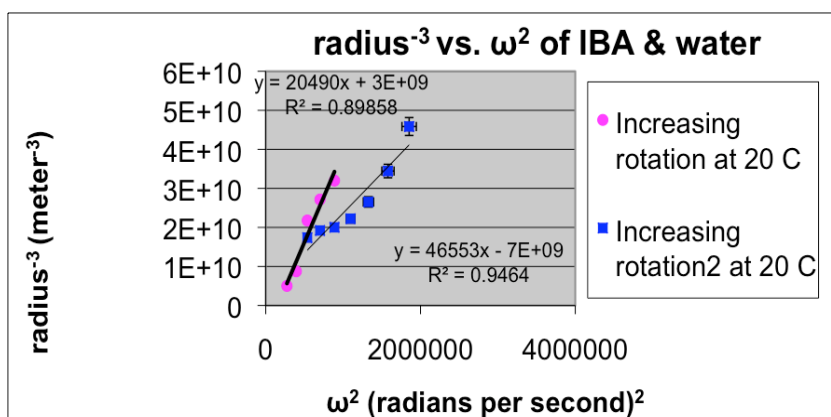


Figure 5.56. Graph of r^{-3} vs. ω^2 for IBA/DTAC/water of 5.74 mM DTAC.

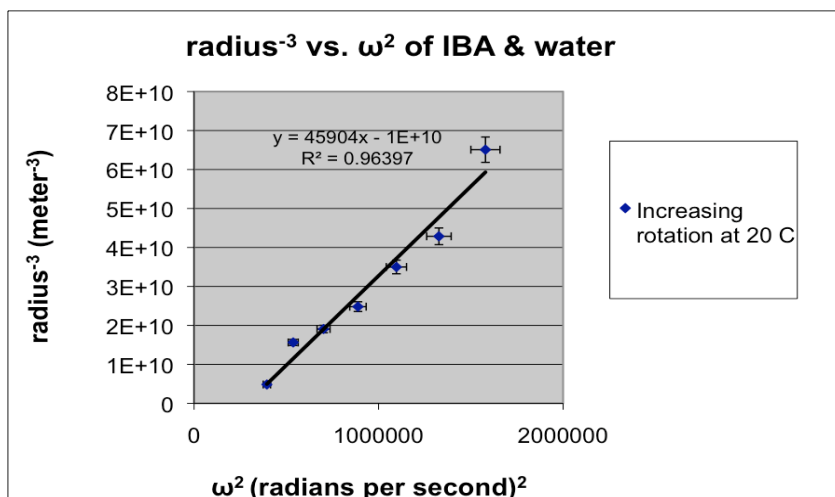


Figure 5.57. Graph of r^{-3} vs. ω^2 for IBA/DTAC/water of 0.610 mM DTAC at 20 °C.

One interesting item that showed up with the increasing and decreasing rotation rates was that, in Figures 5.38 and 5.39, when the rotation rate was closer to 15000 rpm, the IBA-rich phase's boundary was sharper than when the rotation rate was at 6000 rpm; also, the IBA-rich phase's boundary became more diffuse as each rotation rate range was increased or decreased. This behavior was typical of IBA/water systems.

In comparing the consistence checks of r^{-3} vs. ω^2 for the recrystallized surfactant experiments except for 0.6 mM SDS, which was not purified, the results had a linear regression line. However, in comparing the EITs calculated from the linear regression lines, the EITs ranged greatly. So, we looked at the averaged EITs calculated using the method of Vonnegut.³⁷ One of the reasons that some averaged EITs were so different from the linear regression EITs was because of the range of radii. For some cases, when the range between the radii was only 40 pixels, both types of EITs were closer, but, when the range between the radii was 15 pixels, the averaged and linear regression EITs had a greater

difference. When the radii's difference was smaller and then divided by a larger number, the resulting slope is much smaller than what the averaged EIT used, creating a big difference between the averaged and linear regression EITs. One way to solve this problem is to calculate your own slope by first subtracting the r^3 and then dividing the rotation rate squared over r^3 . This method allows a bigger difference between the radii to be divided by a large rotation rate squared and so be closer to the averaged EIT. So, looking at both averaged linear regression, new slope EITs were done.

In comparing the three smaller concentrations of the SDS to each other, the first rotation rate increase did have the largest concentration having the smaller Vonnegut³⁷ averaged EIT. For a long volume drop, the drop is assumed to be a cylinder shape with its length four times (or more) the diameter. This was stated by Vonnegut.³⁷ His formula was a static-based method that stated:

$$\sigma = \frac{\Delta\rho\omega^2 r^3}{4} \quad (\text{Eq. 29})^{37}$$

where σ is interfacial tension, $\Delta\rho$ is density difference, ω is rotation rate, and r is radius. For Princen *et al.*,⁴⁵ they modified Vonnegut's formula so that the interfacial tension could be calculated for drops whose length was less than four times the diameter volume. Princen *et al.*⁴⁵ included a correction factor, C , so that the formula was now:

$$\sigma = \frac{\Delta\rho\omega^2}{4C} \quad (\text{Eq. 30})^{45}$$

The correction factor is determined from the ratio of the length to the diameter volume. The correction factor is only good for drops with a ratio of 1:1 to 4:1. Princen *et al.*⁴⁵ included a table.

The largest concentration of SDS had a slightly larger (0.05 mN/m) averaged EIT than the largest averaged EIT measured from the three SDS concentrations below the cmc. These results agree with what is expected. However, in comparing the EITs of the IBA/water systems using surfactant, the averaged EIT closest to 0.11 mN/m, which is the measured EIT for equilibrated IBA/water, was the system with the 0.312 mM SDS concentration. The 0.6 mM SDS concentration was smaller than the equilibrated IBA/water while systems with 11.8 and 0.06 mM SDS were larger. All densities are assumed to be 15.4 kg/m³ because very density difference was not known for IBA/water/surfactant.

We also looked at rotational rate decreases and additional increases when possible. In previous research, we were able to look at the increase and decrease of IBA/water.⁵² The decreasing rotational rate was only slightly smaller (0.002 mN/m). For the SDS surfactants, the decreasing and additional increasing of the rotation rate varied. For the system with 0.312 mM SDS, the first decrease had one of the largest measured averaged EITs. Each subsequent additional rotational rate would be larger than the previous rotational rate increase. However, the second rotational decrease would be smaller than the first rotational increases. For 0.06 mM SDS, the second decrease had the largest EIT with each subsequent decreasing EIT being smaller. Similar to 0.312 mM SDS, the system with 0.06 mM SDS also had each sequential additional

rotational rate increase have a larger EIT than the previous one. Also, similar to 0.312 mM SDS, the decreased rotational rate would have a higher averaged EIT. Unlike 0.312 mM and 0.06 mM SDS, the systems with 11.8 mM SDS had the first three rotational rates (both increase and decrease) have smaller averaged EITs as each sequential increase and decrease occurred, with the largest EIT out of those six measurements being the first measured averaged EIT. However, for the fourth, fifth, and sixth rotational rates, the fifth rotational rate decrease was the largest with each of the corresponding increase having a smaller averaged EIT than the decreasing rotational rate. This behavior was similar to the 0.312 mM and 0.06 mM SDS.

For the increasing and decreasing rotation rate, each subsequent increase or decrease broadened the drop's radius of the same rotation rate, i.e. the drop's radius of 8000 rpm after the first rotation rate increase would be larger than the drop's radius of 8000 rpm after the second rotation rate. Also, with each additional each increase, the 15000 rpm would have a slightly darker, sharper boundary while each 6000, 7000, or 8000 rpm would have a less sharp, lighter boundary. This behavior generally occurred at 30 °C.

In comparing the 20 °C and 30 °C averaged interfacial tensions or EITs, respectively, the 20 °C would have been with the IBA/SDS/water systems being in the immiscible phase while the 30 °C being in the miscible phase. For the systems with 0.312 mM concentrations, there was a wide range of results in the averaged EITs at 20 °C. Part of this may be explained because of the methodology of the system being made. For the 0.312 mM concentration, the

SDS was first added into the jar, followed by IBA and then water. For all of the other concentrations of SDS and DTAC, the surfactant was completely dissolved into water and then IBA was added. For Figure 5.36, the SDS that was used was not recrystallized. For all of the other figures, the SDS was recrystallized.

Discounting the really low IT from 0.312 mm 20 °C, the IBA/water system with 11.8 mM SDS had the largest averaged IT (0.27 mN/m) while the system with a surfactant concentration of 0.06 mM was 0.10 mN/m and 0.312 mm and 0.6 mM SDS were about 0.10-0.17 mN/m. Like the 30 °C, in general, any additional increases for 0.6 mM and 0.06 mM would have a slightly larger IT than the previous increase. Each of the 20 °C averaged IT of the systems with 11.8 mM and 0.312 mm SDS concentrations was smaller (0.01-0.03 mN/m) than the averaged EITs at 30 °C while IBA/water systems with 0.06 and 0.6 mM SDS had the 30 °C having smaller averaged EITs (0.01-0.07 mN/m for the 0.06 mM and 0.15 mN/m for 0.6 mM). Part of this difference might be because the IBA/water systems with 11.8 mM and 0.312 mM SDS had, respectively, the SDS in bulk concentration above the cmc and in the IBA.

Hence, for the SDS concentrations, we did get the expected results of decreasing IT while concentration increased and that the cmc concentration was about the same as the smallest concentration of SDS. One unexpected results was having the middle concentration of the range tested below the cmc being extremely similar to the IBA/water system's IT. A second unexpected result was how dissolving SDS in IBA allows the 20 °C IT to being similar to the largest concentration SDS at 20 °C.

For DTAC, all of the concentrations were below the cmc so that the EIT should decrease like the SDS concentration below the cmc though temperature should affect the averaged EITs as it did for SDS and in Mehta *et al.*⁵¹ For the DTAC results, we got similar results of IBA/water systems with the larger surfactant concentration having the smallest averaged EIT, possibly indicating that the solutions were below the cmc. The system with 0.610 mM DTAC was about twice the IBA/water system's EIT (0.1 mN/m) while the IBA/water system with 5.74 mM DTAC was about 0.1 mN/m less than IBA/water system's EIT. Like system with SDS, this would put the IBA/water system's EIT in the middle of the calculated averaged EIT's of the IBA/water system with DTAC.

Looking at the 20 °C and excluding the smallest IT calculated for the IBA/water system with DTAC, which was not close to the other results, all of the concentrations were between 0.13-0.17 mN/m similar to the averaged ITs of the IBA/water system with SDS at 20 °C and slightly higher than the 0.11 mN/m of the IBA/water system at 30 °C. These measurements also placed between the 30 °C's EITs of IBA/water systems with 5.74 mM and 0.610 mM DTAC.

So, for the systems with DTAC, the expected results were similar to the IBA/water systems with SDS results below cmc. An unexpected result was that the 20 °C systems' EITs, like systems with SDS, were slightly higher than the IBA/water systems' EITs. One expected result for both SDS and DTAC is that temperature did have an effect on the calculated averaged EITs. One unexpected result for both surfactant-containing systems was that the IBA/water system's EIT being in the middle of the concentrations below cmc. Hence,

surfactants can affect the EITs of IBA/water in both expected and unexpected ways.

In comparing the linear regression line to the Vonnegut EIT to the r^3 EIT, the r^3 EIT for 30 °C was closer to the Vonnegut averaged EIT than the linear regression EIT. In these instances, the 0.312 mM SDS and 5.74 mM DDTMACI either had a really short rotation rate or drops behaving unusually. Another reason for this difference might be that the drops were not completely settled. For Tables 5.1-5.4, the green highlighted results indicate instances where the linear regression line is closest to the Vonnegut EIT, and the cyan highlighted results indicate results where the Vonnegut EIT is closer to the r^3 EIT. In the other cases, by using the radius³ slope rather than the linear regression line slope, the Vonnegut averaged EIT was more similar to the radius³ EIT since the radius³ 's slope more closely resembled the 1/Vonnegut's ($r^3 * \omega^2$) than the linear regression line's slope.

In comparing the linear regression line IT to the Vonnegut averaged IT to the radius³ IT, most of the linear regression lines' ITs more closely resembled the Vonnegut than the radius³ ITs. For example, according to Table 5.3, linear regression IT values for 0.312 mM were 0.125 mN/m and 0.288 mN/m for two of the datapoints. The corresponding Vonnegut averaged ITs were, respectively, 0.131 mN/m and 0.261 mN/m whereas the corresponding radius³ ITs were, respectively, 0.153 mN/m and 0.0678 mN/m. A possible reason for the slope of the linear regression line more closely resembling the 1/Vonnegut's ($r^3 * \omega^2$) than the radius³ slope is that the drops were not as settled as seen by the third, fourth,

and fifth rotation rate at 20 °C having the Vonnegut EIT more closely resembling the radius³ EIT. For 30 °C, the drops had been running for more than five minutes while for the 20 °C, the drops had only been rotating for a minute.

So, a good thing to do is to use all three types of EITs and ITs but to keep in mind that using the radius³ EIT is better in comparing it to Vonnegut EIT at 30 °C and to use the linear regression line when (a) unusual behavior rates is seen, (b) a smaller range of rotation rates is used, and (c) the IBA-rich drop does not seem settled.

Table 5.1

Summary of EIT for Different Surfactants at 30 °C

Linear Regression EIT (mN/m)	Surfactant Concentration (mM)	Rotation Range (rpm)	Vonnegut <i>et al.</i> Averaged EIT (mN/m)	Radius ³ EIT (mN/m)	From Figure
0.0621	0.6	8000-13000	0.0812	0.0813	5.34
0.286	0.312	8000-10000	0.190	0.0247	5.35
1.77	0.312	15000-8000	0.572	0.286	5.35
1.76	0.312	15000-10000	0.596	0.134	5.36
0.334	0.312	6000-14000(2 nd rotational rate increase)	0.167	0.0949	5.37
2.16	0.312	6000-14000 (3 rd rotational rate increase)	0.308	0.110	5.37
2.10	0.312	14000-6000 (3 rd	0.325	0.143	5.37

		rotational rate decrease)			
0.881	0.06	7000- 15000	0.232	0.130	5.38
0.678	0.06	15000- 6000	0.243	0.258	5.38
0.977	0.06	6000- 14000 (2 nd rotational rate increase)	0.250	0.209	5.38
1.16	0.06	14000- 6000(2 nd rotational rate decrease)	0.295	0.221	5.38
0.876	0.06	6000- 14000(3 rd rotational rate increase)	0.241	0.165	5.39
0.993	0.06	14000- 6000(3 rd rotational rate decrease)	0.252	0.155	5.39
0.880	0.06	6000- 14000(4 th rotational rate increase)	0.256	0.155	5.39
1.13	0.06	14000- 6000(4 th rotational rate decrease)	0.309	0.0384	5.39
0.482	0.06	9000- 15000	0.165	0.0574	5.40
0.442	0.06	15000- 6000	0.163	0.160	5.40
0.815	0.06	6000- 15000 (2 nd rotational	0.175	0.105	5.41

		rate increase)			
0.540	0.06	15000- 8000(2 nd rotational rate decrease)	0.240	0.159	5.41
0.529	0.06	8000- 15000(3 rd rotational rate increase)	0.210	0.154	5.41
0.588	0.06	15000- 7000(3 rd rotational rate decrease)	0.214	0.168	5.41
0.638	11.8	8000- 15000	0.287	0.244	5.42
0.774	11.8	15000- 6000	0.248	0.250	5.42
0.900	11.8	6000- 15000(2 nd rotational rate increase)	0.269	0.224	5.42
1.10	11.8	15000- 7000(2 nd rotational rate decrease)	0.267	0.145	5.42
0.574	11.8	7000- 15000(3 rd rotational rate increase)	0.246	0.219	5.43
0.721	11.8	15000- 7000(3 rd rotational rate decrease)	0.236	0.160	5.43
0.555	11.8	7000- 15000 rpm	0.162	0.0954	5.44
0.514	11.8	15000- 7000 rpm	0.189	0.196	5.44

0.519	11.8	6000-15000 rpm (2 nd rotation increase)	0.168	0.178	5.44
0.388	11.8	15000-7000 rpm (2 nd rotation decrease)	0.207	0.201	5.44
0.333	11.8	7000-15000 rpm (3 rd rotational increase)	0.172	0.224	5.44
0.290	11.8	15000-7000 rpm (3 rd rotational decrease)	0.190	0.292	5.44
0.475	11.8	7000-15000 rpm (4 th rotational increase)	0.214	0.257	5.45
0.523	11.8	15000-1000 rpm (4 th rotational decrease)	0.143	0.395	5.45
0.629	11.8	1000-15000 rpm (5 th rotational increase)	0.172	0.337	5.45
	11.8	15000-3000 rpm (5 th rotational decrease)	0.167	0.177	5.45
0.492	11.8	3000-15000 rpm (6 th rotational increase)	0.121	0.261	5.45
0.649	11.8	15000-	0.157	0.0898	5.45

		7000 rpm (6 th rotational decrease)			
0.0241	5.74	8000- 14000 rpm	0.0457	0.148	5.46
0.0175	5.74	7000- 14000 rpm	0.0315	0.0932	5.47
0.226	0.610	8000- 15000 rpm	0.0815	0.0505	5.48

Table 5.2

Summary of EIT and Slopes for Different Surfactants at 30 °C

Linear Regression EIT (mN/m)	Linear Regression Slope	Radius ³ Slope	Vonnegut <i>et al.</i> Averaged EIT (mN/m)	Radius ³ EIT (mN/m)	1/Vonnegut ($r^3 * \omega^2$)
0.0621	6.20*10 ⁴	4.74*10 ⁴	0.0812	0.0813	4.74*10 ⁴
0.286	1.34*10 ⁴	1.56*10 ⁵	0.190	0.0247	2.02*10 ⁴
1.77	2.17*10 ³	1.35*10 ⁴	0.572	0.286	6.73*10 ³
1.76	2.43*10 ³	2.87*10 ⁴	0.596	0.134	6.46*10 ³
0.334	1.15*10 ⁴	4.06*10 ⁴	0.167	0.0949	1.13*10 ⁴
2.16	1.79*10 ³	3.49*10 ⁴	0.308	0.110	1.25*10 ⁴
2.10	1.83*10 ³	2.69*10 ⁴	0.325	0.143	1.1*10 ⁴
0.881	4.37*10 ³	2.96*10 ⁴	0.232	0.130	1.66*10 ⁴
0.678	5.68*10 ³	1.49*10 ⁴	0.243	0.258	1.59*10 ⁴
0.977	3.94*10 ³	1.84*10 ⁴	0.250	0.209	1.54*10 ⁴
1.16	3.31*10 ³	1.74*10 ⁴	0.295	0.221	1.31*10 ⁴
0.876	4.40*10 ³	2.33*10 ⁴	0.241	0.165	1.59*10 ⁴
0.993	3.88*10 ³	2.48*10 ⁴	0.252	0.155	1.53*10 ⁴
0.880	4.37*10 ³	2.48*10 ⁴	0.246	0.155	1.56*10 ⁴
1.13	3.41*10 ³	1.00*10 ⁵	0.309	0.0384	1.24*10 ⁴
0.482	7.99*10 ³	6.70*10 ⁴	0.165	0.0574	2.33*10 ⁴
0.442	8.70*10 ³	2.40*10 ⁴	0.163	0.160	2.36*10 ⁴
0.815	4.73*10 ³	3.65*10 ⁴	0.175	0.105	2.20*10 ⁴
0.540	7.13*10 ³	2.42*10 ⁴	0.240	0.159	1.61*10 ⁴
0.529	7.28*10 ³	2.51*10 ⁴	0.210	0.154	1.83*10 ⁴
0.588	6.54*10 ³	2.29*10 ⁴	0.214	0.168	1.80*10 ⁴
0.638	6.04*10 ³	1.58*10 ⁴	0.287	0.244	1.34*10 ⁴
0.774	4.97*10 ³	1.54*10 ⁴	0.248	0.250	1.56*10 ⁴

0.90	$4.28 \cdot 10^3$	$1.72 \cdot 10^4$	0.269	0.224	$1.43 \cdot 10^4$
1.10	$3.50 \cdot 10^3$	$2.65 \cdot 10^4$	0.267	0.145	$1.44 \cdot 10^4$
0.574	$6.71 \cdot 10^3$	$1.76 \cdot 10^4$	0.246	0.219	$1.56 \cdot 10^4$
0.721	$5.34 \cdot 10^3$	$2.40 \cdot 10^4$	0.236	0.160	$1.63 \cdot 10^4$
0.555	$6.94 \cdot 10^3$	$4.04 \cdot 10^4$	0.162	0.0954	$2.37 \cdot 10^4$
0.514	$7.48 \cdot 10^3$	$1.96 \cdot 10^4$	0.189	0.196	$2.04 \cdot 10^4$
0.519	$7.42 \cdot 10^3$	$2.16 \cdot 10^4$	0.168	0.178	$2.29 \cdot 10^4$
0.388	$9.92 \cdot 10^3$	$1.91 \cdot 10^4$	0.207	0.201	$1.86 \cdot 10^4$
0.333	$1.16 \cdot 10^4$	$1.72 \cdot 10^4$	0.172	0.224	$2.24 \cdot 10^4$
0.290	$1.33 \cdot 10^4$	$1.32 \cdot 10^4$	0.190	0.292	$2.03 \cdot 10^4$
0.475	$8.11 \cdot 10^3$	$1.50 \cdot 10^4$	0.214	0.257	$1.80 \cdot 10^4$
0.523	$7.36 \cdot 10^3$	$9.75 \cdot 10^3$	0.143	0.395	$2.69 \cdot 10^4$
0.629	$6.12 \cdot 10^3$	$1.14 \cdot 10^4$	0.172	0.337	$2.24 \cdot 10^4$
0.990	$3.89 \cdot 10^3$	$2.18 \cdot 10^4$	0.167	0.177	$2.30 \cdot 10^4$
0.492	$7.82 \cdot 10^3$	$1.47 \cdot 10^4$	0.121	0.261	$3.18 \cdot 10^4$
0.649	$5.93 \cdot 10^3$	$4.29 \cdot 10^4$	0.157	0.0898	$2.44 \cdot 10^4$
0.0241	$1.60 \cdot 10^5$	$2.60 \cdot 10^4$	0.0457	0.148	$8.42 \cdot 10^4$
0.0175	$2.20 \cdot 10^5$	$4.13 \cdot 10^4$	0.0315	0.0932	$1.22 \cdot 10^5$
0.226	$1.71 \cdot 10^4$	$7.62 \cdot 10^4$	0.0815	0.0505	$4.72 \cdot 10^4$

Table 5.3

Summary of IT for Different Surfactants at 20 °C

Linear Regression EIT (mN/m)	Surfactant Concentration (mM)	Rotation Rate Range (rpm)	Vonnegut <i>et al.</i> Averaged IT (mN/m)	Radius ³ IT(mN/m)	From Figure
0.0612	0.6	5000-8000	0.126	0.238	5.34
0.125	0.312	5000-8000	0.131	0.153	5.35
0.288	0.312	5000-8000	0.261	0.0678	5.36
0.0940	5.74	5000-8000 rpm	0.0692	0.0482	5.46
0.265	11.8	6000-15000 rpm	0.271	1.22	5.49
0.0222	11.8	15000-6000 rpm	0.0150	0.0334	5.49
0.176	0.312	6000-15000 rpm	0.162	0.984	5.50

0.136	0.312	15000-7000 rpm	0.0710	0.0353	5.50
0.169	0.312	7000-15000 rpm (2 nd rotational increase)	0.0738	0.0819	5.50
0.0775	0.312	7000-15000 rpm (3 rd rotational increase)	0.113	0.159	5.50
0.121	0.06	6000-10000 rpm	0.104	0.0779	5.51
0.355	0.06	6000-15000 rpm (2 nd rotational increase)	0.167	0.191	5.51
0.276	0.06	15000-6000 rpm	0.246	0.569	5.51
1.18	0.06	6000-15000 rpm (3 rd rotational increase)	0.361	0.294	5.51
0.334	0.603	6000-12000 rpm	0.176	0.108	5.52
0.188	0.603	6000-15000 rpm (2 nd rotational increase)	0.143	0.264	5.52
0.259	0.603	15000-6000 rpm	0.192	0.433	5.52
0.237	0.603	6000-14000 rpm (3 rd rotational increase)	0.154	0.333	5.52
0.211	0.603	14000-6000 rpm (2 nd rotational increase)	0.156	0.324	5.52

		decrease)			
0.943	0.603	6000-14000 rpm (4 th rotational increase)	0.249	0.156	5.53
0.748	0.603	14000-6000 rpm (3 rd rotational decrease)	0.286	0.270	5.53
0.723	0.603	6000-14000 rpm (5 th rotational increase)	0.293	0.263	5.53
0.0827	5.74	5000-9000 rpm	0.137	0.398	5.54
0.188	5.74	7000-13000 rpm (2 nd rotational increase)	0.164	0.181	5.54
0.234	0.610	6000-15000 rpm	0.162	0.358	5.55

Table 5.4

Summary of IT and Slopes for Different Surfactants at 20 °C

Linear Regression EIT (mN/m)	Linear Regression Slope	Radius ³ Slope	Vonnegut <i>et al.</i> Averaged IT (mN/m)	Radius ³ IT (mN/m)	1/Vonnegut (r ³ * ω ²)
0.0612	6.29*10 ⁴	1.62*10 ⁴	0.126	0.238	3.06*10 ⁴
0.125	3.07*10 ⁴	2.52*10 ⁴	0.131	0.153	2.95*10 ⁴
0.288	2.19*10 ⁴	5.68*10 ⁴	0.261	0.0678	1.47*10 ⁴
0.0940	4.10*10 ⁴	7.98*10 ⁴	0.0692	0.0482	5.56*10 ⁴
0.265	1.45*10 ⁴	3.16*10 ³	0.271	1.22	1.42*10 ⁴
0.0222	1.73*10 ⁵	1.15*10 ⁵	0.0150	0.0334	2.58*10 ⁵
0.176	2.18*10 ⁴	3.91*10 ⁴	0.162	0.984	2.37*10 ⁴
0.136	2.84*10 ⁴	1.09*10 ⁵	0.0710	0.0353	5.42*10 ⁴
0.169	2.27*10 ⁴	4.70*10 ⁴	0.0738	0.0819	5.22*10 ⁴

0.0775	4.97×10^4	2.42×10^4	0.113	0.159	3.41×10^4
0.121	3.17×10^4	4.94×10^4	0.104	0.0779	3.72×10^4
0.355	1.08×10^4	2.02×10^4	0.167	0.191	2.31×10^4
0.276	1.40×10^4	6.77×10^3	0.246	0.569	1.56×10^4
1.18	3.25×10^3	1.31×10^4	0.361	0.294	1.07×10^4
0.334	1.16×10^4	3.56×10^4	0.176	0.108	2.19×10^4
0.188	2.05×10^4	1.46×10^4	0.143	0.264	2.70×10^4
0.259	1.49×10^4	8.88×10^3	0.192	0.433	2.00×10^4
0.237	1.62×10^4	1.16×10^4	0.154	0.333	2.50×10^4
0.211	1.83×10^4	1.19×10^4	0.156	0.324	2.47×10^4
0.943	4.08×10^3	2.47×10^4	0.249	0.156	1.55×10^4
0.748	5.14×10^3	1.43×10^4	0.286	0.270	1.35×10^4
0.723	5.32×10^3	1.47×10^4	0.293	0.263	1.31×10^4
0.0827	4.66×10^4	9.68×10^3	0.137	0.398	2.81×10^4
0.188	2.05×10^4	2.13×10^4	0.164	0.181	2.35×10^4
0.234	1.64×10^4	1.08×10^4	0.162	0.358	2.50×10^4

Graphs of EIT as a function of concentration of surfactant and as a function of change in rotation rate are shown in Figures 5.58-5.63 and summarize the EIT/ITs from Tables 5.1 and 5.3.

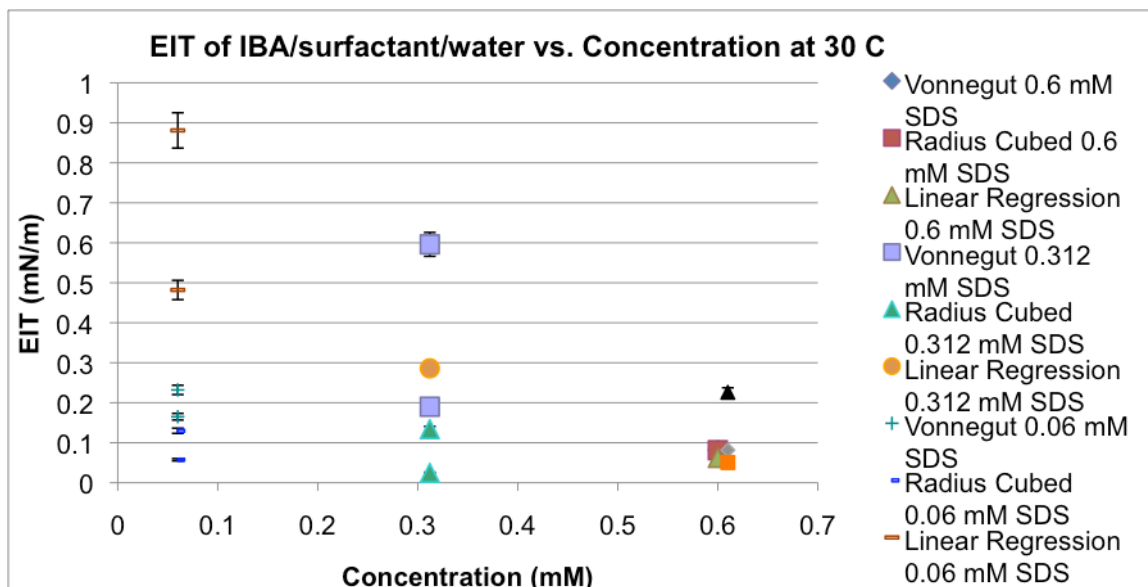


Figure 5.58. Graphs of EIT of IBA/surfactant/Water vs. Concentration at 30 °C.

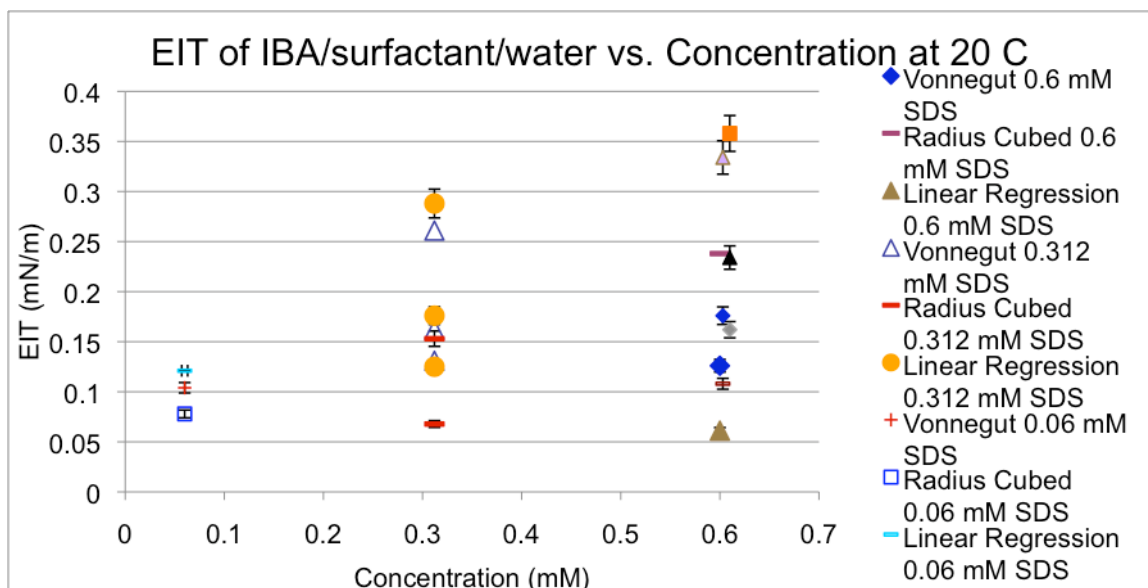


Figure 5.59. Graphs of EIT of IBA/surfactant/Water vs. Concentration at 20 °C.

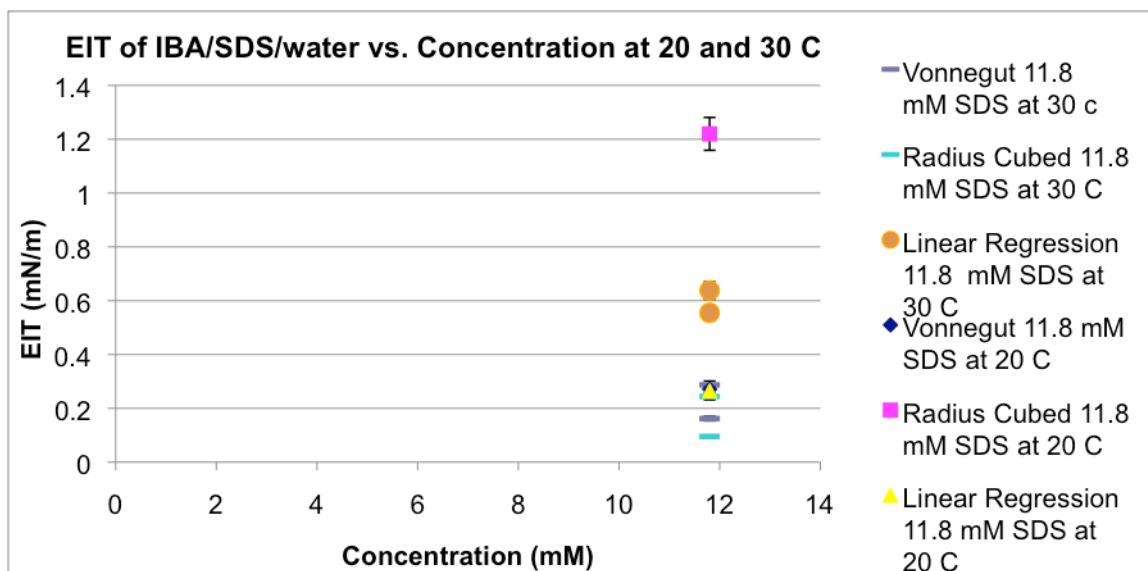


Figure 5.60. Graphs of EIT of IBA/SDS/Water vs. Concentration at 20 and 30 °C.

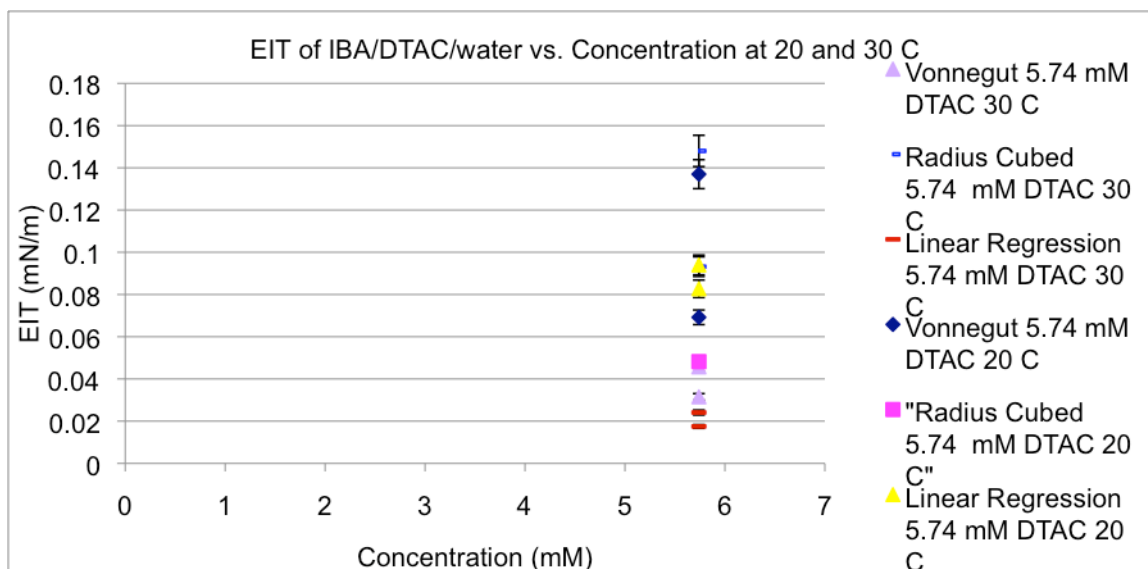


Figure 5.61. Graphs of EIT of IBA/DTAC/Water versus Concentration at 20 and 30 °C.

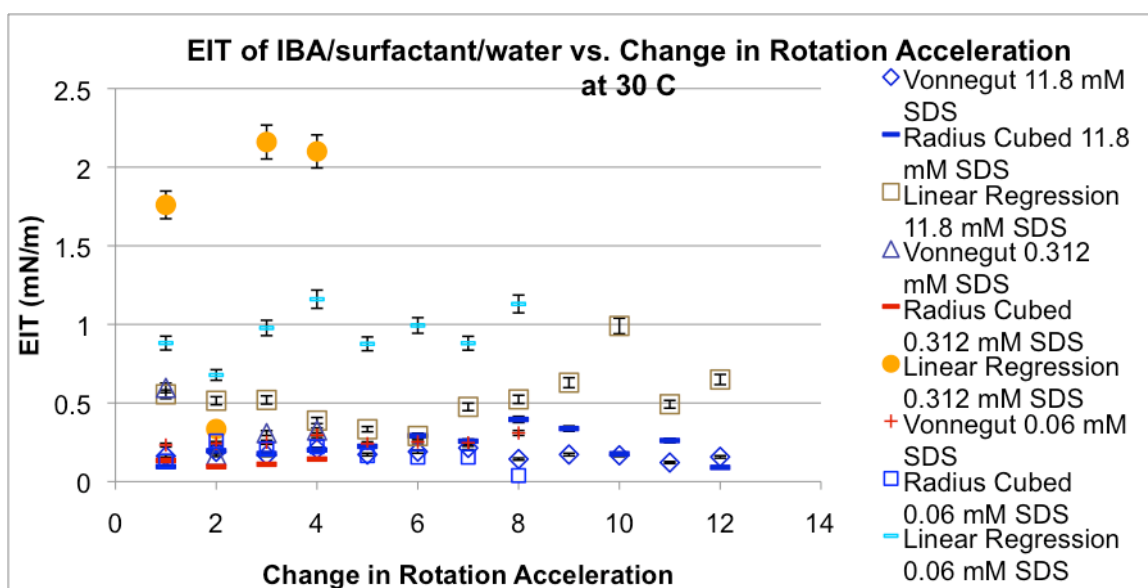


Figure 5.62. Graphs of EIT of IBA/surfactant/Water vs. Change in Rotation Rate at 30 °C.

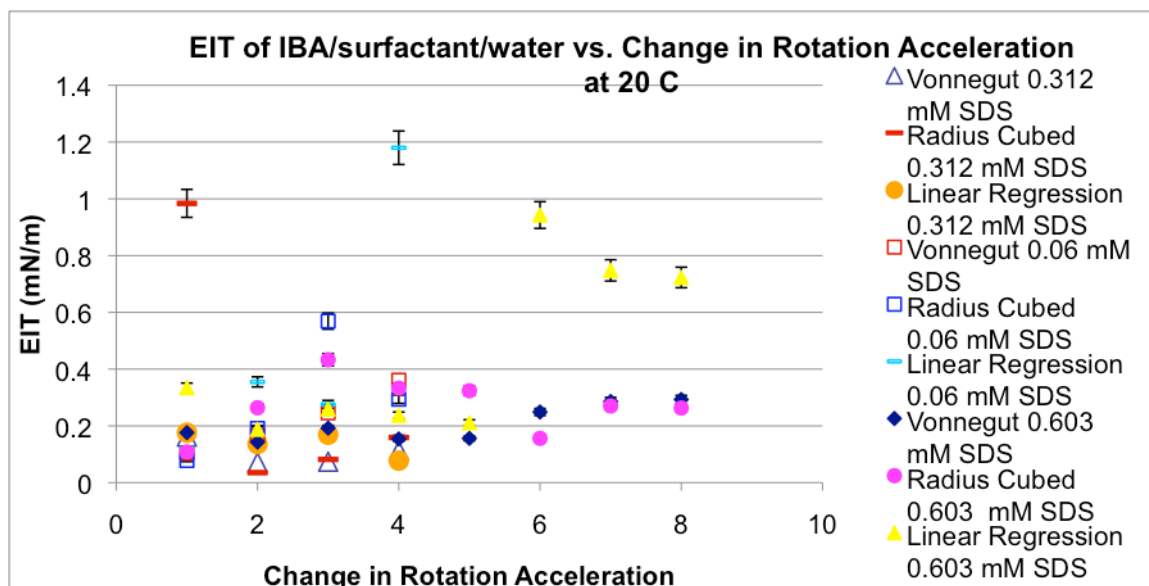


Figure 5.63. Graphs of EIT of IBA/surfactant/Water vs. Change in Rotation Rate at 20 °C.

Figures 5.58-5.61 show the calculated EIT/IT from each surfactant and concentration. Figures 5.62 and 5.63 show how the rotation rates change after the rotation rate is increased or decreased. The values of 1.8 mN/m, 0.98 mN/m, and 0.40 mN/m were cut, respectively, from Figures 5.58, 5.59, and 5.61 so that the rest of the values could be easily seen and not lumped together. Only one value was cut from each of these three graphs because they pushed the y-value too high to see the other distinct, singular y-values rather than a few group of y-values. The number in the x-position of the EIT vs. Change in Rotation Rate refers to whether that was the number of times the rotation rate was increased or decreased. For example, according to Table 5.1 and Figure 5.62, the first datapoint at 1 in the x-axis for 11.8 mM refers to the first rotational increase from 7000 to 15000 rpm or 0.56 mN/m, 0.16 mN/m, and 0.095 mN/m for linear regression, Vonnegut averaged EIT, and radius³ EIT, respectively. In Figures

5.62 at 30 °C, most of the surfactant concentrations show a final EIT as being higher than the initial EIT. In Figure 5.63 at 20 °C, the surfactant concentration of 0.603 mM and 0.06 mM SDS have the final IT being higher than the initial IT while the 0.312 mM SDS has the final IT being slightly lower or the same as the initial IT. In Figures 5.58-5.63, the Vonnegut equation values are generally closer to the Radius Cubed values. In the cases where the linear regression values are closer to the Vonnegut values, the temperature is usually 20 °C.

Conclusions

Before analyzing any results, we had to distinguish among surfactant-rich phase, IBA-rich phase, water-rich phase, and any impurity or unknown component that could be present in the sample. Differences in color contrast and the appearance of a lack a real boundary were used to distinguish the surfactant-rich phase from IBA-rich phase and any impurity. Color contrasts occurred at different temperatures, and sharper, darker boundaries for IBA-rich phase could be identified by decreasing and then increasing the rotation rate.

Similarities and differences in behavior occurred between IBA/water and IBA/surfactant/water systems. For example, the IBA/water system more easily end pinched than the IBA/surfactant/water systems. The more easily end pinching means that the IBA/water systems can more easily affected by Korteweg stress and hat the IBA/surfactant/water systems would have a larger EIT. N-butanol/water also had a hard time end pinching and Pojman *et al.*¹ attributed this behavior to n-butanol/water having a larger EIT than IBA/water.

Immiscible systems also demonstrated the ability to exhibit drop break up.¹ One difference between a miscible system and either of the IBA/water or IBA/surfactant/water system is that the IBA/water and IBA/surfactant/water systems' light phase expanded and then contracted in the heavy phase while dodecyl/polydodecylacrylate had its light phase keep expanding into the heavier phase.^{53, 1} Another behavior that is shown in immiscible systems, IBA/surfactant/water, and IBA/water systems is Marangoni instability.^{1, 49} A difference is that the IBA/surfactant/water systems demonstrated more fluid/flow motions than IBA/water systems. The demonstration of the fluid/flow motions can more easily show any Korteweg stress, indicating that any change in Korteweg stress can be more easily observed in an IBA/surfactant/water system than an IBA/water system, even if the Korteweg stress is higher or lower.

Plots of radius of the drop cubed vs. rotation rate squared were used to determine EIT, and the impact of surfactants on EIT produced some expected and unexpected results. The EITs for the systems with SDS concentrations below the cmc matched the predicted trend of decreasing with increasing concentration of the surfactant. Another expected result was that temperature affected the EIT. EITs for DTAC did change as a function of surfactant concentration because the concentrations of the surfactants were below the cmc for IBA/water. The cmc values for the surfactants were determined in water and not in IBA/water so that the cmc values calculated in water may not be the same as the ones calculated in IBA/water. We expected the interactions between the surfactant and the components of the binary system to be stronger than the

original interactions between the IBA and water, but this result did not occur because the original interactions between the IBA and water were stronger than the ones between the hydrophilic group of the surfactant and water and between the hydrophobic group of the surfactant and IBA. Hence, the EITs of the IBA/water systems using surfactant were greater than EIT of the original binary systems.

The results in this dissertation showed that the EITs of the IBA/water systems using surfactant was similar to the Gaussian curve and that the 0.11 mN/m was in the middle range for the EIT for the IBA/water system using surfactant. Originally, we expected that the EIT of the systems using surfactant would decrease, but our experimental results did not demonstrate this.

Temperature affected the EITs in unexpected ways by having the surfactant-containing systems at 20 °C's ITs slightly higher than the IBA/water system's IT. With equilibrated IBA/water systems, Pojman *et al.*¹ had the EIT not changing with temperature. In the previous chapter of small volume pure IBA/pure water, increased temperature correlated with decreased averaged EIT. Pojman *et al.*¹ also had the EIT stay almost constant over time. For the increasing and decreasing rotation rate, the averaged EIT and radii became larger, especially at 30 °C. The broadening of the radius and the decreased sharpness of the boundary at the lower rotation with each increased or decreased rotation rate indicates Fickian diffusion. In general, the IBA/water system only showed non-Fickian diffusion with a sharp concentration gradient while other miscible systems like dodecylacrylate/polydodecylacrylate showed

Fickian diffusion while maintaining a sharp concentration gradient.^{53, 1} Without the increase or decrease of rotation rate, the IBA/surfactant/water system showed only non-Fickian diffusion rate, indicating that changing rotational acceleration (even a small range) can affect diffusion and showing that barodiffusion can affect EIT in IBA/surfactant/water systems.

The increasing and decreasing rotation rate change had unexpected results for an EIT comparison of different surfactant concentrations below the cmc and above to the IBA/water system.

In comparing the different EITs and ITs calculated using different methods, it is important to use all three types (radius³, Vonnegut, linear regression line) of EITs and ITs, but using the radius³ EIT is better in comparing it to Vonnegut EIT at 30 °C. Also, we found that we should use the linear regression line when (a) unusual behavior rates is seen, (b) a smaller range of rotation rates is used, and (c) the IBA-rich drop does not seem settled.

CHAPTER VI

MICROFLUIDICS

Another way of studying the effects of interfacial tension of a system such as IBA and water is with a microfluidic device. Microfluidics is the study of miniaturized systems and fluidic manipulation and offers a variety of possibilities from solving biological and chemical system integration problems to studying microfluidic physics.³⁸

We wanted to see if we could observe similar behaviors such as drop breakup, drop shape, and Maragoni instability. We also wanted to determine if we could measure the EIT using the current method that we used and described in Chapter IV for direct comparison of EITs of systems using SDT and EITs of systems using microfluidic devices.

In the microfluidic device that we built, we wanted to study behavior of miscible systems that were not mixing because we wanted to see if the mixing in the SDT was causing some of the unusual behavior that we observed or whether that behavior could be attributed to partially miscible and miscible systems. We designed a type of microfluidic device similar to one that exhibits a large Péclet number,¹⁶ which is a dimensionless number that relates convection to diffusion, would work better than either an H junction or a J junction because this type of device would allow multiple laminar flows. We tested different materials with different systems to determine which material worked best for the most number of different systems. For example, we tested the IBA/water system with polycarbonate (PC) and poly(methylmethacrylate) (PMMA). We evaluated

different properties including wettability, hydrophilicity, and the systems' affinity for the material. Different tests such as measuring contact angles and placing microfluidic devices in a sealed jar of water for several days to determine whether the device would dissolve, have water adhere to the surface of the microfluidic device, or whether water had no impact on the device were done to evaluate the wettability of the microfluidic devices. These properties of the microfluidic devices can and did affect the results that we obtained and could distort our findings, thus rendering the microfluidic device useless for studying the effects of the effective interfacial tension of a system. We also tested how well the microfluidic device worked or remained in pristine condition (no scratches, no dissolving by tested system, etc.) after being used multiple times.

If two immiscible fluids are placed into the microfluidic device, the interfacial tension between the two fluids affects the dynamics of the surface between the fluids. If no interfacial tension existed between the oil and water, then the streams would flow alongside each other, but the interfacial tension works to reduce the interfacial area as viscous stress works to extend and drag the interface downstream.¹⁶ The interface is destabilized by these competing stresses, causing droplets to form.¹⁶ Smaller droplets can be formed through flow focusing of either increasing shear gradients or by drawing the stream into a thin jet that breaks up by the Rayleigh-Plateau instability.¹⁶

One problem with the large surface-to-volume ratios of microfluidic devices are the surface effects, particularly when free fluid surfaces are present.¹⁶ The interfacial tensions can cause bulk liquid movement, meaning

that, because of capillary forces, fluids tend to wet microchannels.¹⁶ Previous research showed that fluids that are situated without continuous wetting moved to the more highly wetting side and to even travel uphill on a surface with an interfacial tension gradient.¹⁶ So, in building our microfluidic device, we had to make sure that the neither fluid was overly attracted to the microchannels and adhered to the them and did not move.

Different materials for microfluidic device were tested to determine which ones worked best for studying IBA and water because one or both chemicals could interact with the material of the device by dissolving the material or adhering to the sides of the wall and not moving. For example, IBA can interact with PMMA or adhere to the sides of the wall and not move. For other materials such as polycarbonate (PC), both water and IBA could have similar affinities for it and did not dissolve the microfluidic device.

Besides testing different materials for the microfluidic device, the orientation with respect to the gravitational vector was also evaluated. The interfacial tension of the two fluids depends upon different factors including temperature, electrostatic potential, and surfactant concentration. By externally inducing a gradient in one of these properties, an interfacial tension gradient can be created.¹⁶ Marangoni flow is a fluid flow when the “gradients in interfacial tension along a free surface set the interface itself into motion.”¹⁶

Hagedorn *et al.* studied the capillary instability (Rayleigh-Plateau instability) in a confined system.⁵⁴ This instability can result from the effects of the fluid’s viscosity and interfacial tension. The instability can occur when the

length of the restrained cylindrical drop of one fluid in a second fluid is much greater than $2\pi r$; the unconstrained cylinder has a final drop size of $2\pi r$. When the drop breaks up into smaller droplets, the drop loses surface area but retains the same volume. The rate of drop break up is a function of viscosity and interfacial tension. They also found that the system could break up because of a combination of the capillary and “end-pinch” instabilities of the confined system.⁵⁴ Their study demonstrated that fluid “wetting” properties can impact the stability of the flow of immiscible fluids in microchannels and that interactions between the fluid and “confining wall” are important. Thus, it is important to know the wetting properties of the tested system and to know whether the system will interact with the microfluidic device by reacting with the material of the microfluidic channels or dissolving the microfluidic channels.

PMMA and PC Microfluidic Devices

To see if we could observe similar behaviors such as drop breakup, drop shape, and unusual behavior that occurred in the SDT in the microfluidic device, the initial microfluidic device was built from poly(methyl methacrylate) (PMMA) and had channels that were 100, 250, and 500 micrometers as shown below in Figure 6.1.

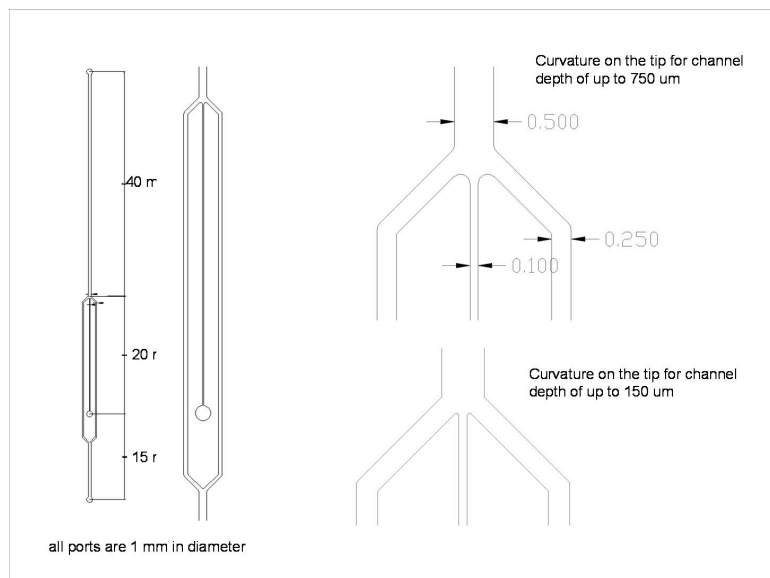


Figure 6.1. A drawing of the microfluidic device that we used.

Figure 6.2 shows a schematic of the device (channel depth of 500 μm , channel length of 7.5 cm, and channels with widths of 0.10 mm, 0.20 mm, 0.50 mm, 2 mm, 3 mm, and 5 mm). Six capillaries were inserted into the microfluidic device, and two fluids were injected via special syringe tips to the capillary. The flow rate of the fluids was controlled by how much pressure was put on the syringe either through hydrostatic pressure or with the syringe plunger.

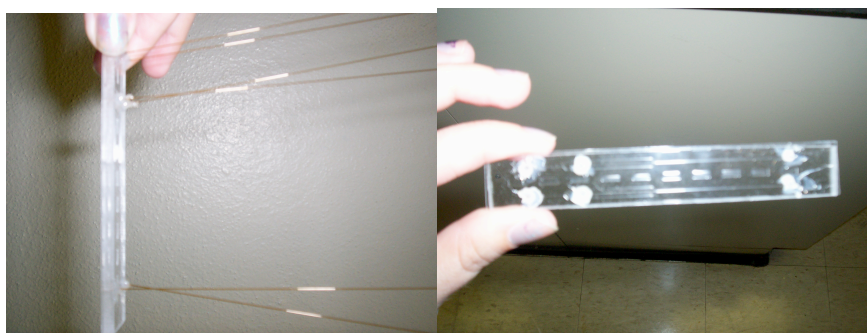


Figure 6.2. Images of the microfluidic device.

One problem that we had was controlling the flow rate. Figures 6.3- 6.6 show images that were taken from an experiment in which a solution of IBA/water, which was shaken and left to equilibrate for 24 hours at room temperature, was injected into the microfluidic device.

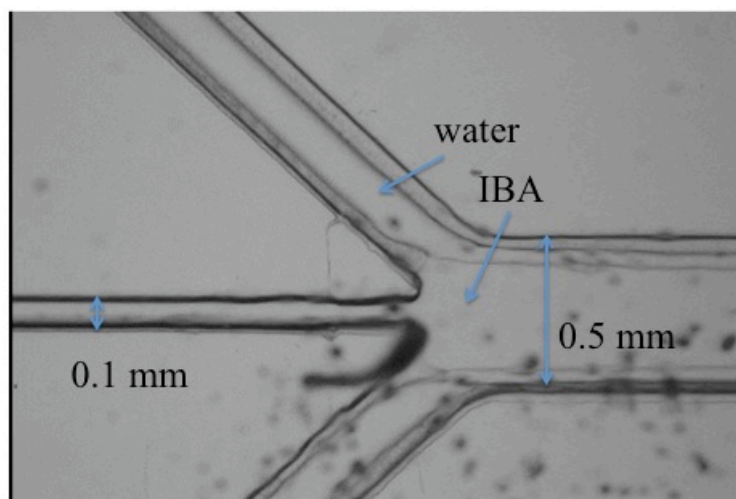


Figure 6.3. An image of the microfluidic device in which the IBA-rich phase was in the center and the water-rich phase was in the side channels, and more of the IBA-rich phase was flowing in than the water-rich phase.

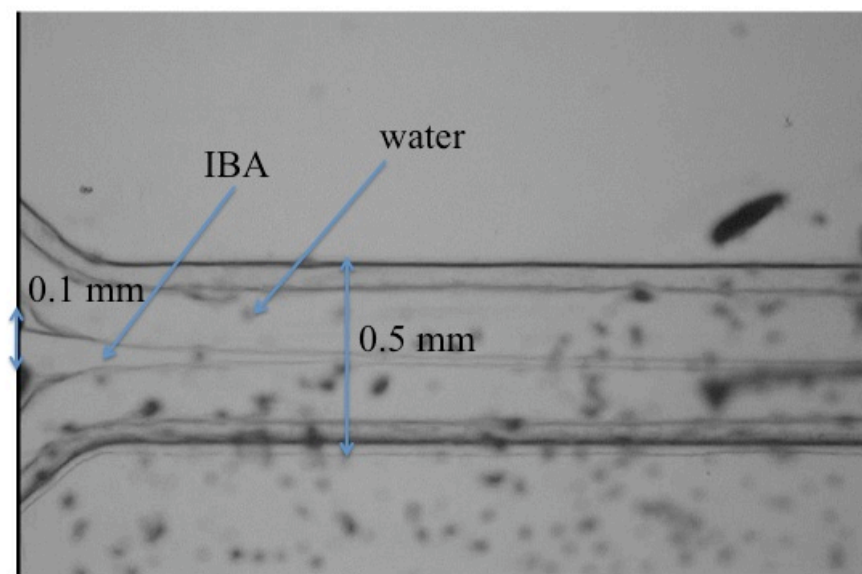


Figure 6.4. An image of the microfluidic device in which the IBA-rich phase was in the center and the water-rich phase was in the side channels, and more of the water-rich phase was flowing in than the IBA-rich phase.

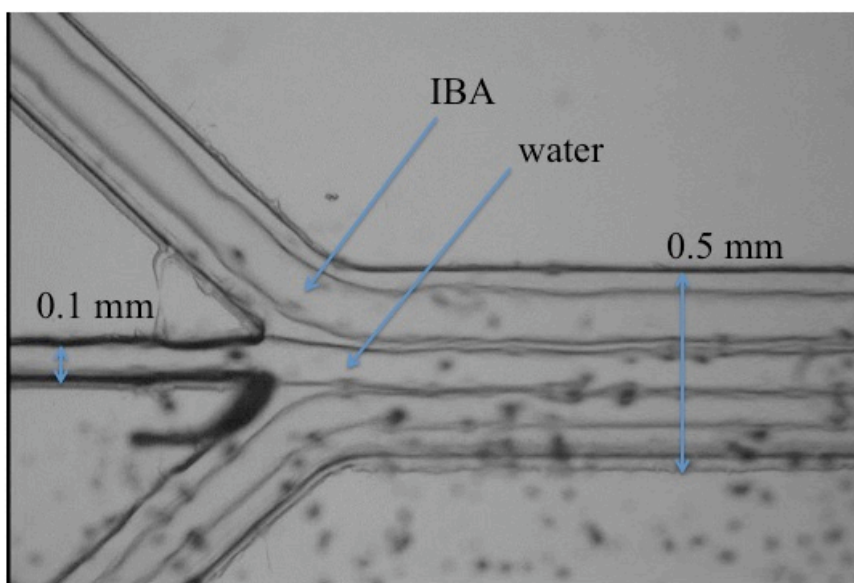


Figure 6.5. An image of the microfluidic device in which the water-rich phase was in the center and the IBA-rich phase was in the side channels, and the more of the IBA-rich phase was flowing in than the water-rich phase.

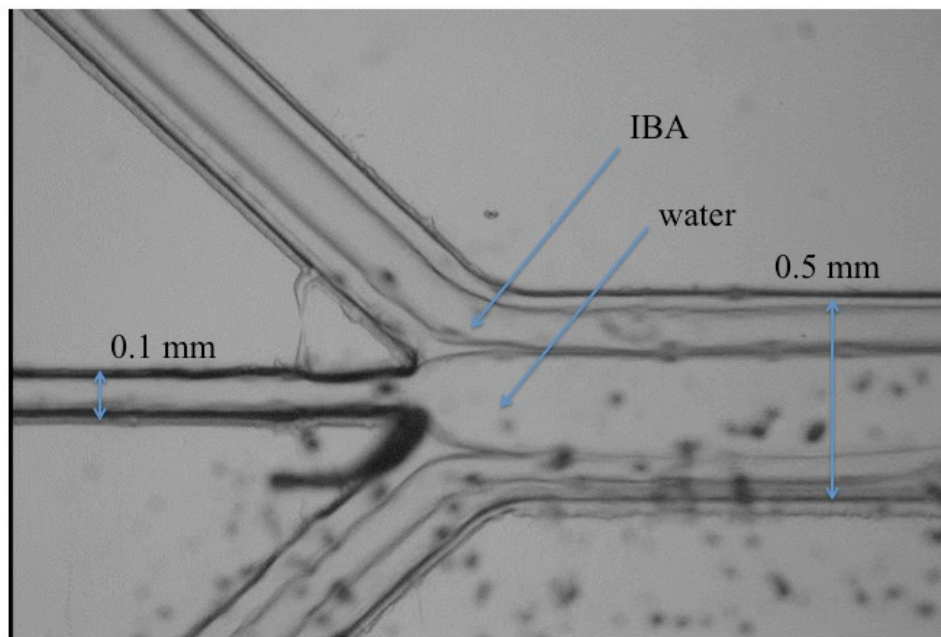


Figure 6.6. An image of the microfluidic device in which the water-rich phase was in the center and the IBA-rich phase was in the side channels, and more of the water-rich phase was flowing in than the IBA-rich phase.

Figures 6.3 and 6.4 had the IBA in the center channel and the water in the side channels so that, with the IBA clinging to the walls, when more IBA was flowing in than water, water had two very small channels while IBA had one large channel and two small channels. However, when more water was flowing in, IBA had three small channels while water had two bigger channels. Figures 6.5 and 6.6 show the microfluidic device with water flowing in the center channel and IBA in the side channels. For this condition, with the IBA clinging to the walls and more water flowing in, IBA and water had, respectively, four small channels and one big channel with two smaller channels while, when more IBA was flowing in, water and IBA had, respectively, three medium-sized channels and two small channels with two medium-sized channels.

Another problem that we had with this device was that the IBA was attaching to the walls and, as demonstrated in solubility tests, the IBA dissolved the PMMA channels. After one hour, the PMMA was showing indications that the IBA was clinging to its water. After one day, the PMMA had been partially dissolved by the IBA, as shown in Figure 6.7. When we tested IBA/water with polycarbonate (PC), the IBA and water had similar affinities and neither the IBA nor the water dissolved the sample of PC.

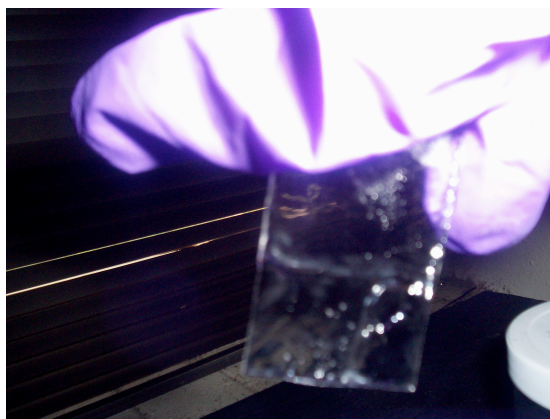


Figure 6.7. An image of the partially dissolved PMMA after one day in IBA/water.

On the other hand even after four days neither the IBA nor the water dissolved the PC. Though, on a drop test, the contact angle for IBA was smaller, indicating that IBA had a slightly greater affinity for the PC than water, after about thirty seconds, the IBA and water had similar contact angles.

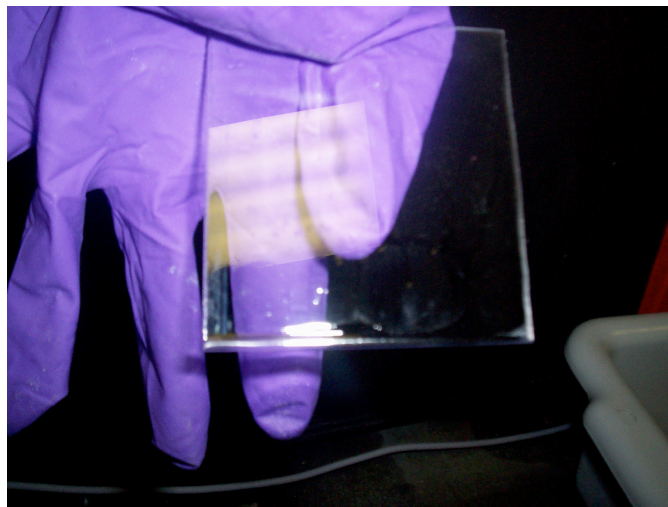


Figure 6.8. An image of the PC after four days in IBA/water.

So, we went with PC in 2-mm, 3-mm, and 5-mm channels. In some of the initial experiments, we tried different positioning of the microfluidic device. In Figure 6.9, the microfluidic device was perpendicular to the floor with gravity pulling the IBA towards the bottom of the image.

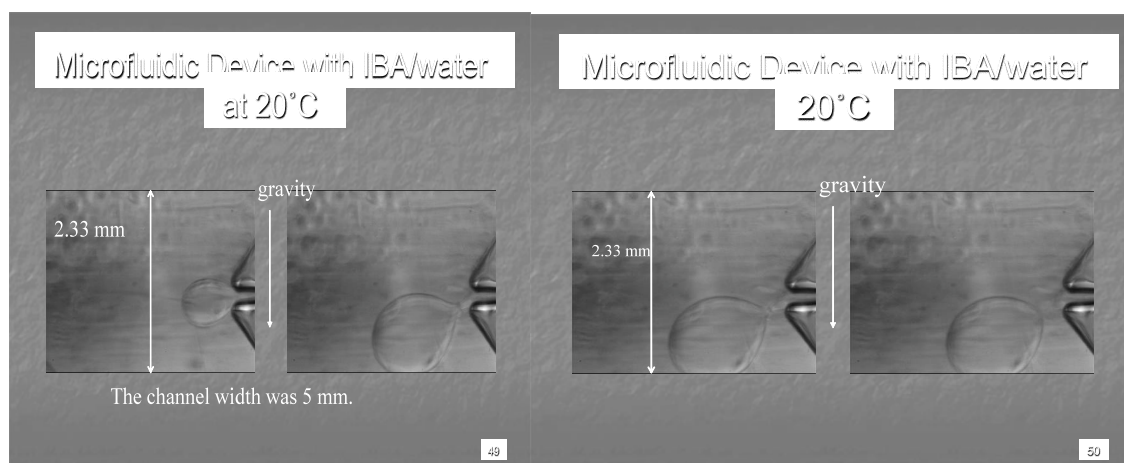


Figure 6.9. Microfluidic device with IBA/water at 20 °C.

The IBA drop was breaking off when it exited the channel but the breakup was most likely affected by gravity. The next position had the microfluidic device parallel with the floor but with changing flow rates.

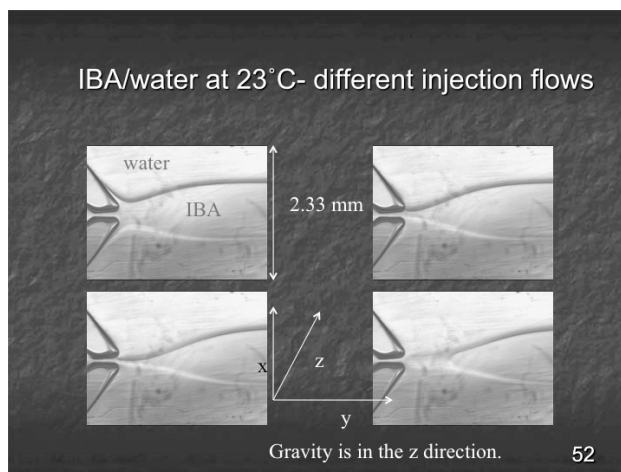


Figure 6.10. Microfluidic device with different injection flows of IBA/H₂O at 23 °C and had 2-mm wide channels.

Though the IBA drop was pinching off, the desired result was for IBA to pinch off by the Rayleigh-Plateau instability rather than gravity or changing flow rates (injection flows). Interfacial tension was part of the process. In the next group of experiments, we quickly injected a small amount of the lighter phase into the central channel and the heavier phase into the two outer channels at the same time and then let the phases equilibrate.

We also tried ethanol/water in this microfluidic device at 24 °C because ethanol dissolved too rapidly in the SDT. The 5-mm width channel was used. The first attempt had water injected into all three channels and then ethanol was added to the central channel and both syringes were pulled away. The ethanol would appear only briefly and then start to dissolve.

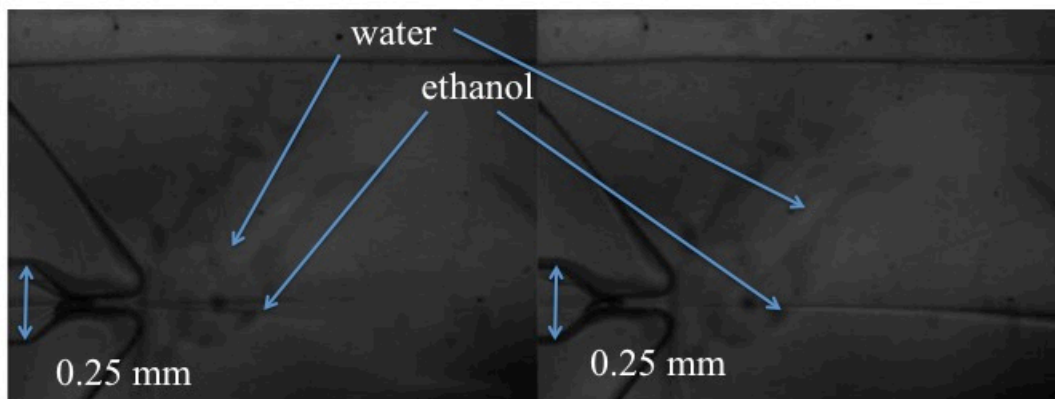


Figure 6.11. Ethanol being injected into 5-mm PC microfluidic device.

As the ethanol was injected into the water-rich phase, the ethanol would become fainter or more diffuse over time.

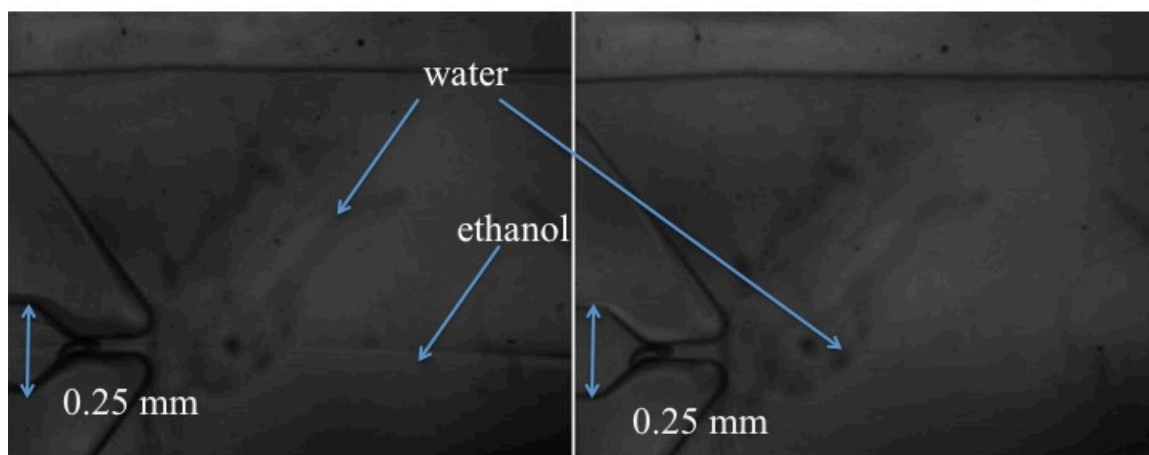


Figure 6.12. The ethanol became fainter or more diffuse as it was continually injected.

When the water and ethanol syringes were pulled out, both the ethanol and water would flow backwards through the central channel because when the syringes were removed, a void of pressure occurred.

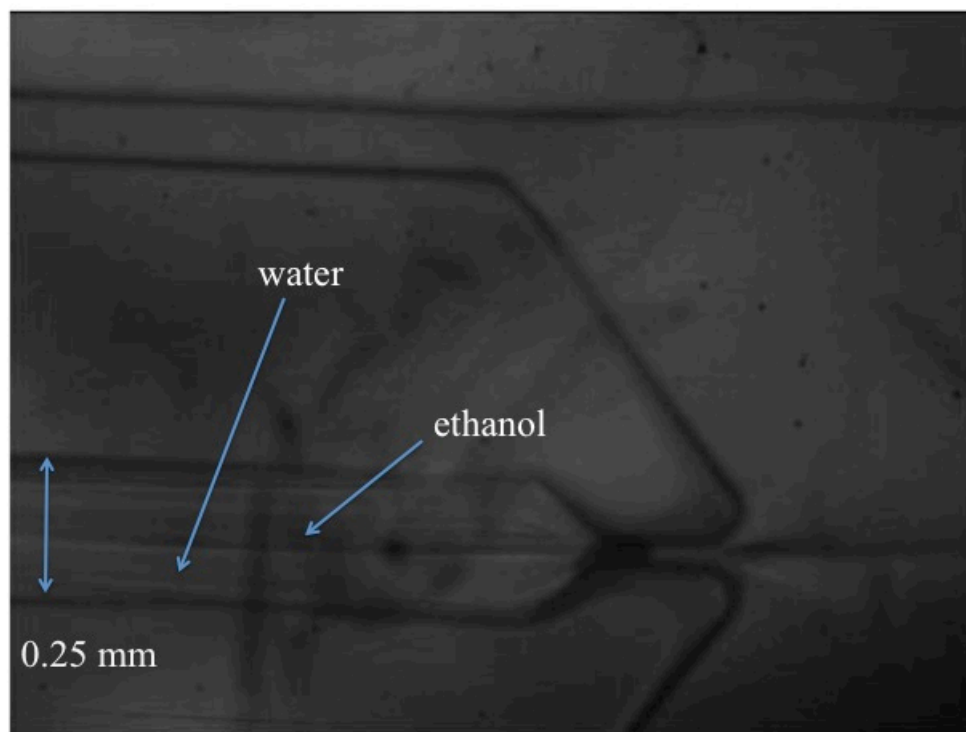


Figure 6.13. The syringes being pulled out and both ethanol and water flowed backwards through the central channel.

When both ethanol and water were injected at the same time, the ethanol became harder to see but was still slightly visible as faint lines. The next three figures show how faint ethanol was and that the flow of ethanol would become slightly wider and then narrow. The first of these three figures show the typical narrow band of ethanol flow. The next two figures show how the flow of ethanol first widened out and then narrowed as the ethanol and water were injected at the same time (the ethanol was injected into the central channel and water was injected into the two outer channels). The ethanol is below the black arrows for the first image. The next two figures have the ethanol between the black arrows.

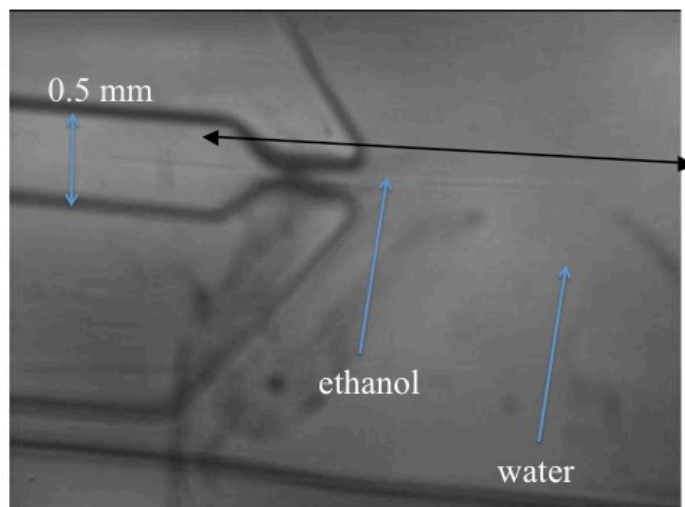


Figure 6.14. Faint lines of ethanol in a 5-mm PC microfluidic device.

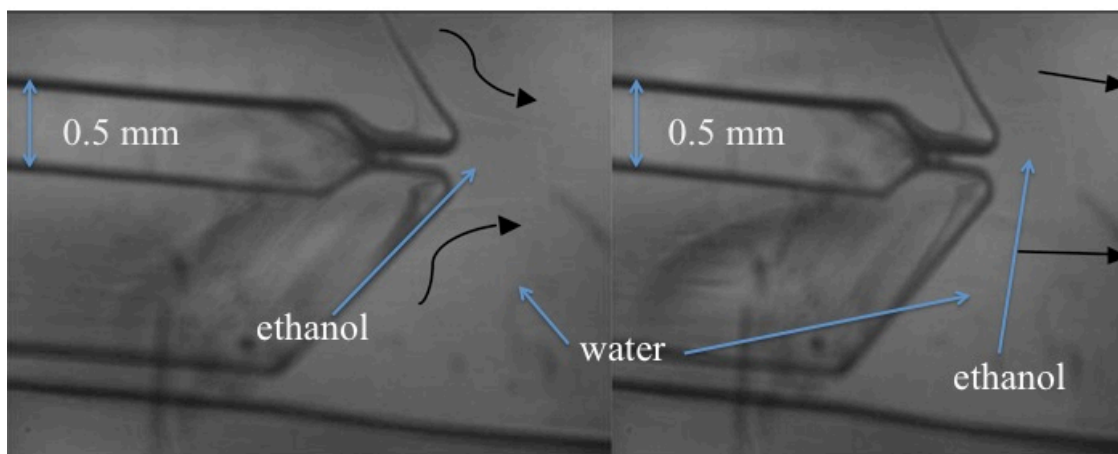


Figure 6.15. Faint lines of ethanol widening in a 5-mm PC microfluidic device.

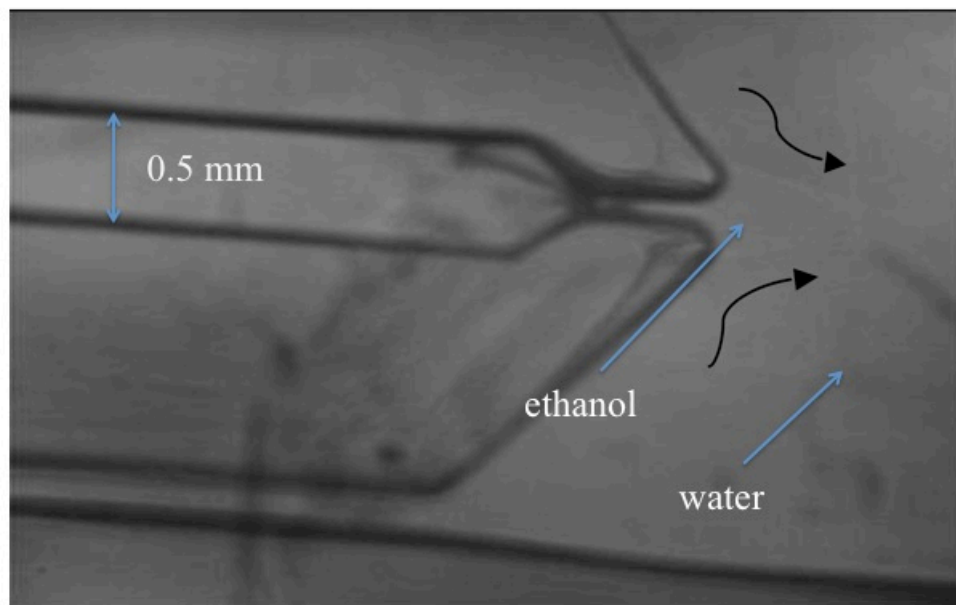


Figure 6.16. The faint lines of ethanol narrowing in a 5-mm PC microfluidic device.

Figure 6.17 shows more ethanol being injected than water and, even then, the ethanol is dissolving.

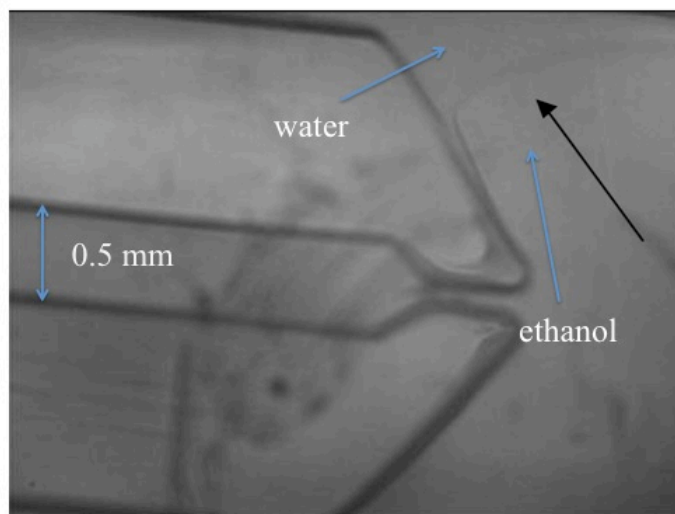


Figure 6.17. Ethanol dissolving in the upper part of the 5-mm PC microfluidic device.

The black arrow points to where the ethanol starts to dissolve. We did not test the ethanol/water system in any more of the microfluidic devices.

The next group of figures shows IBA/water and n-butanol/water in the PC microfluidic device. Figures 6.18 and 6.19 show the behavior of a system consisting of IBA and water at 23 °C in the 5-mm PC microfluidic device. Figures 6.18 and 6.19 show how the two water drops merge. The IBA phase showed no distinct lines while the water-rich phase formed small globules. The water drops merged together. The effect that we were hoping to find was with the cylinder drop breaking up into smaller drops. For all of the channels widths used with IBA/water with a PC microfluidic device, the 5-mm channel had the water drops coming the closest together.

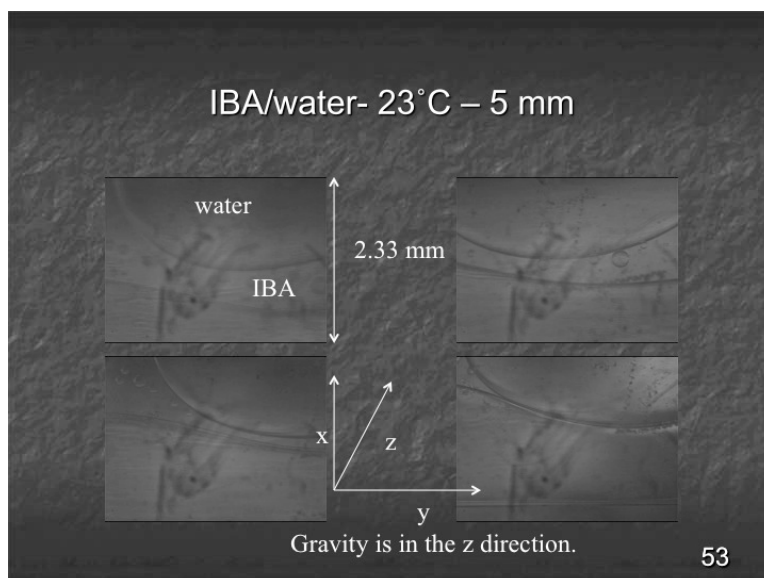


Figure 6.18. PC Microfluidic device with IBA/water in 5-mm wide channel.

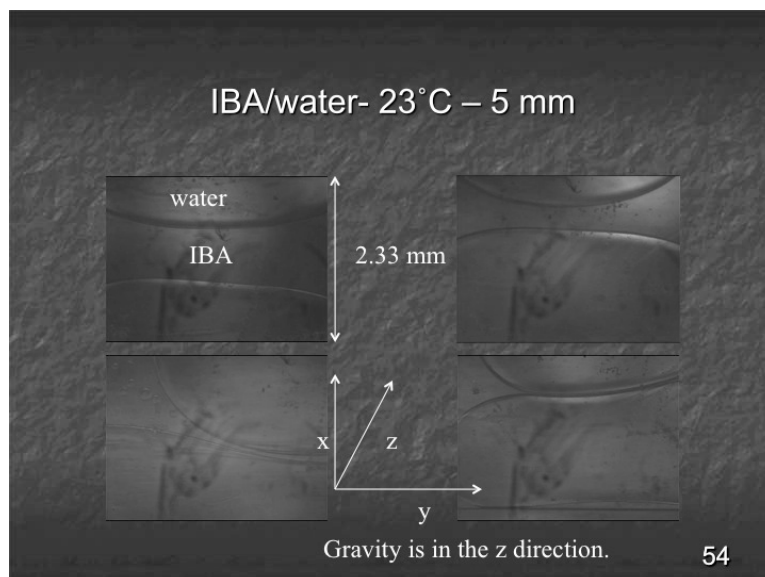


Figure 6.19. Another image of a PC microfluidic device with IBA/water in 5-mm wide channel.

For the 3-mm width channel of the PC microfluidic device, the water drops came close together but never merged. Figures 6.20 and 6.21 show this behavior.

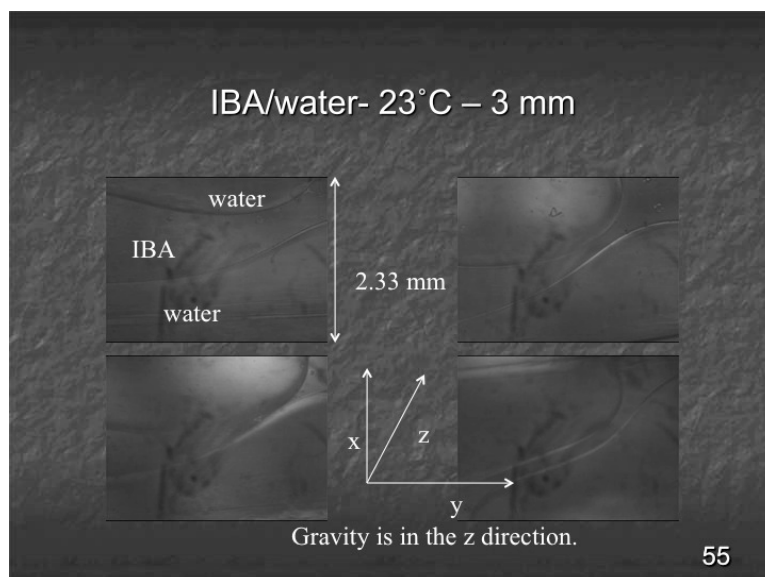


Figure 6.20. PC Microfluidic device with IBA/water in 3-mm wide channel.

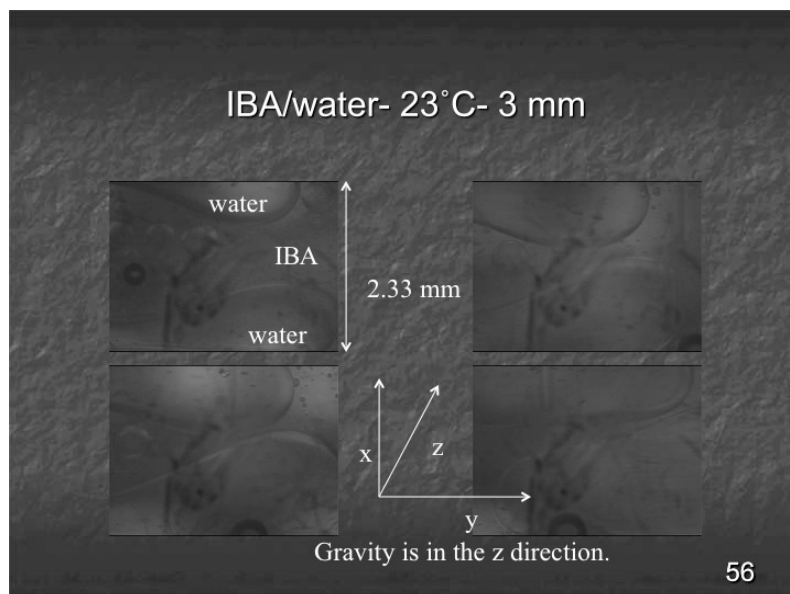


Figure 6.21. Another image of a PC microfluidic device with IBA/water in 3-mm wide channel.

In the 3-mm width channel, the water drops would slide past each other and never touch. The smaller channel restricted the water drop's ability to merge. So, the interfacial tension of the walls of the microfluidic device with the water phase was larger than interfacial tension between the IBA and water-rich phases. Similar to the 5-mm channel, the IBA phase had no distinct boundary lines while the water drops formed small globules and then merged into one large blob.

Like the other two channel widths for PC, the 2-mm channel width PM with IBA/water also had the water-rich phase forming small globules while the IBA phase had no distinct boundary. One interesting difference in behavior that 2-mm width had was the water drops breaking up other water droplets. Two large water drops would flow past each other and in a stream-like manner, and then one (the water drop near the top view of the channel) drop would flow downward

and break up the large stream-like water drop that would be below it into two smaller water drops. Figure 6.22 shows this behavior.

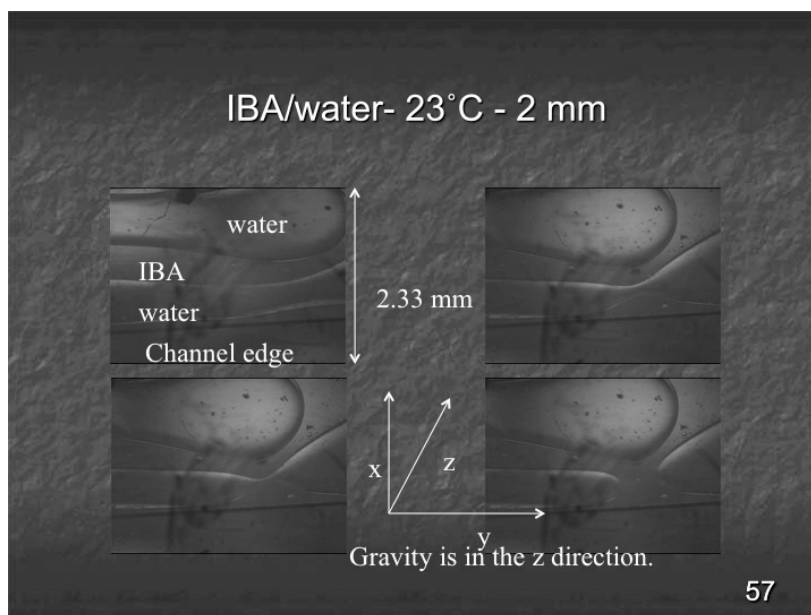


Figure 6.22. PC Microfluidic device with IBA/water in 2-mm wide channel.

Experiments with n-butanol/water in PC microfluidic devices were done similarly. Like IBA/water, the n-butanol/water in the 2-, 3-, and 5-mm width channels showed the water-rich drops forming small globules while the lighter phase did not have a distinct boundary. One major difference in behavior for n-butanol/water in comparison with IBA/water for the 5-mm channel width was that the water droplets moved much more slowly, moving mm per minute versus the mm per second for IBA/water, as shown in Figure 6.23 because of the greater viscosity of n-butanol compared to IBA. To validate that any reported observations were consistent for both systems, images were taken in those moments that did not have the syringe pushed for over a minute and the syringes

had been taken out, thus ensuring that the hydrostatic pressure and how much pressure was applied syringes did not affect what was observed.

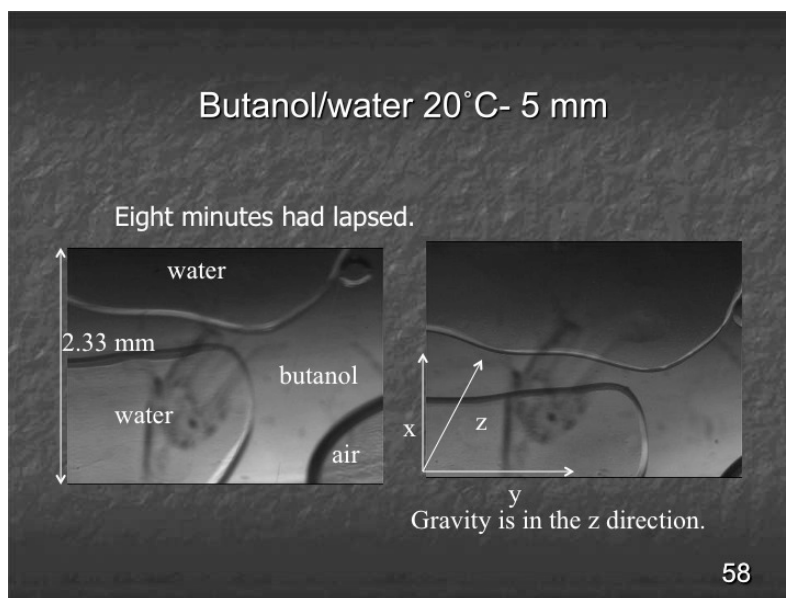


Figure 6.23. PC Microfluidic device with n-butanol/water in 5-mm wide channel.

Another difference was the water drops for n-butanol/water never met in the 5-mm channel width; instead, the water drops would pass by each other like the water drops did for IBA/water in the 3-mm channel. A third difference was that n-butanol/water had a smaller contact angle with the surface and had a slightly sharper boundary between the lighter and heavier phases than IBA/water. One reason in this difference in behavior is the difference in EIT for the two systems. With n-butanol/water having the larger EIT and hence larger viscosity, the water drops would move more slowly.

For n-butanol/water with a 3-mm channel width for the PC microfluidic device, the water drops never moved. Figure 6.24 shows the clearly separated water drops.

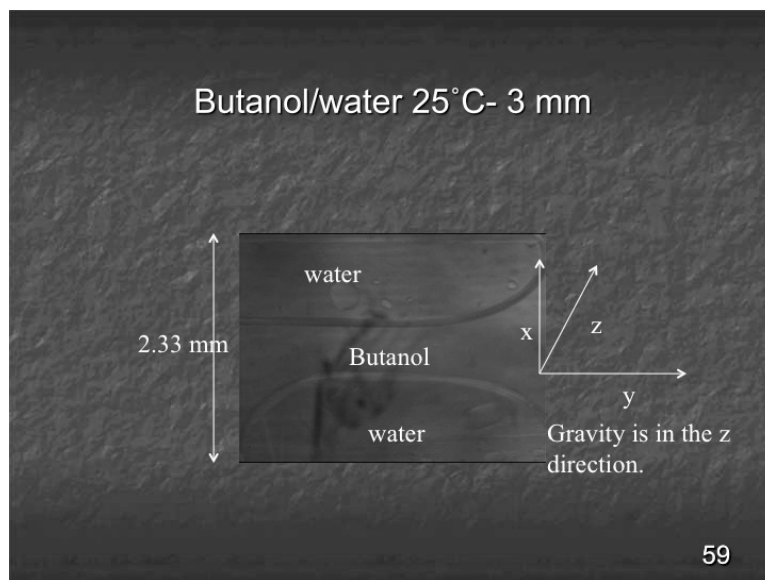


Figure 6.24. PC Microfluidic device with n-butanol/water in 3-mm wide channel.

Like the IBA/water 3-mm channel width for the PC microfluidic device, the smaller channel restricted the water drop's ability to merge or move.

For the 2-mm channel width for the PC microfluidic device with n-butanol/water, the water drop was one large drop rather than several smaller drops as seen in Figures 6.25 and 6.26. This behavior was not seen in any of the other PC microfluidic devices using IBA/water or n-butanol/water.

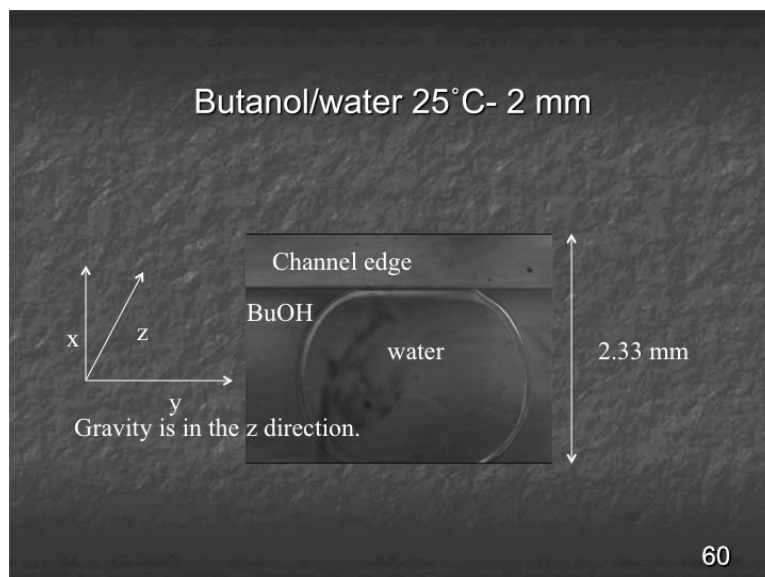


Figure 6.25. PC Microfluidic device with n-butanol/water in 2-mm wide channel.

Figure 6.26 also shows the large water drop moving very slowly similar to the water drop in 5-mm channel width. The systems were injected into the microfluidic device in the same manner with the syringes taken out and then images were taken at least a minute later. So, the motion is only controlled by the properties of the miscible and partially miscible system itself rather than flow rate or hydrostatic pressure.

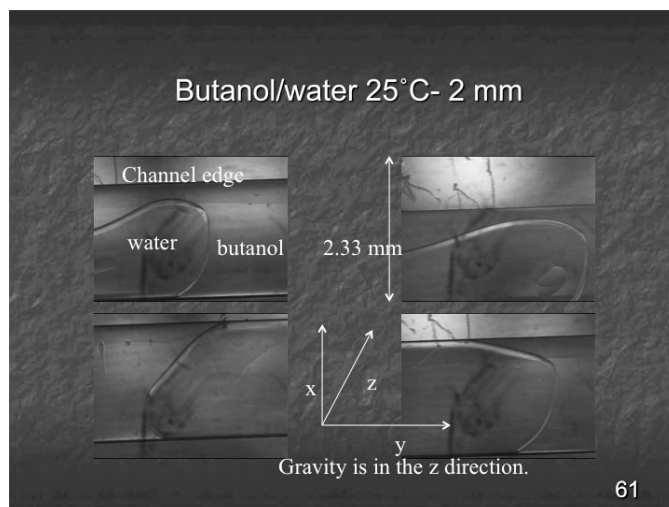


Figure 6.26. PC Microfluidic device with n-butanol/water in 3-mm wide channel.

None of the behaviors seen for n-butanol/water or IBA/water was what we were expecting. Part of the problem was the wettability between the PC and water. We were looking for the IBA and n-butanol drops to be a cylinder that would break up into smaller drops. Our conclusion was that the material was too hydrophobic. The modified PC was processed in two different ways to make it more hydrophilic: (1) exposure to a broad band UV lamp and (2) exposure to 254 nm UV light. To confirm that the wettability was the problem and try to find a more hydrophilic compound, contact angles were taken between PC and two different modified PCs and IBA, n-butanol, and water.

Table 6.1

Contact Angles of Various Systems on Different Surfaces

System	Surface	Contact Angle (Degrees)
Pure BuOH	PC	9.3
Pure IBA	PC	10.6
Pure IBA	PC exposed to IBA	46.3
Equilibrated IBA	PC	6.58
BuOH	Modified PC (broadband)	23.1
BuOH	Modified PC (254)	19.4
Pure IBA	Modified PC (broadband)	11.6
Pure IBA	Modified PC (254)	9.09
Equilibrated IBA	Modified PC (broadband)	12.4
Equilibrated IBA	Modified PC (254)	10.2
Water	Modified PC (broadband)	79.8
Water	Modified PC (254)	81.7
Water	Modified PC exposed to IBA (254)	53.9
Water with IBA drop on top of it	Modified PC (254)	12.7

When pure n-butanol and pure IBA were exposed to pure PC, both had small contact angles. When IBA was re-exposed to the PC after IBA had already been tested, the contact angle increased. Equilibrated IBA had the smallest contact angle between pure IBA, pure n-butanol, and equilibrated IBA because equilibrated IBA had some water in it and had decreased interfacial tension, allowing the equilibrated IBA to have more wettability. However, the pure IBA on the PC with previous exposure to pure IBA had the largest contact angle because the previous IBA had made the PC more hydrophilic so that it left a small residue, making the second exposure made the surface less wettable.

The broadband-modified PC was slightly more hydrophilic than 254-nm-modified PC as shown with the pure n-butanol, pure IBA, and equilibrated IBA having slightly larger contact angles with the broadband-modified PC and the slightly larger contact angle that the pure water had for the 254-nm-modified PC. The modification of the PC also increased the contact angle for pure n-butanol the most out of the pure IBA, equilibrated IBA, and pure n-butanol while pure IBA had the smallest change out of these three conditions. This can be explained by the fact that the UV treatment oxidized the surface, making it more hydrophilic. Another interesting behavior was how the contact angle for pure water decreased significantly when pure water was placed in a spot where IBA had been and then decreased even more when pure water had a drop of pure IBA placed on top of the water drop. The initial drop of pure IBA had made the surface more wettable so that the drop of water had decreased contact angle. The addition of the drop of IBA on top of the water drop decreased the contact angle the most because the IBA drop moved through the water to make contact with the surface, leaving more of the water-rich phase on top rather than having the water-rich phase on bottom.

Overall, both methods decreased the contact angle of water but not extensively. We still obtained similar results to those shown in Figures 6.17-6.26.

One possible problem that we had besides hydrophobicity was identifying which phase was which. A few experiments were done using a fluorescent dye (fluorescein) and regular food dye. When IBA/water with the fluorescent dye was injected into the PC microfluidic device, air bubbles could clearly be seen by the

naked eye, but, in the two syringes, the IBA and water were pretty much the same color and looked the same color when injected into the microfluidic device. The fluorescence was good way to tell the difference between the air and IBA/water (but air and IBA/water could already be differentiated because the air bubble had a very dark boundary around it while the IBA/water phases had a light gray to little difference in boundaries) but not any significant difference between IBA and water. When the food dyes were used, the syringes of IBA and water showed significant color difference, but when these syringes were injected into the microfluidic device, no significant color difference could be seen. No further testing was done with trying to identify the differences between lighter and heavier phases in the microfluidic device.

Polydimethylsiloxane (PDMS) Microfluidic Device

The microfluidic device was made of polydimethylsiloxane and was from Eugenia Kumacheva's research group at the University of Toronto in Canada. Figure 6.27 shows this microfluidic device.

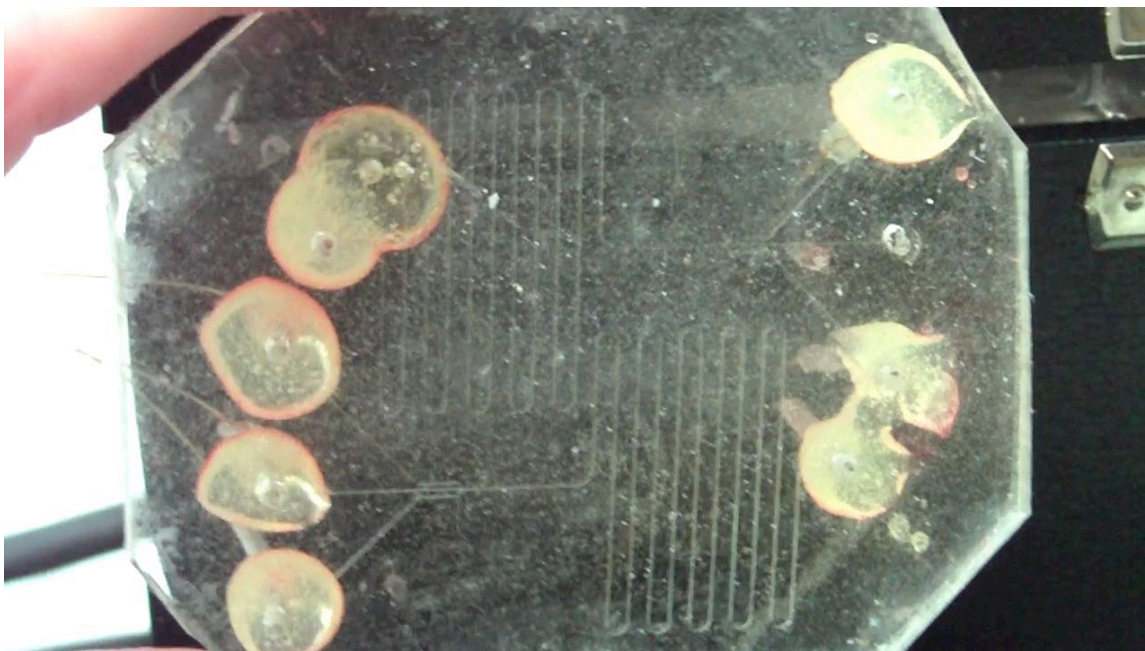


Figure 6.27. Underside view of the PDMS microfluidic device.

The microfluidic device was tested by injecting IBA in the center channel and water in outer channels. Since there were three capillaries for the three channels, one of the capillaries was injected with a 21-gauge needle rather than a glass end (glass ends were used for IBA and one outer water). The procedure was to first press all three at once (with the plastic syringes at 6-8 mLs for best results of long IBA and water drops) with the chip parallel with the ground and then move it perpendicular to the ground so that gravity was pulling down. After the initial press of all three were done parallel, the rest of the presses of all three at one time were done with the chip perpendicular to the floor. The PC-modified chip was tested at the same time as the PDMS chip but nothing could really be seen moving despite first pressing the syringes parallel and then perpendicular to the floor. One problem with the PC modified and PDMS chip was that the glass

syringes kept popping out so that the chips had to be retested. A big problem with the PDMS was having to use another person in order to press all syringes at once. In the initial runs of the PDMS microfluidic device, a lot of IBA and water droplets broke up before meeting and it was hard to distinguish between the IBA and water drops. After several different attempts, the best method to get the fluids to flow with long drops that break up when meeting was to: first press all three at once (with the plastic syringes at 6-8 mLs for best results of long IBA and water drops) with the chip parallel with the ground and then move it perpendicular to the ground so that gravity was pulling down. After the initial press of all three were done parallel, the rest of the presses of all three at one time were done with the chip perpendicular to the floor.

Some of the initial results from the PDMS chip showed the results that we had wanted to see: long cylinder drops breaking up into smaller drops. For a cylinder drop breaking up further away from Y-junction where the IBA and water-rich phases first meet, long fluids flow in a straight line as shown in Figure 6.29 and the two lines are evenly spaced. Then, one of the streaming lines may start to thin out in the bottom part of Figure 6.28 or, as in Figure 6.29-9.31, the evenly spaced streams start to drift to one side so that three streams start to become two streams as show until one long cylinder drop breaks up into smaller drops.

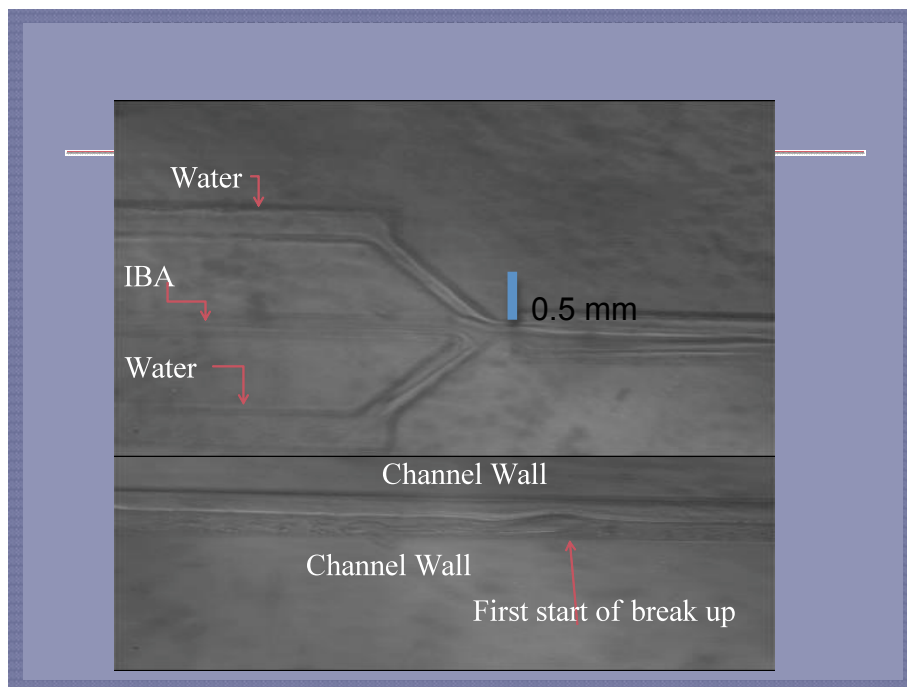


Figure 6.28. Y-junction of PDMS microfluidic chip and initial break up.

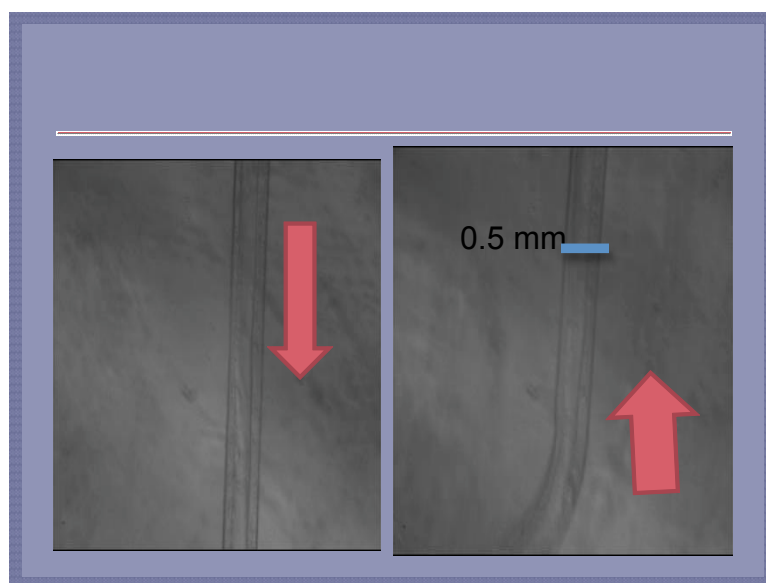


Figure 6.29. Streams start to drift towards one side of channel.

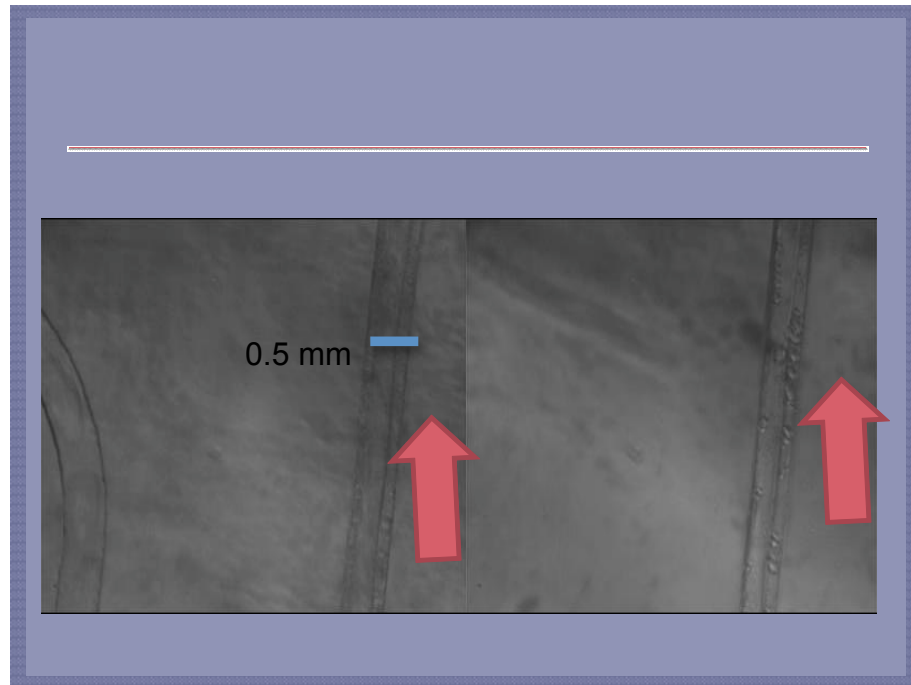


Figure 6.30. Three streams become two streams.

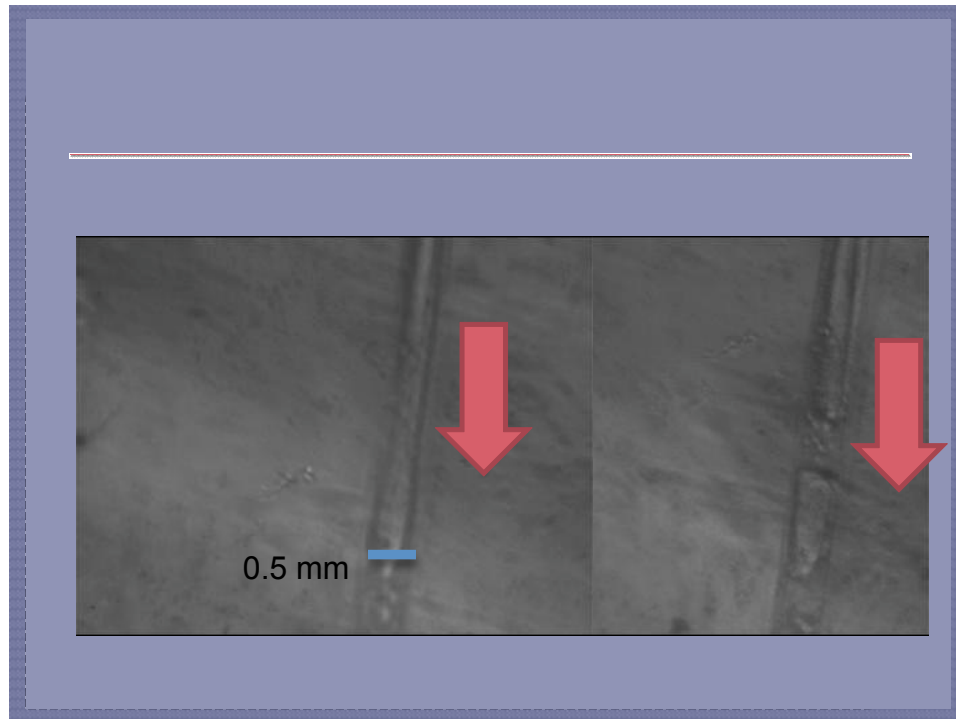


Figure 6.31. Long cylinder drop breaks up into smaller drops.

A long cylinder drop also broke up near the Y-junction of where the central channel of IBA met the two outer channels of water. This break-up occurred in a similar method that occurred in the drop breakup away from the Y-junction except that the break-up occurred more quickly over a shorter distance. Figures 6.32-6.34 show this progression of events.

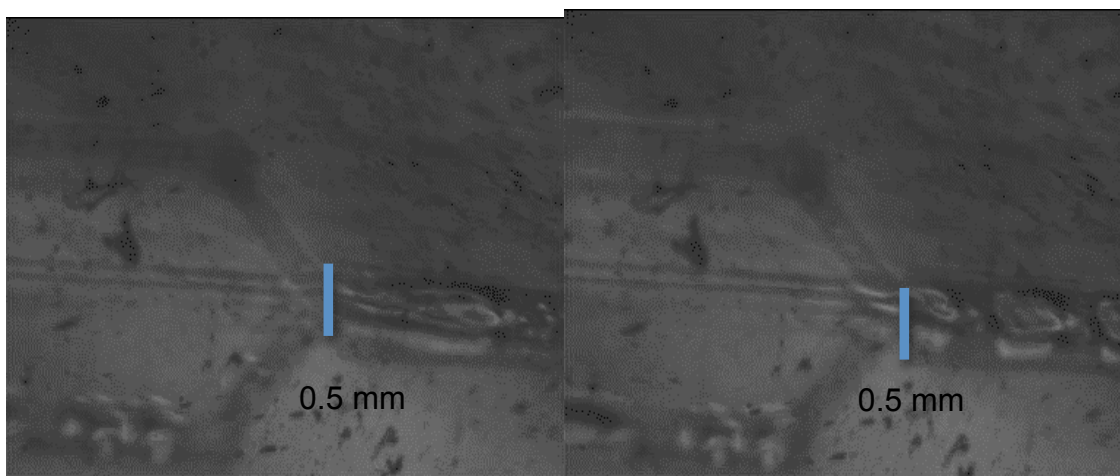


Figure 6.32. Initial start of drop break up.

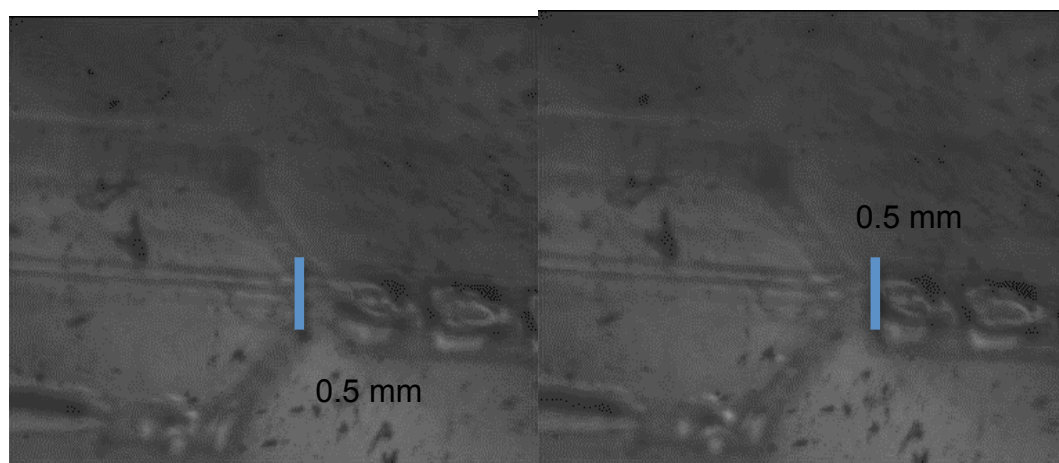


Figure 6.33. Part of IBA stream starts to hit upper, outer channel of water so that the IBA drop breaks off.

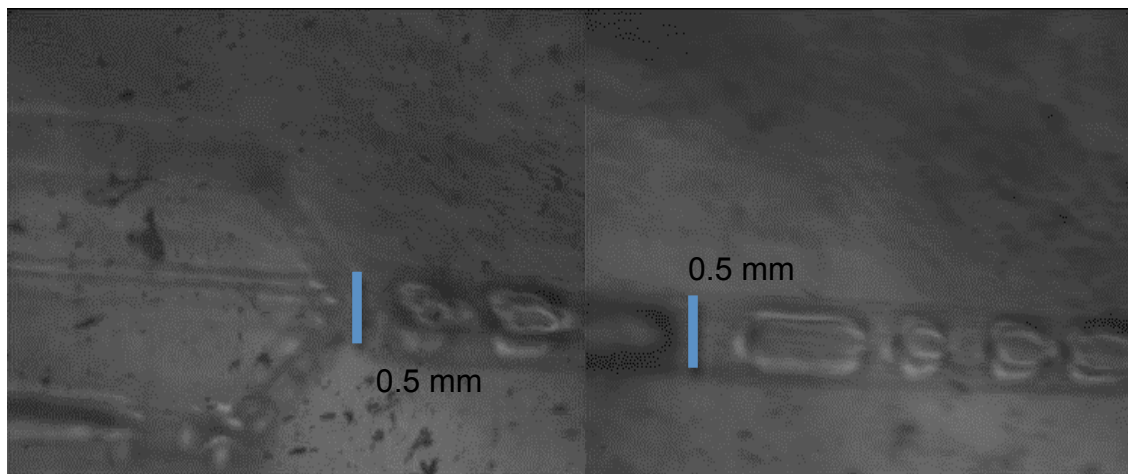


Figure 6.34. The IBA drops are completely broken off and become more clearly defined as separate drops.

Another way of a long cylinder drop breaking up into smaller drops at the Y-junction is shown in Figures 6.35-6.36. The smaller drops just seem to pinch off from the longer cylinder drops in the middle of the channel slightly past where the Y-junction is.

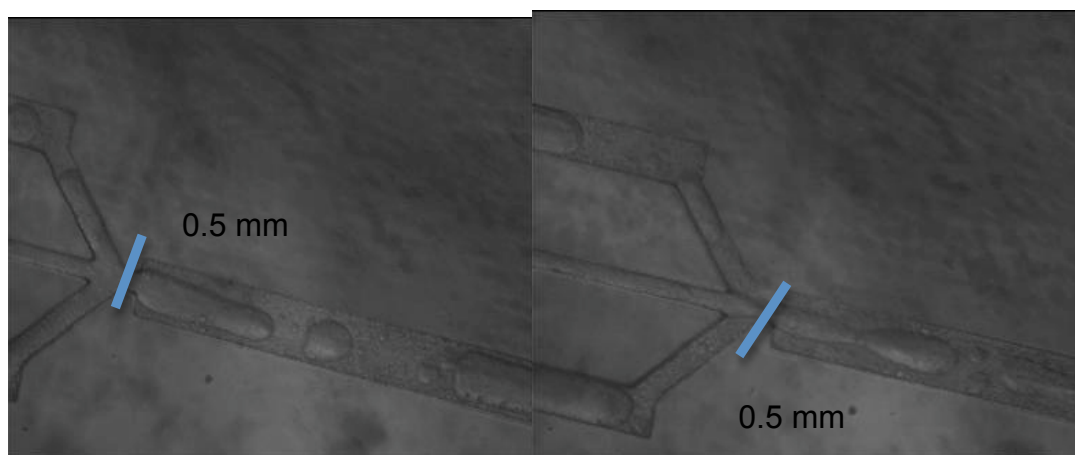


Figure 6.35. Cylindrical IBA drop of breaks up into smaller drops in PDMS chip.

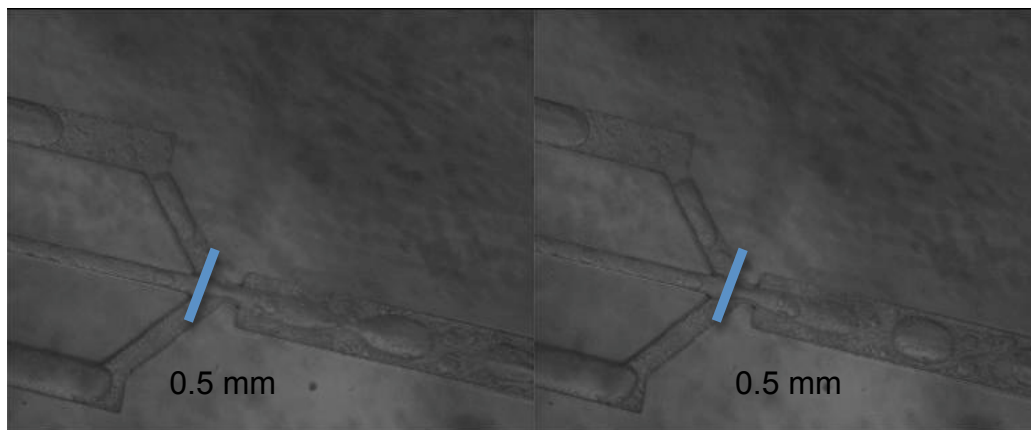


Figure 6.36. Continuation of cylinder IBA drop breaking into smaller drops in PDMS chip.

Some of our initial results also showed how difficult it was to distinguish between IBA and water drops as seen in Figures 6.28-6.34. In all of the instances of the long cylinder drop breaking up into smaller drops, both instances occurred when a brief press of 1-2 seconds of light pressure followed by letting hydrostatic pressure do the rest: neither continuous flow nor changing flow rates occurred as the long cylinder drop was breaking into smaller drops.

However, with these good results, we did have a problem with getting good images because, after a while, the outer surface of the microfluidic device became cloudy so that images were harder to see as shown in Figures 6.32-6.34. Another problem was the difficulty in controlling the initial flow rate with only one person or even two people. Two people were required in order to get three syringes pressed at the same time while recording a movie. Only the immiscible region was done because anything done in the miscible region would immediately dissolve: the IBA would immediately start to dissolve the moment it had any contact with water. Another problem was poor temperature control;

temperature control was done by placing the microfluidic chip on top of a hot oil bath with the temperature taken from the surface of the microfluidic device rather than inside it. By raising the oil bath above 40 °C, the surface of the microfluidic chip was about 30 °C.

Conclusions

In conclusion, the microfluidic PDMS worked best in the obtaining the capillary instability that we sought. In the microfluidic chip design, the three-stream design was chosen because this design allowed multiple laminar flows and less turbulent mixing. Some of the initial problems that we encountered with the PC and PMMA were solved by using PDMS and a different microfluidic design since PDMS had good hydrophilicity and longer, curving distance. One problem that can be solved with the scratching that caused some of the bad images would be the placement of glass on the outside of the microfluidic device. However, one problem that we could not really solve was discerning whether a drop was the lighter or heavier fluid.

For the microfluidic device, unlike the SDT, no observable Marangoni instability was seen. The Marangoni instability was easily be seen in IBA/water or IBA/surfactant/water in the SDT or even in other immiscible and miscible systems in non-microfluidic devices. We did see Rayleigh-Plateau instability for IBA/water in the microfluidic device. Other research has also shown Rayleigh-Plateau instability in immiscible and other miscible systems.³⁸ The drop breakup that we saw in the PDMS microfluidic chip was most likely due to the Rayleigh-

Plateau and end-pinching instabilities while the drop break up that was in the PMMA and both modified and non-modified microfluidic chip was most likely due to either wettability, gravitational forces, Rayleigh-Plateau instability or changing flow rates.⁵⁴

The IBA/water and n-butanol/water systems' behavior in the PMMA and modified PC microfluidic chips are similar to the results seen by the immiscible behavior in Hagedorn *et al.*⁵⁴ Gravitational forces can affect drop breakup because, with two different densities, buoyant forces can drive the more dense fluid downward into the less dense fluid.³⁸ This behavior was easily seen in the PC chips where the water-rich drops would break up other water-rich drops. The drops more easily broke up in the PDMS microfluidic chip than in the PC (both modified and non-modified) or the PMMA chip. The drop breaking up indicates that Korteweg stresses were present in the PDMS chips. Another difference between the PDMS versus the PMMA and modified PC microfluidic chip was that the water drops in the PMMA and modified PC chips were easily seen than in the PDMS chips. The differences in behavior between the PMMA and modified PC versus PDMS is most likely because of the differences in the capillary channels and the materials used. The smaller channels increased the Korteweg stress and any EIT effects. In the PMMA and modified PC chips, any Korteweg was were likely equalized.

We observed that the microfluidic devices, especially the PDMS microfluidic devices, containing miscible and partially systems had IBA/water with less sharp concentration gradients than the ones observed in the SDT. When

the IBA and water phases first met in the microfluidic device, they were sharper than when they were further along and dissolving into each other. As the fluids dissolved into each in the microfluidic device, the IBA-rich drop lost its sharpness, in contrast to the SDT, in which the IBA-rich phase kept its sharp boundary as it dissolved. For the microfluidic because of the large surface area to volume, larger effects from EITs should occur. The larger EITs would occur in the upstream where the IBA-rich and water-rich phases met and have smaller EIT in the downstream, generating a stress toward the upstream. This behavior was seen in our results with the PDMS microfluidic device and in Sugii *et al.*⁵⁵ and would explain why the IBA drops were sharper in the upstream but were less sharp as they went downstream and broke up into smaller dissolving droplets. In contrast, the IBA-rich always remained sharp in the SDT as the drop dissolved, possibly indicating that a stress was occurring in the SDT but that it remained equalized or that an artifact was present.

We were not able to measure the EIT in the microfluidic device using the current equation that we used for IBA/water systems in the SDT in Chapter IV and which is discussed in Chapter IV. We also found some unusual behavior in the microfluidic device that we did not have with the SDT. We had more problems in trying to get a long cylinder drop to break up in the microfluidic device. Using the PDMS microfluidic device, some of our first images of long cylinder lighter phase drop breaking up was observed. In the microfluidic device, the water-rich phase would be observed to merge together without any rotation

while, in the SDT the lighter phase would merge together when the SDT's rotation was started.

CHAPTER VII

CONCLUSIONS AND FUTURE WORK

Before we could test our hypothesis that barodiffusion caused IBA/water and n-butanol/water systems to have sharp boundaries and yet the drop stretched, shrank in length, and then started to dissolve, we first had to replicate the previous experimental results found in the Pojman lab.¹ Problems with trying to replicate the experiment included obtaining measurable drops that were similar in size and in the length of time they lasted before dissolving. We had to test different methods and vary different experimental conditions including how much IBA to add, what initial rotation rate to use, etc.

Using equilibrated systems gave us more reproducible results, but we still had to determine many different experimental conditions including how long to let the systems equilibrate, how much to inject of each system, what initial rotation rate to use, what initial temperature to use, etc. in order to obtain enough analyzable drops that did not dissolve in 10 seconds or less and that were similar in size. From these different methods, we found that lower temperatures and lower rotation rates had fatter (bigger radii across) drops that tended to dissolve slower, thus making them easier to analyze and producing more consistent results. Another interesting result was that long drops of IBA/water can have blurry boundaries after half an hour of spinning at high rotation rates and above the UCST, a behavior not observed previously in other experiments. From these obtuse boundaries, we can conclude that barodiffusion was not the reason for the sharp concentration gradients. Also, evidence of end pinching is indicative of

Korteweg stress and EIT because end pinching and EIT can occur in immiscible systems and other miscible systems like dodecyl acrylate/polydodecylacrylate.¹

Once we developed a usable method, then we were able to observe that miscible fluids such as IBA and water exhibited an effective interfacial tension when brought in contact with each other. We studied the IBA/water system at five different rotation rates (6000, 8000, 10000, 12000, and 14000 rpm) and at three different temperatures (20, 25, and 27 °C) that were close to the consolute point. Five different rotation rates were selected because the rotational acceleration of the SDT could affect the diffusional flux due to the very small diffusion coefficient near the consolute point.

For isobutyric acid and water, we tested if the rotational acceleration affected diffusion by studying the drop volume/surface area, which is proportional to the flux for different rotation rates. With increasing rotation rate at 20 °C, we found that the dissolution rate increased and the averaged IT/EIT decreased. The averaged EIT or IT also decreased when temperature was increased from 20 °C to 25 °C or 27 °C. These results with increasing temperature are different from those previously observed in the Pojman lab when equilibrated IBA/water was used.¹ In initial experiments conducted in this experiment when equilibrated IBA/water was used, smaller dissolution rates and larger volume/surface area than systems with pure IBA/water occurred. Air bubbles sometimes adversely affected the dissolution rate and the averaged IT/EIT. The averaged drop radii and the duration the drop was present also could have an impact on the averaged IT/EIT. These results demonstrated that barodiffusion did not cause the

sharp concentration gradient but did affect the dissolution rate at 20 °C. Cussler states diffusion coefficient is expected to decrease as the temperature is decreased to the consolute point.⁴⁶ A second explanation assumes that “long-range fluctuations dominate behavior near the consolute point” and that diffusion occurs when the fluctuations of concentration and fluid velocity combine.⁴⁶

With increasing temperature, the dissolution rate seems to be relaxing like the relaxation of the concentration gradient over time. Previous research^{24, 26, 33, 35, 47, 48} has demonstrated that gravitational acceleration can affect diffusion near a critical solution temperature. Differences in these researchers’ results and the experimental findings in this dissertation can be attributed to the small range or to smaller difference in rotational acceleration as compared to other researchers. Another possibility is that the immiscible region of small volume is more affected by rotational acceleration than small volume that is near the UCST.

The SDT experiments with IBA-water system demonstrated that an EIT exists between the two fluids and can be measured for IBA-water systems. We also demonstrated how SDT can be used to observe how this phenomenon relaxed with time. Future work with SDT would focus on testing other types of miscible, partially miscible, and immiscible systems and determining whether the behavior for IBA-water system is unique for miscible and partially miscible systems.

Besides examining different types of miscible and immiscible systems, we used SDT to determine whether surfactants lowered the interfacial tension for an immiscible fluid system (IBA-water system) and if so how the EIT is a function of

concentration and type of surfactant (anionic, cationic). Like the SDT experiments with IBA-water systems, we could not just run the system with any surfactant and then analyze the results. We first had to distinguish among the different phases including a water-rich phase, IBA-rich phase, surfactant-rich phase, and sometimes an unknown component or impurity. We did this by differences in shades of gray and the appearance of a lack of a real boundary. The IBA-rich phase typically had a real boundary and was darker in shades of gray than the impurity or unknown component. Also, at different temperatures, different color contrasts occurred for the different phases.

Similarities and differences in behavior occurred between IBA/water and IBA/surfactant/water systems. For example, the IBA/water system more easily end pinched than the IBA/surfactant/water systems because of differences in EIT, which indicates that system without surfactant is more easily affected by Korteweg stress and that systems with surfactant would have a larger EIT. Prior research by Pojman *et al.*¹ attributed difficulty in end pinching to a system having a larger EIT. Two other similar behaviors demonstrated in IBA/water systems using and not using surfactant are Marangoni instability and similar behaviors with air bubbles.^{1, 49} A difference in behavior is that the IBA/surfactant/water systems demonstrated more fluid/flow motions than IBA/water systems, which is indicative of being able to observe Korteweg stress more easily in the system using surfactant than the original IBA/water system with no surfactant. Thus, these differences (or lack of differences) in behavior in the two systems demonstrated how the surfactant affected the interfacial tension between the

miscible and partially miscible fluids, thus helping to determine whether the behaviors observed in the SDT were unique. Although some behaviors were unique to the systems using surfactants or to the systems without surfactant, IBA/water systems with and without surfactant also had some similar behaviors. So there is not a simple yes or no answer as to whether the behaviors of the IBA/water system in the SDT are unique or not.

Thus, future work with other types of immiscible and miscible systems needs to be done with the two surfactants that we tested (SDT and DTAC). Also, other types of surfactants (anionic, cationic, nonionic) also need to be done. We only tested two surfactants that were either anionic or cationic. Other surfactants may cause different or similar behaviors, depending upon their cmc and type of surfactant.

At 20 °C, the ITs of IBA/water systems using surfactants were slightly higher than IBA/water systems without surfactant. Prior research by Pojman *et al.*¹ had results where EIT did not change with temperature, but research in the IBA volume chapter (Chapter IV) correlated increasing temperature with decreased averaged EIT. At 30 °C, increasing and decreasing the rotation rate resulted in the averaged EIT and radii getting higher. This result of the broadening radius and decreased sharpness of the boundary at the lower rotation with each increased or decreased rotation rate is due to Fickian diffusion. Typically, previous research has demonstrated that generally only IBA/water system had non-Fickian diffusion with a sharp concentration gradient whereas other miscible systems like dodecylacrylate/polydodecylacrylate showed Fickian

diffusion while maintaining a sharp concentration gradient.^{53, 1} If the rotation rate was not changed, then the IBA/surfactant/water system showed only non-Fickian diffusion rate, thus proving that changing rotational acceleration (even a small range) can affect diffusion and showing that barodiffusion can affect EIT in IBA/surfactant/water systems.

We calculated EITs and ITs using three different methods or formulas and found that it is important to use all three methods for comparison because of the sometime unusual behavior of drops or extremely short rotation rates. However, at 30 °C, comparing the radius³ EIT to Vonnegut EIT is better because the EITs are closer in value. Also, we found that we should use the linear regression line when (a) unusual behavior rates is seen, (b) a smaller range of rotation rates is used, and (c) the IBA-rich drop does not seem settled.

We plotted radius of the drop cubed vs. rotation rate squared to determine EIT and found that the EITs for the systems with SDS concentrations below the cmc matched the predicted trend of decreasing with increasing concentration of the surfactant, but for systems with surfactant concentrations above the cmc, the EITs should not have changed but did, possible because the cmc values for the surfactants were determined in water and not in IBA/water so that the cmc values calculated in water may not be the same as the ones calculated in IBA/water. Thus, the concentrations of the surfactant could actually have been below the cmc. We expected the interactions between the surfactant and the components of the binary system to be stronger than the original interactions between the IBA and water. However, this result did not occur because the original interactions

between IBA and water were stronger than either component's interactions with the surfactant.

Because of the interesting results produced by the two different surfactants, future work would be to test another type of surfactant other than SDS and DTAC. This surfactant would have at least three concentrations and have the EIT measured above and below the UCST of IBA/water. Other future work would be to test all of the concentrations tested at least three times. DTAC also needs more concentrations, preferably a couple below 0.01 mM and one above 5.74 mM.

We used microfluidics as a method to study different systems such as IBA/water and to determine what type of microfluidic device worked best for studying different types of systems. We found that the microfluidic PDMS worked best in the obtaining the capillary instability that we sought. This device allowed us to introduce miscible fluids without significant mixing. Issues with different microfluidic devices include that some of the systems dissolved the microfluidic device. Use of PDMS with a different microfluidic design than ones designed with PC and PMMA gave us the necessary hydrophilicity and longer curving distance, but we still had issues with determination of whether the drop was the heavier or lighter fluid.

A comparison of the behavior in the IBA/water system in the microfluidic device and in the SDT revealed that we had some unusual behavior in the SDT that we did not observe in the microfluidic device. For example, no observable Marangoni instability was seen in the microfluidic device, but in the SDT,

Marangoni instability was easily observed in IBA/water systems no matter whether a surfactant was added. In the microfluidic device, we observed Rayleigh-Plateau instability for IBA/water, which resulted in drop breakup in the PDMS microfluidic device. Other researchers have observed Rayleigh-Plateau instability in immiscible and other miscible systems.³⁸ The drop breakup observed in PDMS microfluidic chip also could have been due to end-pinching instabilities. Drop breakup in the PDMS microfluidic device indicates that Korteweg stresses were present. The drop break up that was in the PMMA and both modified and non-modified microfluidic chip was most likely due to wettability, gravitational forces, Rayleigh-Plateau instability, or changing flow rates.⁵⁴

Differences in the behavior between the PMMA and modified PC versus PDMS are most likely because of the differences in the capillary channels and the materials used. The smaller channels of the PDMS microfluidic device increased the Korteweg stress and any EIT effects. Any Korteweg stresses in the PMMA and modified PC chips were likely equalized.

The PDMS microfluidic devices showed IBA/water with less sharp concentration gradients than the ones observed in the SDT, thus illustrating that the microfluidic devices had fewer Korteweg stresses than the SDT. Because of the large surface area to volume in the microfluidic device, larger effects from EITs should be in the upstream where the IBA-rich and water-rich phases met and have smaller EIT in the downstream, generating a stress toward the upstream. This behavior observed in this dissertation and in Sugii *et al.*⁵⁵ could

explain why the IBA drops were sharper in the upstream but were less sharp as they went downstream and broke up into smaller dissolving droplets. In contrast, when the IBA-rich drop dissolved in the SDT, the boundary always remained sharp and could indicate that an equalized Korteweg stress was occurring in the SDT.

Although we observed drops breaking up in one of the microfluidic devices, we were not able to calculate the EITs using the current equations employed in this dissertation. Future work would focus on deriving an equation that could be used to calculate the EIT in a microfluidic device and compare it to EITs determined using the SDT.

Although we have started on the critical work for determining whether we observe a system such as IBA/water has the same behavior in the SDT as in the microfluidic device and whether this behavior is due to the mixing from the SDT, much future works need to be done. Other materials and microfluidic devices need to be tested and designed to determine which components of miscible and partially miscible systems will not interact with the microfluidic device and which design will allow distinguishing whether the drop is the lighter or heavy phase. Thus, we could then study other systems that we could not previously study with the SDT such as ethanol/water because the ethanol would dissolve into water when the SDT started. We were not able to accomplish this task in this dissertation but have laid the groundwork for which materials and microfluidic devices do not work.

Although we compared the microfluidic behavior of a system such as IBA/water to the system's behavior in the SDT, future work includes comparing the microfluidic behavior of previously studied system to the microfluidic behavior of systems we were unable to study because of the mixing of the SDT before such as ethanol/water system. Also, future work could determine whether the Rayleigh-Plateau instability could be observed with all three types of systems and whether we could observe similar behaviors in the microfluidic device that we saw in the SDT.

REFERENCES

1. Pojman, J. A.; Whitmore, C.; Turco Liveri, M. L.; Lombardo, R.; Marszalek, J.; Parker, R.; Zoltowski, B., Evidence for the Existence of an Effective Interfacial Tension between Miscible Fluids: Isobutyric Acid-Water and 1-Butanol-Water in a Spinning-Drop Tensiometer. *Langmuir* **2006**, *22*, 2569-2577.
2. Whitmore, C. The University of Southern Mississippi, 2004.
3. Viner, G. Evolution of Transient Interfacial Phenomena in Miscible and Partially Miscible Systems. Master, The University of Southern Mississippi, 2006.
4. Poisson, S., *Nouvelle Theorie de l'Action Capillaire*. Bachelier: Paris, 1831.
5. Freundlich, H., *Colloid and Capillary Chemistry*. Methuen & Col. Ltd: London, 1926.
6. Probstein, R. F., *Physicochemical Hydrodynamics*. Wiley: New York, 1994.
7. Van der Walls, J., *J. Stat. Phys.* **1893**, 1979, 20.
8. Anderson, D. M., G.; Wheeler, A., *Annu. Rev. Fluid Mech.* **1998**, *30*, 139.
9. Joseph, D., *Eur. J. Mech. B. Fluids.* **1990**, *9*, 565.
10. Korteweg, D., *Arch. Neerl. Sciences Exactes et Naturelles, Series II* **1901**, *6*, 1.
11. Quinke, G., *Ann. d. Physik.* **1902**, *9*, 4.
12. Smith, P. V. d. V., M.; Mason, S., *J. Colloid and Interface Science.* **1981**, *80* (1), 302.
13. Pojman, J.; Volpert, V.; Dumont, T.; Chekanov, Y.; Masere, J.; Wilke, H. In *Effective Interfacial Tension Induced Convection (EITIC) in miscible fluids*, AIAA 2001-0764, 39th Aerospace Sciences Meeting, Reno, NV, AIAA: Reno, NV, 2001.
14. Zeldovich, Y. B., About Surface Tension of a Boundary between two Mutually Soluble Liquids. *Zhur. Fiz. Khim. (in Russian)* **1949**, *23* (8), 931-935.

15. Vonnegut, B., *Rev. Sci. Instrum.* **1942**, 13, 6.
16. Princen, H. Z., I.; Mason, S., *J. Colloid Sci.* **1967**, 23 (1), 99.
17. Chan, C. C. V. E., J. A. W.; Williams, M. J., *J. Colloid Sci.* **2003**, 260 (1), 211.
18. Capelle, *Surface Phenomena in Enhanced Oil Recovery*. Plenum: New York, 1981.
19. Issacs, E. M., J; Li, J., *ACS Symposium Series* **1988**, 396, 325.
20. Manning, C. D.; Scriven, L. E., On Interfacial Tension Measurement with a Spinning Drop in Gyrostatic Equilibrium. *Rev. Sci. Instrum.* **1977**, 48, 1699-1705.
21. Zoltowski, B.; Pojman, J. A. In *Using Spinning Drop Tensiometry to Determine the Square Gradient Parameter for Dodecyl Acrylate/Poly (Dodecyl Acrylate) for Use in the TIPMPS Flight Investigation AIAA 2003-0996*, 41st AIAA Aerospace Sciences Meeting and Exhibit, Reno, NV, Reno, NV, 2003.
22. Zoltowski, B.; Chekanov, Y.; Masere, J.; Pojman, J. A.; Volpert, V., Evidence for the Existence of an Effective Interfacial Tension between Miscible Fluids. 2. Dodecyl Acrylate-Poly(Dodecyl Acrylate) in a Spinning Drop Tensiometer. *Langmuir* **2007**, 23, 5522-5531.
23. Landau, L. D.; Lifshitz, E. M., *Fluid Mechanics*. Pergamon: Oxford, 1987.
24. Cicuta, P.; Vailati, A.; Giglio, M., Equilibrium and Nonequilibrium Fluctuations at the Interface between Two Fluid Phases. *Phys. Rev. E* **2000**, 62, 4920-4926.
25. Cicuta, P.; Vailati, A.; Giglio, M., Capillary-to-bulk crossover of nonequilibrium fluctuations in the free diffusion of a near-critical binary mixture. *Applied Optics* **2001**, 40, 4140-4146.
26. Brogioli, D.; Vailati, A.; Giglio, M., Universal behavior of nonequilibrium fluctuations in free diffusion processes. *Phys. Rev. E* **2000**, 61, R1-R4.
27. Brogioli, D.; Vailati, A., Diffusive Mass Transfer by Nonequilibrium Fluctuations: Fick's Law Revisited. *Phys. Rev. E* **2000**, 63, 102-105.
28. Vailati, A.; Giglio, M., Giant fluctuations in a free diffusion process. *Nature* **1997**, 390, 262-265.

29. Vlad, D. H.; Maher, J. V., Dissolving Interfaces in the Presence of Gravity. *Physical Review E* **1999**, *59*, 476-478.
30. Izmailov, A. F.; Myerson, A. S., Concentration gradient formation in supersaturated vertical columns. I. Fokker-Planck approximation. *J. Cryst. Growth* **1992**, *121*, 723-732.
31. Izmailov, A. F.; Myerson, A. S., Gravity Induced Formation of Concentration Gradients in Supersaturated Binary Solutions. *Physica A* **1996**, *224*, 503-532.
32. Jamshidi-Ghaleh, K.; Tavassoly, M. T.; Mansour, N., Diffusion coefficient measurements of transparent liquid solutions using Moiré deflectometry. *Journal of Physics D: Applied Physics* **2004**, *37*, 1993-1997.
33. Giglio, M.; Vendramini, A., Optical Measurements of Gravitationally Induced Concentration Gradients near a Liquid-Liquid Critical Point. *Phys. Rev Lett.* **1975**, *35*, 168-170.
34. Hicks, F. B.; Can Vechten, T. C.; Franck, C., Thermally perturbed barodiffusion in a binary liquid mixture. *Physical Review E* **1997**, *55* (4), 4158-4164.
35. Vailati, A.; Giglio, M., Nonequilibrium fluctuations in time-dependent diffusion processes. *Phys. Rev. E* **1998**, *58*, 4361-4371.
36. Rosen, M. J., *Surfactants and Interfacial Phenomena*. Wiley-Interscience: New York, 2004.
37. Vonnegut, B., Rotating Bubble Method for the Determination of Surface and Interfacial Tensions. *Rev. Sci. Instrum.* **1942**, *13*, 6-9.
38. Squires, T. M.; Quake, S. R., Microfluidics: Fluid physics at the nanoliter scale. *Rev. Mod. Phys.* **2005**, *77* (3), 977-1026.
39. Yamada, M. H., T.; Yasuda, M.; Seki, M., *Lab on a Chip*. **2006**, *6*, 179.
40. Sugii, Y. O., K.; Hibara, A.; Tokeshi, M.; Ktamori, T., *J. of Visualization*. **2005**, *8* (2), 117.
41. Bessonov, N.; Pojman, J. A.; Volpert, V. In *Numerical Simulations of Transient Interfacial Phenomena in Miscible Fluids*, AIAA-2004-631, 42nd AIAA Aerospace Sciences Meeting, Reno, NV, AIAA: Reno, NV, 2004.
42. Hagedorn, J. G. M., N.S.; Douglas, J.F., *Physics Review E* **2004**, *69* (5), 056312.

43. "Plateau-Rayleigh Instability". http://en.wikipedia.org/wiki/Plateau-Rayleigh_instability (accessed 1 November 2006).
44. Michon, G. P. Final Answers: Surface Area of an Ellipsoid. home.att.net/~numericana/answer/ellipsoid.htm (accessed 1 November 2006).
45. Princen, H. M.; Zia, I. Y. Z.; Mason, S. G., Measurement of Interfacial Tension from the Shape of a Rotating Drop. *J. Colloid and Inter. Sci.* **1967**, *23*, 99-107.
46. Cussler, E. L., *Diffusion: Mass Transfer in Fluid Systems*. Cambridge: London, 1997.
47. Righetti, P. G.; Bossi, A.; Giglio, M.; Vailati, A.; Lyubimova, T.; Briskman, V. A., Is Gravity on our Way? The Case of Polyacrylamide Gel Polymerization. *Electrophoresis* **1994**, *15*, 1005-1013.
48. Vailati, A.; Giglio, M., q divergence of nonequilibrium fluctuations and its gravity induced frustration in a temperature stressed liquid mixture. *Phys. Rev. Lett.* **1996**, *77*, 1484-1487.
49. Sternling, C. V.; Scriven, L. E., Interfacial Turbulence: Hydrodynamic Instability and the Marangoni Effect. *A.I.Ch.E. J.* **1959**, *5*, 514-523.
50. Nakamura, H.; Sano, A.; Matsuura, K., Determination of Critical Micelle Concentration of Anionic Surfactants by Capillary Electrophoresis Using 2-Naphtalenemethanol as a Marker for Micelle Formation. *Analytical Sciences* **1998**, *14*, 379-382.
51. Mehta, S. K.; Bhasin, K. K.; Chauhan, R.; Dham, S., Effect of Temperature on Critical Micelle Concentration and Thermodynamic Behavior of Dodecyldimethylammonium Bromide and Dodecyltrimethylammonium Chloride in Aqueous Media. *Colloids and Surfaces A: Physiochem. Eng. Aspects* **2005**, *255*, 153-157.
52. Viner, G. University of Southern Mississippi, 2006.
53. Antrim, D.; Bunton, P.; Lewis, L. L.; Zoltowski, B. D.; Pojman, J. A., Measuring the Mutual Diffusion Coefficient for Dodecyl Acrylate in Low Molecular Weight Poly(Dodecyl Acrylate) Using Laser Line Deflection (Wiener's Method) and the Fluorescence of Pyrene. *J. Phys. Chem. Part B* **2005**, *109*, 11842-11849.

54. Hagedorn, J. H.; Martys, N. S.; Douglas, J. F., Breakup of a fluid thread in a confined geometry: droplet-plug transition, perturbation sensitivity and kinetic stabilization with confinement. *Phys. Rev. E* **2004**, *69*, 056312.
55. Sugii, Y.; Okamoto, K.; Hibara, A.; Tokeshi, M.; Kitamori, T., Effect of Korteweg stress in miscible liquid two-layer flow in a microfluidic device. *J. Visualization* **2005**, *8*, 117-124.